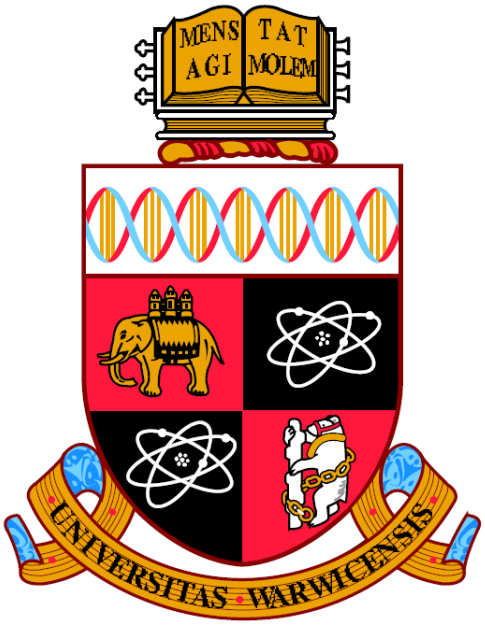

Development on High Energy Lithium-ion Batteries Based on Silicon Electrodes

Qianye Huang

Thesis

Submitted to the University of Warwick

in fulfilment of the requirements for the degree of

Doctor of Philosophy

Warwick Manufacture Group

September 2018

WMG
THE UNIVERSITY OF WARWICK

Table of Contents

List of Tables and Figures

Acknowledgement

I highly appreciate to all the people who kindly gave me advice and trained me for practical skills throughout the process of achieving my PhD degree.

First, I would like to thank my supervisor Dr Rohit Bhagat, who brought me into this promising and exciting research project and always gave financially supports to me for any purchasing requirement related to my PhD as well as sending me to several international conferences to present my work.

Secondly, I would give a big thank to my supervisor Dr Melanie Loveridge, who offered me plenty of guidance during my PhD as well as revised every piece of my writing work with massive patients. Most importantly, she always encouraged me to build up the confidence for my PhD project, for which I started with little knowledge background.

A special thank will give to Ronny Genieser, who is more like a friend other than a colleague. He gave me a lot of useful advice and training for my PhD project. Every time I had problems or was at a loss in my research, he was there providing me with knowledge support as well as critical questions.

Also, I am grateful to Dr Chaoying Wan, who always gave me technical suggestions in polymer synthesis and characterisation, and Dr Marc Walker, who helped me a lot in XPS experiment and analysis.

Additionally, I would like to thank all the colleagues in my group who shared me every useful information and lab skill during my PhD, especially for Romeo Malik and George Papas.

In the end, I would thank my families. A sincere thank goes to my parents, who gave me finance support with their deep love. A big thank to my husband, who always spiritually supported me and took every care for my life. Last but not least, I would thank my dog Bobby, who always accompanied me when I was alone and waited for me no matter how busy I was.

Declarations

I declare that all the work involved in this thesis is subjected to my original unless I referenced. I confirm that this thesis has not been submitted for a degree at another university.

Most experiments and training were conducted on my own in WMG, University of Warwick. XPS analysis was performed together with Dr Marc Walker from the Department of Physics at the University of Warwick. There is no materials from a prior thesis has been included.

Qianye Huang

September 28th, 2018

Published work

The primary findings from Chapter 5 and part of the results in Chapter 6 (regarding binary crosslinked polymer binder system PAA/PVA) have already been published in peer-reviewed journals.

Publication directly related to this thesis:

Huang, Q., Loveridge, M. J., Genieser, R., Lain, M. J., & Bhagat, R. (2018). Electrochemical Evaluation and Phase-related Impedance Studies on Silicon–Few Layer Graphene (FLG) Composite Electrode Systems. Scientific Reports, 8(1), 1386.

Huang Q, Wan C, Loveridge M, Bhagat R. Partially Neutralized Polyacrylic Acid/Poly(vinyl alcohol) Blends as Effective Binders for High-Performance Silicon Anodes in Lithium-Ion Batteries. ACS Appl Energy Mater. 2018;1(12):6890–8.

Publication partly related to this thesis:

Loveridge, M. J., Lain, M. J., Huang, Q., Wan, C., Roberts, A. J., Pappas, G. S., & Bhagat, R. (2016). Enhancing cycling durability of Li-ion batteries with hierarchical structured silicon–graphene hybrid anodes. Phys. Chem. Chem. Phys. Phys. Chem. Chem. Phys, 18(18), 30677–30685.

Abstract

To develop a high-energy lithium-ion battery system based on the silicon (Si) anodes, a comprehensive investigation has been conducted through different approaches. These include optimising the composite formulation of the Si electrode, developing a robust binder system and identifying an appropriate electrolyte system to achieve high voltage in Si full cells.

These studies reveal that the carbon blends (a mixture of graphite, carbon black and few-layer graphene) is a more effective conductive system for Si electrodes, compared with the conventional carbon black. An optimised carbon mixture formulation has been identified and applied to other investigations in this project.

By incorporating few-layer graphene (FLG) as a combined active material, the cyclability of Si electrodes can be largely improved. An optimised formulation for the Si-FLG composite electrode has been identified, and the beneficial mechanism of FLG has been comprehensively studied. The optimised Si-FLG formulation has been further manufactured into electrodes with a scale-up battery pilot line, and fabricated into the full cells with the $LiNi_{0.6}Mn_{0.2}Co_{0.2}O_2$ (NMC622) cathode. Based on this full cell system, ethylene-carbonate (EC)-free electrolyte systems with different additives, have been systematically studied to improve the stability of the system under 4.4 V. The results indicate that, by excluding EC from the electrolyte, the cells could effectively avoid the large capacity loss that occurs during initial cycles due to the oxidation of EC. The optimal combination of electrolyte additives has been identified. The surface chemistries of electrodes, with different electrolytes, have been deeply analysed thoroughly.

The development of binder systems based on polyacrylic acid (PAA) has also been investigated, including partial neutralisation, the synthesis of binary cross-linked polymers and the design of a novel multi-level cross-linked polymer. Different levels of improvement for the cyclability of Si electrodes have been achieved. The multi-level cross-linked binder has delivered the best performance, due to the strong ionic interaction with the Si surface.

Abbreviations

3DM	Three-dimensional Microporous
Alginate-C	Alginate with Dopamine
CB	Carbon Black
CC	Constant Current
CMC	Carboxymethyl Cellulose
C-rate	Current rate based on cell capacity
CVD	Chemical Vapour Deposition
DEC	Diethyl Carbonate
DMC	Dimethyl Carbonate
EC	Ethylene Carbonate
EDX	Energy Dispersive X-ray Spectroscopy
EIS	Electrochemical Impedance Spectroscopy
EMC	Ethyl-methyl Carbonate
EPD	Electrophoretic Deposition
EVs	Electric Vehicles
FEC	Fluoroethylene Carbonate
FLG	Few-layer Graphene
FTIR	Fourier-Transform Infrared Spectroscopy
GO	Graphene Oxide

G-Si-C	Si Particles between Graphene and Amorphous Carbon layers
GSM	Gram per Square Meter
LFP	$LiFePO_4$ (Lithium Iron Phosphate)
LTO	$Li_4Ti_5O_{12}$ (Lithium Titanate Oxide)
LUMO	Lowest Unoccupied Molecular Orbital
MEC	Methylene-ethylene Carbonate
MWCNTs	Multiwall Carbon Nanotubes
Na-PAA	Partially neutralized PAA with 70 mol% NaOH
Na-CMC	Sodium - Carboxymethyl Cellulose
NCA	$Li(Ni_{0.8}Co_{0.15}Al_{0.05})O_2$ (Lithium Nickel Cobalt Aluminium Oxide)
NMC	$Li[Ni_xCo_yMn_z]O_2$ (Lithium Nickel Manganese Cobalt Oxide)
NMC-622	$Li[Ni_{0.6}Co_{0.2}Mn_{0.2}]O_2$
NMC-811	$Li[Ni_{0.8}Co_{0.1}Mn_{0.1}]O_2$
NMP	N-Methyl-2-pyrrolidone
PAA	Polyacrylic Acid
PAA-C	PAA with the Catechol Groups
PANI	Polyaniline
PEIS	Potentio Electrochemical Impedance Spectroscopy
PES	1-Propene 1,3-Sultone
pnPAA	Partially neutralized PAA with 8 mol% NaOH
PR	Ring-slide Polyrotaxane
PVA	Polyvinyl Alcohol
PVdF	Polyvinylidene Fluoride
SBR	Styrene-Butadiene Rubber

SEI	Solid Electrolyte Interface
SEM	Scanning Electron Microscopy
SiMPs	Si micro-powder electrodes
SiNPs	Si Electrodes with Nano-sized Particles
SoC	State of Charge
SPEIS	Staircase Potentio Electrochemical Impedance Spectroscopy
VC	Vinylene Carbonate
VGCFs	Vapour-grown Carbon Nanofiber
VLS	Vapour-liquid-solid
XPS	X-ray Photoelectron Spectroscopy

List of Symbols

Symbol	Description	Units
ρ	Density	kg/m^3
E_{store}	Energy stored in a cell of battery	J
Q_{cell}	Delithiation capacity	mAh
V_{cell}	Cell potential	V
M_W	Molar mass	kg/mol
d	Diameter of a subject	μm (or cm)
$M_{dry\ coating}$	Mass of coating after dried	g
$M_{wet\ coating}$	Mass of wet coating	g
$M_{Cu\ foil}$	Mass of copper foil	g
$R(Series\ Resistance)$	Series resistance	Ohm
$R(SEI)$	SEI resistance	Ohm
$R(Charge\ Transfer)$	Charge Transfer resistance	Ohm
W_s	Warburg Impedance	Ohm
t	Time	s (or h)
T	Temperature	˚C

Chapter 1 Introduction

1.1 Background for Lithium-ion Batteries

In recent years the efficiency of energy generation has been dramatically developed with various types and scales of the power source. As a result, the requirements for energy storage devices with high capacity have gradually become critical. Batteries, as the most common energy storage device, have naturally attracted wide attention.

The lithium-ion (Li-ion) battery was enabled to be commercially launched since the invention of the $LiCoO_2$ cathode by John B. Goodenough in 1980 [1]. In 1991, Sony commercialised the first Li-ion batteries, and it soon became the predominant battery product for portable devices due to its high energy density[1]. Nowadays, the energy that can be stored in a portable Li-ion battery has successfully increased to >3.0 Ah in the 18650 cells and is continually being improved[2], which makes it a promising candidate for applications that require high energy density such as electric vehicles and smart grid applications.

In comparison with other secondary batteries (Figure 1-1), Li-ion batteries hold nearly twice the energy density of nickel-based batteries, and around four times the energy density of lead-acid batteries[3]. Also, Li-ion batteries have other advantages of no memory effect, low self-discharge and being environmentally friendly[4].

During the charging process of Li-ion battery, lithium ions move from the cathode to the anode. As a result, anode materials are susceptible to swelling in order to store lithium ions, and the expansion is proportional to lithium intercalation[5]. During the discharging process, lithium ions will move back to the cathode from the anode, and typically there will be a loss of lithium ions that have been trapped into the solid electrolyte interphase (SEI) layer on the surface of anode material. Therefore, within a battery, the design and type of anode material are one of the main factors that determine higher degrees of reversible storage capacity for lithium ions.

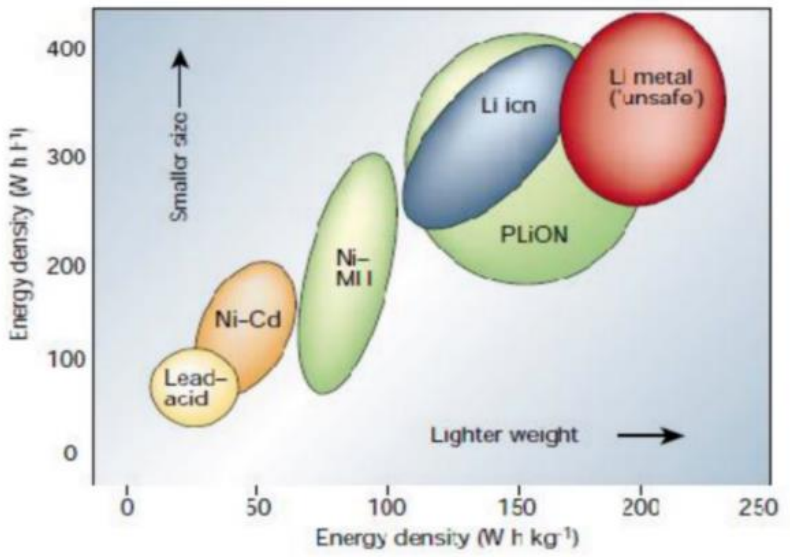

Figure 1-1 Comparison of Different Battery Technologies[3].

1.2 Motivation and Challenge for the Silicon-based Anode

Currently, most commercialised Li-ion batteries use graphite as its anode, which has a theoretical reversible capacity of 372 mAh/g[6], while silicon appeared on the research horizon in recent years due to its higher capacity (3579 mAh/g) at room temperature[7]. Therefore, silicon (Si) based anodes have attracted wide attention for it to be developed into high energy batteries to replace carbon-based anodes.

The mechanism of electrochemical lithiation on Si electrode is illustrated as Reaction (1) – (3)[8]–[10].

During lithiation:

$$Si(crystalline) + xLi^+ + xe^- \rightarrow Li_xSi(amorphous) + (3.75 - x)Li^+ + (3.75 - x)e^- \quad \text{(Reaction 1)}$$

Or $\rightarrow Li_{15}Si_4\ (crystalline)$ (under 50 mV) (Reaction2)

During delithiation:

$$Li_{15}Si_4(crystalline) \rightarrow Si(amorphous) + yLi^+ + ye^- + Li_{15}Si_4(residual) \quad \text{(Reaction 3)}$$

It can be concluded from Reaction (1)-(3) that one Si atom can alloy with maximum 3.75 Li atoms, compared with 6 carbon atoms accommodate 1 Li atom in conventional graphite anode. It has been revealed by several groups that Si undergoes the phase change during the (de)lithiation process[7]–[12]. For the first lithiation, crystalline Si will be lithiated to amorphous Li-Si compound (Reaction 1) until the voltage drops to

below 50 mV, which is regarded as the transformation point for the deep-lithiated crystalline phase $Li_{15}Si_4$ (Reaction 2). The lithiation process before hitting 50 mV is considered as a two-phase region, which is demonstrated as the distinct plateau on the voltage profile (Figure 1-2). Whilst for the first delithiation, the crystalline phase $Li_{15}Si_4$ (if there is any) will be delithiated to an amorphous Li-Si compound firstly and then back to amorphous Si only (Reaction 3). Therefore, from the second cycle onwards, the crystalline Si should have disappeared, and the single-phase cycling is exhibited as the slope is seen to plateau on the voltage profile (Figure 1-2) [12]. It has also reported that if the Si electrode is cycled between Reaction 2 and 3 repeatedly, it will result in a rapid capacity fading; hence it is suggested to control the cycling voltage above 50 mV[12].

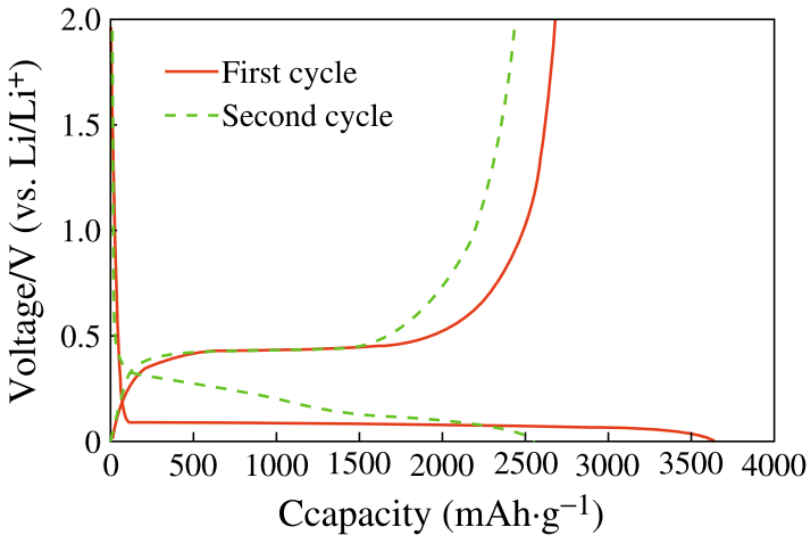

Figure 1-2 Voltage profile for the first two cycles of a typical Si powder electrode

Another advantage for the high specific capacity of Si is that it is not necessary to make thick coatings to achieve high energy density. It has been well recognised that thin electrode coatings exhibit better adhesion force between electrode and current collector[13]. However, for traditional electrodes with much less specific capacity, a thick coating is desired to enhance the energy density, which has to address the challenge to manufacture crack-free thick coating (> 100 μm) and maintain a stable electrode structure[13]–[15].

Despite the high specific capacity, there are some major challenges, which dominate the main degradation mechanisms and limit the commercialisation of Si anodes for Li-ion batteries. Firstly, there is a massive volume expansion during the charge/discharge

cycle. While alloying with lithium ions, the formation of Si-Li compounds such as $Li_{12}Si_7$, Li_7Si_3, $Li_{13}Si_4$ can cause maximum 280 vol % increase[16]. It can lead to a pulverisation of active particles, a loss of connections between the active material and current collector delamination, and also a breakdown of the conductive carbon network (Figure 1-3a, b)[16], and thus results in a continued capacity fade in the battery. Secondly, when the potential of the anode material is around 0.9 V *vs.* Li/Li^+, the decomposition of the $LiFP_6$ based carbonate electrolyte (which is initiated around 1.7~1.3 V *vs.* Li/Li^+) at the electrode surface is thermodynamically favourable[17]. Some side reactions occur between the electrolyte solvent and the negative electrode, and as a result, a passivation film – SEI layer will be formed on the surface of the negative electrode. A stable SEI layer is desirable to protect the active materials on the electrode from further reactions with electrolyte components. However, due to massive volume expansion of silicon, the SEI layer is unstable. It becomes successively thicker during the continual breaking and reforming (Figure 1-3c)[18]. Furthermore, the formation of the SEI compounds results in continual loss of lithium ions, which causes irreversible capacity reduction.

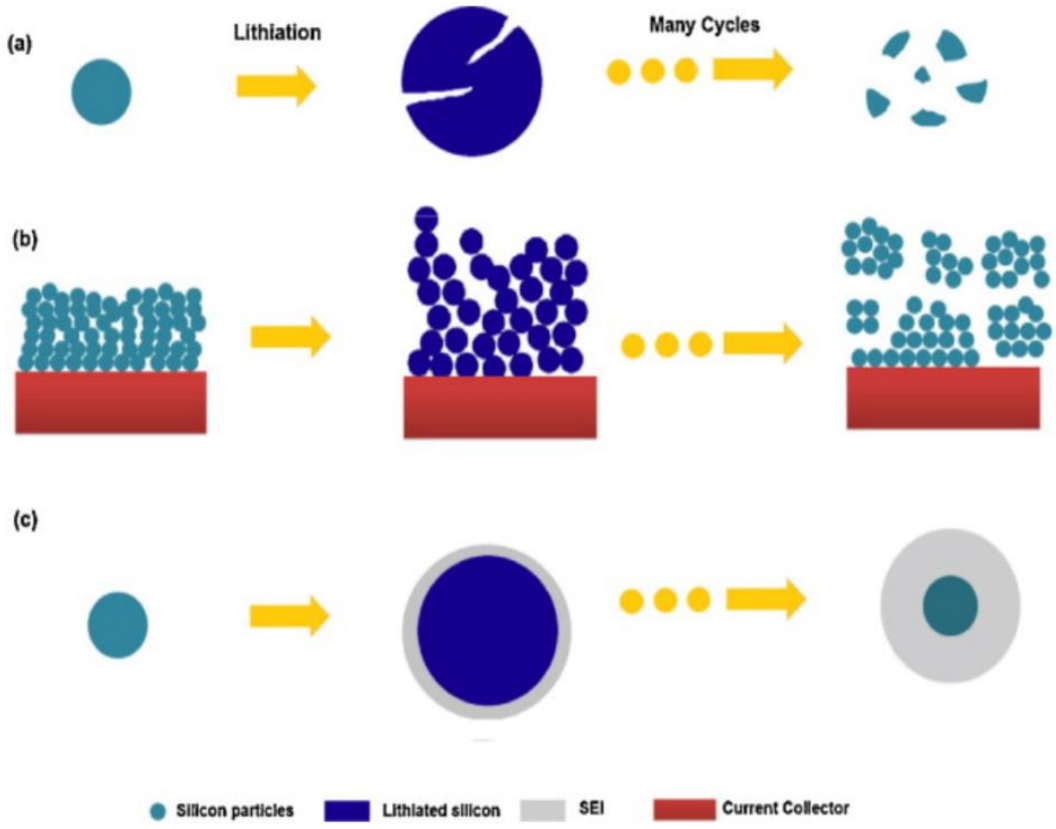

Figure 1-3 Si electrode failure mechanisms: (a) material pulverisation (b) morphology and volume change of the entire Si electrode (c) continuous SEI growth[17].

To address these problems, many studies have been conducted using different approaches, which, in general, can be divided into two main categories as follows:

a. The morphology and microstructure of the silicon anode to better adapt the volume expansion, such as small particle size, porous structures or nano-structuring[17], [19].
b. The electrode composite formulation, including the chemistry of binder, the ratio of different electrode materials (active materials, carbon black, binder, solvent), hybrid active materials (consisting of silicon and other materials). This aims to optimise the specific property, including extending the life cycle, improving conductivity or capacity[20].

Among these approaches, attractive results have been achieved via modifying the morphology of the silicon (e.g. nano-structuring) so that electrodes can effectively accommodate Si expansion [28]-[38]. However, it is difficult and expensive to scale up such methodology industrially. Compared to this approach, optimising the electrode formulation and microstructure is more practical and innovative. This also constitutes a more realistic approach to be applied within an industrially-relevant scale, as there is no requirement for complicated manufacturing processes and expensive materials. Therefore, this approach embodies and drives the central themes of this research.

1.3 Other Challenges for the Full Cell with the Si-based Anode

The cell's energy that can be stored is governed by the relation $E_{store} = Q_{cell} \times V_{cell}$, where Q_{cell} refers to the charge capacity and the V_{cell} is the cell potential. This relation suggests that to develop a high energy battery, the electrode materials should satisfy not only a high capacity but also a high potential between anode and cathode material[21].

Generally, to select the right material for Li-ion batteries, characteristics including high discharge voltage, high-energy capacity, long life cycle, high power density, lightweight, low self-discharge rate, and to be environmentally benign [21]. Since the cathode is not the main research topic here, there is no investigation in developing high voltage cathode materials in this study. The commercially available material $Li(Ni_{1/3}Mn_{1/3}Co_{1/3})O_2$, which is also called NMC, has been selected for the cathode

material to pair with Si anode since NMC can operate at a high voltage of 4.5 V with a capacity of around 200 mAh/g[21].

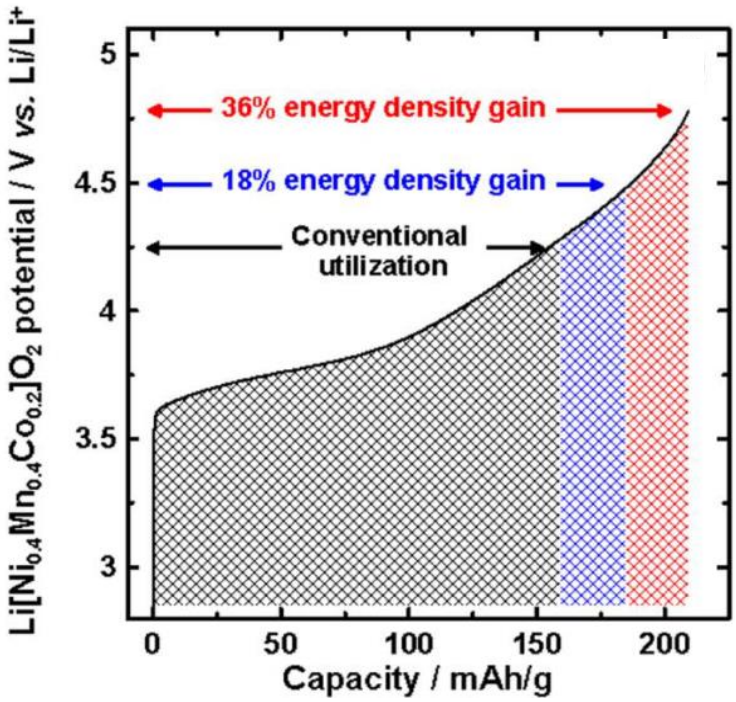

Figure 1-4 Potential vs. gravimetric capacity of Li[Ni0.4Mn0.4Co0.2]O2 positive electrode materials[22]

For most conventional cathodes, 4.3 V is applied as the upper cut-off voltage, since higher than this voltage, the electrolyte oxidation on cathode becomes the main challenge to achieve a stable cyclability[22]. Plenty effort have been made to push up the upper boundary of cell operation voltage through optimising electrolyte systems; however improvements were slowly achieved [23]–[26]. 4.5 V for cathodes was considered as the most practical target cut-off voltage in literatures, since with this enhancement of 0.2 V, a remarkable gain of energy density could be achieved (would 18 % energy density gain for NMC) as shown in Figure 1-4[22], [27].

Therefore, to achieve higher energy density in full cells, electrolyte is the most critical component. The electrolyte mostly used for the current commercialised Li-ion battery is a mixture of alkyl carbonates including ethylene carbonate (EC), dimethyl carbonates (DMC), diethyl carbonates (DEC) and ethyl-methyl carbonates (EMC) solvating in the salt $LiPF_6$ [28]. Generally, they exhibit acceptable stability for high voltage cathodes (~4 V), good ionic conductivity, a reasonable temperature window (between freezing and boiling points), low toxicity and acceptable safety[28]. However, it is still quite challenging for electrolyte to perform stably over 4.3 V in

full cells[29]. The upper voltage limit for the stability of electrolytes becomes the main constraint factor for developing high-energy Li-ion batteries.

It has been reported in several studies that EC demonstrated poor stability towards high voltage, and EC free electrolyte with an appropriate "enabler" was suggested for NMC full cells towards high voltage operation[22], [27], [30]. Therefore, for this study, EC free electrolytes with varies additives were investigated, aiming to stabilise the SEI and improve the cyclability for Si/NMC full cells operated under high voltage.

1.4 Research Assumptions and Objectives

Generally, this work aims to extend the operational lifetime of Si as an anode material in Li-ion batteries and to do this a holistic approach is required. In order to improve the energy density and durability of Li-ion batteries with Si-based anodes, an advanced optimisation will be conducted around the electrode's microstructure, the binder system, and the electrolyte for Si-based full cells cycling under higher voltages. The specific objectives can be summarised as the following:

- To optimise electrode composite formulation (including hybrid electrodes with other materials, component ratios and conductive additives etc.) and to understand the improved mechanism with the optimised microstructure.
- To develop a smart binder system which could better adapt to the expansion for Si electrodes as well as to understand the contribution from the corresponding functional groups and chemical bonding within these polymers.
- To investigate the electrolyte additives at high voltage to improve cyclability of Si full cells.

It is proposed that each objective could contribute several novelties to the knowledge system and provide a literature support base and guidance for industrialisation in the future.

1.5 Structure of This Thesis

Chapter 1 outlines the research background and motivation as well as indicates the potential knowledge contribution from this work.

Chapter 2 reviews recent developments of Si electrodes for Li-ion batteries and to validate the approach and motivation for this work. Also, existing studies related to the research objectives have been critically reviewed to identify the research gaps and

seek guidance in designing electrode materials. This includes electrode composite structures, binders and electrolytes, to achieve the objectives of this work.

Chapter 3 provides detailed information about the experimental methodology and relevant techniques used in this work. Relevant guidance from existing literature has also been included to provide a comprehensive experimental outline.

Chapter 4 investigates the effect of different carbon conductive mixtures which provide hierarchical conductive networks to enhance the durable performance of Si. The formulation of the optimised carbon mixture has been identified and will be applied to later studies.

Chapter 5 conducts a comprehensive study around Si-few-layer-graphene (Si-FLG) composite systems. An optimised formulation has been identified, with further studies here including electrochemical evaluation, mechanical testing, impedance and post-mortem structure imaging. This demonstrates the holistic approaches required to facilitate the longer-term use of Si, and also to fundamentally understand the functioning of this optimised formulation.

Chapter 6 examines several polymer systems and aims to improve the electrode's binder system regarding both mechanical and electrochemical performance in Si half-cells (*vs* Li/Li^+). Polyacrylic acid (PAA), PAA-based binary polymers and tailored multi-level crosslinked polymer are all included.

Chapter 7 systematically investigates the EC-free electrolyte with various additives within Si/NMC full cells under high voltage cycling profile. An optimised electrolyte formulation is proposed.

Chapter 8 summarises the main findings from the experimental data in this work and suggestions for further research are indicated.

Chapter 2 Literature Review

2.1 Development of Technology on Si Anodes

As outlined in Section 1.1, the main obstacles for commercialising Si anodes are the large volume expansion and its associated problems including short cycle life and unstable SEI. To address these challenges, several studies have been conducted through different approaches, which can be divided into two main methods – modification of the morphology of Si electrodes and optimisation of electrode formulation and microstructure.

2.1.1 Modification of Si Morphology

Current studies on the modification of Si morphology are generally based on nanomaterials since nanoparticles with reduced dimensions could adapt to a higher rate of alloying with Li and mitigate electrode cracking. Also, since Si exhibits much lower diffusion coefficient (10^{-13} ~ 10^{-12} cm^2 s^{-1}) comparing with graphite ($10^{-8.5}$ ~ $10^{-7.7}$ cm^2 s^{-1}), modifying Si morphology can be an effective approach to minimise the diffusion route of Li ions and thus to achieve higher rate capacity. This approach could be categorised into three main areas – solid nanostructures, hollow structure, and surface coated particles.

- ***Nanostructured Si electrodes***

The development of Si anodes with nano-sized Si particles (SiNPs) has been investigated by several groups. Li *et al.*[31] studied a nano-Si (78 nm) composite anode with carbon black and PVdF and achieved a capacity over 1700 mAh/g for 10 cycles, which was better than their bulk Si powder (faded to 200 mAh/g after only 5 cycles). Kim et at[32] investigated nano Si particles with different sizes (5 nm, 10 nm and 20 nm), and they indicated that nano-Si with the particle size of 10 nm showed the relatively better result with specific capacity over 3000 mAh/g and 81 % capacity retention achieved over 40 cycles. However, these results are not optimistic for Si

electrodes since the life cycle is too short, possibly due to a large amount of SEI layer for nanoparticles, which would continuously consume Li-ions.

Cui's group conducted several studies into designing nanostructured Si electrodes including Si nanowire, nanotube and hollow nanostructures. They introduced a nanowire Si structure in 2008 (Figure 2-1)[33]. The method used to synthesise the electrode was the vapour-liquid-solid (VLS) process on a stainless steel substrate using an Au catalyst. This type of structure provided better accommodation for the large volume expansion of Si electrodes. Also, each Si nanowire is electrically connected to the current collector with a straight electronic conductive pathway for efficient electronic conduction, which maximised the achievable capacity. In this case, there was no need for the binder and conductive additives, which to a large extent enhanced the energy density and charge efficiency[33]. Results showed a reversible capacity around 3500 mAh/g for 20 cycles, which almost maintained the theoretical capacity for Si electrodes at room temperature. However, data for only 20 cycles is insufficiently convincing to indicate or predict whether this structure could achieve a practical long cycle life.

In 2009, Cui's group developed a crystalline-amorphous core-shell Si nanowire structure[34], which was synthesised on a stainless steel current collector (without Au as the catalyst) in a SiH_4 Chemical Vapour Deposition (CVD) furnace. It was considered that amorphous Si had a better cycle performance and reacted with lithium at a slightly higher voltage than crystalline Si, and therefore an amorphous Si shell was designed to store Li-ions while the crystalline core worked as the mechanical support[34]. Their best result showed a capacity of around 1060 mAh/g with 85% capacity retained after 100 cycles and the coulombic efficiency was maintained at 98.4%-99%. This capacity has triple the value of graphite anode, but it still needs to be improved as the coulombic efficiency is not good enough to maintain a long life cycle and be of commercial interest.

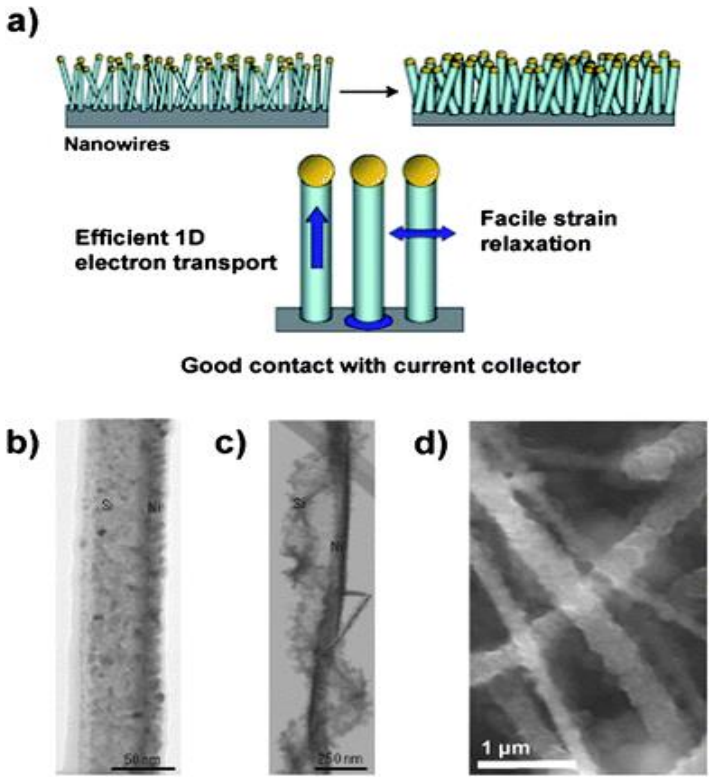

Figure 2-1 Schematic of Si nanowire structure[33].

Si nanotubes (Figure 2-2) can be regarded as hollow nanowires that have a similar structure to carbon nanotubes, which are prepared by CVD. Capacities of 3360 mAh/g at C/20 and 2500 mAh/g at C/5, were achieved with high capacity retention – around 81% after 50 cycles[35], which were promising results for initial research, but the cycle life still needs to be improved to meet commercial requirements. Additionally, all these approaches of one-dimensional structures require the process of CVD or template growth, which make it challenging for large-scale manufacture and commercialisation.

Two-dimensional nanostructures such as Si thin films, deposited by radio-frequency magnetron sputtering on copper foil[36], have also shown improved cell performance, but this varies as a function of the film thickness. Ohara *et al.*[37] indicated that thinner films could deliver higher discharge capacity, and their studies proved that Si thin films with the thickness of 50 nm had much better performance (over 3500 mAh/g for 200 cycles under 1C) compared with 150 nm thickness (around 2200 mAh/g for 200 cycles). This result is significant for Si as it approaches the theoretical capacity for increased cycle numbers even under high charge rate. However, the synthesis method is impractical for large-scale manufacture.

Actually, for all the template-growth approaches mentioned above [33]-[37], it raises most concern that with such thin electrodes (50 nm ~ 5 μm), it will be challenged to pair them with high-energy-density cathode, which is normally above a thickness of 60 μm.

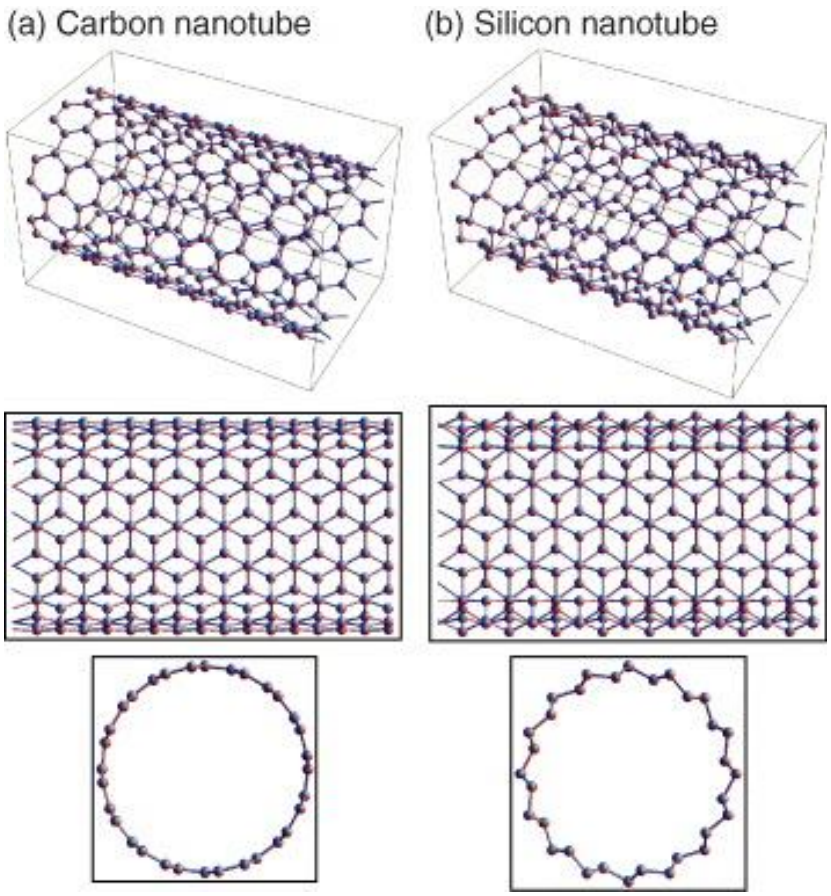

Figure 2-2 Structure of Si nanotubes and comparison with carbon nanotubes[35].

Porous Si nanoparticles are three-dimension nano-structures that have attracted much attention in recent years. One popular approach is the three-dimensional microporous (3DM) structure, which used a chemical etching method to produce porous Si particles that could increase particle surface area and provide better accommodation for volume change[38]. Bang *et al.*[39] demonstrated a simplified method to produce 3DM Si electrodes by depositing Ag on commercial bulk Si powders via a metal-assisted chemical etching process to synthesise the porous particles (Figure 2-3). This kind of electrode showed a high reversible capacity over 2000 mAh/g for 50 cycles and the initial charge efficiency was improved to 94.4 %[39]. Another approach is hollow porous Si nanoparticles, which was reported by Chen *et al.*[40]. They fabricated hollow porous Si nanoparticles via magnesiothermic reduction of hollow porous SiO_2

nanoparticles and followed by silver coating (Figure 2-4). A high specific capacity of 3762 mAh/g was achieved, and 93 % of the capacity was retained after 99 cycles at a current density of 4000 mA/g[40]. Despite this excellent performance for this kind of hollow porous Si nanoparticles, the synthesis method is still too complex and costly to realise large-scale manufacture, and also with the increased surface area of porous Si, problems with a large amount of SEI layers are also associated.

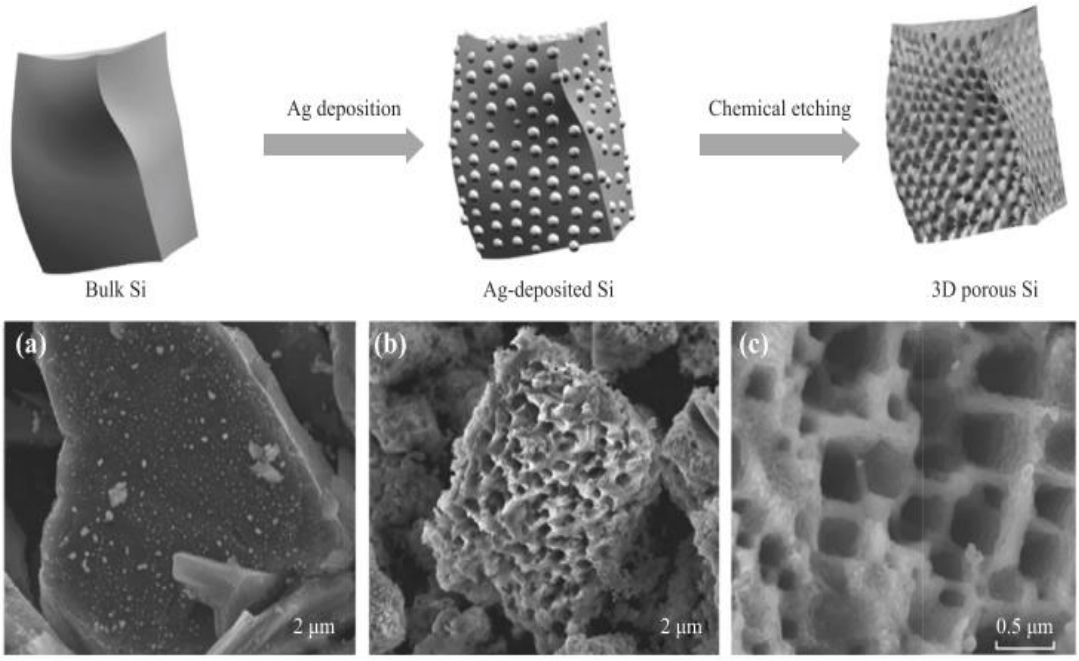

Figure 2-3 Schematic of 3DM bulk Si and the electrode under SEM observation[38].

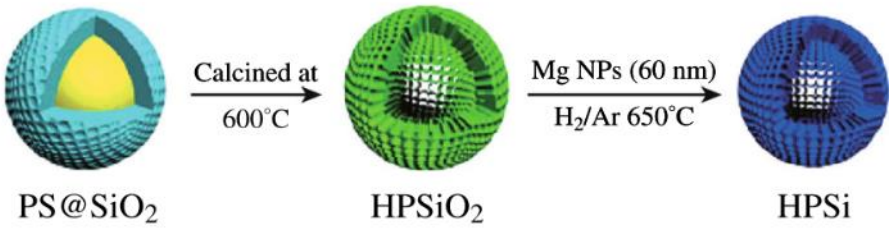

Figure 2-4 Schematic of fabricating hollow porous Si nanopowders[38].

- ***Surface coating***

Surface coating is another approach for Si electrode modification, and carbon-based materials are the most common candidates for the coating material. Liu *et al.* developed a pomegranate-inspired hierarchical structured Si anode (Figure 2-5)[41]. The Si particle was coated with SiO_2 and then encapsulated by a conductive carbon,

then when the SiO_2 was removed by HF solution, the external carbon layer would allow enough space for Si to expand. Also, the SEI outside the carbon layer would remain stable and not be ruptured during cycling. Results showed 97 % capacity retention after 1000 cycles, with a high coulombic efficiency (99.87 %) and volumetric capacity (1270 mAh/cm^3) (Figure 2-6).

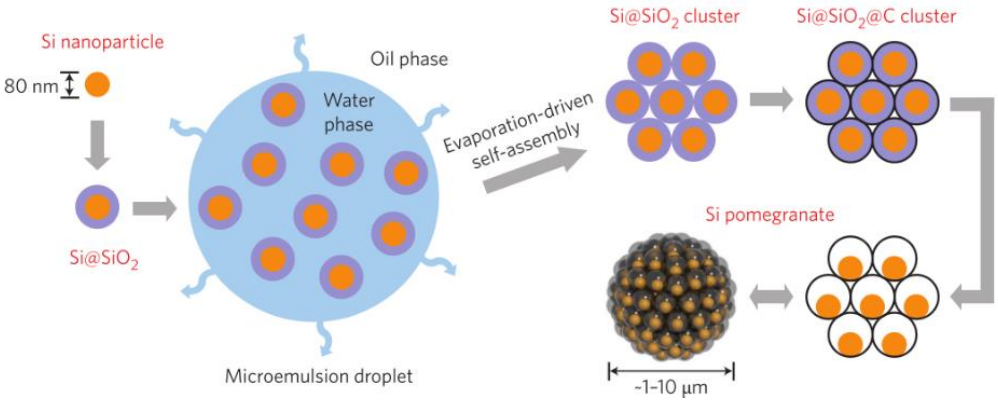

Figure 2-5 Schematic of the fabrication process for Si pomegranates[41].

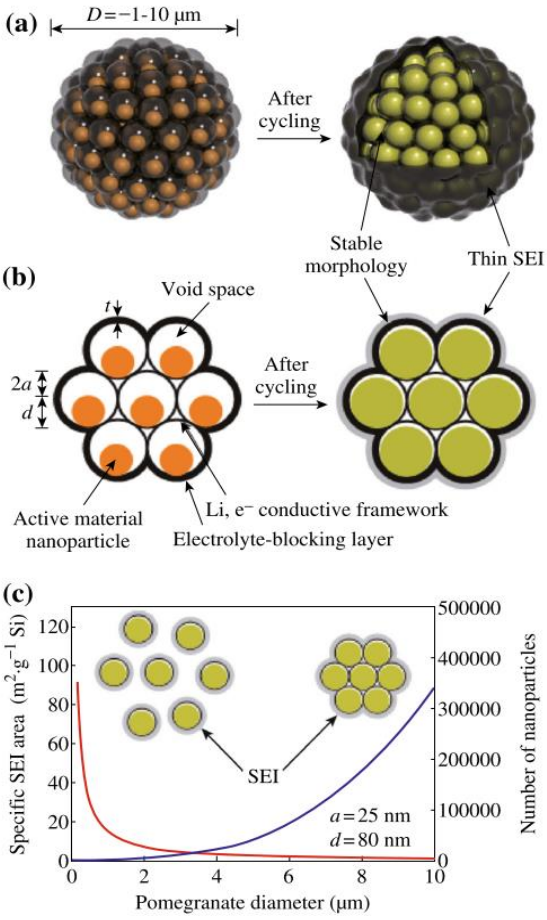

Figure 2-6 Schematic and performance for Carbon encapsulated Si structure[41].

Zhou *et al.* demonstrated a hybrid coated Si nanoparticle, which was wrapped between graphene and amorphous carbon layers (G-Si-C)[42]. They worked together to function as an efficient electrical bridge so that all Si particles were electrochemically active, and also the tensile properties of graphene could adapt to the expansion and contraction of Si. Their result of G-Si-C exhibited a high reversible capacity of 902 mAh/g for 100 cycles at 300 mA/g, by which point the capacity of the graphene-coated SiNPs dropped to below 500 mAh/g, while pure SiNPs dropped to 13 mAh/g after only 50 cycles.

Despite some good performance achieved, using the surface coating method to prepare the identified electrode remains complicated to be considered industrially relevant. Hence more simplified manufacturing methods still need to be investigated. On the other hand, this study indicates that the hybrid graphene/carbon coating could be an approach to improve the cyclability of Si particles. Therefore, for this project, studies of Si integration with graphene will be mainly focused on as drop-in technology using existing manufacturing methods.

2.1.2 Optimisation of Electrode Composition

Optimising electrode composition is another approach to enhance the performance of Si anodes, which includes developing a strong binder system, optimising the formulation of the electrode and conductive additive. Binders play an essential role towards enhancing the performance of Si despite their relatively small mass ratio. Improving the binder system serves to better deal with Si expansion and contraction. This will be discussed in more details in Section 2.2.

- ***Optimising the formulation of Si anodes***

Current studies on the formulation of Si electrodes can be mainly divided into two streams. One applies a small ratio of Si active mass (less than 40%), aiming to improve the capacity based on conventional graphite anode and obtain good capacity retention. Another is to study electrode with a large ratio of Si active mass (more than 60%), targeting for high capacity while balancing a reasonable life cycle.

Beattie *et al.* developed a geometric model to explain the excellent cyclability for electrodes with low Si content, suggesting that it could better accommodate the significant volume change during lithiation and delithiation process[43], as shown in

Figure 2-7. Their model predicted that to achieve a good cyclability, the largest Si loading is supposed to be 20 vol %, but their experiment data showed a higher Si content in an electrode (with 33 wt % Si 100 nm + 33 wt % CMC + 33 wt % carbon C65) could also cycle well with relatively high capacity (1200 mAh/g), as shown in Figure 2-8. This error between experimental and model data was considered to result from electrode porosity, which was not included in the model. However, it is difficult to conclude directly through these data sources to identify whether high Si content is practical or not. With different binders, conductive additives, or combined with other active materials, the best ratio for Si could be very different, and this needs to be demonstrated and verified experimentally.

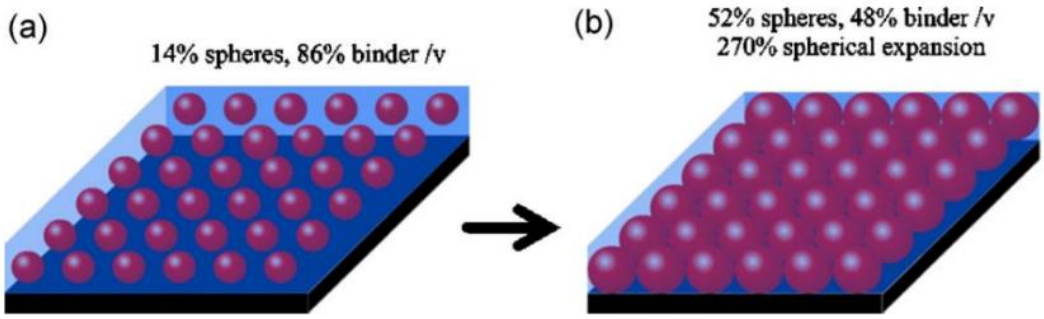

Figure 2-7 Si spheres surrounded by binder: (a) The Si spheres occupy 14 vol % of the electrode and the binder occupies 86 vol % of the electrode; (b) same electrode after 270% expansion of spheres.[43]

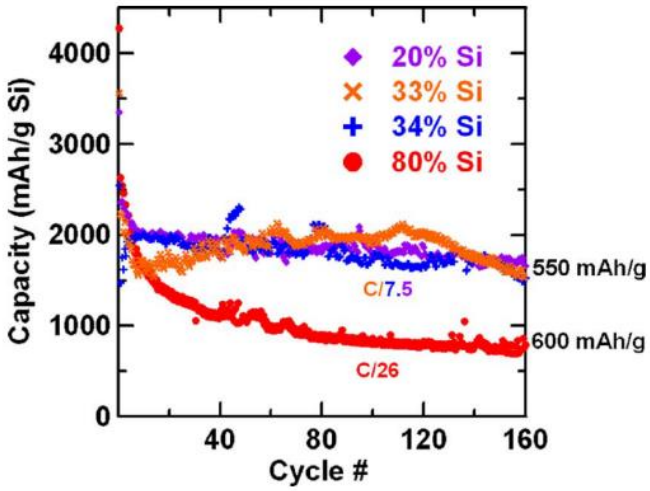

Figure 2-8 Capacity vs cycle number for electrodes made with 20, 33, 34, and 80 wt % Si[43].

A practical approach to optimise Si electrodes is to combine with other active material to form a matrix, which could improve conductivity as well as better buffer the volume

change. Carbon materials would be ideal candidates due to their excellent conductivity, small volume change, lightweight and good ionic conductivity[44]. Yang *et al.* first reported a hybrid Si/carbon/graphite composite electrode, and their results showed that the proper ratio for Si/carbon would result in an enhanced cyclability, and the introduction of graphite into Si/carbon electrodes demonstrated further improvement, as shown in Figure 2-9[45]. Several studies have investigated Si-graphite composite electrodes with improved and stable cyclability achieved, but most of them are focussed on a small ratio of Si incorporation[46]–[49]. Farooq *et al.* investigated the effect of different ratios between Si and graphite and with different binders (PVdF and polyacrylic acid (PAA)) on the anode's cyclability[47]. The Si to graphite ratio was varied from 0:70, 5:65, 10:60, 15:55 to 20:50 and the results are shown in Figure 2-10. It indicated the improvement in capacity for graphite-based electrodes is in proportion to the ratio of Si incorporated. The development of high-energy density Li-ion batteries is the primary objective of this project. Therefore a high content of Si (60 wt% -80 wt% mass ratio) will be considered in this study to ensure the high capacity of the cell.

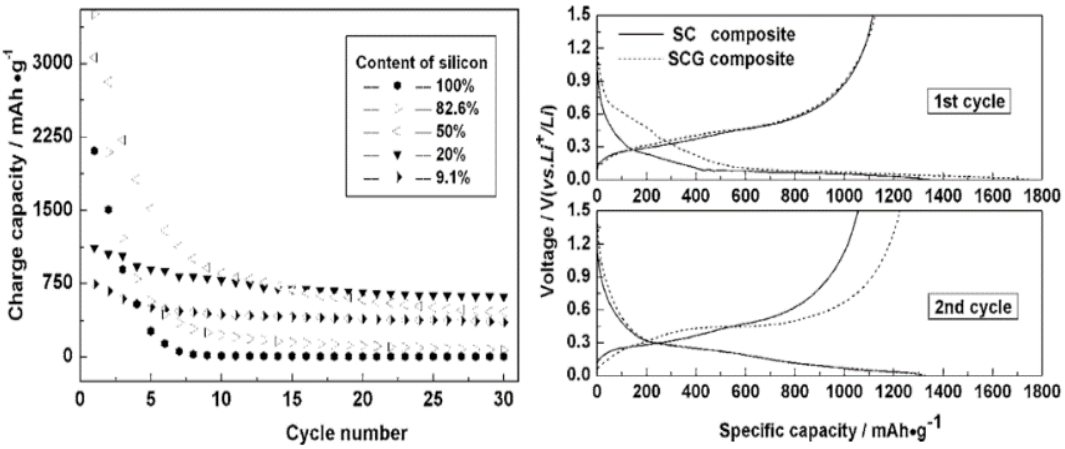

Figure 2-9 Electrochemical performance for (left) different ratio of Si content in Si/Carbon composite electrode and (right) comparison between Si/Carbon and Si/Carbon/Graphite for first two cycles[45].

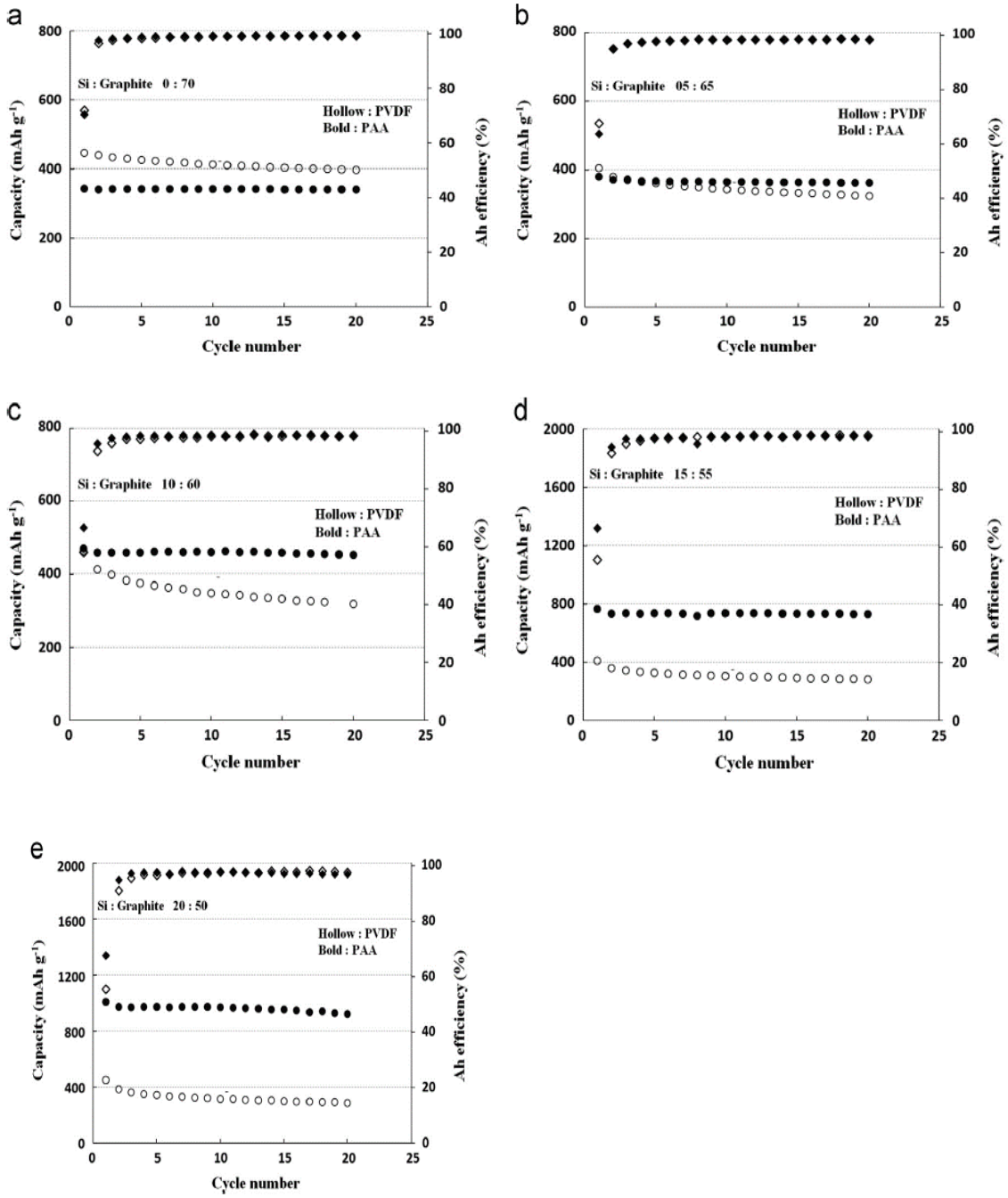

Figure 2-10 Cell performance of Si-Graphite composite electrode with PVDF and PAA electrode: (a) Si 0 wt%, Gr 70 wt%; (b) Si 5 wt%, Gr 65 wt%; (c) Si 10 wt%, Gr 60 wt%; (d) Si 15 wt%, Gr 55 wt%; (e) Si 20 wt%, Gr 50 wt%[47].

Recently, graphene has attracted wide attention, due to its excellent planar (X-Y) electronic conductivity and high surface area, and superior thermal and mechanical properties[50]. Also, multi-layered graphene has been proved for good flexibility due to the lack of rigid connections between adjacent nanosheets, which can be used as the "flexible confinement structure" to reduce pulverisation for electrodes[51]. All these characteristics of graphene make it a promising material to be incorporated into a Si

anode. Several pieces of research on hybrid Si/graphene-nanosheets (GNSs) electrodes have been conducted with promising results achieved[50], [52], [53]. However, most of these studies tried to synthesise Si and graphene through electrophoretic deposition (EPD) or CVD, which is difficult for large-scale production. Whilst for the Si/graphene hybrid electrodes that were demonstrated through merely physically blending, the electrochemical results in the literature are yet to show clear improvements[52], [54], which can be identified as a research gap for this study.

Other carbon materials such as carbon nanotubes and carbon nanofibers have also been applied as the combined active material within Si anodes[55], [56], and they all show different levels of improvement. Among them, carbon nanotubes demonstrated the best performance, in which the capacity of Si has been maintained around 1000 mAh/g for 100 cycles at a high charge/discharge rate of 10 C[55]. Since graphene has been reported for better mechanical property and electronic conductivity than carbon nanotubes (Table 2-1), it is supposed that the Si/graphene hybrid electrode should have even better cycling performance than the reported Si/nanotubes electrode.

Table 2-1 Comparison of properties between graphene and CNTs[57]

Properties	**Graphene**	**CNTs**
Fracture strength (GPa)	~124 (Modulus: ~1100 GPa)	45
Density (g cm^{-3})	>1	1.33
Thermal conductivity (Wm^{-1} K^{-1})	~5000	3000
Electronic conductivity (S cm^{-1})	10^6	5000
Charge mobility (cm^2 V^{-1} s^{-1})	200,000	100,000
Specific surface area (m^2g^{-1})	2630	400

In addition to carbon, other materials have also been studied to be incorporated into Si anodes, aiming to achieve better cycling performance. Tin (Sn) is a popular candidate, as Sn/SnO_2 electrodes have shown a much more stable cycling performance than Si[58]. Ahn *et al.* synthesized the Sn-Si electrodes with three different ratio (Sn: Si = 2:1; Sn: Si = 1:1; Sn: Si = 1:3), while Si-only electrodes were used as the controlled sample[59]. Their result indicated that the incorporation of tin could effectively delay

the electrode degradation but compromise the electrode capacity, whilst smaller amounts of Sn could help to maintain the capacity and cyclability as well as to improve the overall conductivity of the electrode, as shown in Figure 2-11.

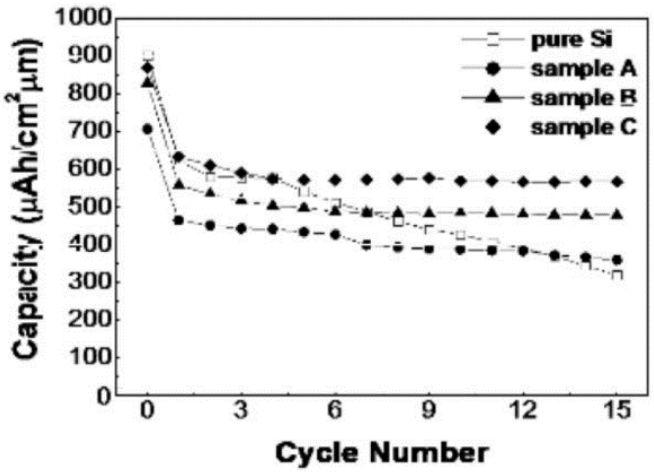

Figure 2-11 The cycle number dependence of the capacities of Li/Sn–Si cells fabricated with the three different Sn–Si nanocomposite electrodes (Sample A, Sn: Si = 2:1; Sample B, Sn: Si = 1:1; Sample C, Sn: Si = 1:3)[59].

Another promising candidate to combine with Si anode is $Li_4Ti_5O_{12}$ (LTO). LTO has been reported with a specific capacity of 175 mAh/g if the cell discharged to 1V[60]. The negligible volume change, an SEI free potential (~1.55V vs Li/Li^+), ultra-fast charging rate and a high thermal stability, make LTO a promising electrode to meet high power and abuse tolerance requirements for electric vehicles[61]–[63]. Also, these characteristics of LTO appear to be the complementary to Si anodes concerning to improve the SEI stability and rate capacity. However, with the operation condition of Si electrodes, the hybrid Si/LTO electrodes would be charged to lower voltage to achieve higher capacity; hence there would likely be SEI formed on LTO as well. Chen *et al.*[64] studied the hybrid LTO/Si electrodes with different ratios and various current density, and the result (Figure 2-12) stated that the hybrid LTO/Si electrodes could get benefit from both the high capacity contributed by Si and the excellent cycling performance contributed by LTO. However, it compromised the energy density for Si-LTO hybrids compared to the pure Si electrodes and rate capacity for Si-LTO was not ideally improved. It indicates that without proper conductive additives, Si electrodes could not cope with high-rate charging incorporation of LTO.

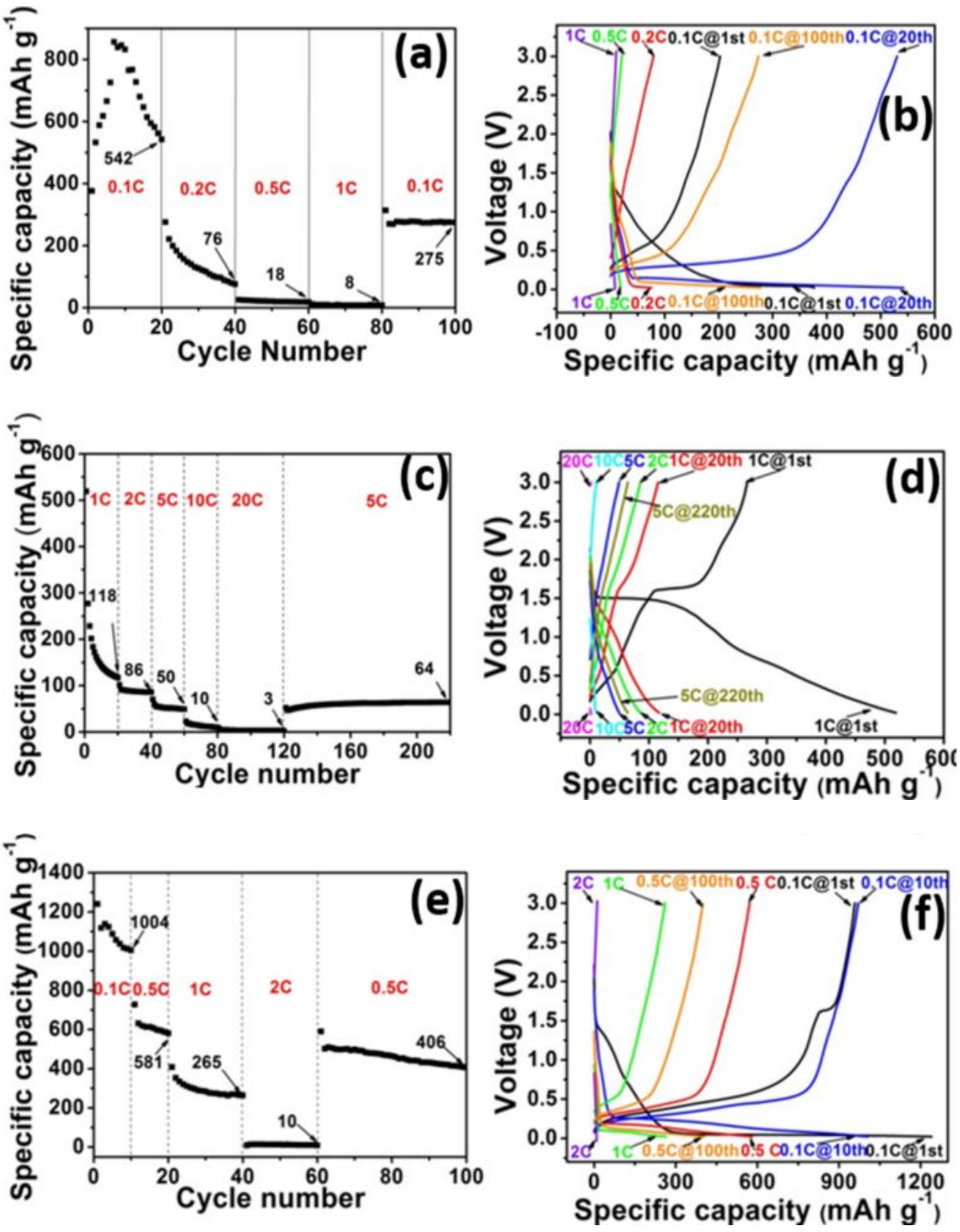
(a)
Specific capacity (mAh g-1)
Cycle Number
0.1C
0.2C
0.5C
1C
0.1C
542
76
18
8
275
(b)
Voltage (V)
Specific capacity (mAh g-1)
1C 0.5C 0.2C 0.1C@1st 0.1C@100th 0.1C@20th
1C 0.5C 0.2C 0.1C@100th 0.1C@1st 0.1C@20th
(c)
Specific capacity (mAh g-1)
Cycle number
1C 2C 5C 10C 20C 5C
118
86
50
10
3
64
(d)
Voltage (V)
Specific capacity (mAh g-1)
20C 10C 5C 2C 1C@20th 1C@1st
5C@220th
5C@220th
20C 10C 5C 2C 1C@20th
1C@1st
(e)
Specific capacity (mAh g-1)
Cycle number
0.1C 0.5C 1C 2C 0.5C
1004
581
265
10
406
(f)
Voltage (V)
Specific capacity (mAh g-1)
2C 1C 0.5C@100th 0.5 C 0.1C@1st 0.1C@10th
2C 1C 0.5C@100th 0.5 C 0.1C@10th 0.1C@1st

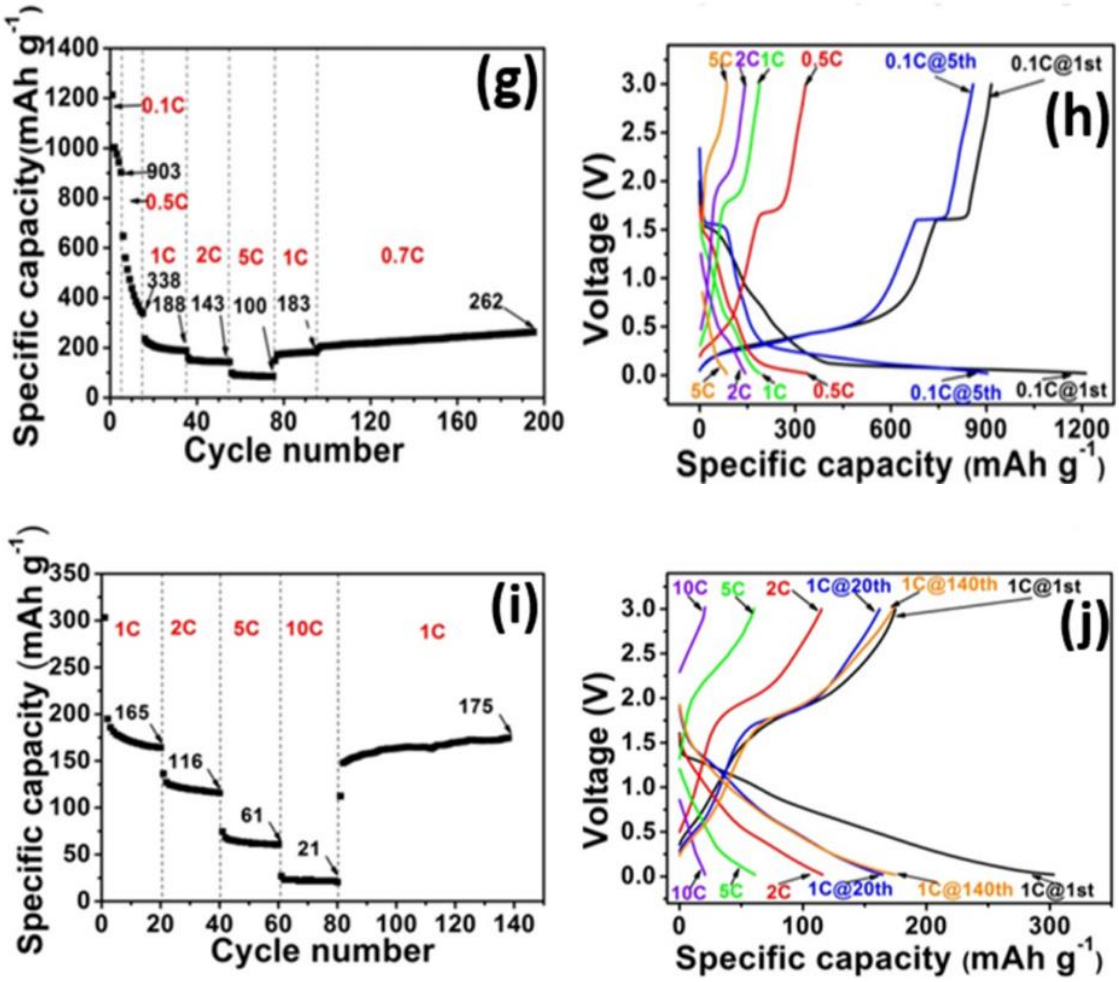

Figure 2-12 The rate performance and corresponding charge-discharge curves for electrodes based on (a,b) pure-Si, (c,d) pure-LTO, (e,f) LTO:Si = 35:35, (g,h) LTO:Si = 50:20 and (i,j) LTO:Si = 65:5[64].

- ***Conductive additives***

Si, as a semiconductor, is well known for its low electronic conductivity, which in theory is 6.7 x 10^{-4} S/cm. Therefore, conductivity-boosting additives are essential to enhance the overall electronic conductivity of Si-based anodes[65]. Normally carbon materials are used as conductive additives due to their high electronic conductivity, environmentally benign properties[66], and the capability of capacity contribution. They can be incorporated into Si-based anodes through two different methods: (1) coating of high conductive phase onto Si particles, which has been discussed in Section 2.2.1; (2) physically blending conductive additives into electrodes to form a conductive network around active materials[65]. The second method is a more accessible and cheaper approach to exploit but has a high requirement for sufficient mixing and dispersion techniques as nano-sized carbon materials are generally difficult to disperse.

Common carbon materials to be used as conductive additive in Li-ion batteries and their electrical properties have been summarised in Table 2-2. Carbon black and graphite are the most common conductive additives due to their low price, high electronic conductivity and commercial availability[66]. Both have been studied with Si anodes and the improvement of cycling performance has been achieved[65], [67], [68]. When comparing carbon black and graphite, carbon black has a higher specific surface area (45 m^2/g for C45 and 65 m^2/g for C65, compared to 17 m^2/g for graphite SFG6) due to its spherical shape and smaller particle size, which can contribute to the enhancement of rate capability and resistance for fracture. It has been proven by Rezqita *et al.* that carbon black (Super C65) had better performance than conductive graphite within Si/mesoporous carbon electrode[65]. However, a major concern here is that a larger surface area is more likely to cause a high irreversible capacity loss at the first cycle due to a large amount of SEI formation.

Table 2-2 Common carbon conductive additive and their electrical property[57], [69], [70]

Properties	Graphite	Carbon black	Graphene	CNTs
Density ($g\ cm^{-3}$)	2.24~2.27	1.10~2.005	>1	1.33
Electronic conductivity ($S\ cm^{-1}$)	$2.6*10^4$	$1.25 * 10^5$ ~$2*10^5$	10^6	5000
Charge mobility ($cm^2\ V^{-1}\ s^{-1}$)	15,000	-	200,000	100,000
Specific surface area (m^2g^{-1})	5-27	45~250	2630	400

Hierarchical carbon combinations have also been studied as conductive additives within Si electrodes. Lestriez *et al.* reported a hierarchical and resilient conductive network combing multiwall carbon nanotubes (MWCNTs) and vapour-grown carbon nanofiber (VGCFs) in Si anodes[71]. Their findings showed that the electrode with this complex conductive network had better performance than the electrode with the

single conductive additive (Figure 2-13). Therefore, with this kind of hierarchical system, both long and short range of conductivity can be covered, thus to provide an efficient electronic transport within the composite electrode. Also, the electrode's so-called "wiring" structure is supposed to better tolerant the volume change due to the tensile benefits of a fibrous structure.

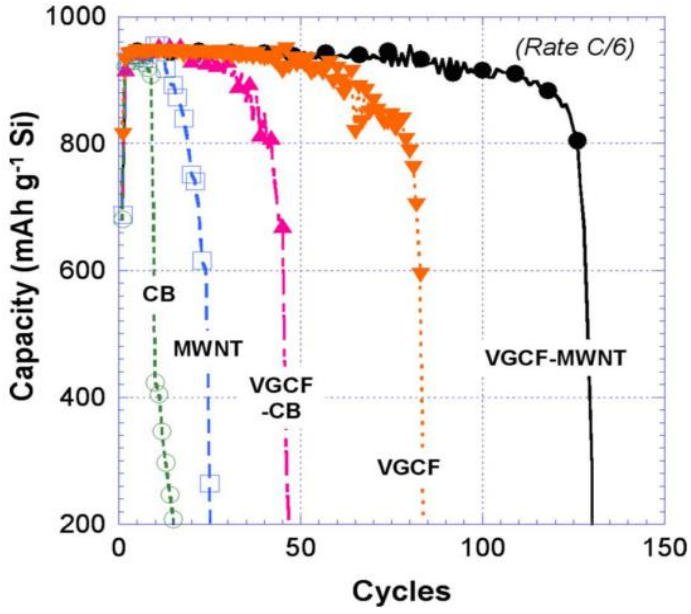

Figure 2-13 Charge capacity vs cycle number for electrodes made with VGCF-MWCNT, VGCF, VGCF-CB MWCNT, CB. The rate is C/6.[71]

Regarding the recommended amount of carbon conductive additive in electrode, Spahr *et al*. has conducted research into the relationship between the electronic resistivity of electrode and the volume fraction of carbon conductive additive. As shown in Figure 2-14, it indicates that there is a sharp rise in electrode conductivity when the volume percentage of carbon conductive additive is increasing within certain range. Beyond this range, there is no significant increasing of the electrode conductivity. From which point, other factors like surface area, dispersion difficulty with active material, absorption effect of binder, and electrode mechanical property should be taken into consideration.

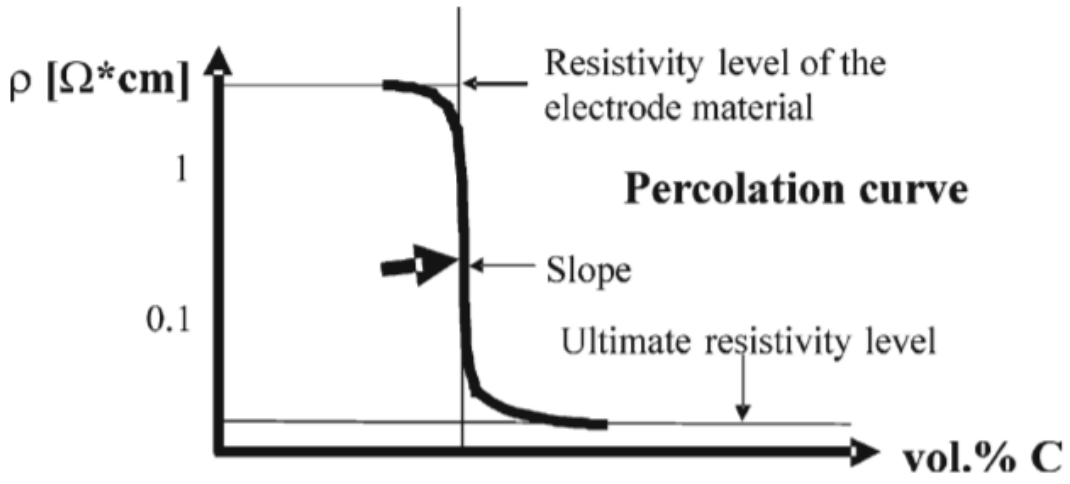

Figure 2-14 The effect of a conductive additive at various carbon concentrations on the electronic resistivity of an electrode. [70]

2.2 Development on Binder Systems to Enhance the Cyclability of Si Electrodes

The binder is an essential component in electrode materials, despite it only occupy 2-5% of the mass in a typical commercialised electrode of Li-ion batteries[72]. It helps to maintain electrical contact between active materials and the current collector, facilitating the connection between active materials and conductive additives in X, Y and Z direction. In other words, it maintains the adhesion and cohesion of the electrode coating. Otherwise, the onset of capacity fade would occur once the contact with the current collector or the connection with the conductive additive breaks down. Therefore, to a large extent, the binder can indeed affect the life cycle of cells by improving the composite stability. This is especially critical for Si electrodes, given the severe problems of large volume change during the alloying/de-alloying reaction that would result in the pulverisation of the electrode and thus the gradual failure of the cell.

Typically, a suitable binder suitable for Si-based anode should include following characteristics[20]:

i. To build effective connections between Si particles as well as with conductive additives, and maintain good adhesion to current collectors during cycling. It requires a good flexibility and adhesion force to adapt to the volume expansion.

This condition could be better achieved if the chemical bond between polymer chain and the surface of Si is a covalent bond or stronger chemical interactions.

ii. To form a Li-ion conductive conformal layer at the surface of Si particles, which could work as an artificial SEI (e.g. binders which contain a higher concentration of –COOH can better exchange H^+ with Li^+ to promote Li^+ hopping, thus result in a more stable conformal layer).

iii. To help maintain the electronic conductivity.

iv. To keep good electrochemical stability over a wide potential range and insoluble into electrolyte solution[73].

This section will review some common binders that could be considered for Si-based electrodes and possibilities for further improvement on the binder system will be discussed.

2.2.1 Polyvinylidene Fluoride

Polyvinylidene fluoride (PVdF), whose functional group is $–(CH_2\text{-}CF_2)_n\text{-}$, has been the conventional binder widely used in Li-ion cells for either anode or cathode because it has excellent electrochemical stability and possesses a high binding strength between the active material and the current collector. Additionally, the amorphous region in PVdF is a good matrix for Li-ions to pass through, which could effectively ensure excellent conductivity and enhances the overall cell performance[73]. However, for Si materials, PVdF binder does not chemically interact with the active material, because the contact between PVdF and Si particles is achieved by weak Van der Waals forces (between its fluorine atoms and hydrogen atoms on Si-OH), which would result in losing contact upon volume expansion[74]. Even for electrodes with a small amount of Si, those electrodes incorporating PVdF demonstrate worse cycling performance than the ones with PAA binder, and the difference becomes more significant with increasing the ratio of Si[47].

In recent years, some studies have been conducted on improving the elasticity of the PVdF binder for Si anodes. Li *et al.* [75] reported that with heat-treatment at 300^{o}C, the performance of the PVdF binder could be effectively improved for Si electrodes. In his report, a capacity of 600 mAh/g could be retained after 50 cycles, and according to SEM observation and adhesion test, the carbon black was better distributed on the surface of Si particles[75]. However, this kind of result is still not ideal for Si

electrodes as the capacity of 600 mAh/g is too low for Si and 50 cycles is too short to indicate a good capacity retention, but to some extent, it suggested that the heat treatment could be an effective method to enhance the performance of binder.

Additionally, as a non-aqueous binder, PVdF has a requirement to be solved in *N*-Methyl-2-pyrrolidone (NMP), which is a toxic and expensive organic solvent. Hence more researchers and industries have turned to more environmentally friendly and aqueous-based binders such as CMC or PAA for the replacement of PVdF.

2.2.2 Polyacrylic Acid

Polyacrylic acid (PAA), similar to other members of the polyvinyl acids family, is a type of aqueous based polymer. PAA possesses a high concentration of functional groups (especially carboxyl groups) which can effectively control the space with other monomers via copolymerization[76].

Magasinski *et al.*[76] firstly studied the performance of PAA for SiNPs and compared with PVdF and CMC. Their result showed that a high capacity (3300~3700 mAh/g) was achieved for both PAA and CMC, while PVdF showed much lower capacity (~2000 mAh/g). Also, PAA demonstrated 94 % capacity retention after 20 cycles, whereby CMC and PVdF only achieved 42 % and 13 % capacity retention, respectively[76]. Additionally, with VC electrolyte additives, the cells with PAA binder could still achieve 2400 mAh/g after 100 cycles, even at a high charge rate (C/2) and 100% Depth of Discharge[76]. This result showed the best performance for Si anodes with PAA binder despite only 40 wt% active Si.

Farooq *et al.*[47] studied the performance of Si/graphite electrodes with PAA binder at different ratios (ranging from 0% to 20%) and made comparisons with a control electrode containing PVdF. The result revealed that a composite electrode fabricated with PAA binder using a maximum content of Si powder (20 wt%) showed high specific capacity around 1000 mAh/g with 94% capacity retention after 20 cycles. With PVdF the capacity was only around 447 mAh/g, and the capacity retention was only 66 %, as shown in Figure 2-10. This study indicated that with higher Si active ratio, the electrode with PAA binder demonstrated much better performance than that with PVdF, which proved that PAA is a better option for Si-based anodes.

Their studies are all based on un-neutralised PAA with a low pH, while partially neutralised PAA may produce an even better result in Si anode since the un-neutralised PAA would suppress the electrolytic dissociation. In this case, the carboxyl groups in PAA are prone to aggregate through their hydrogen bonds (Fig 2-15). Once the neutralised hydrolysis of the alkali salts PAA-Na is induced in aqueous solutions, the polyacrylate chain will be stretched due to the electrostatic repulsion between neighbouring dissociated carboxyl groups (Fig 2-15)[61]. Also, the neutralised PAA exhibits a higher viscosity because the stretched polyacrylate chain increases the flowage resistance of the solution[61].

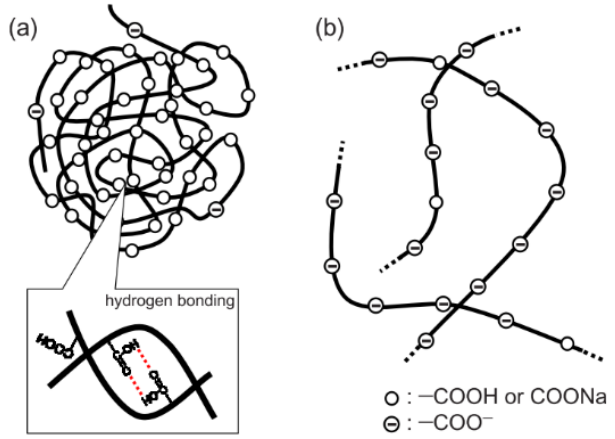

Figure 2-15 Schematic illustration of polymer chain conformation of (a) PAAH and (b) sodium polyacrylate dissolved in water[77].

Han *et al.* studied the effect of neutralisation degree of PAA on the performance of Si/graphite composite electrodes[78]. Their result showed that 80% of the neutralised PAA had the best electrochemical performance with the Si-graphite electrodes compared with 60% neutralised, full neutralised and un-neutralized PAA. They also indicated that the slurry with a partially neutralised polyacrylate has a unique rheological property, which could assist to form a moderate porous structure during the drying process[78].

With the premier cyclability with Si electrodes and various reports in the literature, PAA based binders are a good starting point for conducting further systematic studies of the effects of binder properties on the performance of Si anodes.

2.2.3 Bio-derived Polymers

Bio-derived polymers are materials that are extracted from renewable resources, so most of them are aqueous and environmentally benign. Recently, more and more attention is paid to bio-derived polymers to be used as the binder for Li-ion due to their abundant availability and ease for further functionised[79]. The requirement for bio-polymers that to be applied as the binder in Li-ion batteries, especially for Si-based electrodes, is the involvement of plenty carboxyl groups so that they can form an effective covalent bond with the –OH group on the surface of Si particles[80]. The most typical bio-polymers that have been investigated for Li-ion batteries include carboxymethyl cellulose[81], [82], chitosan[83], and alginate-based systems[80], [84], [85].

- ***Carboxymethyl cellulose***

Carboxymethyl cellulose (CMC), whose molecular structure is shown in Figure 2-16, is a linear polymeric derivative of cellulose with varying levels of carboxymethyl substitution. The carboxymethyl groups are combined with carboxylate anionic functional groups, which are responsible for the aqueous solubility of CMC[81].

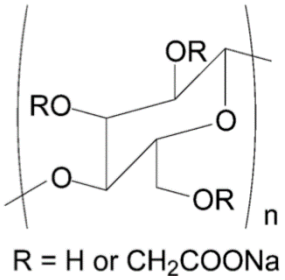

Figure 2-16 The molecular structure of CMC[72].

CMC was firstly reported by Lee *et al.*[86] to be used as a binder for graphite and showed improved cycling performance with Si with more than 90% of the initial capacity retained after 200 cycles, due to the enhanced adhesion strength within electrodes. Following this, Liu *et al.* demonstrated that if CMC is combined with elastomeric styrene butadiene rubber (SBR) (1:1) it can be used as the binder for C/Si anode. This is because CMC is a brittle polymer and SBR could contribute tensile strength[87]. Significant improvement was observed in electrode cycling performance, which achieved a capacity of 1000 mAh/g and cycled stably for 50

cycles. Furthermore, Buqa[82] made the comparison between the combined binder SBR/Na-CMC (1:1) and PVdF and declared that nano-Si electrodes containing 1 % SBR and 1 % Na-CMC had the same cycle stability with the identical electrodes that included 10% PVdF binders. It means that SBR/Na-CMC is 10 times more efficient than PVdF. However, while comparing the behaviour between the combined binder of SBR/Na-CMC and pure Na-CMC binder on the performance of Si/C electrodes, the pure Na-CMC, which was more brittle, exhibited better capacity retention[88]. The reason could be SBR is too electronically resistive, which would compromise the cell conductivity, hence the ratio of CMC to SBR should be further investigated in Si electrodes.

- ***Chitosan***

Chitosan is one of the most abundant naturally abundant polymers, which is the de-acetylated extract from of chitin[89]. This is a polysaccharide composed mainly of β-(1,4)-linked 2-deoxy-2-amino-d-glucopyranose units[90], which molecular structure is shown in Figure 2-17.

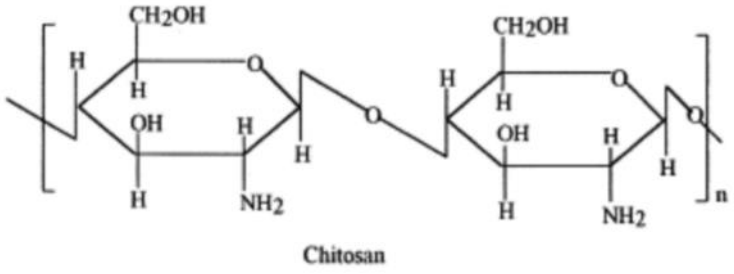

Figure 2-17 Molecular structure of chitosan[89].

Chitosan-based aqueous polymers possess proper viscosity and can be considered as an effective binder. Chai *et al.* conducted a comparison study between chitosan and PVdF, to investigate their behaviours on the graphite anode[90]. The result showed that with chitosan-based binders, the initial loss, rate capability and cycling behaviour were considerably improved compared with PVdF. Yue *et al.* first applied carboxymethyl chitosan as a binder for Si-based electrodes. The results showed that the Si/C-chitosan anode (Si : carbon black : C-chitosan = 62:30:8 in weight ratio) exhibited a high first discharge capacity (4270 mAh/g) with a first coulombic efficiency of 89%, maintaining a capacity of 950 mAh/g at the current density of 500 mA/g over 50 cycles[83]. Tang *et al.*[91] studied chitosan oligosaccharides, which are

the hydrolysed product of chitosan (poly-beta-(1,4)-2-amino-2-deoxy-glucopyranose), to use as the alternative binder to PVdF for $Li_2ZnTi_3O_8$ electrodes. The result demonstrated improved performance in terms of the initial coulombic efficiency, cycling behaviour, rate capability and long life cycle.

- ***Alginate***

Alginate, whose molecular structure is shown in Figure 2-18, is a linear polysaccharide which is synthesised by brown seaweed and by soil bacteria. Sodium alginate is the most commonly used alginate form in the industry since it is the first by-product of algal purification[79]. Recently, alginate has come into view to be used as an aqueous binder for Li-ion batteries as it possesses properties including high viscosity and good electrochemical stability[92].

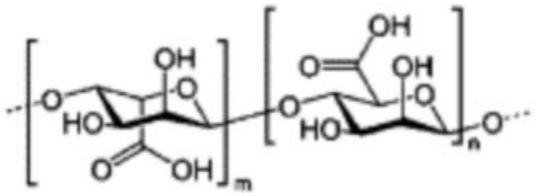

Figure 2-18 Molecular structure of alginate[92].

Kovalenko *et al.* first reported the electrodes containing SiNPs and alginate that extracted from brown algae[80]. Their result illustrated a stable reversible capacity around 1700-2000 mAh/g for 100 cycles, which was better than the Si electrodes with PVdF and CMC binders. With a similar microstructure of the alginate to CMC's, the considerable difference in their performance within Si electrodes could be explained by the small structural differences in their polymer chains. In alginate, carboxylic groups are naturally presented and evenly distributed in the polymer chain, whereas in CMC they are synthetically induced, and their distribution is random (where some monomeric units may have more than one carboxylic group and the others have none.) The higher concentration and a more uniform distribution of the carboxylic groups along the chain in alginate could be responsible for the better transport of Li ions within Si particles. Also, more uniform coverage, and more efficient assistance in the formation of a stable SEI layer on the Si surface[80].

2.2.4 Binary Crosslinked Polymers

Cross-linking of polymers are generated by linking the polymer chains in three dimensions, which can produce a strongly interconnected network[93]. Due to their superior mechanical properties, crosslinked polymers are very promising to be incorporated into Si-based electrodes as a multifunctional binder to enhance the interaction with Si and other components. Since PAA has proven to be able to maintain a relatively stable cyclability for Si electrodes, due to its abundant carboxyl groups, existing studies of crosslinked polymers in Si anodes are mostly focused on interacting PAA with another polymer. Those with rich hydroxyl groups such as polyvinyl alcohol (PVA)[94], CMC[93], dopamine hydrochloride[95] and ring-slide polyrotaxane[96] have been studied.

- ***PAA-PVA***

It will be of major benefit for Si anodes to take advantage of both good adhesion from PAA and good flexibility from PVA. It is known that PAA is rich in carboxyl groups, while PVA contains hydroxyl group[97], hence the esterification reaction can take place between them. In the meantime, the carboxyl group from PAA can also react with the hydroxyl groups from native SiO_2 on the surface of Si. This will result in strong covalent bonds between Si particles and the polymer network (Figure 2-19)[94].

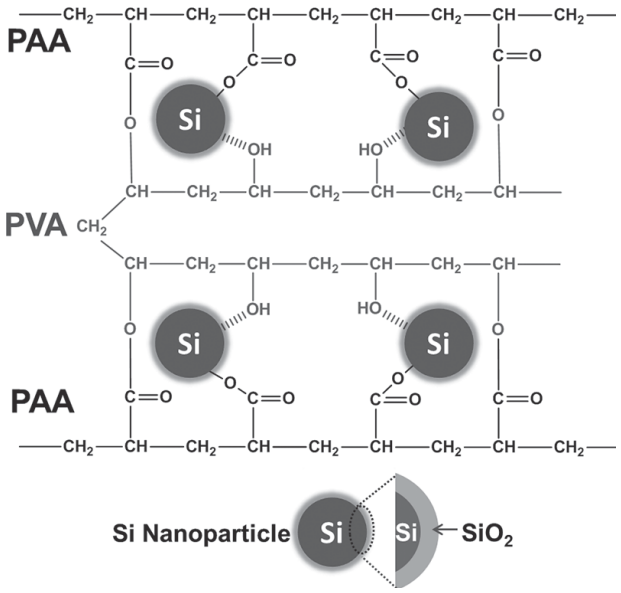

Figure 2-19 The illustrative interaction between PAA-PVA and Si particles[94].

Song *et al.* first investigated the effect of the binary crosslinked polymer PAA-PVA in Si-based anodes which included 60 wt% Si nanoparticles, 20 wt% carbon black and 20 wt% PAA-PVA (the weight ratio of PAA to PVA is 9:1) [94]. Their results showed that cells with PAA-PVA achieved a high specific capacity (2283 mAh/g) maintained after 100 cycles, much improved compared to CMC in their experiments. However, their ratio of PAA to PVA can be optimised as the ratio of PVA was too small. The result for PAA-PVA was also similar to that achieved by pure PAA in other literature[76], so the advantage of the crosslinked binder has not been completely demonstrated nor elucidated to date.

Additionally, the interaction strength between PAA and PVA can be further improved. Kumeta *et al.* investigated the cross-link conditions in PAA-PVA systems, including the time and temperature for heat-treatment as well as the partial neutralisation effect[98]. They specifically suggested that partially neutralisation of PAA (5-10%) could facilitate the formation of a stronger interconnection between different functional groups.

- ***PAA-CMC***

Similar to PVA, CMC also contains plenty of free hydroxyl groups. Therefore the covalent ester bond could also be formed while crosslinking PAA with CMC. Koo *et al.* first reported the crosslinked binder PAA-CMC and applied it to Si electrodes[93]. They effectively built the interpenetrating interaction through a condensation reaction between PAA and CMC at 150°C under vacuum (Figure 2-20a and b). Also, a covalent ester bond is also formed between the free carboxylic groups of PAA and the hydroxyl groups of the SiO_2 layer on the Si surface (Figure 2-20 c)[93]. Their results (Figure 2-21) indicated an obvious improvement of cycling performance for the cells with PAA-CMC binder when compared to those involving only PAA, CMC or PVdF. The capacity was maintained at above 2200 mAh/g after 100 cycles, and a high coulombic efficiency of over 99.5% was achieved.

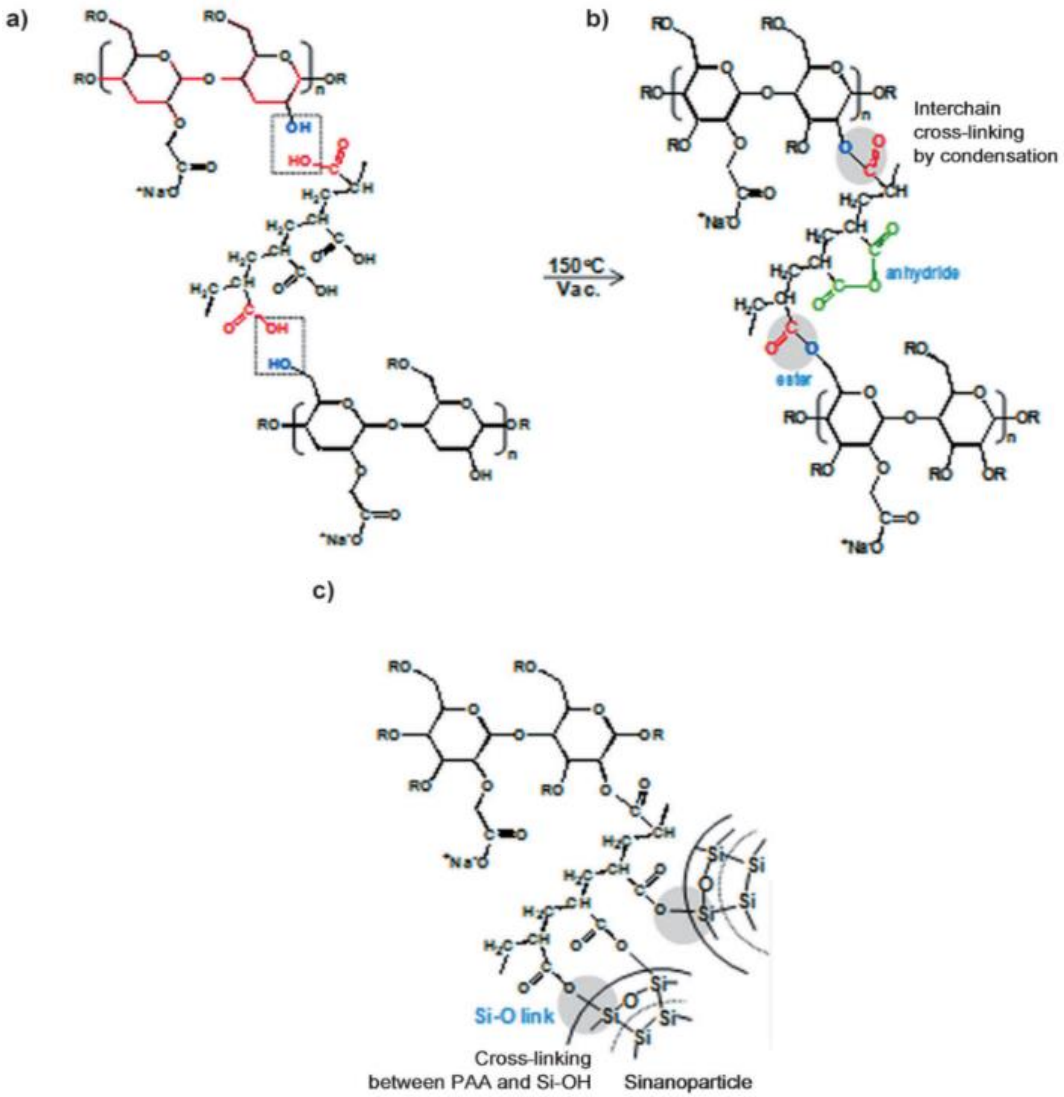

Figure 2-20 The illustrative interaction between PAA-PVA and Si particles[93].

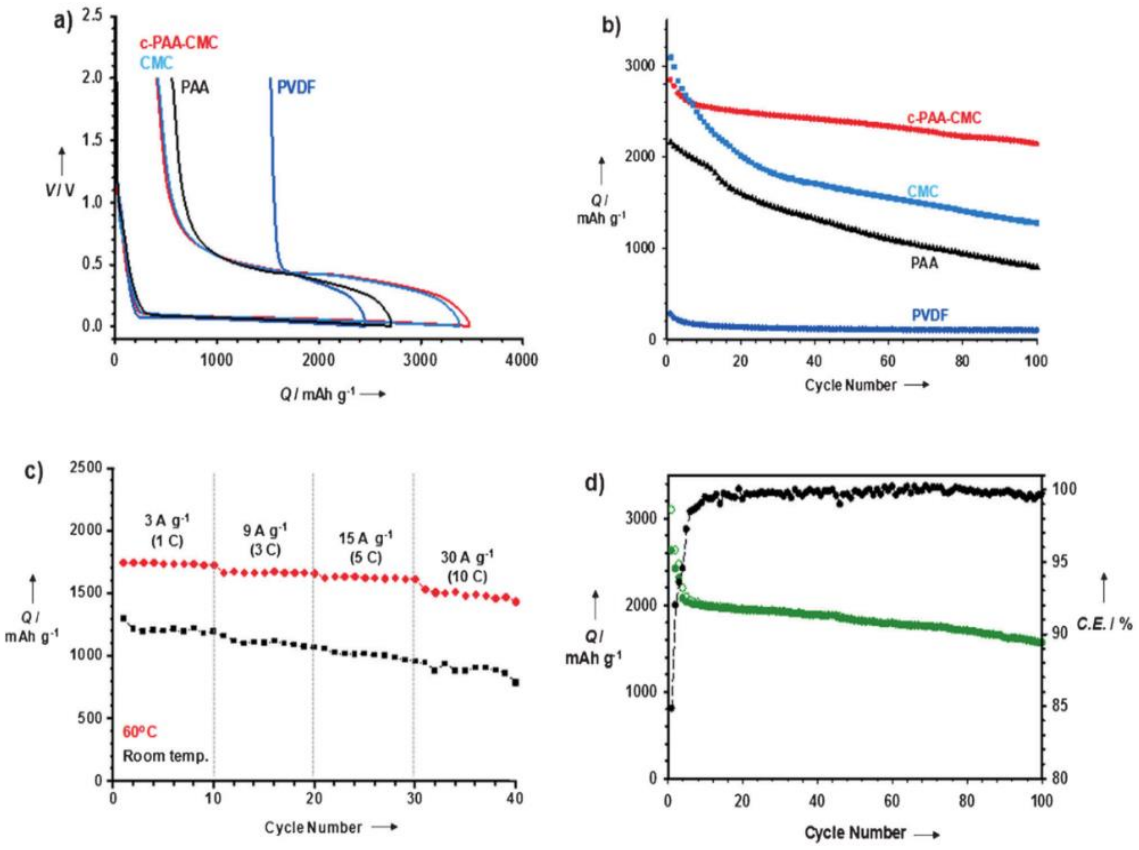

Figure 2-21 a) Initial charge–discharge profiles of Si composite electrodes between 0.005 and 2.0 V versus Li/Li$^+$. b) Specific capacity *vs* cycle number for the Si composite electrodes at a current density of 300 mA/g . c) Lithium extraction capacity of Si anodes with c-PAA-CMC for various high current densities at room temperature and 60°C. d) Specific capacity retention (green circle) of Si composite anodes with c-PAA-CMC binder (electrode density=0.4 g cm^{-3}) *vs* cycle number at a current density of 1500 mA/g (corresponding to 0.5C).[93]

- ***PAA- dopamine hydrochloride***

Inspired by mussels, Ryou *et al.* introduced a new binder system that conjugated PAA with the catechol groups (PAA-C) from dopamine hydrochloride, which interacted through the covalent bond between carboxylic from PAA and hydroxyl group from the catechol moieties (Figure 2-22)[95]. In this conjugated binder system, PAA served as the backbone while catechol moieties from dopamine worked as the "tentacles", with strong wetness-resistant adhesion. They also synthesised alginate with dopamine (alginate-C) in the same way. Their results demonstrated that SiNPs electrodes with both PAA-C and alginate-C binders achieved higher reversible capacity and better cyclability compared with those with pure PAA and pure alginate, respectively. The improvement was more significant for SiNPs electrodes with the alginate-based binder.

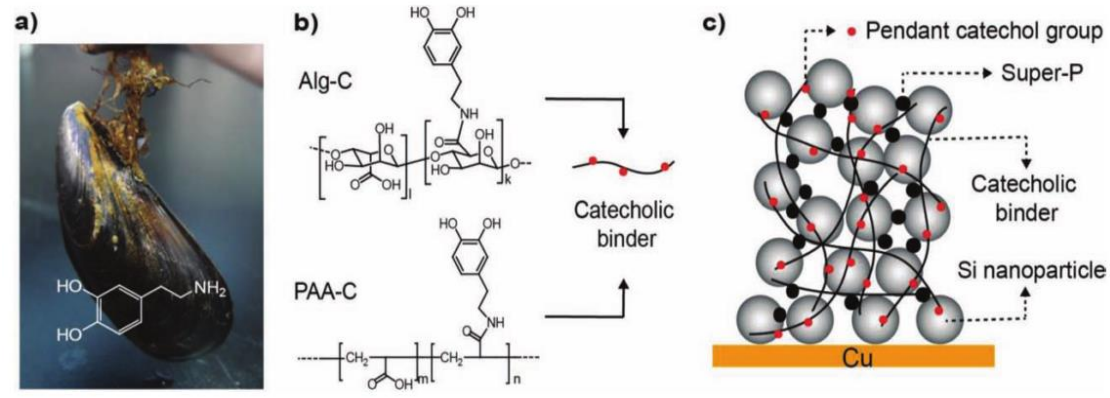

Figure 2-22 Schematic of catechol conjugated polymer binders and Si anode structure

- ***PAA- polyrotaxane***

Choi *et al.* incorporated 5 wt% ring-slide polyrotaxane (PR) with PAA and applied it to Si micro-powder electrodes (SiMPs), connecting parts of PR rings with PAA chains through covalent bonds[96]. Compared with pure PAA binder, PAA-PR exhibited extraordinary elasticity in the network due to the ring sliding motion of polyrotaxane. It dissipated the stress during the volume expansion of Si, similar to the mechanism of a series of moving pulleys lifting an object (Figure 2-23). This could help to retain the homogenous and integration of the whole structure during cycling. Their results were in high agreement with the hypothesis that Si-PAA/PR electrodes showed a high reversible capacity of 2.43 mAh/cm^2 (Si loading: 1.07 mg/cm^2) over 150 cycles while Si-PAA achieved less capacity and started to fail after around 50 cycles. Moreover, proved by post-mortem cross-section SEM images, the Si-PAA/PR electrodes demonstrated less particle disintegration which resulted in a less amount of SEI layers.

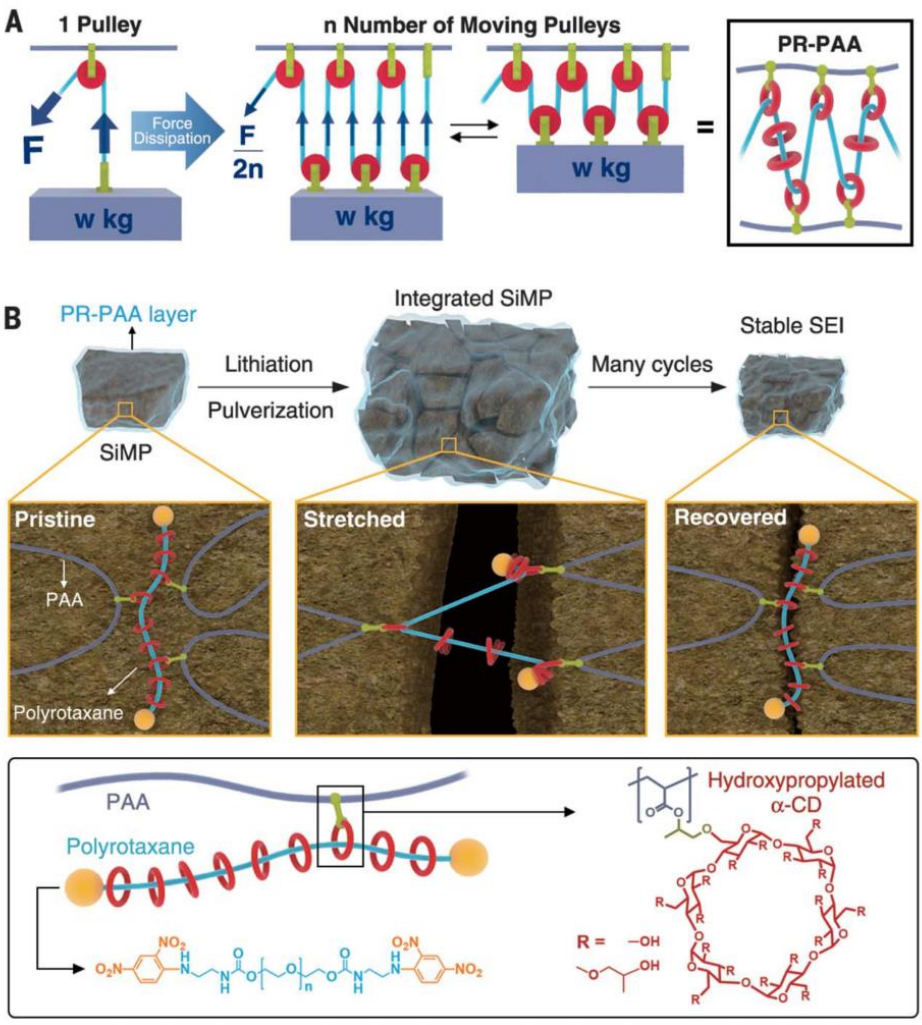

Figure 2-23 Illustration of schematic for PAA-PR for SiMPs electrodes[96]

2.2.5 Conductive Polymers

As most polymers are not electronicly conductive and whilst they usually account for 10-20 wt% in Si-based electrodes, using conductive polymers is considered to be an effective approach to enhance conductivity, as well as maintain good adhesion in the network. Liu *et al*. reported a novel polyfluorene based polymer poly (9,9-dioctylfluorene-co-Suorenone-co- methylbenzoic acid)[99]. They introduced carbonyl functional groups (C=O) for tailoring the lowest unoccupied molecular orbital (LUMO) electronic states, which resulted in improved conductivity. They also used methylbenzoic ester -PhCOOCH$_3$ to provide strong covalent bonds to enhance the polymer adhesion. The schematic of the structure of this polymer is shown in Figure 2-24. This new conductive binder was applied to SiNPs electrodes and achieved 2100 mAh/g for 650 cycles, which was the best performance for Si electrodes without

the conductive additive. However, the toxic nature of the binder is still the main drawback here[72].

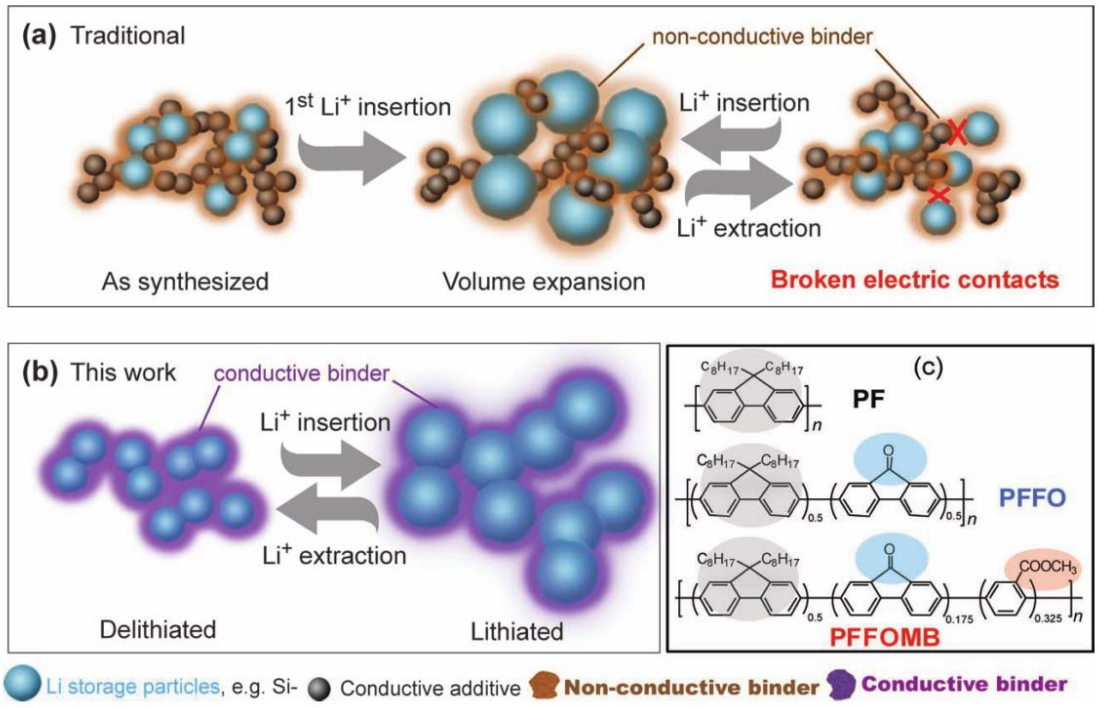

Figure 2-24 Schematic of PF-type conductive polymers (a) Traditional approaches use acetylene black as the conductive additive and PVDF binder. (b) Conductive polymer with dual functionality (c) The molecular structure of the PF-type conductive polymers[99].

Inspired by this study, Wu *et al.* further developed a porous conductive polymer hydrogel with multiple functions, including a continuous electrical conductive polyaniline network, strong chemical bonding with the Si particle surface (via both the cross-linked hydrogen bond with phytic acid and the electrostatic interaction with the charged polymer), and porous structure for volume expansion[100]. Polyaniline (PANI) is a well-known conductive polymer, and its application to Li-ion batteries has been studied since 1987[101]. However, the typically used p-type PANI is not phase-stable below 1 V (Li/Li^+), and this causes loss of conductivity in Si anodes, whose working potential ranges from 0.01V – 1V (Li/Li^+)[102]. To address this challenge, Wu's group developed an n-type PANI polymer, which could be cathodically doped for high electronic conductivity under the reducing environment for anodes[103]. Their approach was to utilise phosphoric acid groups from phytic acid and react with the nitrogen group from PANI, to form of a 3D interconnected network surrounding Si nanoparticles. When Si nanoparticles were mixed into the solution during

polymerisation, the phosphoric acid groups from the phytic acid form a strong hydrogen bond with the SiO_2 on Si particle surface (Figure 2-25)[100]. The SiNP-PANI hydrogel electrodes demonstrated a stable reversible specific capacity of 1600 mAh/g for 1000 deep cycles using a current density of 1 A/g^{-1}, and the coulombic efficiency from 2nd to 5000 cycles was stable at around 99.8%, even better than the Si nanowire they reported previously[33], [34].

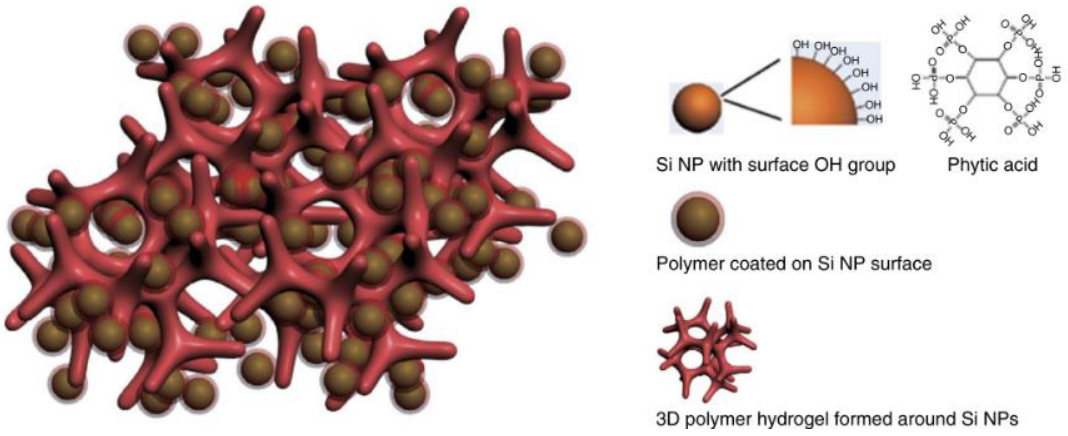

Figure 2-25 Schematic illustration of 3D porous SiNPs/conductive polymer hydrogel composite electrodes[100].

2.2.6 Self-healing Polymers (Multi-level Cross-linked Polymers)

Bao's group first introduced self-healing polymers (SHPs) and applied them to SiMPs electrodes in Li-ion batteries[104]. Whilst undergoing a mechanical disruption of the structure, this kind of polymer could be spontaneously self-healed through the dynamic re-association of hydrogen bonds at room temperature. The chemical structure of this SHPs is illustrated in Figure 2-26. In order to improve the conductivity of the polymer, they also included some carbon black during synthesis. Their electrochemical cycling result showed that the SiMPs electrodes with SHPs demonstrated remarkable improvement in cyclability compared with those containing alginate, CMC and PVdF binder (Figure 2-27a). Moreover, due to the involvement of carbon black, the conductivity for SiMPs/SHPs electrodes was improved, and this resulted in achieving a high rate capacity (around 1700 mAh/g at the current density of 2 A/g) (Figure 2-27b).

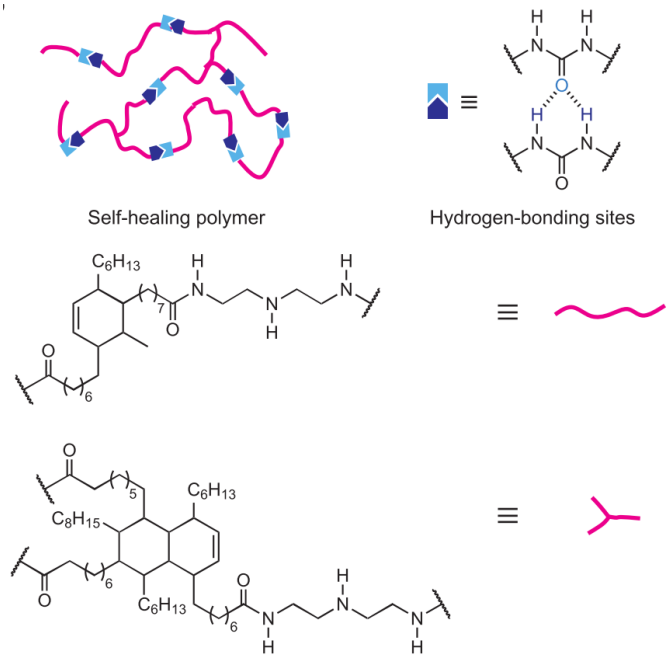

Figure 2-26 Illustration of chemical structure for SHPs

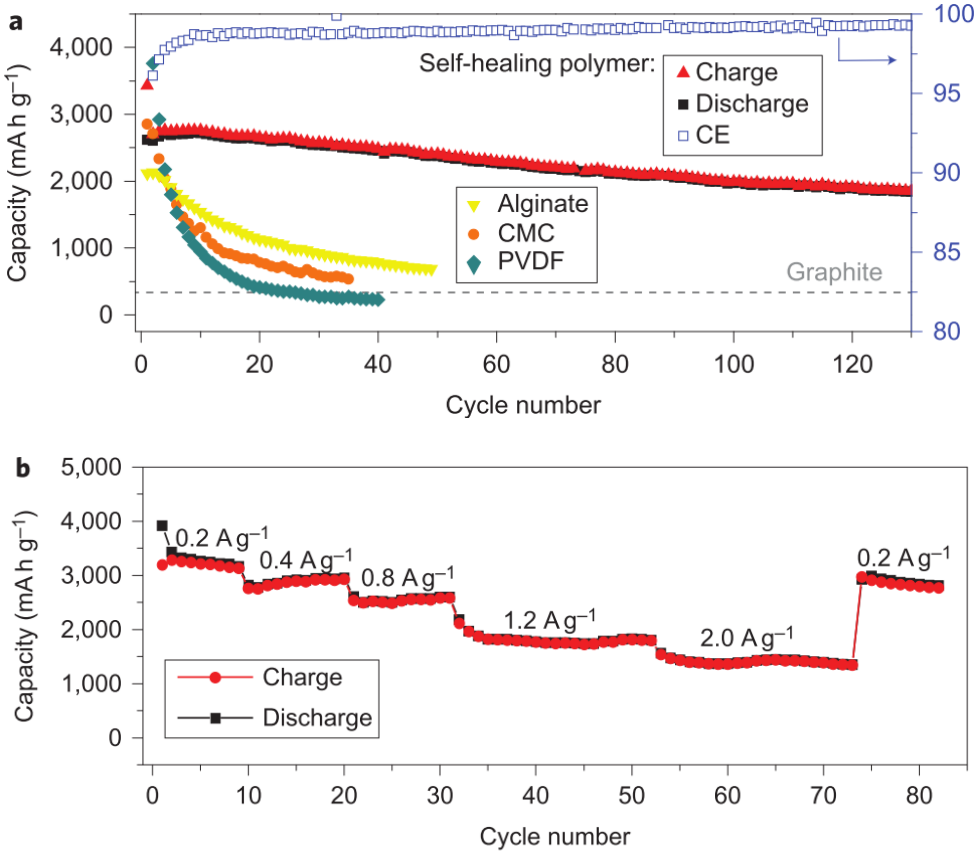

Figure 2-27 Electrochemical properties of SiMPs with SHPs a)Capacity retention of SiMP electrodes with different polymer additives b) rate capacity profile.[104]

Kwon *et al.* systematically investigated a series of polymeric binders incorporating Meldrum's acid with distinctive properties (Figure 2-28)[105]. They fabricated the

self-healing binder through hydrolysing K 100 in the presence of LiOH. The ratio was varied for different monomeric units to verify different polymer parameters including covalent crosslinks, stiffness and flexibility for improving the performance of Si electrodes. Their results indicated that Si electrodes with self-healing polymers exhibited the best cyclability among all cells, maintaining nearly 1800 mAh/g for 500 cycles. Whilst for the others, the polymer with the strongest cross-linked covalent bonds with the Si surface achieved higher reversible capacity achieved and longer cycle life. It suggests that a strong covalent bond was the most critical factor to be considered when designing the optimal binder for Si electrodes.

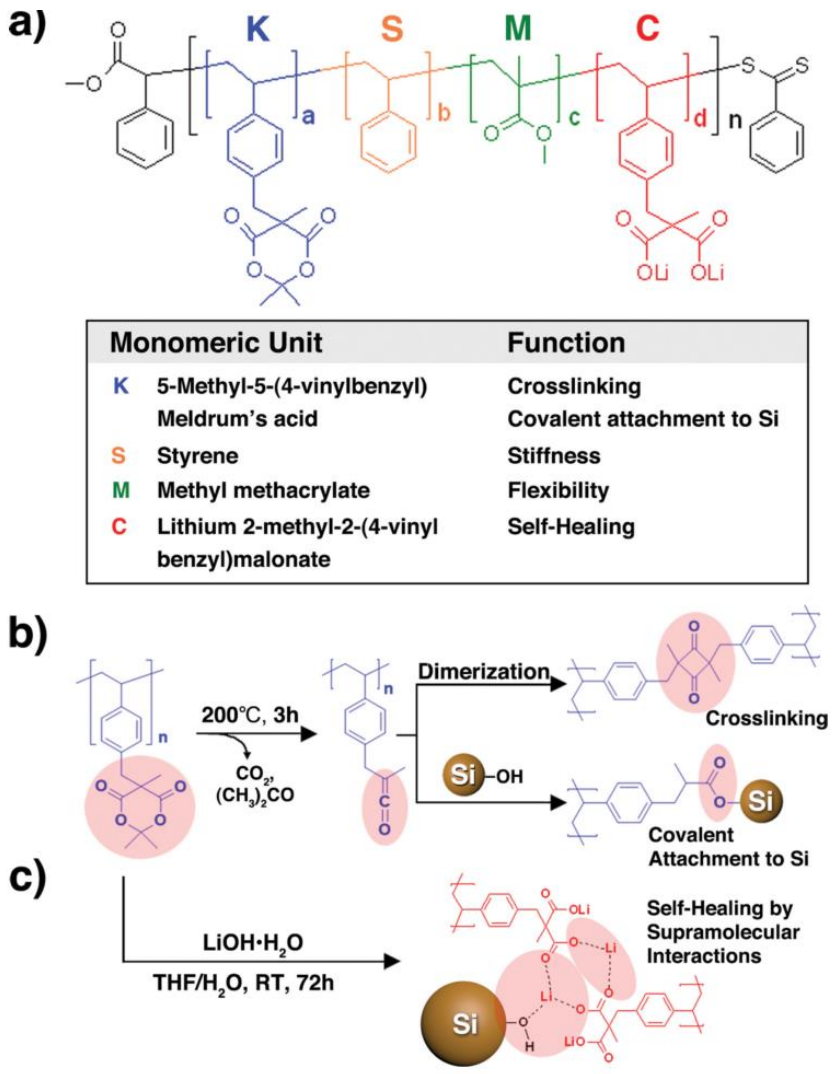

Figure 2-28 Structure of polymers and interaction with Si surface[105]

Zhong *et al*. fabricated a PAA-based self-healing hydrogel through building a dynamic coordination bond between graphene oxide and PAA matrix with Fe^{3+} ions as the cross-linker[106]. It was hypothesised that an ionic cross-linking would be formed

among PAA chains, as well as with the oxygen functional groups on graphene oxide (Figure 2-29). With only 0.5 wt% GO and 0.5 mol % Fe^{3+}, the mechanical property of PAA was significantly improved. GO nanosheet was used as a stress transfer centre to dissipate energy from PAA chains. Additionally, the ionic interaction along the PAA chains would break and recombine simultaneously to maintain the polymer structure. This robust and self-healing binder has not been applied to energy storage studies, so it could be a novel study to apply this self-healing polymer for Si electrodes.

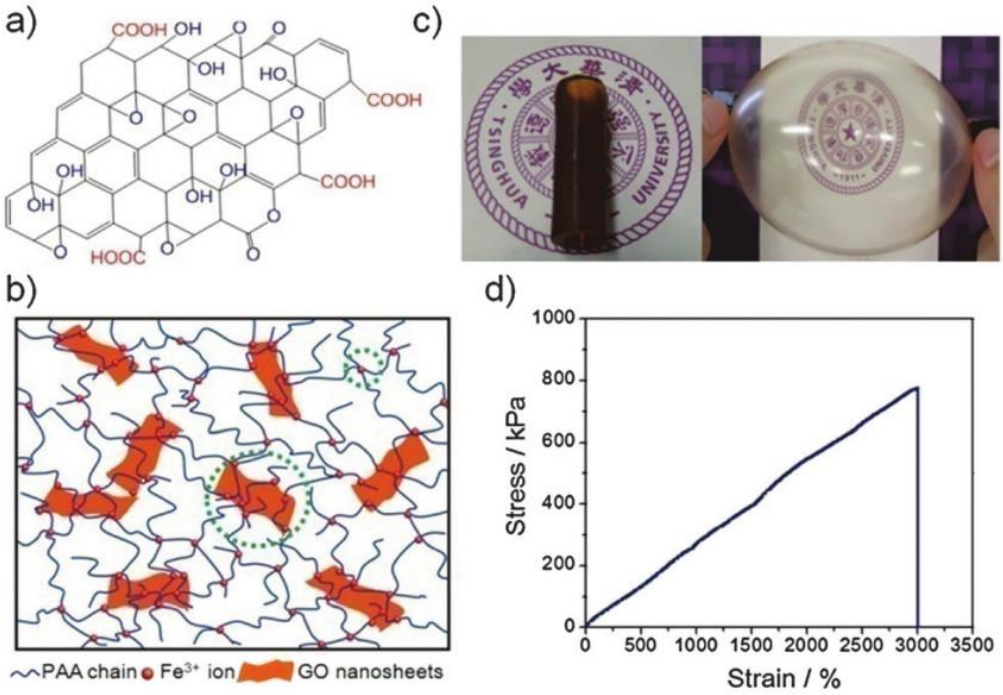

Figure 2-29 Illustration of PAA-Fe^{3+}-GO polymer and its tensile property[106].

2.3 Challenges for Si Full Cells

It is efficient and convenient to investigate and compare the electrochemical behaviour of novel materials in Si half-cells with Li foil as the counter electrode. However, Si half-cells (*vs* Li/Li^+) cannot provide enough convincing information towards the practical application, especially regarding long-term cycling performance. In half-cells, Li-ions are unlimited from the Li foil counter electrode, whilst they are finite from the cathode and electrolyte in full cells. It will exhaust the Li-ions more readily and is the main reason for the degradation in performance of the full cell. Additionally, the capacity fading of the lithium foil electrode could also affect the cycling performance, which could not be excluded from half-cells. Therefore, studies on Si full cells are necessary and more relevant for the further industrial application.

Moreover, besides the cyclability and storage capacity of Li-ions in anode, there are much more factors to be considered to achieve a long cycle life in full cells such as capacity balance between anode and cathode, the stability of cathode structure, a stable operational voltage window for both anode and cathode, and corresponding choice of stable electrolyte under this voltage window.

2.3.1 Cathodes for High Energy Batteries

The cathode, as the positive electrode, is defined as the oxidising electrode that accepts electrons from the external circuit and is reduced during the electrochemical reaction.

Generally, when selecting the right material for cathodes, characteristics including high discharge voltage, high-energy capacity, long life cycle, high power density, lightweight, low self-discharge rate, and environmentally benignity should be considered. Current research on high voltage cathode is mainly focussed on three types materials[21]:

- Layered oxides;
- Oxides with a spinel structure;
- Poly-anion oxides with the olivine and olivine-related structures.

The layered oxides generally have a formula of $LiMO_2$, where M stands for the transition metals, and most are structured in anionic stacking layers, as shown in Figure 2-30. This type of structure provides a 2D pathway for Li-ion diffusion (in X-axis direction and Z-axis direction). Typical layered oxide cathode material includes $LiCoO_2$, $LiNiO_2$ and $LiMnO_2$[21]. Amongst them, $LiCoO_2$ was the first commercialised cathode applied in Li-ion batteries, which showed an operated voltage 3.7 V *vs* Li/Li^+ and an excellent specific charge capacity (about 150 mAh/g)[107]. However, the high cost due to expensive Co and the associated toxicity with high exposure levels, are the main disadvantages which have made it unsustainable commercially. $LiNiO_2$ has a higher energy density and better availability, but it is less stable due to its less ordered structure[108]. $LiMnO_2$ is an attractive material currently, as Mn is cheap and more environmentally benign than Co and Ni, and also shows a smooth voltage profile despite it suffers from the problem of unstable phase transformation[21]. While extracting Li ions from layered $LiMnO_2$, some manganese ions will penetrate the interlayer lattice space, which can result in the formation of crystal areas with a spinel structure, thus compromising the cycle life and reduce the

working potential (the observing work potential for $LiMnO_2$ is lower than 4.1 V). To solve this problem, investigations into doping of different elements such as Co, Ni, Cr etc. have been conducted, and it is reported that $Li(Ni_{1/3}Mn_{1/3}Co_{1/3})O_2$, which is also known as NMC, could operate at a high voltages of up to 4.5 V with a capacity of above 200 mAh/g[21]. NMC has been commercialised and included into most electric vehicles (EVs) including Chevy Volt and BMW i3.

Lithium-nickel-cobalt-aluminium oxide (NCA), is a further development of lithium nickel oxide with adding aluminium to improve the chemical stability. Similar to NMC, NCA has a high reversible capacity (~200 mAh g^{-1}) and long storage calendar life compared to conventional Co-based oxide cathodes. Despite this, it was reported that capacity fade might be severe at elevated temperatures (40–70°C) due to solid electrolyte interface (SEI) growth and micro-crack growth at grain boundaries[109], [110]. NCA has also been widely used commercially, and a successful example are the Panasonic battery pack that has been applied in Tesla EVs.

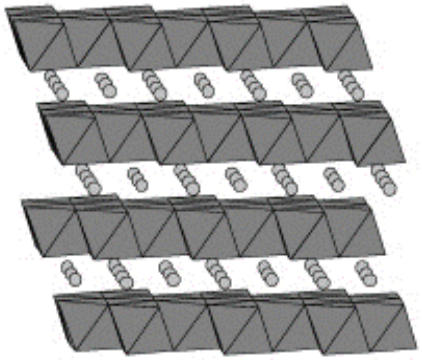

Figure 2-30 Illustration of schematic for layered oxide structure[111].

Spinel oxides generally have a formula of LiM_2O_4, and contain octahedrally coordinated M-cations and Li-cations in a cubic-closed-packed lattice, as shown in Figure 2-31[21]. This type of structure represents a more stable framework to allow Li-ions to reversibly move between the tetrahedral sites. It provides 3D pathways for Li-ion diffusion through the spinel framework and this makes spinel oxide materials possess a good Li-ion conductivity. The disadvantage is that generally they have lower charge capacity as there are fewer spaces for Li-ions with this structure[21]. Due to the good stability of spinel oxides, it is easy to blend different transition metal based on this structure to enhance the performance and reduce the cost. Some existing high

voltage cathode materials based on spinel-structured oxides have been summarized in Table 2-3.

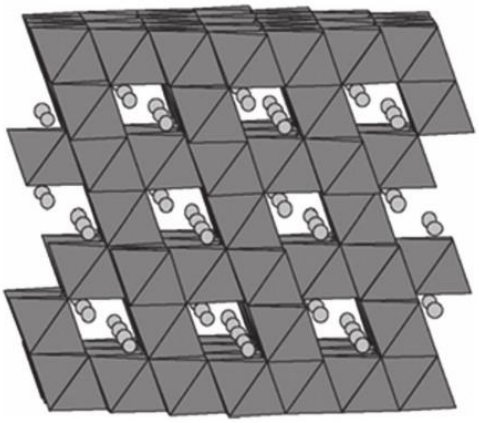

Figure 2-31 $LiMn_2O_4$ spinel structure representation; $LiMn_2O_4$ shown being composed of dark grey MnO_6 octahedral and Li-ions (light grey balls) occupying interconnected tetrahedral positions[21].

Table 2-3 Structural data for high-voltage lithium cathode materials based on spinel-structure oxides[107]

Composition	Mid-discharge voltage at the plateau over 4.5 V/V	Redox couple to operate at the plateau over 4.5 V	Potential range/V
$Li_2CrMn_3O_8$	4.8	$Cr^{3+/4+}$	3.4–5.4
$LiCrMnO_4$	4.8	$Cr^{3+/4+}$	3.4–5.4
$Li_2FeMn_3O_8$	4.9	$Fe^{3+/4+}$	3.0–5.3
$Li_2CoMn_3O_8$	5.1	$Co^{3+/4+}$	3.0–5.3
$LiCoMnO_4$	5	$Co^{3+/4+}$	3.0–5.3
$LiNiVO_4$	4.8	$Ni^{2+/3+/4+c}$	3.0–4.9
$Li_2NiMn_3O_8$	4.7	$Ni^{2+/4+}$	3.0–4.9
$Li_{2.02}Cu_{0.64}Mn_{3.34}O_8$	4.9	$Cu^{2+/3+}$	3.3–5.1

Poly-anion compound materials have also attracted wide attention in recent years due to their premier cyclability, safety, environmental compatibility and potentially low cost[21]. Typically, these materials have an open 3D framework, as shown in Figure 2-32, which are suitable for Li-ion diffusion. A typical example of this structure is $LiFePO_4$ (LFP), which has an average discharge voltage of 2.98 V for the $LiFeO_2$ cathode, whereas the discharge voltage is 3.5 V for $LiFePO_4$ cathodes[21]. The similar

structure is demonstrated by the lithium-metal-oxide with cobalt-based redox couple: where the discharge voltage is ~4.1 V for a $LiCoO_2$ cathode but is 4.8 V for a $LiCoPO_4$ cathode[21]. Calculations indicate that Ni-based poly-anion materials such as $LiNiSO_4F$, $LiNiPO_4$, and $LiNiO(SO_4)$ may have the highest voltage (above 5 V)[112], but the experimental results are still ambiguous, and the electrochemical activities of nickel have not been confirmed. Above all, the notable shortcoming for poly-anion materials is the low electronic and ionic conductivity[113], which limits the rate-capacity and the cyclability under the high current density of the material.

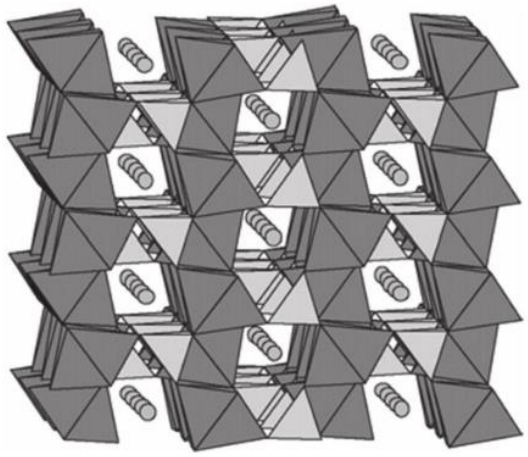

Figure 2-32 $LiFePO_4$ (olivine structure) representation; the oxide shown being comprised of dark grey FeO_6 octahedral and light grey PO_4 tetrahedral Li-ions are shown as light grey balls occupying octahedral[21].

The properties of different cathode materials that are commonly used in current EVs are summarised and compared in Figure 2-33. Cathode materials that are involved in existing Si full-cell studies are mostly found from these five materials, including NMC[114], NCA[56], [115] and LFP[116], [117]. However, the maximum cut-off voltages for these studies are mostly below 4.2 V since, when cycling to high voltages (> 4.2 V), the cycle efficiency will drop and the higher the voltage, the faster the capacity fade[115]. Huang *et al.* applied Li-rich cathode - graphene and carbon nano-tubes with modified NMC (GNL-modified LMNCO) for Si/graphite electrodes and cycled up to 4.65 V[118]. A significant enhancement has been notified in terms of the specific capacity of the full cell (around 250 mAh/g). However, cycling data for 20 cycles is not yet compelling enough to address the improvement. The challenge for Si full cells cycling under high voltage (> 4.2 V) could be due to the limitation of the voltage window of the electrolyte.

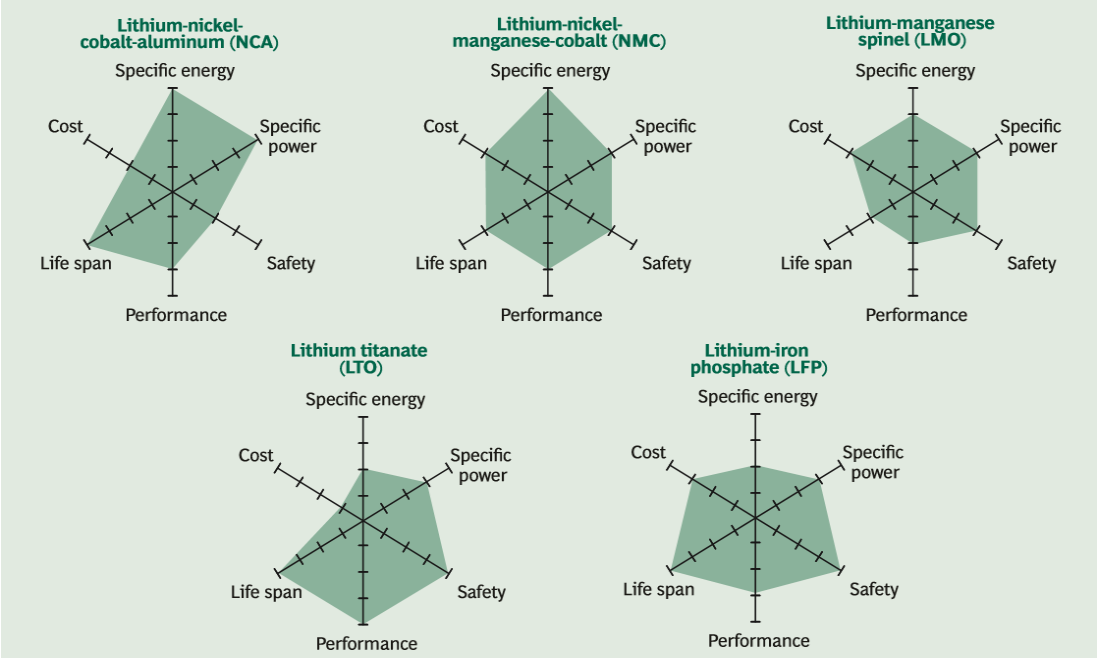

Figure 2-33 Tradeoffs among the five pricipal Li-ion battery technologies[119]

2.3.2 Electrolyte Additive for Si Full cells under High Voltage

The electrolyte is also an essential component in Li-ion batteries, which face challenges including wide electrochemical window, a wide range of operation temperature, safety properties, good ionic conductivity and ability to form efficient passivation layers[28]. With these criteria in mind, the electrolyte that is mostly used for current commercialized Li-ion batteries is a mixture of alkyl carbonates including ethylene carbonate (EC), dimethyl carbonate (DMC), diethyl carbonate (DEC) and ethyl methyl carbonate (EMC) for dissolving the salt $LiPF_6$, which demonstrates acceptable stability under voltages of around 4 V[28].

It has been addressed above that a stable SEI layer is a crucial factor that determines the cyclability of Si electrodes, and also affects the kinetics of Li-ion transport and interfacial stability. The SEI is the product of the electrochemical reduction of the organic solvents and salts and is strongly dependent on the components and properties of the electrolyte.

In most alkyl carbonate electrolytes, PF_6^- anions in solvent undergo an equilibrium as following[120]:

$LiPF_6$ (sol.) ↔ LiF (s) + PF_5 (sol.).

The PF_5 is likely to attract any moisture that is present in the electrolyte solution, and P-F bonds will be hydrolysed as presented in the following reaction[121]:

$LiPF_6(sol.) + H_2O \rightarrow POF_3(sol.) + LiF(s) + 2HF(sol.)$

$PF_5\ (sol.) + H_2O \rightarrow POF_3\ (sol.) + 2HF\ (sol.)$

The resulting HF will start the following reaction that induces cracks in the Si-Si network. This will also result in a consumption of Si-based active material as the Si in SiF_6 becomes inactive, thus constituting a constant capacity fading[120].

$Si + 4HF + 2F^- + 2H^+ \rightarrow SiF_6^{2-} + 2H^+ + H_2\ (g)$

To address these problems, electrolyte additives are applied to improve chemical stability. Currently, there are various electrolyte additives commercially available and according to diverse functions and can be categorised into 6 types. These are (1) SEI improver; (2) cathode protection agent (protect cathode from dissolution and overcharge); (3) $LiPF_6$ salt stabilizer (to enhance thermal stability of $LiPF_6$); (4) safety protection agent (low flammability and overcharge protection); (5) Li deposition improver (improve cycle efficiency of metallic Li); and (6) other agents such as solvation improver, Al corrosion inhibitor, and wetting agent[122]. For Si-based anodes, due to its unstable SEI caused by volume change, electrolyte additives with a function of improving SEI are favoured. Additives such as fluoroethylene carbonate (FEC)[123], succinic anhydride[124], vinylene carbonate (VC)[125] to $LiPF_6$ electrolyte have been reported to help generate smoother and more stable components in SEI layer and this in turn improve coulombic efficiency. Dalavi *et al.* conducted a comparison study between all these reported additive for Si thin film electrodes (Figure 2-34)[126], which indicated VC could best facilitate capacity retention when compared with other additives.

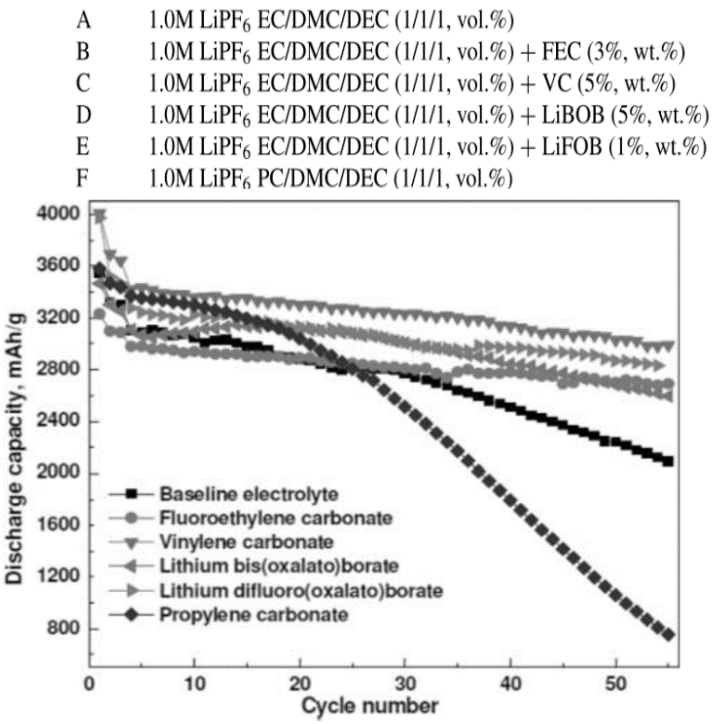

Figure 2-34 Discharge capacity (mAh/g) *vs* cycle number of Si half cells (*vs* Li/Li^+) with and without additives.

For common layered cathodes mostly used in commercial batteries, the usable potential range is limited due to electrolyte oxidation and polarisation growth under high voltage[23], [24], [127]. For most commercially available NMC cathodes, the cut-off potential *vs* Li/Li^+ is generally set as 4.28 V to best maintain the cycle life despite having structural stability up to 4.78 V *vs* Li/Li^+ [10], [25], [127]. In order to operate Li-ion batteries under high voltage, strategies including the application of novel solvent blends, electrolyte additives and coatings have been investigated. New solvent blends that involve fluorinated compounds[128]–[131], nitriles or dinitriles[132], [133] and sulfones[134], [135] have been reported for their high oxidation potential (> 5 V *vs* Li/Li^+), which is much higher than alkyl carbonates electrolyte[136]. However, these new blends have also been critiqued for their poor wettability, high viscosity, gas production, high impedance and safety concerns[128], [135], [137].

EC-free electrolytes for high voltage Li-ion batteries were first introduced by Dahn's group, which has proven that removing EC from the electrolyte and adding small amounts of additives could result in better performance than those cells including EC[22]. Their result also showed that with a proper additive as the "enabler", NMC/ graphite cells with EC free electrolyte could demonstrate excellent cyclability up to

4.4 V. Further to this study, the effect of different additives with various ratio in EC free electrolyte in high voltage NMC/graphite full cells has been investigated by the same group[27]. They compared additives including VC, methylene-ethylene carbonate (MEC), FEC and difluoro ethylene carbonate (DiFEC), and addressed the importance of the proper ratio for these additives to be involved. It indicates that if the "enabler" was insufficient, the cells could result in the gas generation and rapid capacity fading. On the other hand, excess "enabler" would result in large impedance and gas generation, but this did not include FEC (Figure 2-35). In their study, NMC/graphite cells with 3% FEC or 5% FEC in the electrolyte of 1 M LiPF6 in EMC demonstrated the best cycling performance.

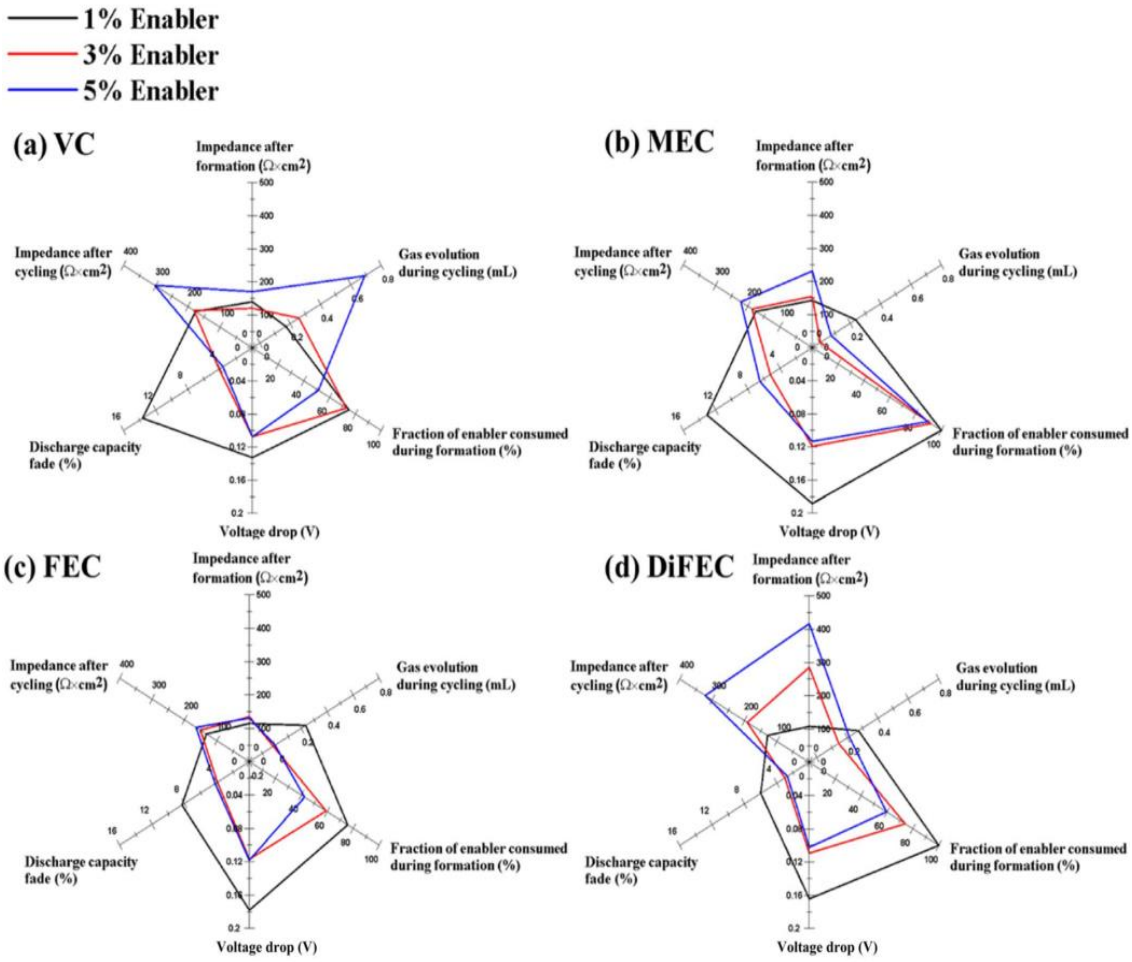

Figure 2-35 Radar plots summarizing the effects of selected enablers (1%, 3% and 5%) on NMC442/graphite in "EC-free" electrolyte system (a) VC (b) MEC (c) FEC (d) DiFEC[27]

Prop-1-ene-1, 3-sultone (PES) has also been reported as a novel additive to improve the stability of SEI on the anodes in Li-ion batteries, and it helped maintain the cyclability even under high voltage[134], [138], [139]. Xia *et al*. conducted a

comparison study to compare the performance of PES, VC and the combination in the EC-free electrolyte for graphite/NMC pouch cells under high voltage -the result is concluded in the radar plots in Figure 2-36[140]. They concluded that PES is a beneficial additive to maintain a reasonable cyclability under high voltage and high temperature and it can be considered as a replacement to VC for the industrial electrolyte.

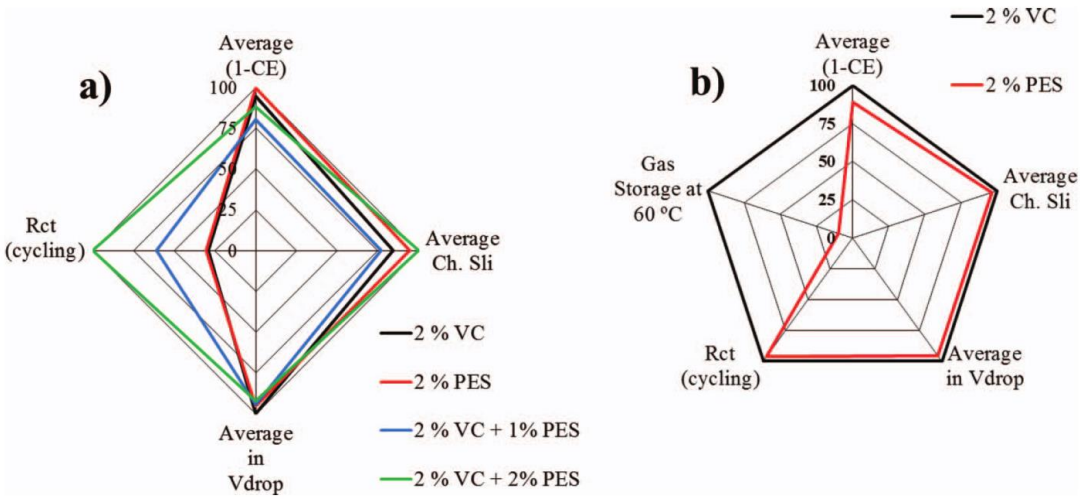

Figure 2-36 Radar plots summarizing the comparison result between different electrolyte additives (a) 2% VC, 1% PES, 2% P ES, 2% VC + 1% PES and 2% VC + 2% PES; (b) 2% VC and 2% PES.[140]

However, existing studies of EC free electrolyte are mostly focussed on graphite/NMC systems while there are few investigations for EC-free electrolyte system in Si full cells. Hence it is novel to systematically investigate the EC-free electrolyte system and appropriate additives for Si-based full cells under high voltage.

2.4 Overview of Literature

Si anodes show great potential to be industrialised into the next generation of Li-ion batteries, and much effort has been given to improve the electrochemical performance of Si-based anodes. Despite promising results achieved by several groups through modification of Si morphology, all of them used complicated chemical deposition methods[1-13], which is not ideal for large-scale industrialisation. Therefore, optimising the electrode composition is considered more realistic from a "drop-in" perspective, which supports the research approach of this study.

With this approach, studies from literature have given a lot of information on current progress in optimising Si electrode composite[14-33], which are used as the guidelines

for designing experimental parameters. Regarding optimising electrode composite, factors including the mass ratio of Si, choice of conductive additive, binder systems, and incorporation of other active materials are considered. The mass ratio of Si represents a comprehensive balance between the energy density and the life cycle. Since the research objective for this project is to develop high-energy Li-ion batteries, relatively high content of Si (60 % - 80 %) will be applied into the anode formulation to address this. Also, considering that Si needs more space to accommodate its expansion as well as to necessarily maintain its electronic contact during the volume change process, a sufficient amount of binder and conductive additives should be used. Graphene can be considered as an ideal co-active material to be incorporated into Si because it can contribute additional Li storage capacity as well as supplying good flexibility and conductivity[15-28].

For the choice of conductive additive, carbon materials are the most common candidates[34-38]. Among the diverse array of carbon materials, graphene may have the best overall conductivity, even better than carbon nanotubes[26]. A hierarchy of conductive combinations is considered here to be an optimal choice to provide the conductive network with the short and long-range order within the electrodes

Regarding the application of binder, the literature has shown that the binder plays an essential role in increasing the durable performance of Si anodes[39-73]. Among the common polymer binders, PAA has exhibited superior performance to maintain the cyclability of Si electrodes, as has been documented well in literature, with good baseline performance[17, 43, 44, 61]. There are several studies on binary polymer binders, and it has been shown in these studies that binary polymers could have better performance with Si anodes compared with single binder systems. It can be considered a good approach to combine a polymer with good adhesion (rich in carboxyl groups for example) with a polymer with excellent tensile properties, given the expansion stresses emanating from Si. Also, existing binary polymer systems as PAA-PVA can be further optimised concerning polymer ratio and crosslinking conditions, which are addressed in this study. Conductive polymer binders have demonstrated substantial enhancement of cycling performance in several studies[39, 67-71], but issues including toxicity, unstable voltage and complicated synthesis process are yet to be improved. Self-healing polymers have been recommended for its superior performance in terms of enhancing the cyclability for Si anodes even under the full capacity condition

despite their complex fabrication process[72-73]. It can be concluded that the most essential factor for self-healing polymer is to possess multi-level crosslinks including dynamic ionic interactions within the polymer chain. Inspired by the super tough self-healing hydrogel GO-Fe^{3+}-PAA that introduced by Zhong *et al.* with relatively simple synthesis process[74], similar polymer graphene-Fe^{2+}-PAA could be considered as an effective self-healing binder for Si electrodes. The reason to use graphene instead of GO is graphene possesses good conductivity and flexibility, which are favoured for Si electrodes. The functional group on the reduced product of graphene can form ionic interaction with Fe^{2+} as well as covalent bond with PAA, following the same mechanism as stated in Zhong *et al.*'s study. Considering that the ionic interaction with Fe^{3+} will be strong such that it will be easily gelled and difficult to disperse in the slurry, Fe^{2+} will be chosen as the ionic cross-linker for this novel self-healing polymer.

Since this study is mainly focussed on the anode, there is not the scope to include the considerable investigation into the cathode. Among the common cathode candidates from literatures[75-88], NMC will be chosen as the cathode chemistry to pair with Si anodes to manufacture full cells in later-stage investigations. This is due to its relatively high voltage (4.5 V) and reasonable capacity (200 mAh/g)[83, 88].

Electrolytes are essential components that limit the upper cut-off voltage for full cells, so a comprehensive study will also be conducted on an electrolyte with varies additives for Si full cells under high voltage. Much research efforts have been carried out into the electrolyte with novel solvent blends that are stable up to 5 V during cycling and storage[101-108]. However, disadvantages including poor wettability, high viscosity, gas production, high impedance and safety concerns prevent them from being industrialised in short-term perspective[128], [135], [137]. Dahn's group first introduced EC free electrolyte to be applied in high-voltage graphite/NMC full cells with merely removing EC from the electrolyte and involving appropriate additives that can function as "enablers". These result in significant improvement of the cell's performance in terms of cyclability, impedance, stability for storage and gas generation[112, 113]. Therefore, EC free electrolyte is applied to Si full cells for use towards higher voltages is another objective of this study and could be another point of knowledge contribution since most existing studies were conducted on graphite-based electrodes. Regarding the choice of additives in EC free electrolyte, FEC, VC and PES will be considered since FEC and VC have been reported in various studies

as to how they could effectively stabilise the SEI of Si[93, 95, 96]. Additionally, they are shown to achieve good performance in EC free electrolyte under high voltage[112, 113]. PES was introduced recently for its contribution to forming stable SEI and suggested to be the replacement for VC[108, 114-116].

In conclusion, with sufficient knowledge support from the literature, the hypothesis to develop the high-energy Li-ion batteries can be summarised as follows:

- It is an industrial-favoured approach to improve the Si performance through optimising the electrode composite other than modifying the structure of the active material, and high-content Si electrodes (60 wt% ~ 80 wt% active mass) will be focused in this study to obtain the high capacity. Graphene can be incorporated as the co-active material with considerations around the binder type and content for increased surface area scenarios.
- Carbon combinations to supply hierarchies of conductive networks and thus result in better rate capacity for Si electrodes than common single conductive additives.
- Regarding the binder system for Si electrodes, PAA has proven superior for its performance in Si electrodes among other single binder systems. For this reason, it can be used as the baseline for further improvements. Interpenetrating polymer networks that combined a polymer with strong adhesion and one with the premier tensile property are reported to achieve better performance than single binder system in Si electrodes. Further improvement may be accomplished by optimising polymer ratios and crosslink conditions. Also, the multi-level crosslinked polymer PAA-Fe^{2+}-FLG is proposed to be a novel robust binder that could better tolerate the volume expansion and maintain the cyclability within Si electrodes.
- To achieve high energy full cells based on Si/NMC, the choice of electrolyte is essential. EC-free electrolyte with beneficial additives will be aimed at extending the cycle life under high voltages. This performance improvement with Si is still yet to be proved and will constitute an important part of this project. Therefore, it is hypothesised that removing EC from existing EC/EMC based electrolyte could result in improved cyclability for Si full cells under high voltage. A comprehensive study will be conducted to identify the optimised additive among the candidates of FEC, VC, PES and the combination.

Therefore, the structure of this project can be categorised into four main parts:

1. Formulation-based matrix study for Si electrodes and incorporation/ hybridisations of FLG.
2. Study of carbon mixture as a hierarchy of conductive additives for Si-based electrodes.
3. A comprehensive study of the optimisation of PAA-based binder chemistries for Si-based electrodes.
4. Investigation of EC free electrolyte to be used in Si/NMC full cells under high voltage (4.4 V).

Chapter 3 Research Methodology

3.1 Si Anode Formulation

3.1.1 Carbon Conductive Mixture

Carbon black (SUPER C65, C-NERGY), graphite (SFG6, TIMREX), Few-layer Graphene (FLG) (xGnP-M5, XG Sciences) and multi-wall carbon nanotubes (MWCNTs) (SMW=200, Aldrich) were weighed according to the formulation listed in Table 3-1. Deionized water was added to make a solution targeted at 11 wt% solid mass and 1 g Na-PAA solution (12.5% concentration) was added to increase the viscosity and adhesive property of the mixture. However, for carbon mixture 3, due to the large surface area of particles, additional deionised water has to be added to get the MWCNTs dissolved, and this resulted in a solid mass of 8%. The mixture was medium-sheer processed using an overhead high-speed homo-disperser (Model 2.5, PRIMIX) at 1000 rpm for 30 mins. The resulting slurry was further processed using an ultrasonic probe (UP400S, SciMED) for 15 mins using an amplitude of 60 % and a frequency of 24 Hz, followed by further dispersion using a high-speed homo-disperser for 30 mins at 1000 rpm. Following dispersion, a small aliquot of the resulting mixture was cast onto copper foil and dried for SEM imaging.

Table 3-1 Carbon mix formulation

	Carbon black	**Graphite**	**FLG**	**MWCNTs**
Carbon mixture 1	50 wt%	50 wt%		
Carbon mixture 2	25 wt%	25 wt%	50 wt%	
Carbon mixture 3	25 wt%	25 wt%		50 wt%

3.1.2 Binder Formulation

- ***PAA solution***

PAA powder (M_W = 450 K, purity ≥ 99.5%, Sigma-Aldrich) was purchased from Sigma Aldrich. 13g PAA powder was dissolved in 87 g of deionised water using a Planetary Centrifugal Mixer (ARE310, Thinky) operated at 1000 rpm for 20 mins, followed by a degassing procedure at 400 rpm for 10mins. The solution was left to stand in a parafilm-sealed vessel for 24 hours before use.

- ***Partially neutralise PAA solution***

The resulting PAA solution was neutralised with sodium hydroxide (NaOH) to achieve the target neutralisation degree of 70 mol%. The NaOH pellets (BioXtra 99 % purity, Sigma-Aldrich) were dissolved into deionised water to make the NaOH solution with 50% concentration. The resulting NaOH solution was added to the PAA solution formulated above. The solution was stirred with a spatula for 5 mins and left overnight for reaction completion.

- ***Preparation of PAA/PVA and pnPAA/PVA blends***

Considering the crosslink reaction between PAA and PVA is favoured in acidic conditions[98], a low neutralisation degree of PAA is chosen for this study. To make a partially neutralised PAA solution (pnPAA), 0.35 g sodium hydroxide pellets (NaOH, Sigma-Aldrich) were dissolved in deionised water and then added to 60 g PAA solution with stirring for 10 mins. This resulted in a PAA solution with a neutralisation degree of 8 mol% and was allowed to de-gas for 24 hours before blending it with a PVA solution.

PVA aqueous solution with a concentration of 13 wt% was prepared by dissolving PVA powder (Mw ~98K, Sigma Aldrich) into the pre-heated de-ionised water at 80°C. To identify the optimised ratio between PAA and PVA, the prepared PVA solution was mixed with un-neutralised PAA solution to make blend solutions with designed PAA/PVA mass ratio from 100% to 0% at ambient temperature. The resulting solution was mixed at 200 rpm for one hour using an overhead impeller disperser (IW15, IKA) with a PTFE-coated propeller blade. The resulting solution was left to stand for 24 hours to exclude any gas bubbles generated. To make the pnPAA/PVA blend solution,

the same procedure was followed by replacing PAA with pnPAA, and only the optimised ratio between PAA and PVA was applied.

- ***Preparation of Na-PAA/SBR blends***

NaPAA solution was prepared through the method described previously. Both NaPAA/SBR (2/1) and NaPAA/SBR (5/1) were prepared to identify the optimum weight ratio between NaPAA and SBR. To synthesise NaPAA/SBR blends for the purpose of polymer characterisation, SBR solution (Styrene-Butadiene Rubber, MTI) was added into PAA solution according to different weight ratio and mixed at 200 rpm for 5 mins using an overhead impeller disperser (IW15, IKA) with a PTFE-coated propeller blade. The resulting solution was left to stand for 24 hours to exclude any gas bubbles. For applying into Si-NaPAA/SBR slurry, NaPAA/SBR was blended during the electrode mixing process, which will be described in section 3.1.3.

- ***Synthesis of dually cross-linked PAA-Fe2+-FLG polymer***

0.1 g FLG powder (xGnP-M5, XG Sciences) was dissolved into 100 g deionised water and followed by an ultra-sonication process (UP400S, SciMED) for 3 mins at 60% amplitude. 0.7 g $FeSO_4 \cdot 7H_2O$ was added, and the resulting solution was placed under a high-speed homo disperser (Model 2.5, PRIMIX) at a speed of 400 rpm. 25 g PAA powder (M_W = 450 K, purity ≥ 99.5%, Sigma-Aldrich) was gradually added to the mixing solution at the same speed for an additional 30 mins to ensure powder dissolution. The final blend was placed overnight to allow for self-polymerisation and degassing to complete.

To systematically study the dually cross-link effect, PAA-FLG and Fe^{2+}-PAA have also been synthesised to compare the mechanical and electrochemical properties. The processes mostly follow the steps demonstrated above, with the exception of adding $FeSO_4 \cdot 7H_2O$ to make PAA-FLG and excluding FLG for making the Fe^{2+}-PAA solution.

3.1.3 Slurry Mixing and Electrode Manufacture

- ***Manufacturing Si electrodes with different carbon conductive mixtures***

The electrode formulation for the study with different conductive carbon mixtures included 70 wt% Si powder (d=3.1 µm, purity 99.7 %, Elkem), 16 wt% selected

carbon conductive additive and 14 wt% Na-PAA (prepared through the method described above.) Carbon mixtures with formulation 1, 2, 3 are listed in Table 3-1 and were manufactured and applied as the carbon conductive additives respectively. Carbon black (SUPER C65, C-NERGY) was also used as the control conductive additive to compare with the performance of the other carbon combinations.

The slurry was initially mixed using an overhead high-speed homo-disperser (Model 2.5, PRIMIX) at 1000 rpm for 30 mins. Following this the slurry was ultrasonically processed (UP400S, SciMED) for 7 mins at 60 % amplitude, followed by manual stirring with a spatula and subsequent ultra-sonication for a further 7 mins. The binder was added into the slurry and mixed using a high-speed homo-disperser at 1000 rpm for 30 mins. Finally, the mixed slurry was transferred to a Filmix (high shear processor, Model 40-40, PRIMIX) to ensure a homogeneous distribution of the nanosize particles and to prevent secondary agglomeration. The solution was processed at a speed of 10 m/s for 30 s, then 25 m/s for another 30 s.

The resulting slurry was coated onto the copper foil (10 μm, Oak Mitsui, electrodeposited) using a draw-down coater (RK Instruments Ltd) with a micro-meter-controlled spreading blade (K control coater Model 101, RK Print), and a blade gap of 80 μm. Slurry made for all studies in this thesis was coated on the same day or the next day by the latest to avoid any uncertain side reactions in aqueous solution.

The coated copper foil was dried on a hot plate set to 50 °C to evaporate the solvent for 10 mins. The coated sheet was placed in a vacuum chamber set to 50 ^{o}C for 12 hours under dynamic vacuum to ensure minimising of any water prior to cell construction. All electrodes in this study were made into half cells or full cells within a week to minimise the risk of being oxidised under high temperature, considering they could be contacted with oxygen during open the door of the vacuum oven by other people.

- ***Manufacturing Si-FLG electrodes***

To investigate the effect of the FLG to the cyclability of Si anodes, a matrix formulation study was conducted with four different formulations to vary the ratio between the Si and FLG (Table 3-2).

Table 3-2 Si/graphene formulation matrix

Formulation	Mass ratio %			
	Si	**Few-layered Graphene**	**Na-PAA**	**Carbon mix**
A	76	0	12	12
B	70	8	12	10
C	65	12	14	9
D	60	16	14	10

The electrode materials included active material powder, a mixture of carbons and deionised water, with mass proportions according to their designated formulation. The slurry mixing process was the same process as outlined in the method to prepare Si slurries with different conductive carbon mixture as stated above.

To investigate the electrochemical performance of Si-FLG electrodes, electrodes based only on either Si or FLG were manufactured under the same process based on formulations in Table 3-3.

Table 3-3 Formulation for further comparison study

Electrode	Mass ratio %			
	Si	**Few-layered Graphene**	**Na-PAA**	**Carbon mix 2**
Si/FLG hybrid	60	16	14	10
Si only	76	-	14	10
FLG only	-	76	14	10

The mass of electrode and pure copper foil were measured by a precision semi-microbalance (Satorius, SE2, d=0.01 mg). The thickness of coating and copper foil were measured by digital thickness gauge (Kafer, d=0.001 mm). In most study of this thesis, the thickness for Si-based electrode is between 40 μm ~ 50 μm.The area of the electrode is known as 1.72 cm^2, in which case the electrode density ρ can be calculated by Equation 1.

$$\rho = \frac{mass_{coating} - mass_{copper\ foil}}{1.72 \times (thickness_{coating} - thickness_{copper\ foil})} \quad \text{(Equation 1)}$$

- ***Differential capacity analysis (dQ/dV)***

dQ/dV peaks are associated with the structural phase change of anode and cathode materials through alternating amounts of lithium ions within their lattices[141]. The data is collected during the cycling process under the C rate of C/5 and recalculated in software based on the difference value of capacity and potential within a specific voltage step, which is 3 mV for this project.

- ***Si-FLG large scale coating***

Si-FLG slurry was manufactured through the process as described above. Slurry viscosity was measured first through a viscometer (RheolabQC-18318, Anton Paar) in combination with a B-CC27 measuring cylinder to verify the feasibility for large coating. The viscosity at the shear rate of 10/s was taken into consideration since that is the shear rate for the reel-to-reel coater of the large coating line. Solid content and gram per square meter (GSM) of the coating were calculated to get the control parameter for coating thickness. The solid content was calculated through Equation 2.

$$Solid\ content = \frac{M_{dry\ coating} - M_{Cu\ foil}}{M_{wet\ coating} - M_{Cu\ foil}} \times 100\% \quad \textit{(Equation 2)}$$

The target capacity for Si-FLG electrodes was selected as 2.8 mAh due to the capacity of available NMC (NMC622, Argonne), and the theoretical capacity applied on Si-FLG electrodes was 1200 mAh/g. The active ratio for Si-FLG electrodes was chosen to be 60 wt%. The target GSM for wet coating is calculated according to Equation 3.

$$GSM = \frac{2\ mAh/cm^2}{1200^{mAh}/_{g} \times 60\% \times solid\ content\% \times 10^{-4}} \quad \textit{(Equation 3)}$$

The coating was applied using a pilot-scale battery coating line (MEGTECH LabCoater, B&W) with a reel-to-reel setup approach. The line speed was set at 0.5 m/s, and the comma bar was adjusted from 80 μm to 15 μm to monitor the actual GSM. The temperature of all three thermal chambers of the coating line was set to be 50°C, and the airspeed was set at 5 m/s.

- ***Manufacturing Si electrodes with cross-linked and self-healing polymer binders***

The electrode formulation was 70 wt% Si powder (d_{50}=3.1 μm, purity 99.7 %, Elkem), 16 wt% carbon mixture and 14 wt% selected binder. The slurry was initially mixed without binder using an overhead high-speed homo-disperser (Model 2.5, PRIMIX) at 1000 rpm for 30 mins. Following this the slurry was ultrasonically processed (UP400S, SciMED) for 7 mins at 60 % amplitude, followed by manual stirring with a spatula and subsequent ultra-sonication for a further 7 mins. The binder was added into the slurry and mixed using an overhead stirrer (IW15, IKA) at a speed of 200 rpm for 1 hour.

For Si and PAA/SBR electrodes, most mixing procedures were same as illustrated above before adding the binder. PAA was added firstly into the slurry and mixed using a high-speed homo-disperser at 1000 rpm for 30 mins, followed by Filmix dispersion (high shear processor, Model 40-40, PRIMIX) at a speed of 10 m/s for 30 s, then 25 m/s for another 30 s. Finally, SBR solution (Styrene-Butadiene Rubber, MTI) was added into the slurry and mixed at 400 rpm for 5 mins. This is to better protect the polymer elastic from SBR.

The resulting slurry was coated onto the copper foil (15 μm, Oak Mitsui) using a draw-down coater (RK Instruments Ltd) with a micrometer-controlled spreading blade (K control coater Model 101, RK Print) with a blade gap of 80 μm. The coated copper foil was dried on a hot plate set to 50 °C to evaporate the solvent for 10 mins.

For Si with PAA/PVA or PVA/biopolymer electrodes, an additional heat-treatment process was applied at this stage to form the cross-link between Si particles and binder. The dried coatings were placed in a vacuum oven set to 150˚C for 20 mins under a compression of 20 N with a brick on top of a stainless steel plate to facilitate the formation of the cross-linking between polymer chains and the surface of Si.

All the dried coatings were transferred to the vacuum oven set to 50˚C in a dry room for an overnight period before coin cell assembly.

3.2 Polymer Characterisation

The polymer blend free-standing films were prepared by solution-casting onto a petri dish and dried at room temperature until constant weights were achieved.

3.2.1 Fourier Transform Infrared Spectroscopy (FTIR)

Fourier transform infrared spectroscopy (FTIR) was conducted using an FTIR Spectrometer (TENSOR 27, Bruker) to identify the functional groups present between different polymer films. The resolution setting was 4 cm^{-1} with 20 scans from the wavenumber range of 4500 to 500 cm^{-1}.

3.2.2 Tensile Test Characterisation

The polymer films with the thickness of 0.13-0.2 mm were cut into tensile specimens according to ASTM D638, with the gauge width of 4 mm and the gauge length of 26 mm. The tensile testing was conducted using a universal tensile machine (AGS-X Series, Shimadzu) with a load of 500 N, and a tensile rate of 2 mm/min.

3.2.3 Polymer Swelling Test

Polymer films were firstly dried in a vacuum oven under 60˚C overnight, and then soaked into the electrolyte, which was used in half-cells, and placed in an oven with a constant temperature of 25˚C. The weight of each polymer film was measured hourly immediately after removing any electrolyte solution on the polymer surface. Three samples for each type of polymer were made to get the average value for comparison purposes.

3.3 Electrode Characterisation

3.3.1 Scanning Electron Microscope (SEM) and Cross-section Imaging

SEM analysis was performed using a Carl Zeiss Sigma Field Emission Scanning Electron Microscope (FE-SEM) to generate the SEM images of electrodes and cross sections applying an accelerated voltage of 5 kV and in-lens detection. The working distance was around 2.5 mm.

Energy Dispersive X-ray Spectroscopy (EDX) analysis was conducted using the same FE-SEM with an accelerated voltage of 15 kV and an in-lens detector. The working distance was adjusted to 8.5 mm for the EDX scanning.

Cross-sections were obtained using an ion-milling system (IM4000 Plus, HITACHI) at an accelerating voltage of 4 kV for 3 hours.

3.3.2 Electrode Nano-indentation Test

Indention testing is conducted on a nano-indenter (NanoTest Extreme, Micro Materials Ltd) with a Berkovich indenter with a diameter of 25 μm. 20 indentations were applied to each electrode to establish and minimise the error of measurement.

The test procedure is:

1. Apply the load to the electrode to 15 mN.
2. Hold for 300 s to ensure the creep exponent has been removed during unloading.
3. Remove the load and thermal drift correction for 60 s.

3.3.3 Electrode Adhesion Test

The adhesion strength of electrodes was tested using the Tensile and Compression Test system (AGS-X Series, Shimadzu) with the sensor of 1 kN. A 3D printed counterpart (d=10 cm) was used as the sample holder in parallel with the compression plate. The electrode (1.72 cm^2) was fixed between these planes with double-sided polyacrylate tape on a polypropylene substrate (Tesafix 5696, Tesa). Initially, a compression velocity was applied to the system of 0.75 mm/min until the compressing force reaching 20 N; subsequently, the system was held for 10 seconds before a pull-up velocity of 100 mm/min was applied.

As indicated in a previous adhesion study[142], three different failure mechanisms may appear as a result:

a) adhesion failure between coating and copper foil, which means the internal adhesion strength amongst electrode components is larger than the adhesive force between electrode coating and current collector;

b) cohesion failure inside the coating, which indicates the internal adhesion force of the electrode is smaller than the adhesive force from the tape;

c) failure of adhesive, which is an invalid result if the compression force is too big that the adhesive from the double-sided tape has penetrated down through the electrode and current collector.

For all electrodes that undertaken the adhesion test in this study were result in cohesion failure as shown in Figure 3-1.

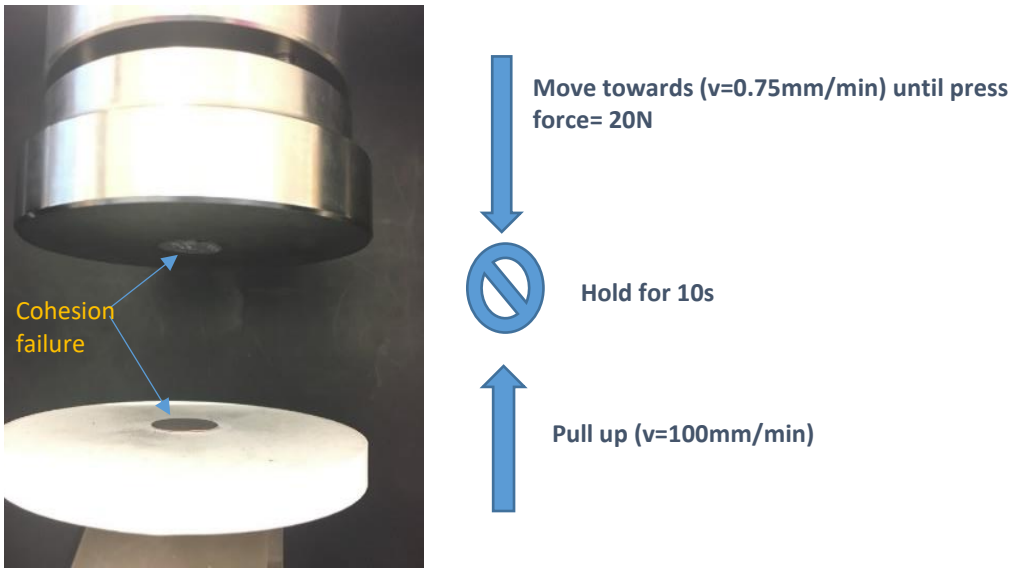

Figure 3-1 Illustration of adhesion force test of an electrode

3.4 Electrolyte Mixing and Characterisation

3.4.1 Electrolyte Mixing

Different electrolyte formulations based on $LiPF_6$ salt and EMC solvent were selected (shown in Table 3-4) to investigate the effect of EC free electrolyte with various additives for Si-FLG full cells under high voltage of 4.4 V. $LiPF_6$ (battery grade, Sigma-Aldrich) was weighed according to the formulation in Table 3-4 and added into 10 ml EMC (98% purity, Sigma-Aldrich). FEC (99% purity, Sigma-Aldrich), VC (97% purity, Sigma-Aldrich), PES (95% purity, Sigma-Aldrich) were weighed according to the mass ratio to $LiPF_6$ and added into the corresponding electrolyte solution based on the formulation in Table 3-4. The resulting solution was placed on a magnetic stirrer and mixed under 500 rpm overnight. The weighing and mixing processes were performed in an Argon-filled glovebox (O_2 and H_2O less than 10 ppm). Commercially available electrolytes (as shown in Table 3-5) were used as the control electrolytes to compare the effect of EC.

Table 3-4 Selected electrolyte formulation for EC free electrolyte study

Electrolyte Formula	$LiPF_6$ Salt mol/L	EMC solvent ml	FEC wt%	VC wt%	PES wt%
Baseline	1	10			
H01	1.2	10	15	3	
H02	1.2	10	15		
H03	1.2	10	15		2
H04	1	10			2
H05	1	10		3	

Table 3-5 Formulation for commercial electrolyte RD265 and RD165

Electrolyte Formula	$LiPF_6$ Salt mol/L	Solvent	FEC wt%	VC wt%
RD265 (PuriEL, Soulbrain)	1.2	EC:EMC (1:3)	12	3
RD165 (PuriEL, Soulbrain)	1	EC:EMC (1:1)		

3.4.2 Water Content Measurement

The water content measurement was conducted using a moisture measurement equipment (Karl Fisher CA-200, MITSUBISHI Chemical Analytech Co. Ltd.). AQUAMICRON® anode solution (AKX, Mitsubishi Chemical Co. Ltd) and cathode solution (CXU, Mitsubishi Chemical Co. Ltd) were applied for the measurement. 1 ml check solution (AQUAMICRON Check Solution P, Mitsubishi Chemical Co. Ltd) was injected into the Karl Fisher apparatus to test the moisture in the standard solution. When the measurement is between 3900 – 4100 µg, the test result can be considered reliable. Followed that, 1 ml tested electrolyte would be injected for analysis. For each electrolyte, two measurements were taken to get a more precise result.

3.5 Cell Build

For each characterisation on one material in this project, three coin cells were made to get a reliable electrochemical performance. If any of them performed with a clear difference, a fourth cell was constructed and characterised until consistent and comparable results were acquired.

3.5.1 Half-cell Assembly

The electrodes were assembled into Hohsen CR2032 coin cells in a dry room with a dewpoint of -45 °C to reduce the water content from the electrodes and cell components. Lithium foil (D=15.6 mm, PI-KEM) was used as the counter electrode with a trilayer membrane (PP-PE-PP, Celgard) as the separator. The default electrolyte for investigating Si electrode formulations and varies binders is 1.2 mol $LiPF_6$ dissolved in the solvents EC/EMC (1/3), 15 % FEC, and 3 % VC (PuriEL, Soulbrain). Whilst for electrolyte additive studies for high-voltage full cells, the modified electrolytes with different additives were applied.

3.5.2 Full-cell Assembly

- ***Si-FLG half-cell test for lithiation potential at cut-off capacity***

Si-FLG half-cells (*vs.* Li/Li^+) were cycled in a constant current mode as demonstrated in Section 3.6.1 with the capacity limitation of 1200 mAh/g. The lithiation potential of Si-FLG half-cells at cut-off capacity was monitored through the voltage-capacity profile as shown in Figure 3-2, and it can be concluded that the lithiation potential for Si-FLG electrodes at the State-of-Charge of 1200 mAh/g is about 0.1 V.

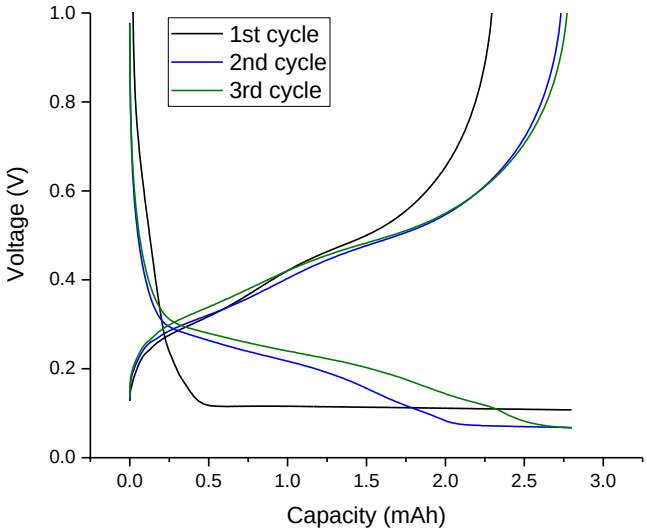

Figure 3-2 Lithiation potential test (*vs*. Li/Li^+) for Si-FLG electrodes at cut-off capacity

- ***NMC half-cell capacity test***

NMC coating (NMC622, Argonne) was purchased from Argon Laboratory and made into half-cells (*vs.* Li/Li^+) according to the method described above. The target cut-off voltage for the full cell is 4.4 V, and the lithiation potential of Si-FLG electrodes at the cut-off capacity is 0.1 V, therefore under this condition, NMC electrodes will be cut off at 4.5 V in the full cell. The actual capacity of NMC half-cells within the voltage range of 2.75 V - 4.5 V was tested with the same constant current density as the Si-FLG anode (240 mA/g). The actual capacity was also demonstrated through the voltage-capacity profile as shown in Figure 3-3.

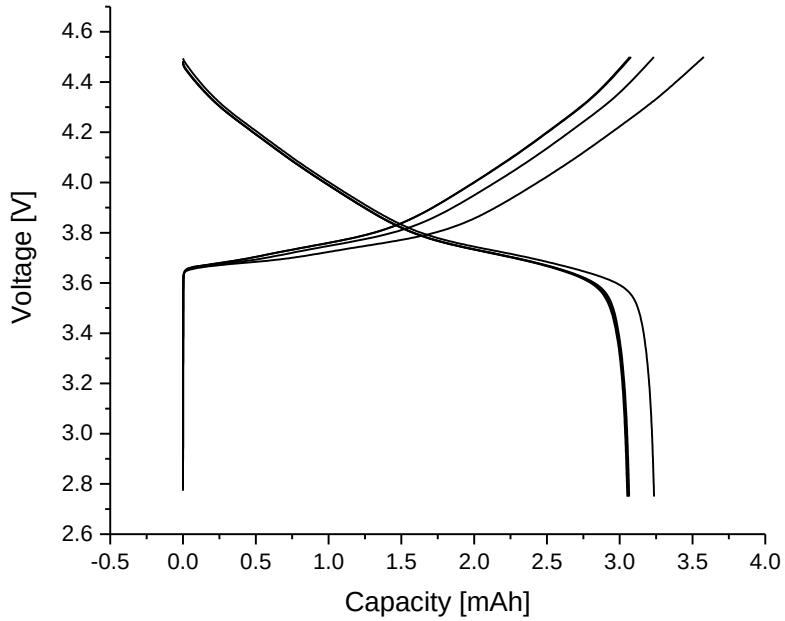

Figure 3-3 Capacity test at the cut-off voltage (*vs*. Li/Li$^+$) for NMC electrodes

- ***Full cells assembling***

The electrode capacity (anode *vs.* cathode) was balanced through matching NMC cathode with Si anode according to the same electrode capacity. The capacity for NMC was obtained through Figure 3-3, while the capacity for Si anode was paired based on a theoretical capacity of 1200 mAh/g.

Full cells were assembled in a dry room through the method described in Section 3.5.1, placing an NMC electrode at the bottom as the cathode and a Si-FLG electrode on top as the anode. A trilayer membrane (PP-PE-PP, Celgard) was used as the separator in between. Electrolytes with different additives listed in Table 3-4 and Table 3-5 were applied to investigate the benefit of electrolyte additives in full-cells cycling under high voltage.

3.6 Electrochemical Evaluation

3.6.1 Constant Current (CC) Cycling Test

Si half-cells (*vs.* Li/Li$^+$) were cycled at constant current mode between 10 mV and 1 V on a Maccor Series 4000 system with an initial C-rate at C/20 for the formation cycle, followed by repeated cycling at the C-rate at C/5. For Si electrodes with different cross-link binders, cells were cycled under a capacity limitation of 2000 mAh/g (400 mA/g). For the study of Si-FLG hybrid electrodes study, cells were cycled

under a capacity limitation of 1800 mAh/g, which corresponds to the current density of 360 mA/g.

The Si-FLG/NMC full cells were tested (BCS-805, BioLogic) and cycled between 2.5 V and 4.4 V with a formation cycle at C-rate of C/20, followed by constant C-rate cycling at C/5, corresponding to the current density of 60 mA/g and 240 mA/g, respectively.

3.6.2 C-rate Test Study for Si Electrodes with Different Conductive Carbon Combinations

Si half-cells (*vs.* Li/Li^+) including different carbon conductive mixture were cycled (BCS-805, BioLogic) between 10 mV and 1 V with a capacity limitation of 1200 mAh/g. The C-rate of C/20 was applied for a formation cycle, followed by cycling at different C-rates in the order of C/10, C/5, C/2, C and C/10. 10 cycle repeats were performed for each C-rate.

3.6.3 Electrode ImpedanceTtest

- ***Potentio Electrochemical Impedance Spectroscopy (PEIS) study***

To demonstrate improvements in conductivity by the incorporation of FLG, SPEIS test and PEIS test were carried out using a potentiostat cycler (VMP3, Bio-Logic).

The PEIS test was used to measure the impedance change as a function of cycle number. The test was conducted with a voltage amplitude of 10 mV, measured between frequencies of 500 kHz and 100 mHz at 50 % SoC of each cell. The first measurement was taken after the formation cycle with an additional 10 mins relaxation time and repeated with every 10 cycles.

Typically, the Nyquist plot of electrodes in a Li-ion battery contains two semi-circles and a diagonal line with a slope of ~45˚ to follow. It has been widely agreed that the intersection point of the X-axis refers to the series resistance, which includes electrolyte resistance, electronic resistance of the electrode as well as the contact resistance between the electrode and current collector[143], [144]. The first semi-circle represents the resistance when Li-ions are diffusing through the SEI layer, and the second refers to the charge transfer at the interface between the electrolyte and the active material. However, previous impedance studies on Si-based electrodes[145], [146] have suggested that interphase electronic contact resistance between the active

material and the current collector (which normally reacted at medium-high frequency range) should also be taken into consideration. The straight-line tail followed is referred to as Warburg impedance, which includes the diffusion impedance of Li ions within active material. Based on the EIS spectra of the electrodes in this study and the previous literature, the fitting equivalent circuit is shown in Figure 3-4. It consists of a resistor representing series resistance and is followed by a series of three resistors in parallel with a constant phase elements and a Warburg diffusion element at the end. They respectively account for the SEI resistance, interphase electronic contact resistance and charge transfer resistance.

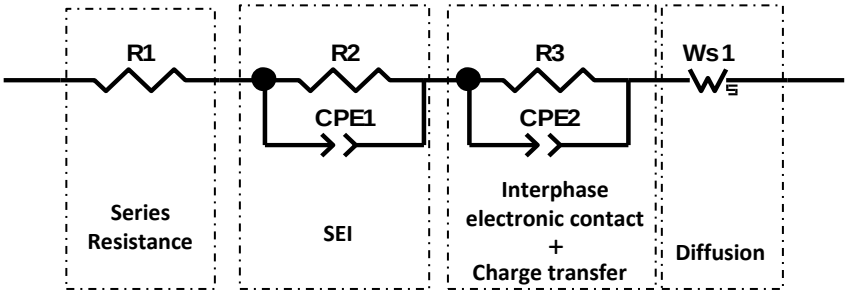

Figure 3-4 The equivalent circuit for fitting the impedance spectra

- ***Staircase Potentio Electrochemical Impedance Spectroscopy (SPEIS) Study***

The SPEIS test in this study measured impedance at different voltage steps within one cycle. Half-cells (*vs.* Li/Li^+) with Si-FLG, Si only and FLG only electrodes were charged and discharged using the same constant current mode and measured for every 10 cycles. SPEIS was conducted with a staircase potential swept from 1 V to 0.1 V with 20 steps (10 mins rest after reaching each voltage step) during lithiation, followed by another SPEIS measurement repeated from 0.1 V to 1 V during delithiation. The voltage profile is shown in Figure 3-5.

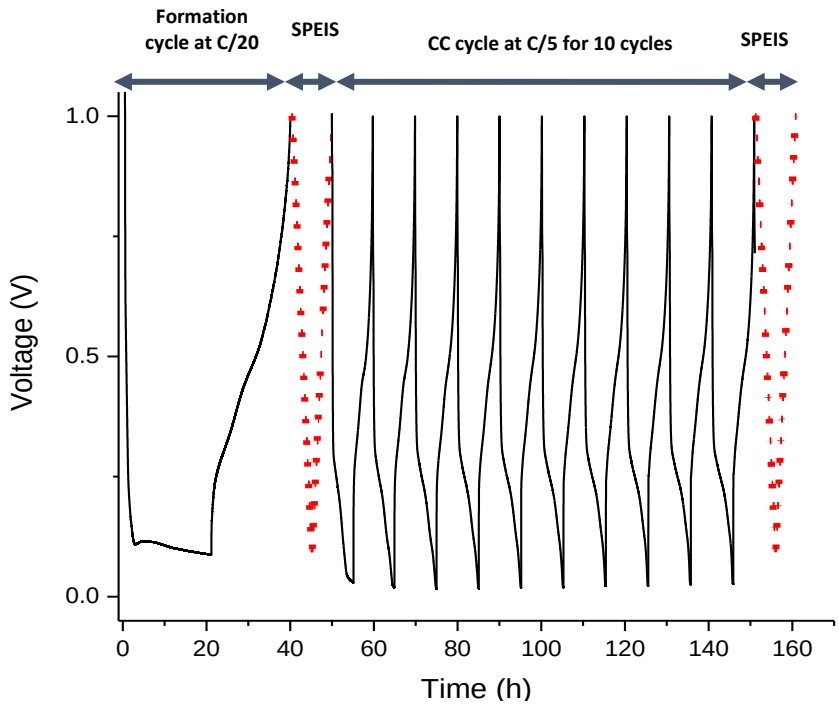

Figure 3-5 Continuous voltage profile for SPEIS test

3.6.4 Oxidative Stability Test for Electrolytes

The traditional method to test the oxidative stability of electrolytes was mostly conducted on inactive cathode materials such as Pt, stainless steel or glassy carbon. However, it was revealed that inactive cathode materials significantly affect the anodic decomposition limit of the electrolyte. Alternatively, galvanostatic cycling tests at very slow C-rate (less than C/100) on NMC half-cells (*vs.* Li/Li^+) were proven to be a more effective approach to verify the oxidative limitation for electrolytes[147].

Therefore, in this study, the oxidative limit for each electrolyte was investigated through NMC vs Li half-cells which were built through the method in Section 3.5.1. The half cells were cycled (BCS-805, BioLogic) and charged between 3 V to 5.5 V at a very slow C rate of C/110 to ensure the detection of reliable oxidation limits[147].

3.7 Post-mortem Characterisation

3.7.1 SEM Image for Cycled Electrodes

The cycled cells were dissembled in a dry room and rinsed with dimethyl carbonate (DMC), and followed the same procedure as stated above to obtain the SEM or cross-section SEM images.

3.7.2 X-ray Photoelectron Spectroscopy (XPS) Study

Surface compositional and chemical state analysis was carried out using x-ray photoelectron spectroscopy (XPS) measurements conducted on a Kratos Axis Ultra DLD spectrometer at the University of Warwick Photoemission Facility. Both pristine and cycled electrodes (anodes and cathodes) were investigated. For pristine electrodes, samples were mounted onto a copper bar with electrically conductive carbon tapes and transferred to the XPS facility under ambient atmosphere. The cycled electrodes were dissembled in an argon-filled glove box and rinsed with DMC. Afterwards, the samples were mounted on to copper stubs using electrically conductive carbon tapes and loaded into the instrument via an inert transfer unit under an argon atmosphere.

XPS measurements were performed in the main analysis chamber, with the sample being illuminated using a monochromated Al Kα x-ray source. The measurements were conducted at room temperature and a take-off angle of 90° with respect to the surface parallel. The core level spectra were recorded using a pass energy of 20 eV (resolution approx. 0.4 eV), from an analysis area of 300 microns x 700 microns. The spectrometer work function and binding energy scale of the spectrometer were calibrated using the Fermi edge and 3d5/2 peak recorded from a polycrystalline Ag sample prior to the commencement of the experiments. The data were analysed in the CasaXPS package, using Shirley backgrounds and mixed Gaussian-Lorentzian (Voigt) lineshapes. For compositional analysis, the analyser transmission function has been determined using clean metallic foils to determine the detection efficiency across the full binding energy range. The samples were found to charge slightly under the x-ray beam and to overcome this the samples were flooded with a beam of low energy electrons during the experiment. In turn necessitated charge referencing of the binding energy scale, with the C-C/C-H component of the C 1s region at 284.8 eV used as the reference energy.

In order to study the underlying transition metals on the cathode samples, the surfaces were sputtered using a monatomic argon ion beam with a beam energy of 4 keV. A 4x4 mm area of the surface was sputtered to ensure that subsequent XPS data were acquired from within the crater.

Chapter 4 Incorporation of Combined Carbon Hierarchies as the Conductive Network to be Applied in Si Electrodes

4.1 Introduction

As introduced in Chapter 2, conductive additive is one of the essential electrode component for Si electrodes, especially for charge/discharge process under high current density. This chapter investigates the performance for using different carbon materials combinations including carbon black (CB), graphite, few-layered graphene (FLG) and multi-wall carbon nanotubes (MWCNTs) as hierarchical conductive network to be incorporated into Si electrodes. Different carbon Carbon Blends formulations are listed in Table 3-1 of Chapter 3. Carbon black is used as the control conductive additive to compare with the hybrid conductive systems. Considering that the primary influence of the conductive additive for Si electrodes is to improve the discharge rate over cycling, the rate capacity (delithiation capacity for half-cells (*vs* Li/Li^+) cycling under different C-rate) and the long-term cyclability test under the C rate of C/3 were conducted and compared between different Carbon Blends formulations.

4.2 SEM Images

The structural hierarchy of different carbon materials could be clearly observed in the SEM images shown in Figure 4-1. For Carbon Blends 1 (Figure 4-1 (a)), it shows that carbon black particles are evenly distributed around large graphite chunks. While incorporating Carbon Blends 1 into Si electrodes (Figure 4-1 (b)), there can be an agglomeration of carbon black due to its substantial surface area and the surface adsorption effect, which could leave some Si particles uncovered with conductive

materials, thus reducing the transport rate of Li-ions in the electrode. Comparing to Carbon Blends 1, with additional FLG included, there are more connections between carbon black clusters in Carbon Blends 2, where FLG is working as the "bridge" to form extra electronic connections in this structure as well as the "separator" to break large carbon agglomerations. With these benefits, it can be noticed that in Si anodes with Carbon Blends 2, there are much fewer and smaller carbon black clusters, which indicate that there are more homogenously distributed regions around Si particles. Moreover, with Carbon Blends 2, carbon black provides short-range conductivity with graphite while FLG could provide long-range conductivity for Si particles due to its thin 2D structure and high aspect ratio. For Carbon Blends 3, it can be noticed that on top of graphite, MWCNTs appear like the fibres that connect single carbon particles within the network as well as build additional pathways between carbon black and graphite, which is supposed to make the electronic contact in this structure more stable. With Carbon Blends 3, both carbon black particles and MWCNTs are evenly dispersed around Si particles. Also, similar to the FLG in Carbon Blends 2, MWCNTs are working as the tiny "electronic cables" between Si and other composite materials, which can be regarded as the efficient electronic pathway within the electrode structure.

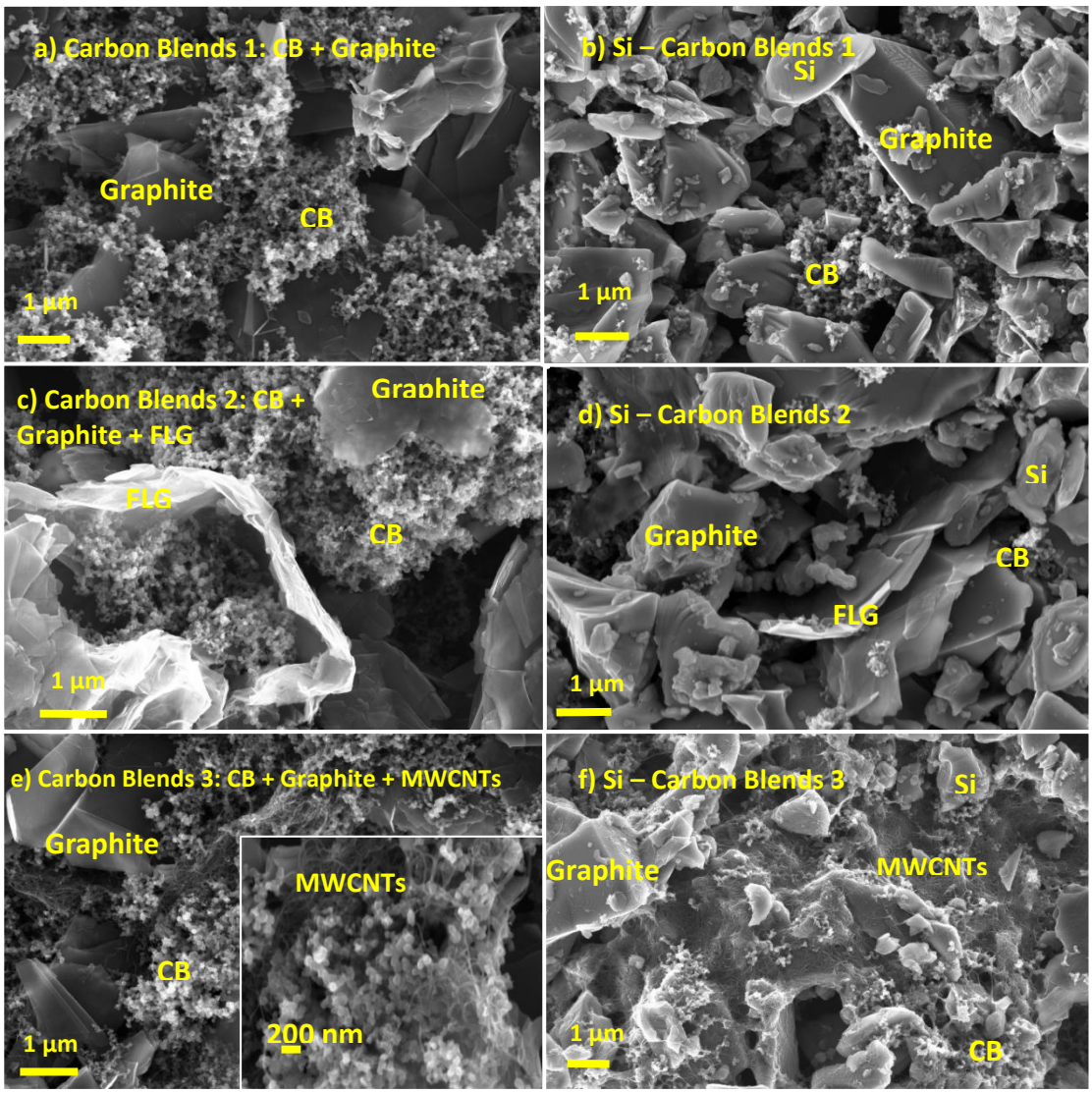

Figure 4-1 SEM image for dried Carbon Blends paste with different formulation (left) and pristine Si electrodes with different Carbon Blends (right).

4.3 Rate Capacity Test under Different C-rate

It can be observed from Figure 4-2 that under a C-rate of C/10 (120 mA/g) and C/5 (240 mA/g), all the Si half-cells (*vs* Li/Li^+) could maintain a stable delithiation capacity around 1200 mAh/g. When the C-rate increases to C/2 (600 mA/g), the capacity of Si electrodes with only CB dropped dramatically, continually decreasing from 1199 mAh/g to 626 mAh/g during 10 cycles. There is also significant capacity drop for Si-Carbon Blends 1 electrodes, which include CB and graphite, but the dropped capacity is maintained around 1010 mAh/g over 10 cycles. While for Si-Carbon Blends 2 and Si- Carbon Blends 3, there is no visible capacity change, maintaining stable around 1199 mAh/g. For a higher C rate at 1C (1200 mA/g), Si electrodes with both CB only and Carbon Blends 1 demonstrate a rapid and continuous

decrease over 10 cycles. The capacity of Si electrodes with Carbon Blends 2 also drops to the level of 1000 mAh/g but maintains relatively stable performance until the last three cycles. Whilst for Si electrodes with Carbon Blends 3, the capacity maintains the same stability at the higher C rate despite a small capacity decrease (to 1160 mAh/g) for the last three cycles. It also can be noticed that when the C rate gradually reduced to the previous low levels, the capacity can be restored for all Si electrodes, suggesting the capacity fading under high C rate within 10 cycles is mostly due to Si not sufficiently alloy with Li-ions under such fast charging rate other than electrode pulverisation. From these results, it can be concluded that with Carbon Blends 3, Si electrodes could best maintain the cyclability even under high current density up to 1200 mA/g. This is possibly due to the benefit from MWCNTs that worked as a more efficient electronic pathway between Si particles and other composite materials. While for Si electrodes with Carbon Blends 2, this also shows much better rate performance than for Si electrodes with just CB/graphite, which proves that with a conductive hierarchy network incorporated with CB/graphite/FLG, the electronic conductive efficiency has also been improved despite the cyclability under 1C which is not as good as those incorporating MWCNTs.

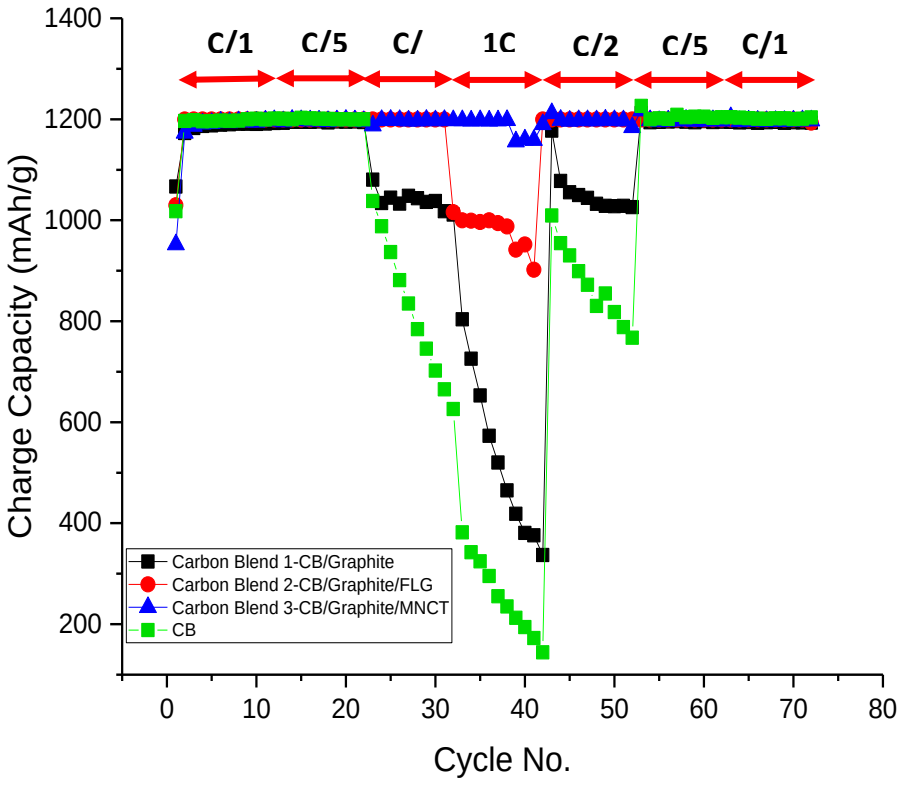

Figure 4-2 Rate capacity test for Si half-cells *(vs Li/Li⁺)* with different Carbon Blends.

4.4 Long-term Cycling Test under High C-rate

A C rate of C/2 appears quite challenging for Si-Carbon Blends 1 and Si-CB during rate testing, and so a slightly lower C rate at C/3 (400 mA/g) was applied for the long-term cyclability test. The results in Figure 4-3 show that under this higher C rate, Si-CB reversible electrochemical performance starts to drop from 36 cycles compared to Si-Carbon Blends 1 resulting in relatively longer cycle life, reducing after 93 cycles. Si-Carbon Blends 2 demonstrates much better cyclability compared with C-mix 1, maintaining stable performance at 1199 mAh/g for 152 cycles. It proves that with additional FLG incorporated into the conductive mixture, the cyclability for Si electrodes could be largely improved. Whilst Si-Carbon Blends 3 still displays the best cyclability among these four different types of electrodes, remaining at a delithiation capacity of 1196 mAh/g for over 170 cycles.

These results suggest that Carbon Blends 3 provides the most stable conductive network for Si electrodes that delivers the longest cycle life amongst the four electrode formulations, indicating that MWCNTs could not only improve the efficiency for Li-ion transfer within the electrode but also provide a more homogeneous lithiation/delithiation process. It also proves that the hierarchical carbon conductive system could largely improve the cyclability of Si electrodes compared with a single conductive additive. Here, more hierarchy exists within the network thus better performance under higher current densities can be achieved.

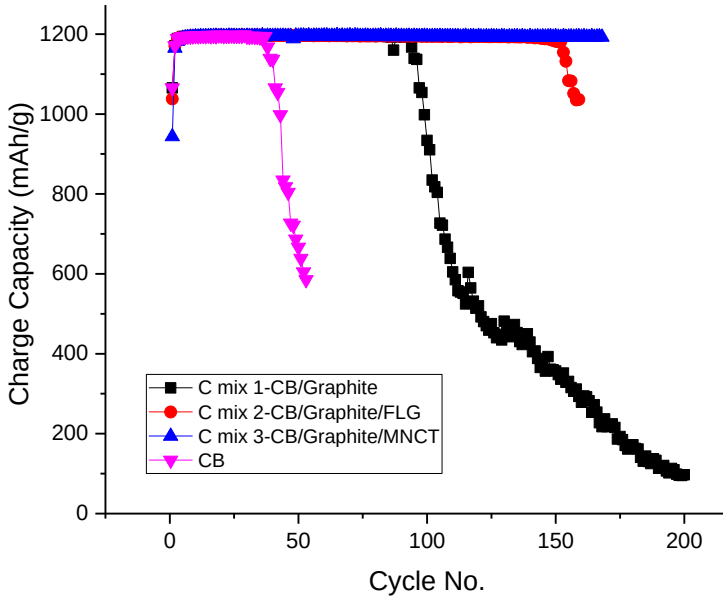

Figure 4-3 Long-term cycling performance for Si half-cells *(vs Li/Li⁺)* with different Carbon Blends under the C-rate of C/3

4.5 Viscosity Considerations to Verify the Feasibility for Scale-up Coating

As industry-relevant electrode formats as produced on a battery scale-up pilot line are applied for a later study, additional viscosity measurements have been carried out to verify whether Si formulations with these C combinations are applicable for the large scale coating equipment. For such a coating facility, the shear stress at rate of 10 /s is the critical value that should be taken into account. This is the roll speed rate for the reel-to-reel slurry coater on the electrode coating line and shear stresses above 15 Pa (symbolled as star in Figure 4-4) is recommended from the supplier of the coating line as applicable for large-scale coating. It can be observed from Figure 4-4 that Si-Carbon Blends 2 is well above this value whereas Si-Carbon Blends 1 is just over 15 Pa at the shear rate of 10 /s. This could be attributable to the FLG included into Carbon Blends 2, more solution was consumed to be solved particles with the increased surface area. For Si-Carbon Blends 3, the shear stress at 10 /s is only 11.4 Pa, which is below the recommended value for coating. This possibly also results from the large amount of additional water used to disperse the MWCNTs, plus when the binder solution is added, the slurry will be further diluted and this in turn results a low viscosity.

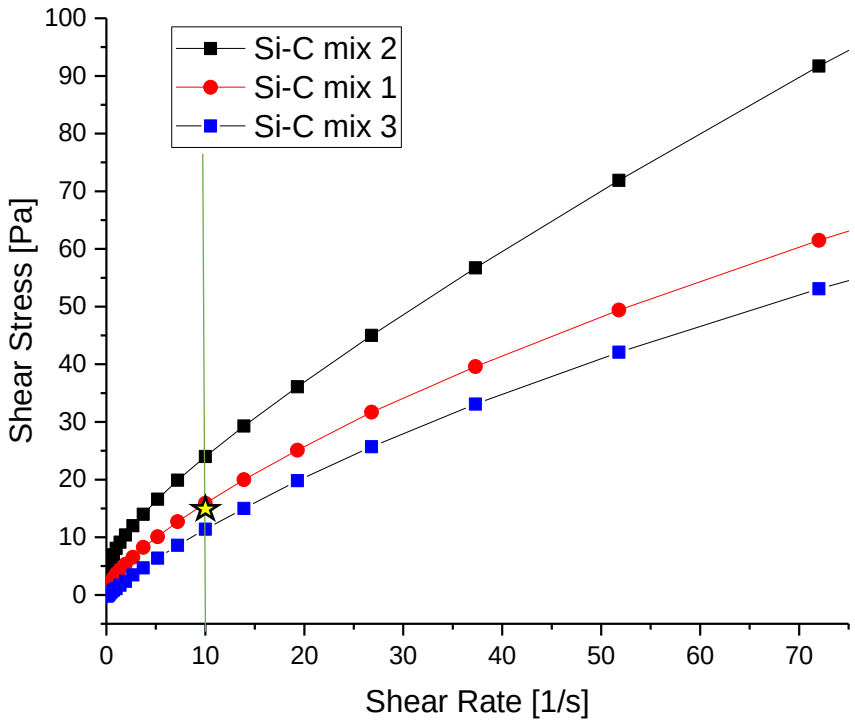

Figure 4-4 Viscosity measurements for Si slurry with different Carbon Blends (the yellow star refers to lowest viscosity limit for the slurry to be coated on the large coater).

4.6 Chapter Conclusion

This chapter compared the rate capacity and the long-term cyclability of Si electrodes with a variety of differing carbon combinations. It can be concluded that a multi-scale carbon mixture with a hierarchy structure could provide much efficient and stable conductive network for Si electrodes compared with single morphology conductive additives. The greater the hierarchy of conductivity, the better the rate capacity and cyclability that can be achieved. Among the Carbon Blends formulations that were investigated in this chapter, the Carbon Blends 3 that contains CB/graphite/MWNCTs demonstrate the best rate capability (1160 mAh/g under C-rate of 1C) and long-term cyclability under higher C rates (over 180 cycles stable at 1200 mAh/g). However, the viscosity results indicate that Si-Carbon Blends 3 synthesised with the default method used in this project is not applicable to a larger scale-coating facility for further study. To better apply Carbon Blends 3 into Si electrodes, a systematic study to optimise the manufacturing process parameters should be further carried out, but this is beyond the scope of this project. Therefore, Carbon Blends 2 that includes CB/graphite/FLG will be mainly applied for the following studies since it also indicated a much improved performance in terms of rate capacity and cycling stability compared with Carbon Blends 1 and single CB systems.

Chapter 5 Comprehensive Investigation into Si-FLG Hybrid Electrode Systems

5.1 Introduction

This chapter conducts in-depth research on interconnecting few-layer graphene (FLG) with Si, which is supposed to be a practical solution to enhance the cycling stability through the formation of a conductive, hierarchical and mechanically more robust microstructure[148]. The results demonstrate that the incorporation of FLG results in significant performance improvement in terms of cyclability, electrode resistance and diffusion properties. The Warburg diffusion impedance during Si phase changes, as well as the variation against cycle number, is elucidated through Staircase Potentio Electrochemical Impedance Spectroscopy (SPEIS): a more comprehensive and straightforward approach than the previous state-of-charge (SoC) based diffusion studies. Additionally, further characterisation of failure mechanism including tensile property test, post-mortem SEM imaging on cross-sections is conducted to give more evidence for the benefit of electrode structure change with the incorporation of FLG into Si electrodes.

5.2 Si-FLG formulation matrix study

The half-cell (*vs* Li/Li^+) cyclability of the Si-FLG electrodes using different formulations is shown in Figure 5-1. It can be observed from Figure 5-1 (a) that initially all half-cells are demonstrating a dramatic increasing. This can be explained by that with a fixed lithiation capacity, the delithiation capacity at first few cycles can be quite low due to the consumption of Li-ions to form the SEI. With the SEI layer becoming gradually stable, all half-cells are cycled stably at 1800 mAh/g specific lithiation capacity (based on the active mass of Si), but they fade dramatically at a certain point of cycling, which is generally referred to as the "roll-over" effect[149]. It can be caused by either electrode deterioration or the continued growth of the SEI layer on the surface of Si becoming thick enough to resist Li-ion penetration[150].

Figure 5-1 (b) shows that the cyclic coulombic efficiency profile, which increases after formation of the initial SEI layer and subsequently decreases due to the side reactions with electrolyte, continuously forming products such as lithium fluoride and lithium carbonate[151]. Amongst the matrix Formulation D, which contains the highest proportion of FLG (60 % Si: 16 % FLG: 14 % sodium-polyacrylic acid (Na-PAA): 10 % carbon mix), delivered the best performance in terms of cycle life and coulombic efficiency, with 80 % capacity retention after 230 cycles. It indicates that by incorporating FLG, the "roll-over" effect is significantly delayed, possibly due to the enhanced tensile properties from the FLG, which reduces the rate of the pulverisation of the electrode microstructure.

However, according to Figure 5-1 (c), it is obvious that with reducing mass ratio of Si in electrode, the specific capacity based on electrode mass is decreasing, indicating that Si still dominates the capacity contribution within the electrode. Additionally, in the plot of the specific capacity based on the mass of whole coin cell (Figure 5-1 d), it is found that the specific capacity becomes lower than 1 mAh/g. This result gives the fact that in the cell prototype of coin cell, the active mass for energy contribution only account for less than 0.05 wt% in the whole weight of the cell. To meet further requirement of industrialisation, a high content of active material in the cell is desired to increase the overall energy density. To address this issue, a thick coating and the pouch cell prototype may be favoured, but it requires further engineering study which is beyond the scope of this thesis.

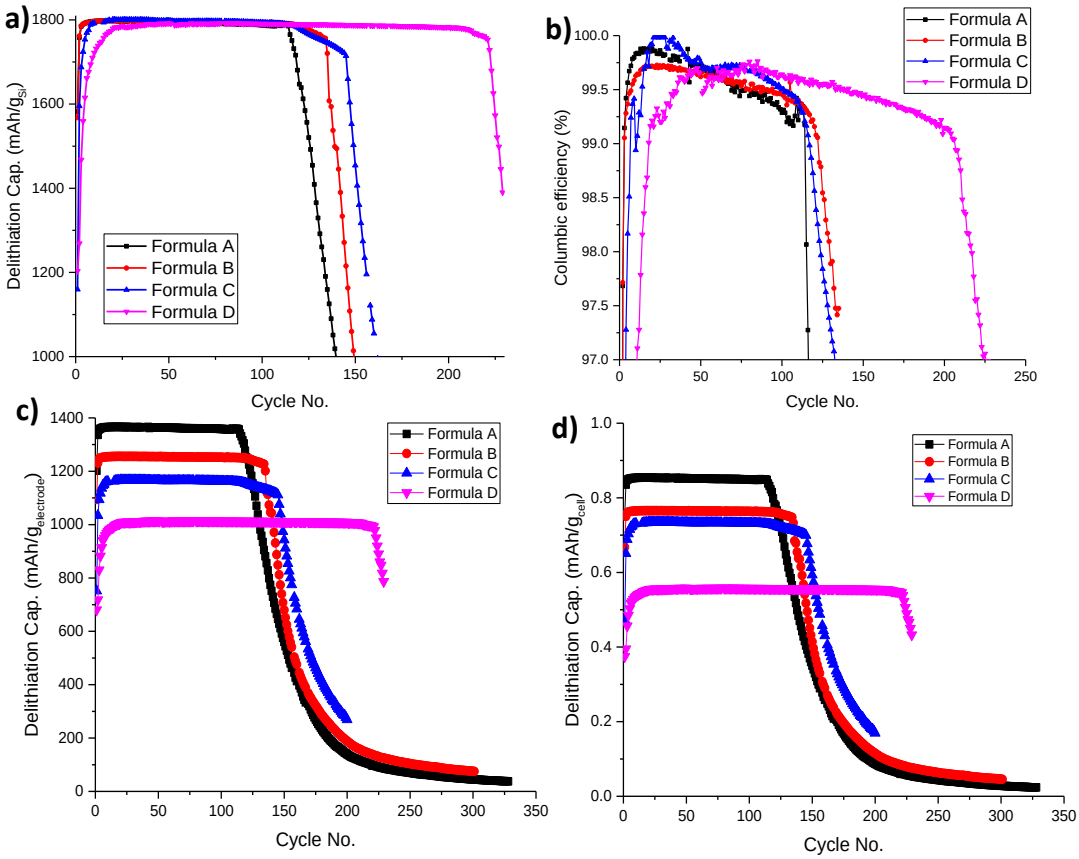

Figure 5-1 a) Half-cell *(vs* Li/Li$^+$*)* delithiation capacity based on the mass of Si, b) columbic delithiation efficiency under capacity limitation of 1800 mAh/g, c) half-cell *(vs* Li/Li$^+$*)* delithiation capacity based on the mass of electrode, and d) half-cell *(vs* Li/Li$^+$*)* delithiation capacity based on the mass of cell for Si-FLG formulation matrix (Formula A- 76 % Si: 0% FLG: 12 % Na-PAA: 12 % Carbon. Formula B – 70 % Si: 8 %FLG: 12 % Na-PAA: 10 % Carbon. Formula C – 65 % Si: 12 % FLG: 14 % Na-PAA: 9 % Carbon. Formula D – 60 % Si: 16 % FLG: 14 % Na-PAA: 10 % Carbon).

5.3 A further Comparison study between Si-FLG electrode and Si only electrodes

5.3.1 Mechanism of structural benefit and SEM image characterisation

Figure 5-2 shows the microstructure change for Si and Si-FLG composite electrode (Formula D, as specified in Table 3-2). Figure 5-2 (a) shows the mechanism of how FLG helps to mitigate the Si particles electrochemically alloying together through their SEI species. Figure 5-2 (b) shows that the particles in the Si-FLG electrodes (Formula D, as specified in Table 3-2) are evenly distributed, and have formed a hierarchical network between the Si, FLG and carbon black. Within this network, we suggest that FLG augments long-range planar conductivity while carbon black provides short-range conductive pathways between the graphene layers and Si particles.

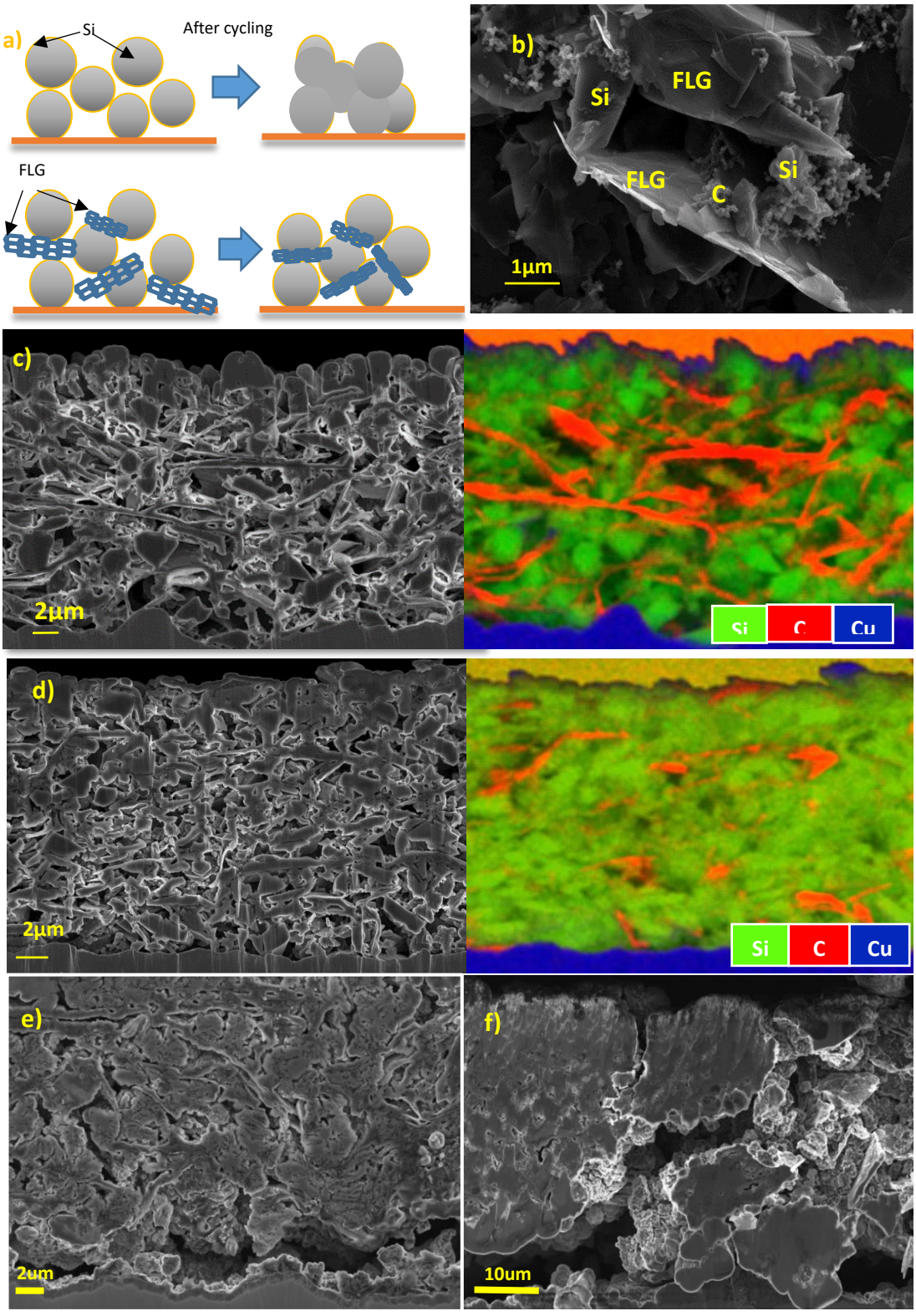

Figure 5-2 a) Schematic of FLG preventing Si electrochemically "fused" together; b) SEM image for Si-FLG electrode (60 % Si: 16 %FLG: 14 % Na-PAA: 10 % Carbon mix); c) Cross-section image and EDS mapping for Si-FLG composite electrode; d) Cross-section image and EDS mapping for Si only electrode; **e)** Cross-section image for Si-FLG electrode after 100 cycles and f) Cross-section image for Si only electrode after 100 cycles.

Cross-section SEM images and energy dispersive X-ray spectroscopy (EDS) mapping (Figure 5-2 (c)-(d)) show that by incorporating FLG into the Si-based anode, the

density becomes ~0.42 g/cm^3, which indicates a higher porosity in comparison with the Si-only electrodes, which have a density of ~0.75 g/cm^3. It can be observed from Figure 5-2 (e)-(f) that, in the Si-only electrode, Si particles are mostly agglomerated within larger Si masses with non-distinct boundaries. While for Si-FLG electrodes, Si particles remain separated by FLG sheets with particle size ranges consistent with the volume variations. The implication of this is that when Si particles become merged in this way then Li diffusion pathways are effectively increased in such regions, and particles deep within the fused areas may contain electrically isolated Li[152].

The structural benefit with the incorporation of FLG in Si electrodes can also be proved through the nano-indentation test. Hardness and modulus are calculated using data taken from the slope of the tangent to the unloading curve in Figure 5-3, and the value is summarised in Table 5-1. It can be observed from Figure 5-3 that during the nanoindentation test, the FLG electrode can be indented deepest, suggesting it is the softest electrode among these three. Si electrode demonstrates the smallest contact depth, indicating the electrode is quite rigid; while Si-FLG exhibits less hardness with larger contact depth. It can also be proved through the hardness value in Table 5-1. Whilst comparing the reduced modulus for these electrodes (Table 5-1), the modulus was significantly reduced through incorporating FLG into Si electrode, which refers to the enhancement of electrode flexibility.

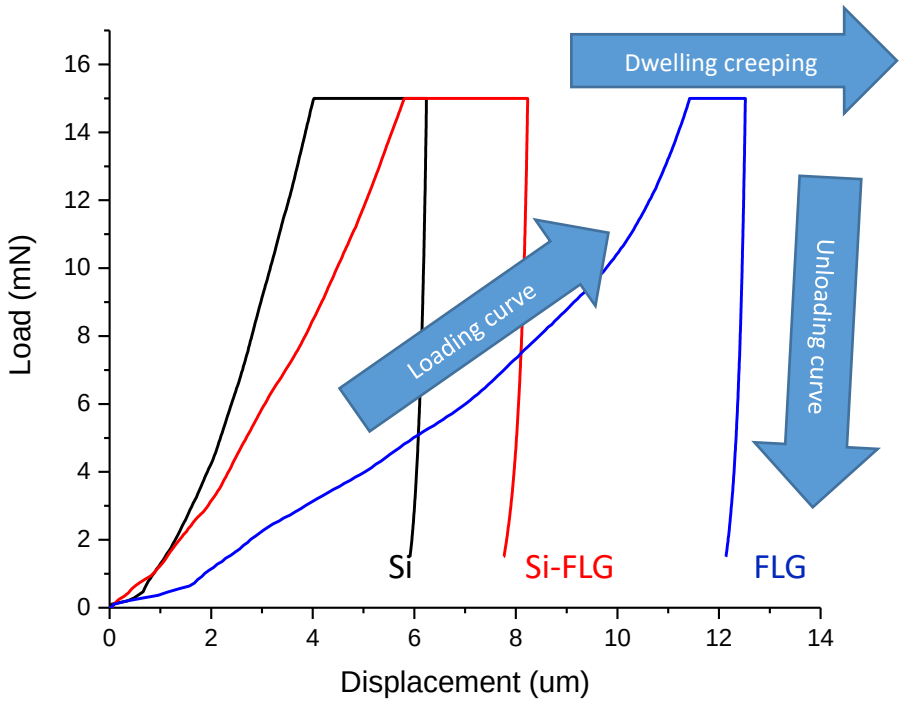

Figure 5-3 Tensile curves from the nanoindentation test

Table 5-1 Maximum contact depth, hardness and Young's modulus achieved from the nanoindentation test

Sample	Maximum Depth (um)	Hardness (GPa)	Reduced Young's Modulus (GPa)
Si	6.22±0.33	0.016±0.002	2.38±0.19
Si-FLG	7.75±0.84	0.010±0.002	1.42 ±0.27
FLG	12.37 ± 0.93	0.004±0.001	1.06±0.11

5.3.2 Capacity contribution from FLG

To investigate the capacity that FLG can contribute within this voltage range, Si-FLG (Formula D) was compared with Si only (76% active mass) and FLG only (76% active mass) under the same current density and without capacity limitation. The comparison of the first cycle voltage profile for electrodes based only on Si only, Si-FLG and FLG only are shown in Figure 5-4. It indicates that with the same current density of 90 mA/g and 5 mV cut-off voltage, the FLG only electrodes (76 % active mass) deliver a maximum contribution of around 330 mAh/g for the first cycle, with a substantial initial capacity loss of about 180 mAh/g. The capacity achieved by the FLG-only electrodes is much lower than the result in a previous study[148], and this could be due to the current density (90 mA/g) being significantly increased during the first cycle. The large initial capacity loss is attributable to the surface area of FLG, resulting in large quantities of lithium ions becoming irreversibly consumed in the SEI layer. For the following cycles at C rate of C/5 (360 mA/g), the delithiation capacity of FLG-only electrode can be only maintained below 50 mAh/g. It indicates that with such high current density in Si-FLG electrode, the capacity contribution from FLG can be neglectable, which agrees with previous result in Figure 5-1 (c).

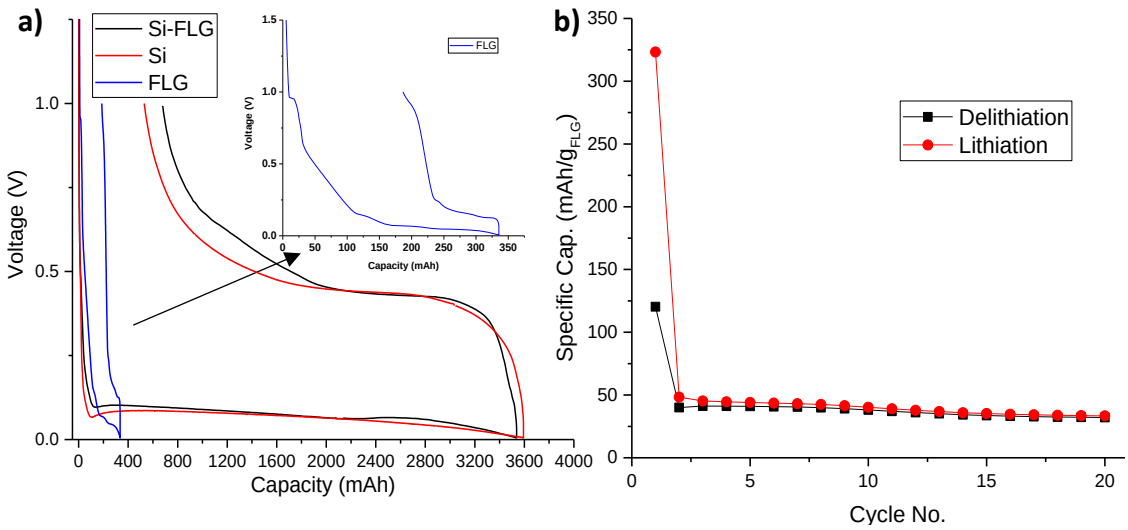

Figure 5-4 a) First cycle voltage profile for half-cells (*vs* Li/Li$^+$)of Si-FLG with Formula D, Si only and FLG only electrodes cycled between 1 V-5 mV without capacity limitation; b) long-term cyclability of FLG only electrode.

5.3.3 Differential capacity analysis

The differential capacity (dQ/dV) plots of Si only and Si-FLG half-cells for different cycle numbers are shown in Figure 5-5. The peaks during the (de)lithiation process correspond to different phase equilibria of Li_xSi. It can be observed from Figure 5-5 that Si-only and Si-FLG electrodes have similar dQ/dV quasi-plateaus, outlined in Table 5-4[12], [148], [153], but the plateaus for Si-FLG electrodes are broader compared to Si-only electrodes. It relates to the quasi-plateaus for Si and FLG components within the electrode overlapping with each other. It can further be seen that for the Si only electrodes, there are apparent reductions in lithiation plateaus and voltage shift around 0.25 V during lithiation and around 0.5 V during delithiation after 50 cycles. It is observed that at this point plateaus become single plateaus for both lithiation and delithiation process. This is possibly related to the resistance on the surface of the electrodes is increased due to the thicker SEI layer, resulting in an increase in overpotential, which delays the lithiation process. In this case, with the 5 mV cut-off voltage limitation, Si electrodes cannot be further lithiated to a-$Li_{3.5}Si$[154]. For the Si-FLG electrodes, there are no noticeable plateau reductions or peak shifting. It supports the observation that Si-FLG composite electrodes show a longer cycle life and reduced voltage hysteresis due to lower resistance, compared with electrodes based only on Si as the active material.

Table 5-4 Corresponding phase change at voltage peaks[12], [148], [153]

Process	Peak voltage	Phase change (after 2nd cycle)
Lithiation	0.25 V	a-Si → a-$Li_{2.0}$Si
	0.1 V	a-$Li_{2.0}$Si → a-$Li_{3.5}$Si
	≤50 mV	a-$Li_{3.5}$Si → c-$Li_{15}Si_4$
Delithiation	0.25 V	a-$Li_{3.5}$Si → a-$Li_{2.0}$Si
	0.5 V	a-$Li_{2.0}$Si → a-Si
	0.45 V	c-$Li_{15}Si_4$ → a-$Li_{1.1}$Si

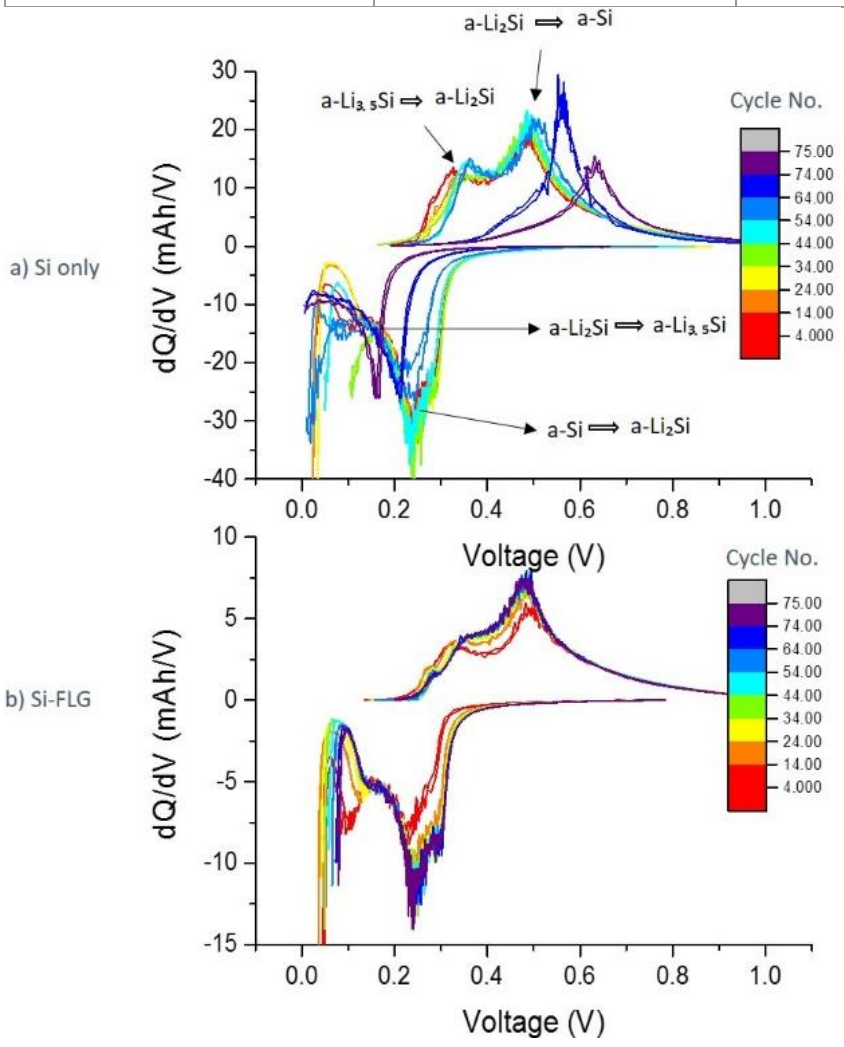

Figure 5-5 dQ/dV plot for cycle 2-60 of (a) Si only electrodes (b) Si-FLG electrodes

5.3.4 Potentio Electrochemical Impedance Spectroscopy (PEIS) study

Figure 5-6 (a)-(c) shows the impedance spectra for the Si-FLG half-cells for different cycle numbers, and Figure 5-6 (d)-(f) compares the fitting results over numbers of cycles between Si only and Si-FLG half-cells based on the equivalent circuit (Figure 3-4). It can be seen that for Si-FLG half-cells from the 1st to 20th cycle, there is a small semicircle related to SEI-derived resistance, but a clear decrease for the second semi-circle that relates to charge transfer resistance. This is in agreement with previous

studies[145] and has been explained by the volume expansion of Si, causing the electrode to be pressurised by the spring inside the coin cell. It results in a better electrical contact between the active material/binder system and the current collector, leading a decrease of interphase electric contact resistance. From the 20^{th} to 50^{th} cycle, it is observed that the series resistance starts to increase, indicating that the ionic conductivity of the electrolyte or electronic conductivity through electrodes or current collector becomes reduced. In the meantime, the SEI-related semicircle increases gradually, which is caused by the growing SEI layer. The increasing SEI is consistent with the growing series resistance because the thicker SEI arises the microstructural changes in the electrode and gradually blocks the electrolyte channels. It is feasible that the electrochemical fusion of Si particles through SEI species or decomposition of the electrolyte is likely phenomena here, suggesting the increase in tortuosity for Li movement and longer diffusion pathways [152]. The interphase contact and charge transfer resistance remain stable, but after the 50^{th} cycle, the SEI resistance grows dramatically, which indicates an inhibited transport of lithium ions through this layer.

Comparing the composite Si-FLG with the Si-only electrodes, Figure 5-6 (d) shows that generally, the Si electrodes show a higher series resistance than Si-FLG, which grows more dramatically during subsequent cycling. This is because, without the FLG, Si particles are more likely to be developed into an electrochemically welded state during cycling, as outlined previously. Thus it becomes more difficult for Li ions to access the surface of Si particles[152]. As the FLG facilitates and maintains Si particle separation in electrodes, the electrolyte channels remain unobstructed. Additionally, since the series resistance is defined by the internal electronic resistance of the electrode, a lower series resistance here indicates enhanced electronic pathways inside the electrode. From Figure 5-6 (e) initially, the Si-FLG electrodes display a more massive SEI resistance than the Si electrodes due to a larger surface area. After 50 cycles, the SEI resistance increases significantly for both electrodes, caused by continual electrolyte decomposition. The relatively slower growth of SEI resistance in Si-FLG may reflect on there being proportionally less Si in Si-FLG electrodes. The SEI layer of FLG is quite stable during (de)lithiation, which improves the general performance stability of the electrode. Figure 5-6 (f) shows the trend for interphase electronic contact and charge transfer for both electrodes (with similar performance), as explained previously.

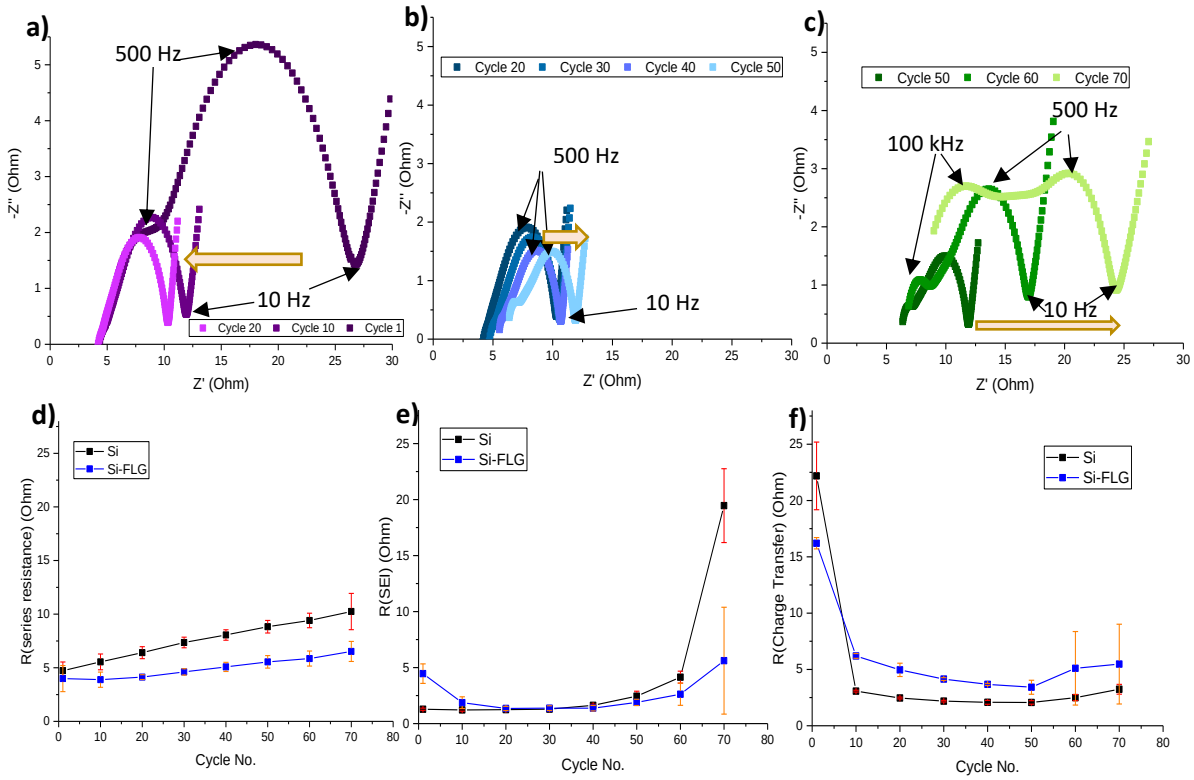

Figure 5-6 Nyquist plots of Si-FLG half cells (*vs* Li/Li^+) at 50 % SoC during charge process from (a) cycle 1 to cycle 20; (b) cycle 20 to cycle50; (c) cycle 50 to cycle 70; impedance fitting result comparison of (d) series resistance (e) SEI resistance (f) interphase contact and charge transfer resistance

5.3.5 Staircase Potentio Electrochemical Impedance Study (SPEIS)

To further investigate the diffusion resistance, SPEIS study has been conducted, which focuses on the impedance variation as a function of a voltage and, by splitting the frequency range, makes it more straightforward to investigate the low-frequency impedance (including the diffusion related Warburg impedance.) Figure 5-7 (a) and (b) show the SPEIS result for the Si-FLG electrodes (Formula D) following the formation cycle for lithiation (Figure 5-7 (a)) and for delithiation (Figure 5-7 (b)). In each graph, there are selected frequency ranges from 1 Hz to 500 kHz. As marked in Figure 5-7 (a)-(c), high-frequency impedance responses (at 10 kHz to 500 kHz) are attributable to the SEI resistance and the series resistance (highlighted green areas in Figure 5b). Impedance responses between 10 Hz and 10 kHz (orange area) represent the interphase electronic contact and the charge transfer resistance. Impedance responses with frequencies less than 10 Hz (blue area) are termed as Warburg impedance, which is mainly determined by diffusion coefficient, is also termed as Warburg diffusion impedance in this study[155].

Figure 5-7 (a) shows that during the lithiation process, the impedance values under the high AC frequency range (series and SEI resistance) remain stable throughout the voltage range, which is in agreement with previous findings[156], [157]. This is because the conductivity of the electrolyte does not change significantly and there is no pronounced decomposition of the electrolyte. Whilst the interphase contact and charge transfer resistance is reasonably stable - starting from 1 V and reaching 0.25 V - it increases at voltages below 0.25 V. This relates to the Si phase change from a-Si to a-Li_2Si and affects the exchange current density, which is a materials-dependent parameter that determines the charge transfer resistance. For the Warburg impedance, there is an initial increase followed by a sizeable decline becoming stable at around 0.25 V. The initial increase is because possibly after the first cycle, the relaxation time (10 minutes) is insufficient to ensure that all the Li^+ has left the Si electrode. The remaining Li^+ provides additional resistance for the subsequent lithiation process. The diminished diffusion resistance may be explained by the Si phase change during the (de)lithiation process. Initially, Si particles mostly exist as “cage-like” crystalline structures, which largely constrain the movement of Li atoms. As the c-Si is lithiated to a-Li_2Si, more and more Si-Si bonds are broken, which release the constrained Li atoms, thus reducing the resistance of Li diffusion. This process has been investigated and clarified by Key *et al*. in an NMR study[12] and other SoC-based diffusion studies on Si, concluding similar results[158]. Additional evidence is the “stopping point” for Warburg diffusion impedance decreases, occurring at around 0.25 V, and coincident with the first lithiation plateau in the dQ/dV plot, representing the phase change equilibria.

For the delithiation process, the trends in the impedance data are similar in reverse to those in the lithiation process, and the "starting point" of the impedance increase (around 0.6 V) relating to the plateau of delithiation in the dQ/dV plot. It refers to the growth of Si clusters. Additionally, the Warburg diffusion impedance after 0.6 V is lower during the delithiation process as compared with lithiation. It is because by following the Si lithiation to an amorphous phase from crystalline during the first cycle, Si will be only delithiated to an amorphous phase in the subsequent cycles (never reverting to crystalline[12]). These results indicate that the impedance variation is highly phase-change correlated.

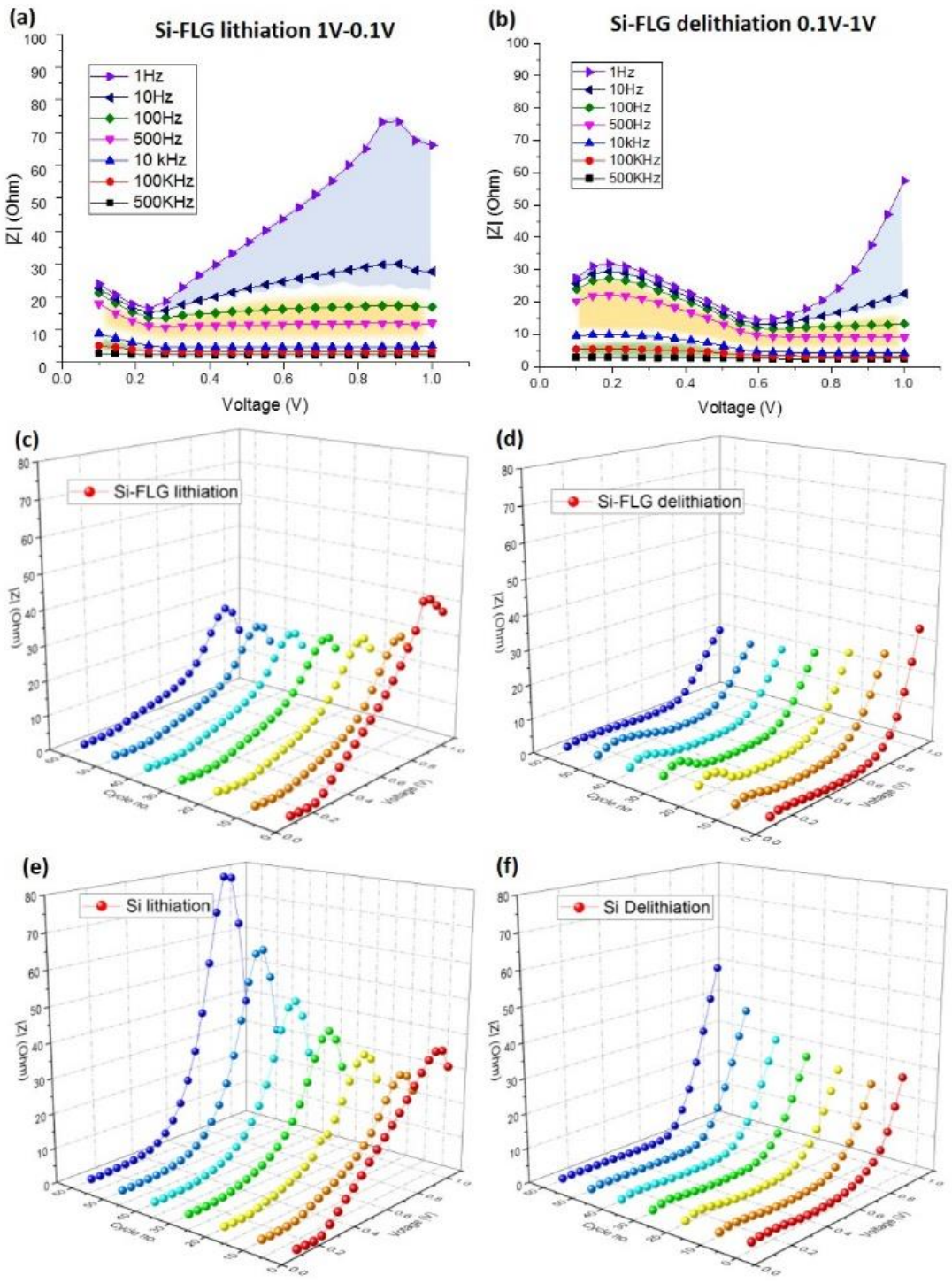

Figure 5-7 SPEIS result of Si-FLG after the first cycle for (a) lithiation process and (b) delithiation process; Warburg diffusion impedance at 1 Hz for Si-FLG (c) during lithiation and (d) delithiation process, and for Si (e) during lithiation and (f) delithiation process.

Additionally, it can be concluded from Figure 5-7 (a) - (b) that it is preferable to take the cyclic PEIS measurement above 0.25 V during the lithiation process because the impedance value under medium and high frequencies is quite stable with a large enough window to account for the voltage shift during cycling. We mainly use PEIS

studies to compare the cyclic series resistance and charge transfer resistance to better understand the degradation mechanism - which occurs in the medium and high range frequency. A stable impedance value within this frequency range is thus essential (despite voltage variability), but previous impedance studies on Si have rarely addressed this issue.

Figure 5-7 (c)-(f) compares the SPEIS result under 1 Hz (the blue area which represents the Warburg diffusion impedance), from Cycle 1 to Cycle 60 for both the Si-FLG and Si only electrodes. It is clear that both electrodes have a similar impedance variation trend against the voltage, but the peak of Warburg diffusion impedance for Si-FLG electrodes is smaller than that of Si-only electrodes after 20 cycles. Due to the poorer cycling performance and more significant voltage hysteresis for the Si only electrodes, it is more likely to drop further below 50 mV to reach a capacity of 1800 mAh/g. In this case, more metastable c-$Li_{15}Si_4$ will be formed in the Si-only electrodes (compared with Si-FLG), which is more resistant to delithiation back to a-$Li_{1.1}Si$ due to more tough Si-Si bonds[12]. As the pulverisation of the electrode progresses, it is possible that some Si clusters become isolated from subsequent lithiation processes, thus further contributing to the capacity loss.

From cycle 1 to 10, the peak diffusion resistance for both electrodes becomes primarily decreased. According to the voltage profile in Figure 3-5, the lithiation in the first cycle has been cut off at around 0.1 V, by which point there could be some crystalline Si remaining within the electrode. Therefore, for the first SPEIS measurement after cycle 1, the remaining crystalline Si clusters are involved in the lithiation process, which shows relatively high Warburg diffusion impedance. After an additional 10 CC cycles, for the second SPEIS measurement, the Si clusters are mostly lithiated to amorphous phases, which are less resistant to diffusion. It can explain why there is more diffusion resistance in the 1st cycle than in subsequent cycles.

5.4 Chapter Conclusion

This chapter comprehensively investigated the performance of Si-FLG composite electrodes, manufactured by an industrially relevant methodology. Electrochemical evaluation and phase-related impedance spectroscopy were the main investigative tools. The reversible electrochemical performance has demonstrated that by incorporating FLG into a high mass % content of Si, the cyclability is largely improved (the best cyclability can be maintained at 1800 mAh/g for 220 cycles with

incorporation 16 wt% FLG). Also, it was shown that FLG could contribute a capacity of around 300 mAh/g under the high limited capacity condition (1800 mAh/g). We recommend that the ratio of FLG to Si needs to be limited due to the significantly large first cycle loss relating to the large surface area of the FLG.

With PEIS and SPEIS, it was shown that FLG helps Si to maintain an overall lower series resistance during cycling. It could also confer performance benefits through some prevention of the Si particles from agglomerating though electrochemical fusion – but this phenomenon warrants further systematic investigation. Additionally, the improved cyclability of Si-FLG keeps the internal Warburg diffusion impedance at a relatively stable level. Combining the dQ/dV analysis with SPEIS, this study has addressed that the Warburg diffusion impedance in Si is highly phase dependent. On the other hand, it indicates that SPEIS could be a more straightforward method to study the change of Warburg diffusion impedance with different voltage as well as to investigate the Warburg diffusion impedance as a function of cycle number. Finally, the SPEIS results suggest that for the Si-based electrodes, a voltage range with a stable impedance is essential and so it is more reliable to take the PEIS measurement above 0.25 V during the charging process.

Chapter 6 Develop a Robust Polymer Binder Systems for Si Electrodes

6.1 Introduction

This chapter investigates several novel binder systems for Si electrodes, aiming to improve the binder property especially in terms of tensile strength and adhesion force so that it can better tolerate the large volume expansion of Si. As indicated in Chapter 2, for single binder systems, PAA demonstrates much better performance than other common polymers such as CMC and PVdF. Therefore Si electrodes with PAA is used as the baseline for further improvement. Approaches applied in this chapter include optimising single binder system through partially neutralising PAA, improving the tensile property of PAA by synthesising PAA-based binary polymer system (e.g. PAA/PVA, PAA/SBR) and fabricating PAA-based self-healing polymer through designing multi-level crosslinked polymer network (FLG-Fe^{2+}-PAA). For each polymer system, comprehensive studies have been conducted to verify both mechanical property and electrochemical behaviours.

6.2 Partial Neutralisation Effect of PAA

6.2.1 FTIR Measurement of Polymer Films

It can be observed from Figure 6-1 that the absorbance signal of C=O region (around 1700 cm^{-1}) is reduced after partial neutralisation, and the same as the C-OH band (between 1170 to 1240 cm^{-1}), indicating the reduction of the carboxyl groups. In the meantime, the absorbance peak attributed to the sodium carboxylate (at 1550 cm^{-1}) is formed from the ionic interaction of the residual group during neutralization[98]. Moreover, the absorbance of OH stretching band is a broad peak from 3240 to 3380 cm^{-1} for NaPAA, while for un-neutralised PAA, it is a variable double peak between 3000 and 3460 cm^{-1} and overlapped with the CH stretching band at 2920 cm^{-1}. Typically, the breadth of the O-H peak indicates the distribution of alcohol group in

carboxyl within PAA[159]. The shift of the O-H absorbance peak to a higher wavenumber level suggests that with neutralising PAA the polymer chain has been stretched rather than aggregated together, and in this case, more free carboxyl groups have been exposed to be able to form the covalent bond with the surface of Si particles. The deformation of inter-chain hydrogen bonds in NaPAA, stretching at 800 cm^{-1}, can be another evidence of stretching of polymer chains[160]. These results agreed with the statement in the previous study that with partially neutralising, the polymer chain within PAA will be extended and stretched, which will present more active carboxyl group[77].

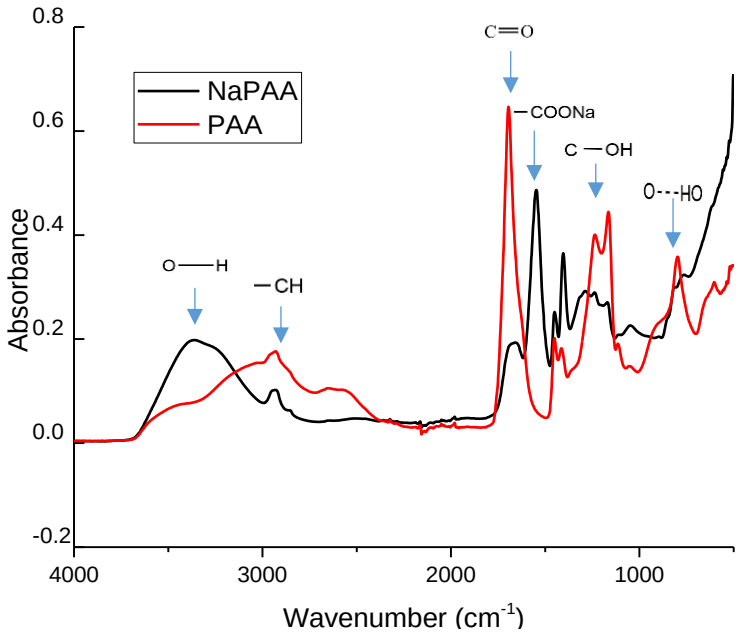

Figure 6-1 FT-IR analysis results for NaPAA and un-neutralized PAA

6.2.2 Swelling Test of Polymer Binders

Figure 6-2 compares the weight gain ratio between NaPAA and un-neutralized PAA during the swelling test, which indicates the electrolyte uptake. It shows that the final electrolyte uptake for NaPAA is about 5%, while the ratio for un-neutralised PAA is only accounting for 3.5%. The improved swelling ability of NaPAA could also be a result from extended polymer chain morphologies with increased free carboxyl groups. This higher electrolyte uptake in NaPAA implies a better transportation efficiency for Li^+, which is beneficial for achieving high capacity and power performance[161].

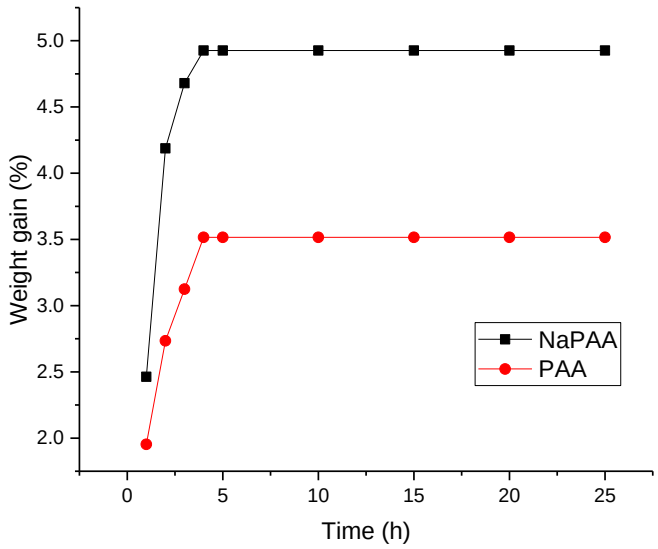

Figure 6-2 Swelling test result for NaPAA and un-neutralized PAA

6.2.3 Tensile Test Result Characterisation

The stress-strain curve from polymer tensile test can be an effective method to evaluate and compare the tensile property of polymer films. The result (Figure 6-3) shows that NaPAA expresses more substantial tensile strength (62 MPa) and a larger elastic region, which refers to a better modulus of resilience. Moreover, NaPAA displays a significant extension prior to the breakpoint, which provides a large strain range for plastic deformation. On the contrary, un-neutralized PAA shows much lower local tensile strength and the absence of plastic region make it more "fragile" than NaPAA. This indicates that after introducing Na^+, the stretched polymer chains can align together and provide stronger tensile strength. These results also suggest that NaPAA could be more tolerant, regarding elastic and plastic deformation, during the significant volume change of the Si electrodes.

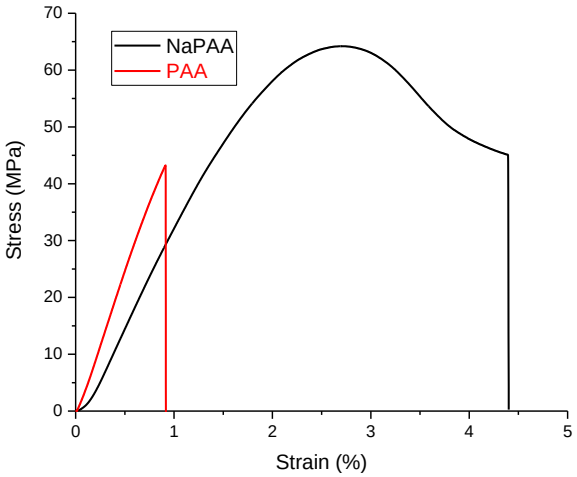

Figure 6-3 Tensile test result to compare NaPAA and unneutralised PAA.

6.2.4 Electrode Adhesion Test

The adhesion test results show that with applying a pull-up velocity of 100 mm/min after 10 s dwelling time, all electrodes are demonstrated cohesion failure in the coating. The positive part is considered as the recovering force from the compression, and the negative part is regarded as the internal adhesion force of the electrode. From Figure 6-4, it is clear that for the same size electrode, the maximum adhesion force for the electrode with NaPAA is 71 N, which is more than twice of the maximum adhesion force for the one with un-neutralised PAA (31 N). It means NaPAA could be more effective to suppress the pulverisation of the electrode and help to maintain the electronic network between active materials and conductive carbons.

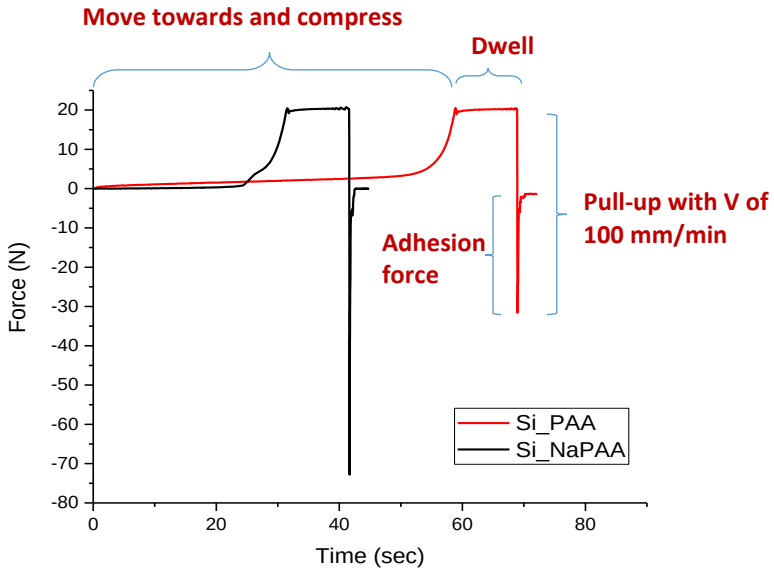

Figure 6-4 Adhesion test results for Si electrodes with NaPAA (black) and un-neutralized PAA (red)

6.2.5 Electrochemical Performance of Electrodes

Cycling performance of half-cells (*vs* Li/Li^+) (Figure 6-5) indicates that the Si electrodes with partially neutralised PAA can achieve much better cycle life, which keeps stable for over 100 cycles, while for the Si electrodes with un-neutralised PAA, it starts to fade from 40 cycles. This is because possibly the Si electrodes with un-neutralised PAA loses electronic contact between active materials and conductive network due to the polymer deformation during Si volume exchange as discussed in previous tensile property results. Additionally, as a result of poorer adhesion strength of un-neutralised PAA, the Si electrodes are more likely to suffer from pulverisation and worse cyclability. Moreover, the better electrolyte uptake of NaPAA also

contributes to the better cyclability through facilitating the Li ions transporting within the electrode.

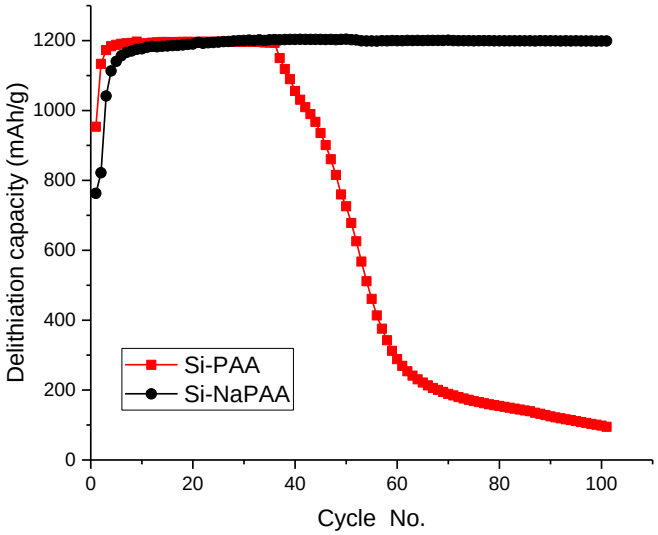

Figure 6-5 Cycling performance of half-cells (*vs.* Li/Li^+) for Si electrodes with un-neutralized PAA and partially neutralised PAA.

6.3 Investigation on PAA/PVA Blends as the Binder System for Si Electrodes

6.3.1 Optimising Weight Ratio between PAA/PVA

The tensile testing results for PAA/PVA blends with different PAA/PVA weight ratios are shown in Figure 6-6. The ratio 60/40 for PAA/PVA shows the highest tensile strength and Young Modulus, with optimal flexibility, which will be further studied as a binder material.

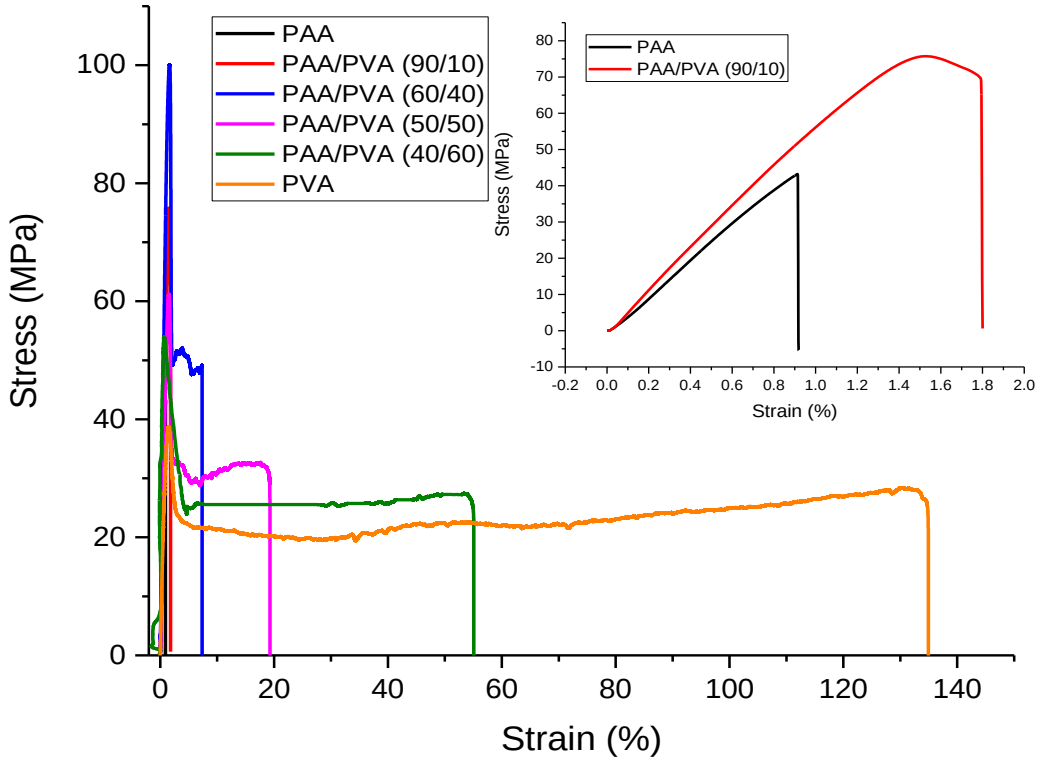

Figure 6-6 Comparison of tensile stress-strain curves for PAA/PVA with different ratios.

6.3.2 Optimising Heat-treatment Conditions

The PAA/PVA (60/40) blend was further heat-crosslinked at 150 ˚C and 200 ˚C, respectively, to optimise the heat-treatment condition. It was observed in Figure 6-7 that the PAA/PVA film did not show noticeable colour change after compress-moulded at 150˚C for 30 mins, but it turned from transparent to a brown colour after being heated to 200˚C, indicating polymer degradation. Similar results were observed for pnPAA/PVA films, which showed a lighter brown discolouration than the heated PAA/PVA. The polymer degradation is characterised by FTIR. As shown in Figure 6-8, after heating to 200 ˚C, the peak intensity for –CH stretching at 2920 cm^{-1} was reduced while the peak intensity for diene bonds (around 1700 cm^{-1}) became stronger compared to that heat to 150˚C. It indicates that there are polymer chain scission and the formation of smaller molecules with carbon-carbon double bonds. Therefore, to exclude the polymer degradation effect, 150 ˚C was chosen as the heat-treatment condition for Si electrodes in this study.

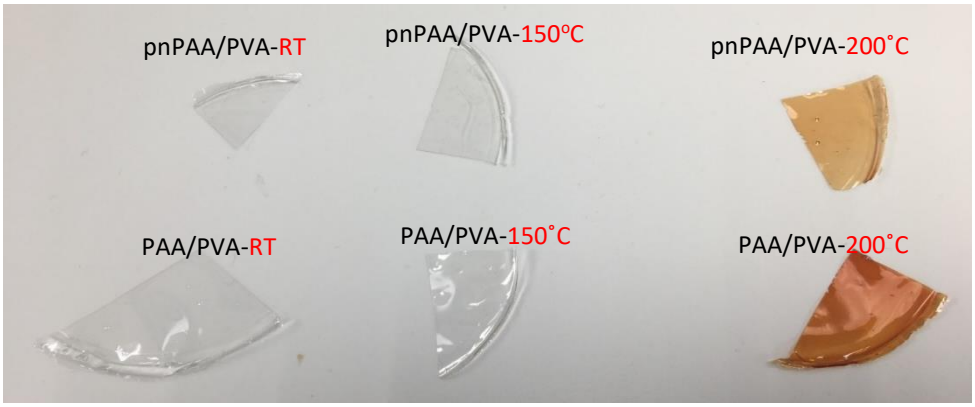

Figure 6-7 Polymer film comparison with different heat treatments

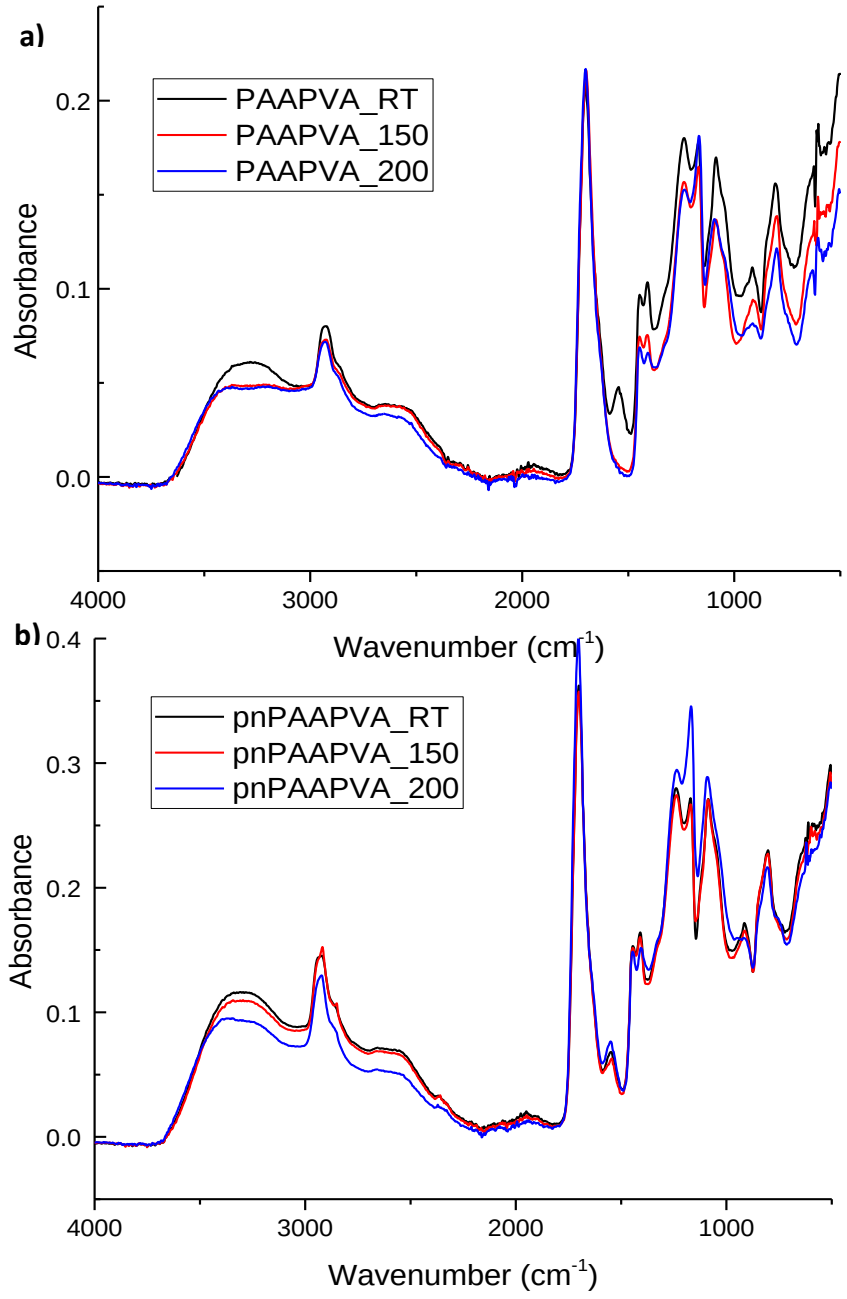

Figure 6-8 FTIR for a) PAA/PVA and b) pnPAA/PVA after different conditions of heat-treatment

6.3.3 Cross-section SEM Imaging

It can be observed from Figure 6-9 that particles are evenly distributed with reasonable porosity for all three pristine electrodes with different binders. After 70 cycles with the capacity limitation of 2000 mAh/g, all three electrodes demonstrate less porosity compared with the pristine ones. This is because during cycling, Si particles are likely to be electrochemically "welded" together, facilitated through the interaction of SEI species (e.g. Li_xSiO_y and insoluble polymers)[152], [162]. For Si-PAA electrodes, there is also apparent electrode pulverisation and separation from the current collector, which indicates that it is a challenge for pure PAA to maintain the electronic contact between the electrode and current collector over long cycling under such high current density. Whilst for Si-PAA/PVA and Si-pnPAA/PVA, there is no such obvious pulverisation observed. Also, the cycled Si-pnPAA/PVA maintains a high degree of porosity after 70 cycles compared with the cycled Si-PAA/PVA. It could support that pnPAA/PVA is a stronger binder which could reduce the rate of the pulverisation of the electrode microstructure as well as the generation of new SEI layers, thus to mitigate the Si fusion through growing SEI species.

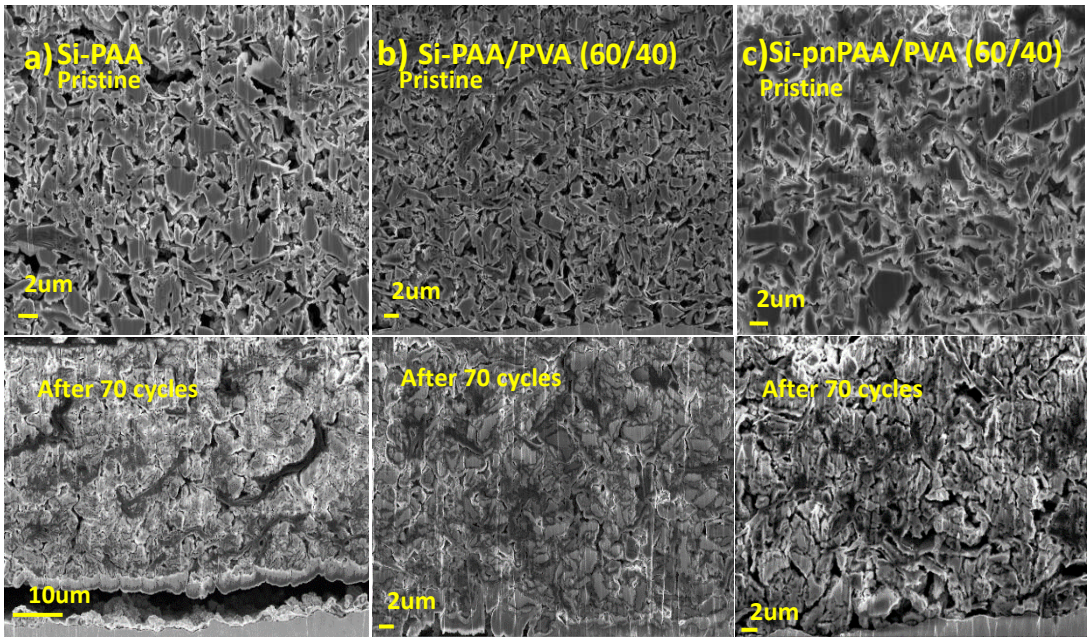

Figure 6-9 SEM image for cross-section of a) pristine and cycled Si-PAA; b) pristine and cycled Si-PAA/PVA (60/40); c) pristine and cycled Si-pnPAA/PVA (60/40).

6.3.4 Tensile Test Characterisation

Stress-strain curves of the polymer films were plotted, and the results are shown in Figure 6-10. The PAA/PVA films show higher tensile strength (100 MPa) than PAA

(45 MPa), and a significant extension before the breakpoint, which provides a larger strain range for plastic deformation. Conversely, PAA shows typical brittle fracture without plastic deformation. The pnPAA/PVA film demonstrates higher stiffness with maximum tensile stress over 120 MPa and a much larger elongation than both PAA/PVA and pure PAA. These results suggest that the tensile properties of PAA can be largely improved through the blending and cross-linking with PVA, and a partially neutralised PAA can generate even higher tensile properties. This is a result of partial neutralisation of PAA in the blends, which has been proven to be able to improve the crosslinking degree between PAA and PVA[98].

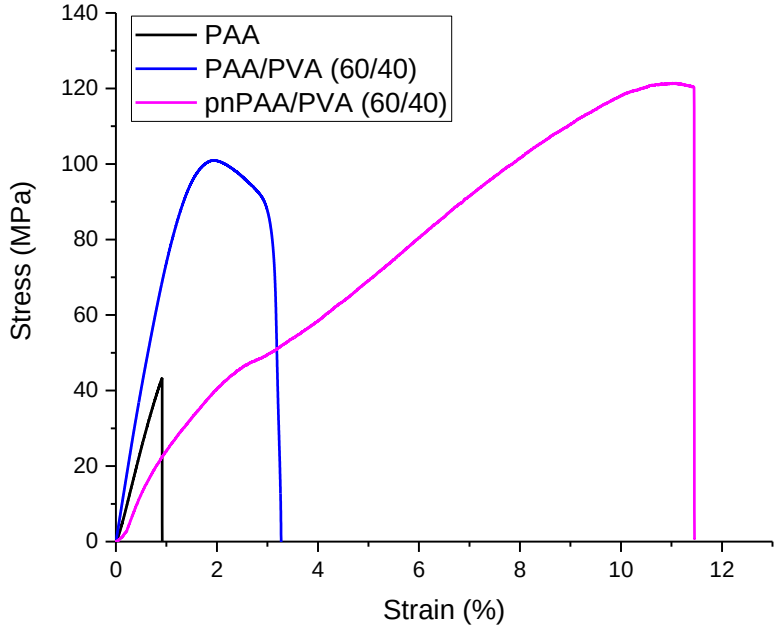

Figure 6-10 Stress-strain curves of PAA, PAA/PVA blends.

6.3.6 FTIR Measurement

Figure 6-11 shows that the absorbance of O-H stretching band in PAA is a variable double peak between 3000 and 3460 cm^{-1} and overlaps with the CH stretching band at 2920 cm^{-1} [159]. After it has been crossed linked with PVA, the O-H band (hydroxyl group) is decreased and is shifted to a higher region. Moreover, the C=O stretching band, which is attributed to the ketone group generated by the oxidative degradation of the hydroxyl group[98], is significantly reduced. It indicates the formation of –COO- caused by the esterification reaction of PAA and PVA[94], [163].

For pnPAA/PVA, the absorbance signal of C=O region (around 1700 cm^{-1}) is reduced compared with PAA/PVA following partially neutralisation, similar to the C-OH band

(between 1170 to 1240 cm^{-1}), indicating the consuming of the carboxyl group. The absorbance peak attributed to the sodium carboxylate (at 1550 cm^{-1}) is formed through esterification reaction. Also, the stretching band at 800 cm^{-1} associated with an out-of-plane OH···O deformation decreased to a lower level, which is similar to previous FTIR analysis for NaPAA.

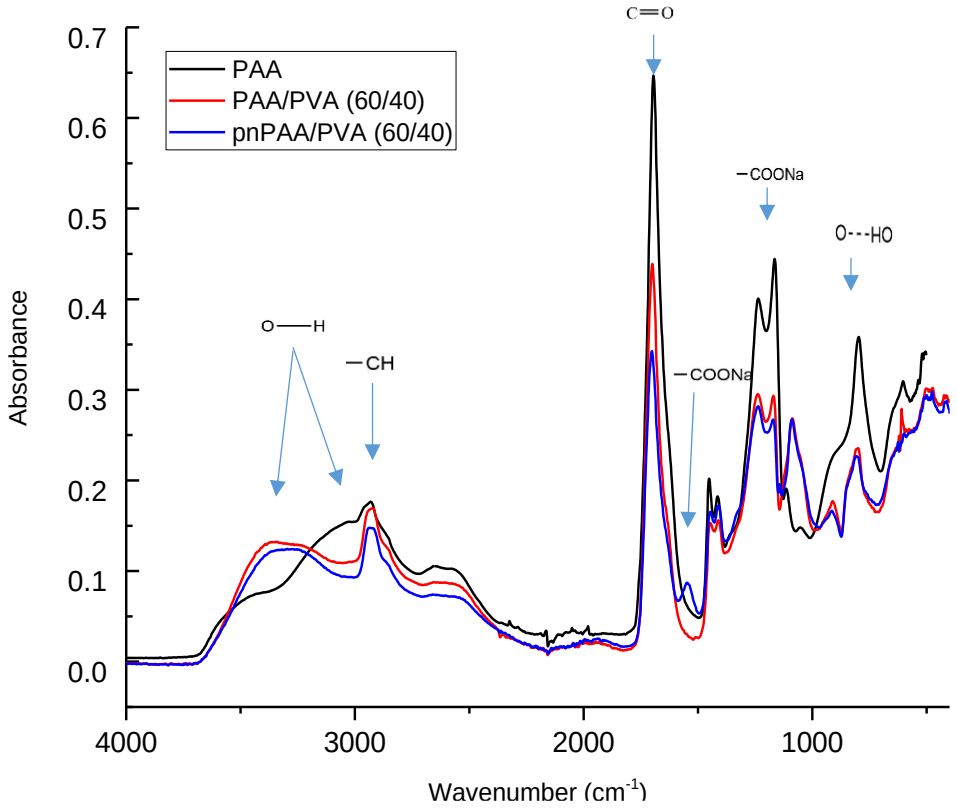

Figure 6-11 FT-IR analysis results for PAA, PAA/PVA (60/40) and pnPAA/PVA (60/40)

6.3.7 Nanoindentation Test

The nanoindentation test results for Si electrodes with different binders are shown in Figure 6-12. Elastic recovery parameter (ERP) and modulus are calculated using data taken from the slope of the tangent to the unloading curve in Figure 6-12a. Figure 6-12b compares the maximum contact depth (the total depth that the indenter penetrates into the electrode) during the nanoindentation test among three electrodes with different polymers, and the plastic depth (the indentation depth that the electrode undergoes plastic deformation) for each electrode material has been calculated. It can be observed that the electrode with PAA demonstrates the smallest contact depth where 96% is plastic contact, indicating the electrode is quite rigid. The electrode with PAA/PVA shows better flexibility with more contact depth and less plastic depth. This parameter has been improved in the electrode incorporating pnPAA/PVA. Whilst

comparing the reduced modulus for these electrodes (Figure 6-12c), the modulus was significantly reduced through the crosslinking of PAA with PVA, and it was further reduced for the electrode with pnPAA/PVA as the binder. The ERP in Figure 6-12d demonstrates an opposite trend but draws the same conclusion that the incorporation of cross-linked polymer PAA/PVA improved the performance of the Si electrode due to its elastic recovery and the partially neutralising PAA of 8% further improved the properties. It is supposed that with the enhanced elastic recovery property, the pnPAA/PVA could best tolerate the massive volume change within the Si electrode upon lithiation, and thus to maintain the electrically conductive network and keep a tight contact between particles within Si electrode during cycling.

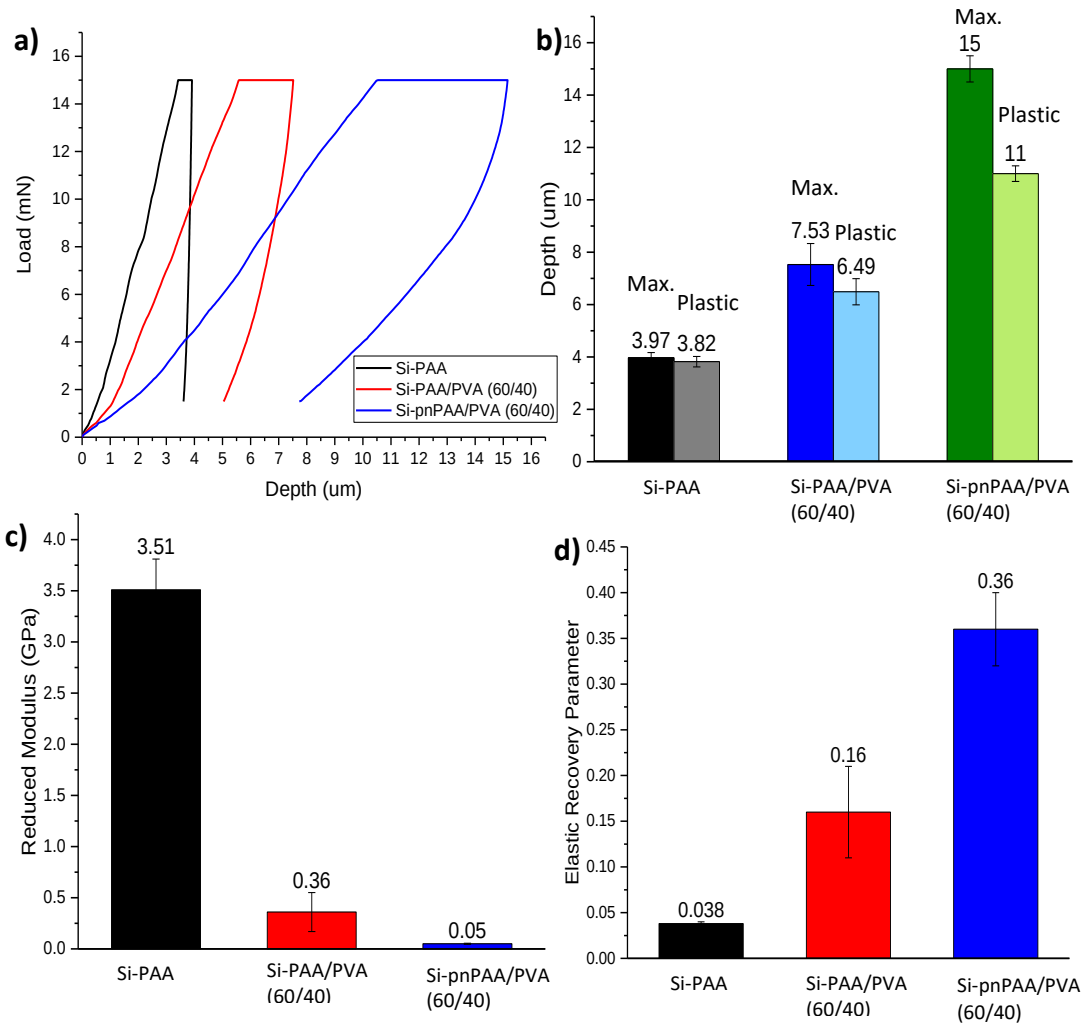

Figure 6-12 Comparison plots for Si-PAA, Si-PAA/PVA and Si-pnPAA/PVA measuring a) Nanoindentation loading vs depth curve for different Si electrodes; b) the ratio of plastic depth among the maximum extent; c) reduced modulus for different Si electrodes; d) elastic recovery parameter comparison for Si electrodes.

6.3.8 Electrode Adhesion Test

From Figure 6-13, it is clear that the maximum adhesion force for the electrodes with PAA is 31 N, and there is not much improvement when compared with the electrodes of Si-PAA/PVA. It indicates that crosslinking with PVA could not improve the adhesion of electrode, which is reasonable since PVA itself does not exhibit good adhesion. However, Figure 6-13 also shows that with pnPAA/PVA, the Si electrodes demonstrates a much higher adhesion force (76 N). This could be due to the benefit of partial neutralisation with NaOH for PAA. As explained near the beginning of this study, following the incorporation of Na^+, there were more extended polymer chains in PAA with free carboxyl groups, in which case more strong covalent bonds would be formed with the hydroxyl groups present on the surface of Si, and thus result in enhanced adhesion force within the electrode. Therefore, Si electrodes with partially neutralised PAA/PVA could effectively suppress the macro degradation of the composite electrode, and as a result, help to maintain the electronic network between active materials and conductive carbon additives.

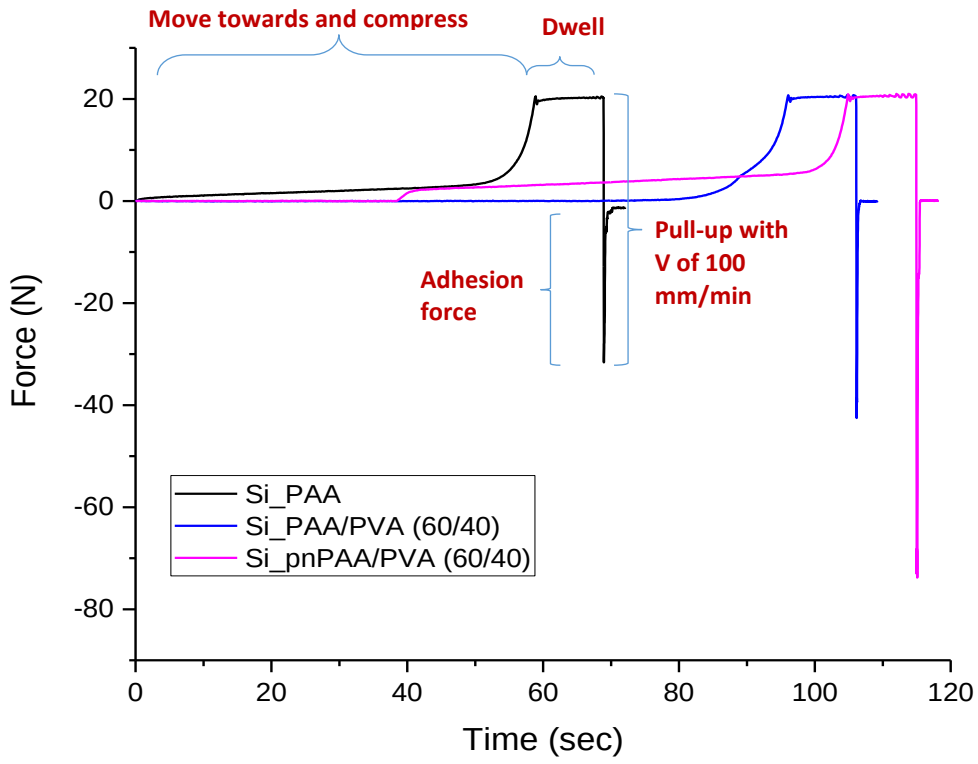

Figure 6-13 Adhesion test result for Si electrodes with PAA, PAA/PVA (60/40) and pnPAA/PVA (60/40)

6.3.9 Electrochemical Performance and Impedance Analysis

The electrochemical cycling performance within half-cells (*vs.* Li/Li^+) indicates that the Si electrodes containing PAA binder start to rapidly decline after only 38 cycles when the capacity is limited to 1200 mAh/g (Figure 6-14 (a)) and only reaches 25 cycles when capacity is capped at 2000 mAh/g (Figure 6-14(b)). It shows that PAA is not robust enough to sustain the Si volume change, and thus fails to maintain the conductive network and microstructure within the Si electrodes. In contrast, Si-PAA/PVA electrodes are more stable after 100 cycles, indicating that the crosslinked PAA/PVA binder could better withstand the massive volume expansion of Si during lithiation due to the improved tensile properties from the PVA fraction. Si electrodes with pnPAA/PVA demonstrate the best cyclability under both cycling conditions (1200 mAh/g and 2000 mAh/g) among these three types of electrodes, which is consistent with its superior tensile and adhesion properties.

From the impedance spectroscopy measurement, the Si electrodes containing the PAA binder show slightly lower series resistance at the beginning, followed by a dramatic increase after 20 cycles; while Si electrodes with PAA/PVA binder and pnPAA/PVA binder exhibit a moderate increase in series resistance (Figure 6-14 (c)). The dramatic growth of series resistance within Si-PAA may be caused by the electrode pulverisation and delamination from the current collector as observed in the SEM images (Figure 6-9 (a)). The SEI resistance for the three types of electrodes is within in similar range for the first 30 cycles. After this, the SEI resistance for Si-PAA grows significantly, with a moderate increase for Si-PAA/PVA from 40 cycles and a slight increase for Si-pnPAA/PVA from 50 cycles (Figure 6-14 (d)). It indicates that the SEI layer of Si-PAA is the most unstable compared with that of the other two electrodes which makes it increasingly difficult for Li-ions to traverse. Also, the higher SEI resistance of Si-PAA/PVA compared with Si-pnPAA/PVA is possibly due to more internal particle cracking for Si-PAA/PVA, which lead to more surface area and subsequent SEI growth (and higher degrees of agglomeration with other particles). This is supported by SEM observations. For the charge transfer resistance, all three types of electrodes undergo a similar trend for the first 30 cycles (Figure 6-14 (e)). The substantial impedance decrease at the beginning is possibly due to the improved contact at the interphase caused by additional pressure from the spring within coin cells during Si volume expansion[145]. After 30 cycles, the charge transfer resistance

of Si-PAA is largely increased, while for the other two electrodes it remains stable (Figure 6-14 (e)). It could be explained by our previous study which states that it is more likely for Si to form c-$Li_{15}Si_4$ with poor cyclability at the same cut-off voltage, and the presence of c-$Li_{15}Si_4$ demonstrates much higher charger transfer and Warburg diffusion impedance compared with a-Li_2Si, which typically exists in electrodes under stable cycling conditions[164]. Therefore, when the performance Si-PAA electrodes starts to decline from 30 cycles onwards, it undergoes a pronounced phase transformation to c-$Li_{15}Si_4$ during deep lithiation, which leads to the dramatic growth of charge transfer resistance.

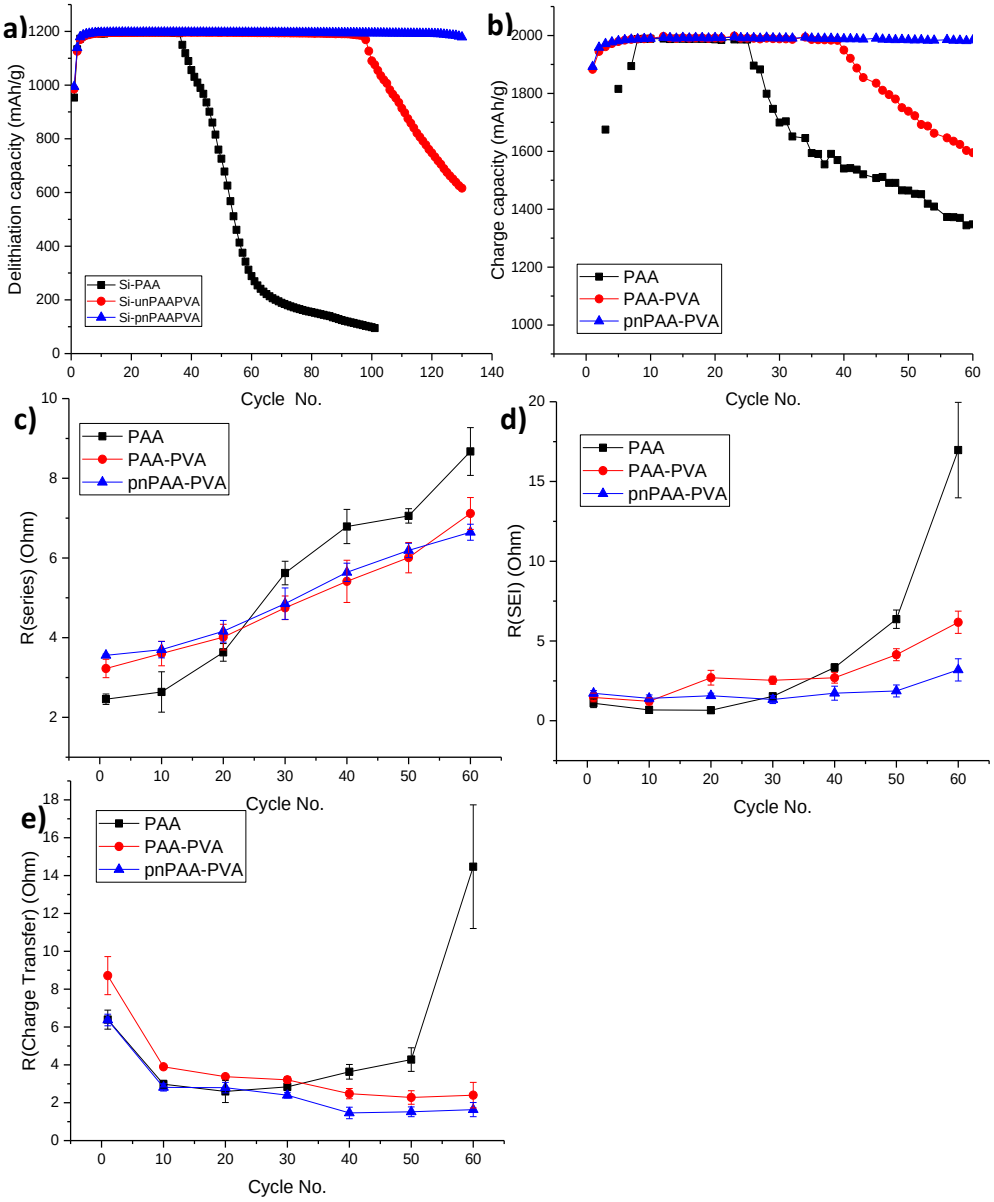

Figure 6-14 Cycling performance for Si half-cells (*vs.* Li/Li^+) with different binders with the capacity limit of a) 1200 mAh/g and b) 2000 mAh/g, and impedance fitting for c) series resistance, d) SEI resistance, and e) charge transfer resistance.

6.4 Investigation on Binary Polymer PAA/SBR as the Binder System for Si Electrodes

6.4.1 Polymer Tensile Test

The tensile test result of polymer films is plotted as the stress-strain curve as shown in Figure 6-15. It indicates that by adding SBR, both binary NaPAA/SBR system demonstrate an enhancement in tensile strength compared with NaPAA (maximum 64 MPa). For NaPAA/SBR (2/1) films, besides the significant improvement of the stiffness (maximum 96 MPa), there is also an obvious extension prior to the breakpoint. Whilst for NaPAA/SBR (5/1) films, the elongation is not significant despite there is an improvement in maximum tensile strength, which is 82 MPa. These results indicate that the stiffness and elongation of PAA can be improved through incorporation with SBR, and the degree of improvement on the tensile property is in proportional to the ratio of SBR added.

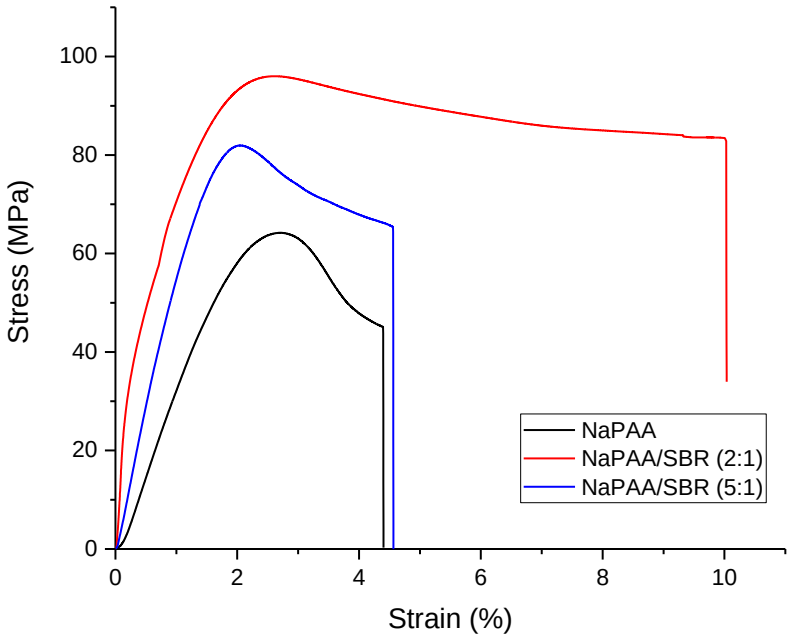

Figure 6-15 Polymer tensile property comparison for NaPAA, NaPAA/SBR (2/1) and NaPAA/SBR (5/1)

6.4.2 Half-cell Electrochemical Characterisation

The half-cell (*vs.* Li/Li^+) cycling performance with capacity limitation of 1200 mAh/g (Figure 6-16) displays that Si electrodes with NaPAA/SBR (5/1) starts to fail first after 88 cycles, and Si electrodes with NaPAA/SBR (2/1) fails after another 20 cycles; while Si electrodes with single binder system NaPAA demonstrates the longest cycle life among them. This result is opposite to the tensile test result of polymer film, indicating

that even with the improved tensile property, the NaPAA/SBR binary binder could not improve the cycling performance of Si electrodes and show worse cyclability than the Si electrodes with NaPAA. It is a similar conclusion for Si electrodes with NaCMC/SBR and NaCMC that reported in the literature, suggesting that Si electrodes with NaCMC/SBR show worse cyclability than that with NaCMC, which might result from high resistance of SBR[88]. Therefore, the electrochemical impedance spectroscopy analysis will be followed to investigate the resistance change in the Si electrodes with NaPAA/SBR system.

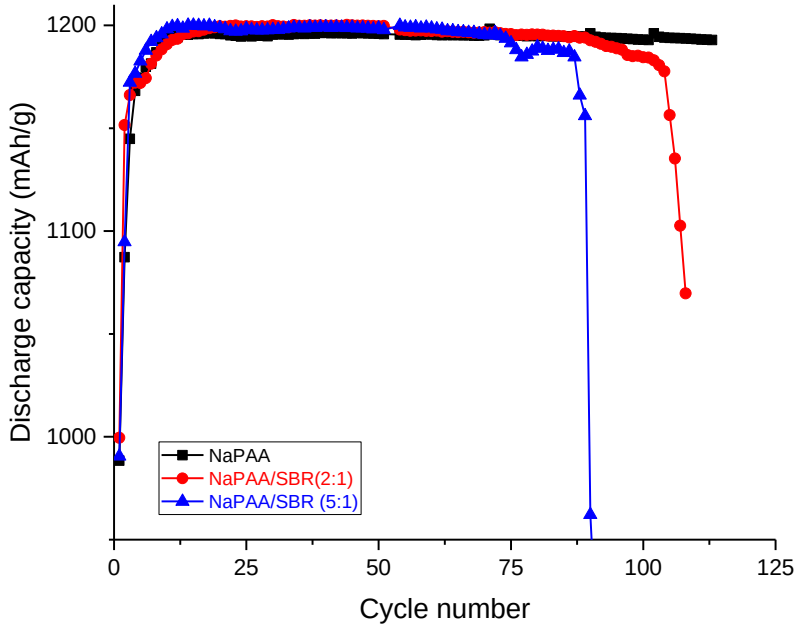

Figure 6-16 Half-cell (*vs.* Li/Li^+) cycling performance comparison between Si-NaPAA, Si-NaPAA/SBR (2/1) and Si-NaPAA/SBR (5/1)

6.4.3 Electrochemical Impedance Spectroscopy Analysis

The fitting result of impedance spectroscopy is shown in Figure 6-17. For the series resistance (Figure 6-17(a)), these two different electrodes show similar value in the beginning. However, the series resistance for Si electrodes with NaPAA/SBR (2/1) demonstrates much higher resistance value and a more significant grow compared to Si electrodes with NaPAA. Whilst for SEI resistance (Figure 6-17(b)) and charge transfer (Figure 6-17(c)), Si electrodes with NaPAA/SBR (2/1) maintain the similar level of resistance with those incorporated NaPAA for first 40 cycles. It is indicated that the dramatic increase in series resistance for Si electrodes with NaPAA/SBR (2/1) for first 40 cycles is not associated with electrode pulverisation; otherwise, it will also lead to a similar increase for SEI resistance. It is likely that the SBR in Si electrodes

makes it more difficult for Li-ion transfer within the electrode. The scenario becomes worse during cycling since Si can be electrochemically welded together through its SEI and narrow the channels for Li-ions transportation. In the meantime, with such a high-resistive binder, the pathway for Li-ions can be even more resistant. From 50 cycles, the SEI resistance of Si electrodes with NaPAA/SBR (2/1) start to significant growing possibly due to the pulverisation of part of Si particles within the electrode, while for Si electrodes with NaPAA, the SEI resistance maintain relatively stable. While for charge transfer resistance, the dramatic increase for Si-NaPAA/SBR occurs after 60 cycles, which is associated with Si phase change that generally happened during cell fading process as explained in Section 6.3.8. Therefore, it can be concluded here the failure mechanism for Si-NaPAA/SBR half cells can be attributed to the high electrode resistance, which is likely blocking the Li-ion pathways and isolating Si particles in the electrode. This in turn accelerate the electrode fading process.

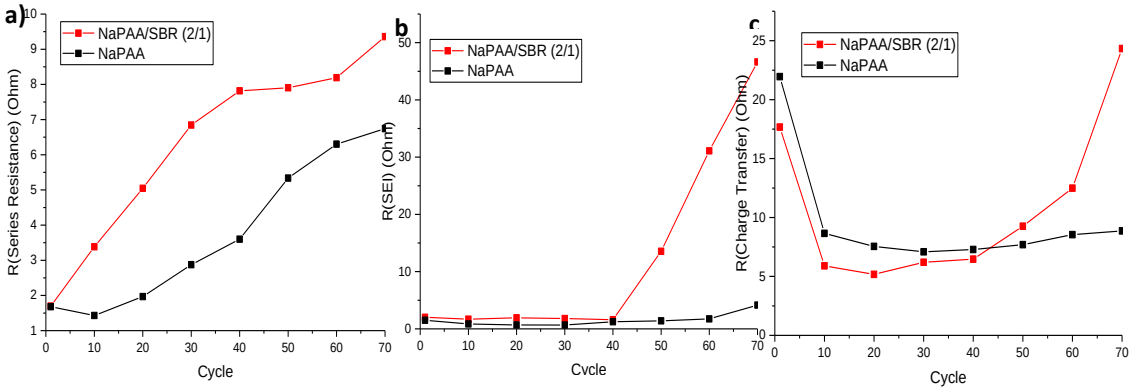

Figure 6-17 Impedance fitting result for different cycles comparing between Si-NaPAA and Si-NaPAA/SBR (2/1)

6.5 Investigation on Multi-level Cross-link Polymer PAA-Fe^{2+}-FLG

6.5.1 Verification of the Multi-level Cross-link Network

FTIR is used to verify the functional group within the polymer structure, and the result is shown in Figure 6-18. The absorbance peaks at 2927 cm^{-1} and 2854 cm^{-1} are attributed to the hydroxyl group that attached to the carbonyl group, and the absorbance peaks at 1234 cm^{-1} and 1163 cm^{-1} are referred to the carbonyl group in carboxyl; hence peak reduction at these positions could relate to the reduction of the carboxyl groups. For absorbance peaks at 1112 cm^{-1} and 1050 cm^{-1}, they refer to the ester group, and peak change at these points suggests the reaction of esterification. It can be observed that compared to PAA there is peak reduction at points referred to

carboxyl groups for all other three polymers, which indicates the part of carboxyl groups from PAA have been consumed in these polymers. Correspondingly, there is a different level of esterification for Fe^{2+}-PAA and FLG-Fe^{2+}-PAA, which proves the formation of the ionic interaction between Fe^{2+} and the carboxyl group in PAA. Additionally, the consuming of the carboxyl group is more dramatic for FLG-Fe^{2+}-PAA, but there are fewer ester groups generated. It could be likely because the carboxyl group on FLG has also been consumed by the ionic interaction with Fe^{2+} in the same way between Fe^{2+} and PAA. However, there is no indication of an ester group generated in FLG-PAA, which suggests that FLG is possibly only formed the hydrogen bond with PAA through their carboxyl groups other than esterification.

Therefore, the cross-linked mechanism can be concluded as shown in Figure 6-19 that there are three different chemical interaction – the dynamic ionic interaction between Fe^{2+} and the carboxyl groups on PAA, the dynamic ionic interaction between Fe^{2+} and the carboxyl groups on FLG and the hydrogen bond between PAA and FLG. Additionally, within the layers of FLG, there is also a strong π-π interaction between two conjugated carbon nets.

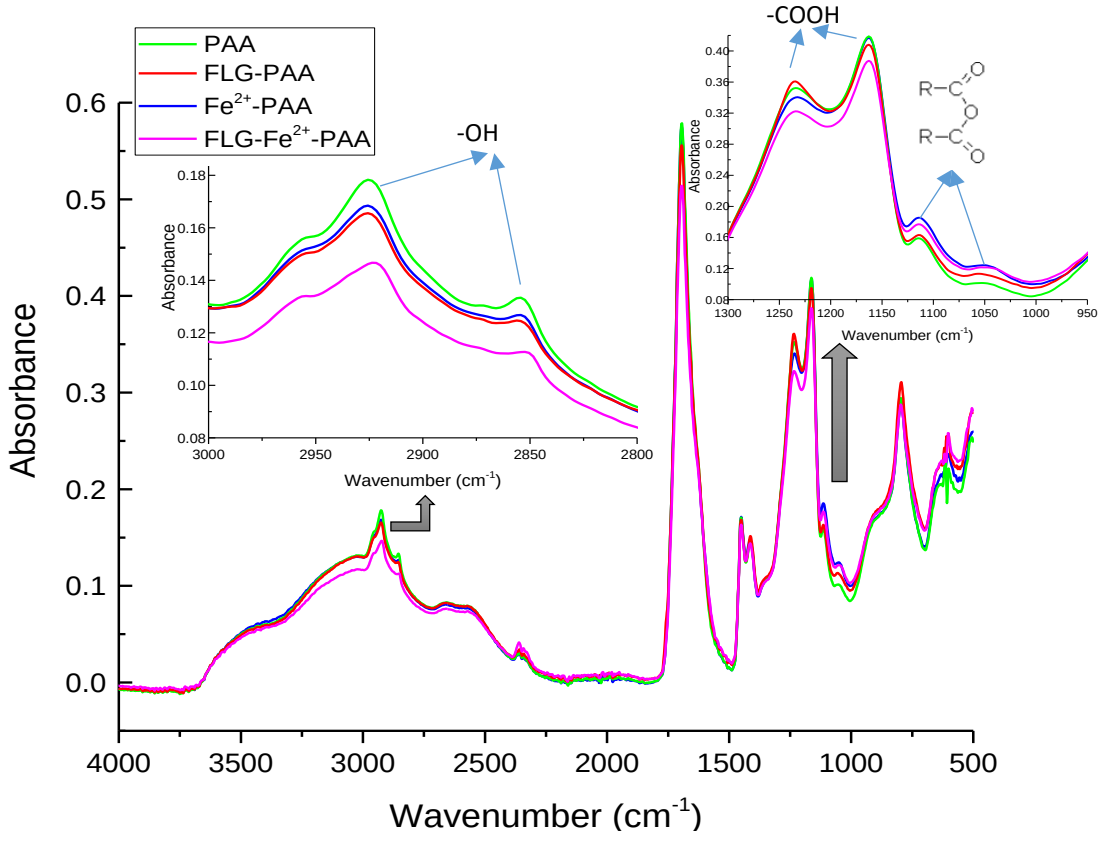

Figure 6-18 FTIR investigation on polymer films of PAA, FLG-PAA, Fe^{2+}-PAA, and FLG-Fe^{2+}-PAA

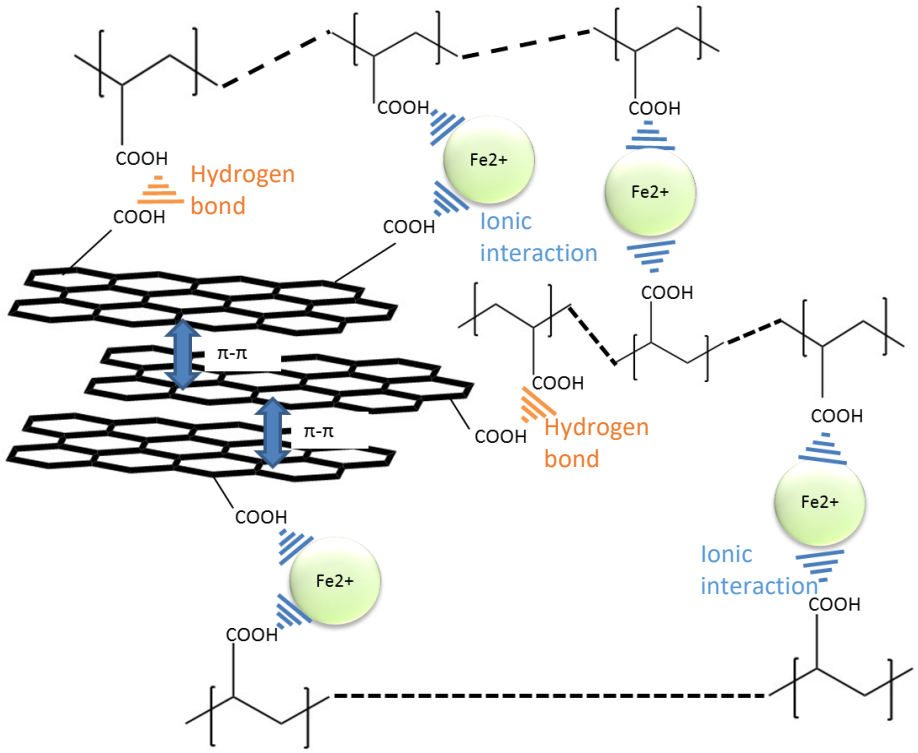

Figure 6-19 Illustration of crosslinking mechanism within FLG-Fe^{2+}-PAA polymer

6.5.2 Tensile Test Characterisation

The stress-strain curve obtained from the tensile test (Figure 6-20) shows that compared to PAA, which maximum tensile strength is around 43 MPa, FLG-PAA displays an increase in stiffness (76 MPa) but not much improvement in terms of plastic extension. While for Fe^{2+}-PAA, similar enhancement achieved in stiffness (71 MPa) and also, there is dramatic extension prior to the breakpoint, indicating a larger strain range for plastic deformation. These results suggest that with extra hydrogen bonds, the stiffness and elastic region could be enhanced but it does not benefit for the plastic region; while with additional ionic interaction, the stiffness of PAA, as well as both plastic and elastic elongation, can be improved. It can be observed for FLG-Fe^{2+}-PAA that, the maximum polymer strength is dramatically increased (108 MPa) and the elongation before the breaking point is more significant, which is possibly due to the variety of binding force, and higher density of ionic interaction existed in this polymer system. It also verifies the high strength of multi-level crosslink within FLG-Fe^{2+}-PAA polymer, and that is supposed to provide a robust network for Si electrodes to better tolerate the large volume change during lithiation.

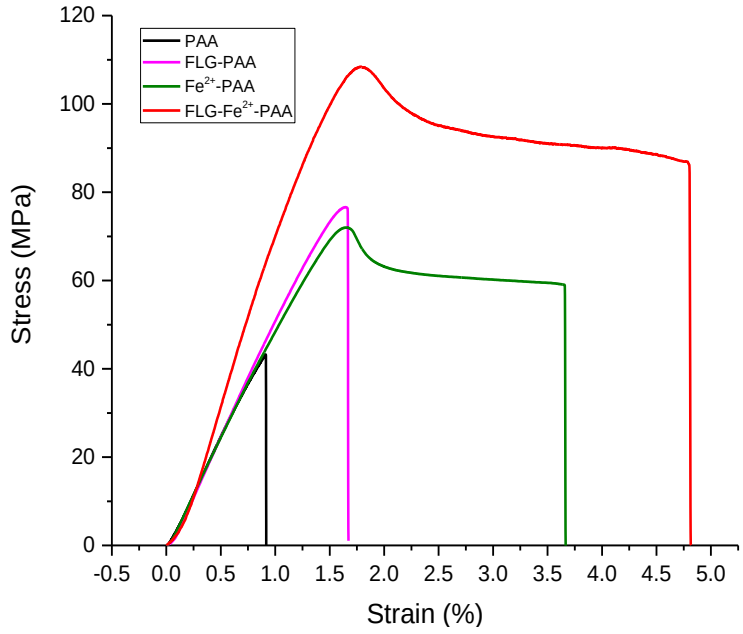

Figure 6-20 Polymer tensile test results for PAA, FLG-PAA, Fe^{2+}-PAA and FLG-Fe^{2+}-PAA

6.5.3 Initial Half-cell Investigation for Binder Performance

To further investigate the electrochemical stability of these polymers during cycling, half-cells (*vs.* Li/Li^+) of constant current cycling under the capacity limitation of 2000 mAh/g were obtained, and the results are shown in Figure 6-21. It displays that Si electrodes with the novel binder FLG-Fe^{2+}-PAA demonstrate a much-improved cycle life compared to those contains only PAA, maintaining near 2000 mAh/g for 75 cycles. While for Si electrodes with only PAA, it starts to fail after 20 cycles. This is a surprising achievement since within the polymer, the FLG and Fe^{2+} only account for 1 wt% in total. However, it can also be noticed that Si electrodes with FLG-PAA and Fe^{2+}-PAA show much worse performance than Si electrodes with PAA, which start to fading from the first cycle, indicating that they could not withstand such high capacity at all. These results are not expected, and the failure mechanism is still needed to be further investigated. Since this section is focused on the performance of FLG-Fe^{2+}-PAA polymers, the following studies will only compare the difference between Si-PAA and Si- FLG-Fe^{2+}-PAA. Also, to better demonstrate the premier performance of FLG-Fe^{2+}-PAA, the optimised single binder system NaPAA will also be incorporated into further comparative studies.

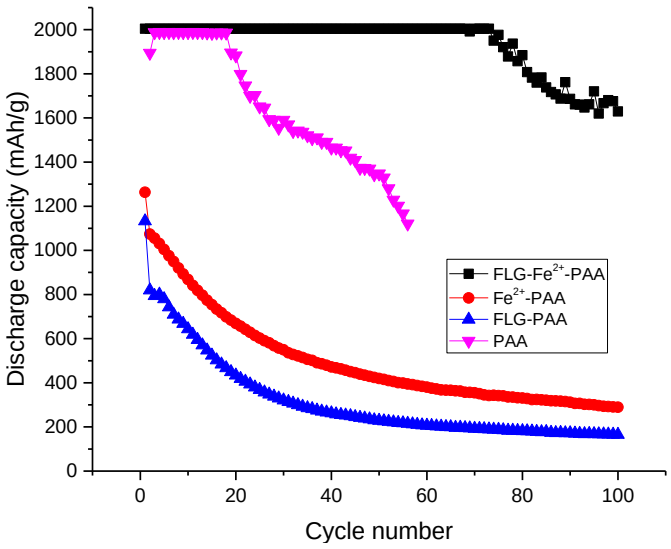

Figure 6-21 Comparison of half-cell (*vs.* Li/Li$^+$) cycling performance for Si electrodes with different polymers

6.5.4 Si Nano-indentation Test

The results for nanoindentation on Si electrodes with different binders (Figure 6-22) indicate that the maximum contact depth for Si-FLG-Fe^{2+}-PAA is significantly larger than Si-PAA, but it remains in the similar region with Si-NaPAA. Also, in term of the reduced modulus, Si-FLG-Fe^{2+}-PAA shows smaller modulus than Si-PAA and keep the similar value with Si-NaPAA. These results indicate that with incorporating only 1 wt% of Fe^{2+} and FLG into PAA binder, the flexibility of Si electrodes has been much improved. A similar improvement is also achieved in Si-NaPAA electrodes, which contains similar ionic interaction with Na^+ and carboxyl group of PAA. It suggests that with ionic interaction, the overall flexibility of electrode can be improved, which is favoured for large volume change in Si electrodes. This is also in agreement with the previous polymer tensile test results.

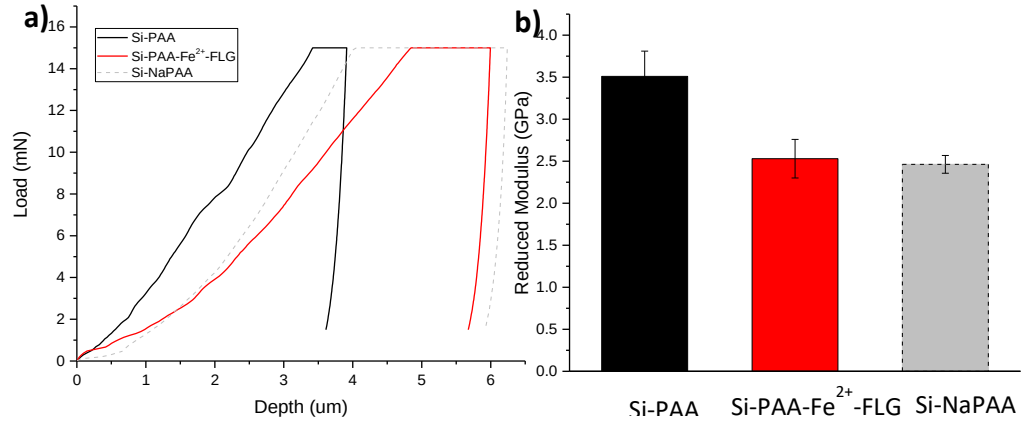

Figure 6-22 Nano-indentation test result for Si-PAA, Si-PAA-Fe^{2+}-FLG and Si-NaPAA

6.5.5 Adhesion Test

In Section 6.2.4, the adhesion strength between Si-PAA and Si-NaPAA has been compared and discussed. In Figure 6-23, it is shown that the adhesion strength of Si electrodes with binder FLG-Fe^{2+}-PAA is as twice as Si-PAA electrodes, which is at the similar level of Si-NaPAA. This improvement could also be attributed to the ionic interaction within polymer chains, which possess a high binding strength that requires more energy to break it.

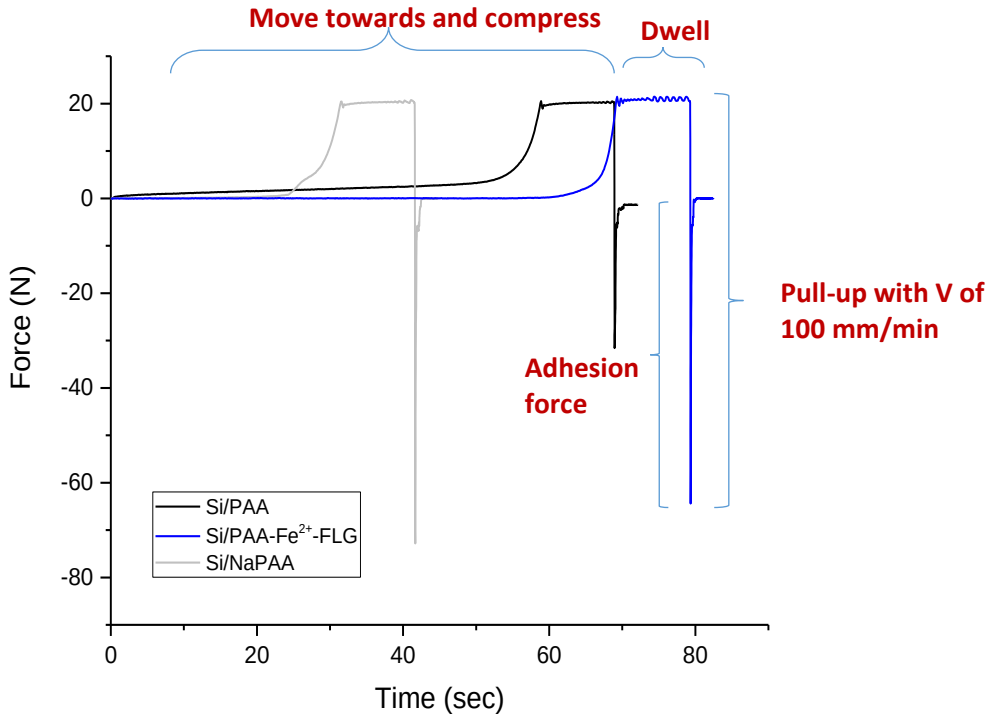

Figure 6-23 Adhesion test result for Si-PAA, Si-NaPAA and Si-FLG-Fe^{2+}-PAA

6.5.6 Electrochemical Testing of Half-cells under Full Capacity

Without capacity limitation, Si particles can undergo the volume expansion by up to 300 %, which is extremely challenging for the binder performance within the electrode. From Figure 6-24, it can be noticed that Si-PAA show the shortest cycle life (drop to 100 mAh/g after 60 cycles). While for Si-FLG-Fe^{2+}-PAA, with the only difference of 1 wt% Fe^{2+} and FLG in binder system compared to Si-PAA, it demonstrates the best cycling performance among these three electrodes, which still maintains above 1000 mAh/g for 200 cycles. The cyclability is even significantly improved based on Si-NaPAA, which starts to fade rapidly from 110 cycles and drop to 100 mAh/g at 160 cycles. It has been proven in previous studies that NaPAA and FLG-Fe^{2+}-PAA have similar ionic interaction within the polymer system, and also

demonstrate similar mechanical performance in terms of tensile property and adhesion force. This dramatic cycling performance between Si-NaPAA and Si- FLG-Fe^{2+}-PAA is possibly attributed to the structural stability of polymers. For FLG-Fe^{2+}-PAA, with multi-level crosslinked through different types of functional group binding, the structure of the polymer is much more stable than NaPAA, which has only one kind of ionic interaction existed and is randomly distributed.

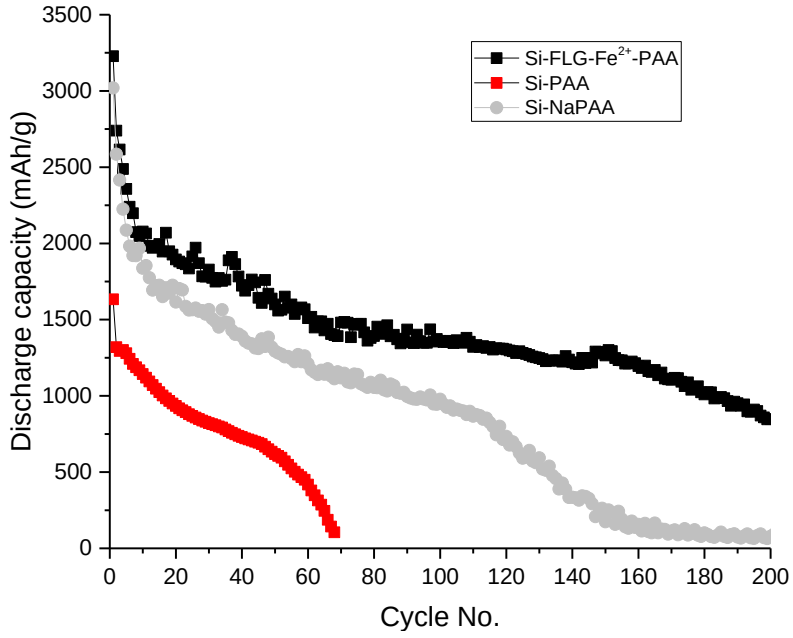

Figure 6-24 Cycling performance of half-cells (*vs.* Li/Li^+) with Si-FLG-Fe-PAA, Si-PAA and Si-NaPAA without capacity limitation

6.6 Chapter Conclusion

This chapter has systematically investigated several approaches to optimise PAA binder system for Si electrodes. To optimise the single binder system, partially neutralise PAA with 70 mol% NaOH has been proven as a practical approach since Si-NaPAA has demonstrated much better cyclability (stable at 1200 mAh/g for over 100 cycles) than Si-PAA, which faded after 40 cycles. This improvement is due to the better tensile strength, adhesion force and the electrolyte uptake capability of NaPAA. Concerning developing PAA-based binary binder system with the premier tensile property, PVA and SBR have been investigated as the incorporated candidates that are well known as "flexibility additive". For the optimised PAA/PVA binder, improved cyclability (100 cycles at 1200 mAh/g) has been achieved for Si-PAA/PVA (60/40) compared to Si-PAA system (40 cycles at 1200 mAh/g), and further improvement has indicated for Si-pnPAA/PVA (60/40) (140 cycles at 1200 mAh/g), which partially

neutralised PAA with 8 mol % NaOH before crosslinking it with PVA. This in turn also proved that partially neutralisation of PAA could improve the effect of crosslinking between PAA and PVA. However, the esterification reaction during crosslinking is favoured for the acid environment; hence it could not be neutralised to 70 mol% as NaPAA. For NaPAA/SBR system, two different ratios (2/1 and 5/1) have been studied. Despite the significant improvement in the tensile property of NaPAA/SBR (both 2/1 and 5/1), the half-cell cycling performance for Si-NaPAA/SBR system is not as good as Si-NaPAA. The failure mechanism of Si-NaPAA/SBR (2/1) have been investigated through electrochemical impedance spectroscopy analysis, and the result indicates that the high resistance of SBR is the main obstacle for Li-ions alloying with Si particles during cycling. This finding is in agreement with NaCMC/SBR in literature. The last section has conducted comprehensive studies for the multi-level crosslinked polymer network FLG-Fe^{2+}-PAA, which indicates a significant enhancement in cyclability of Si half-cells (maintained above 1000 mAh/g for 200 cycles) compared with Si-PAA and Si-NaPAA. It has been proven that FLG-Fe^{2+}-PAA polymer have identical ionic interaction as PAA, and they also possess similar mechanical properties in terms of flexibility and adhesion strength. Therefore, the dramatic improvement of Si- FLG-Fe^{2+}-PAA electrodes can be attributed to the multi-level cross-link structure within the polymer network, which helps to maintain the ionic interaction over cycles.

To conclude, in order to improve the performance of PAA based binder in Si electrodes, it is imperative to build and strengthen the ionic interaction within polymer networks can be the most effective approach, which has been proven through partial neutralisation of PAA and multi-level crosslinked binder FLG-Fe^{2+}-PAA. Compared with flexibility, high stiffness and adhesion force are considered as more important factors when designing binders for Si electrodes, since polymers with improved stiffness and adhesion strength generally demonstrate better cycling performance in Si electrodes in this chapter. Additionally, the resistance of polymer should also be concerned as the high-resistive polymer as SBR is not recommended to be incorporated for Si electrodes unless further approaches for optimising electronic conductivity are also involved.

Chapter 7 Systematic Investigation of Electrolyte Additives for EC Free Electrolytes to be Applied in Si-FLG/NMC Full Cells Cycling under High Voltage

7.1 Introduction

It has been addressed in Chapter 2 that to improve the cyclability of Si full cells under high voltage, an appropriate electrolyte system that can maintain a stable interface between electrodes and electrolyte is essential. Various electrolyte additives including FEC, VC, PES and different combinations are investigated as the "enabler" to help develop an effective SEI for Si-FLG electrodes and to maintain the stability of electrolytes under high voltage. Comprehensive electrochemical performance including differential capacity analysis, constant current cycling, oxidative limitation analysis and electrochemical impedance spectroscopy have been compared. A post-mortem surface chemistry analysis for both anodes and cathodes has also been conducted to further understand the degradation mechanism of cells with different electrolytes cycled under high voltage.

7.2 Moisture Measurement for Electrolytes

According to Table 7-1, it can be noted that the water content involved in the check solution for verifying baseline is about 3990 ppm, which is within the reasonable range as marked by the supplier (3800-4200 ppm); this indicates that the results listed in this table are reliable. It can be concluded from Table 7-1 that the water content of all electrolytes investigated in this study is below 10 ppm. RD265 (EC/EMC+FEC+VC) contains the highest moisture concentration, which is 9.5 ppm. Also, it can be indicated from Table 7-1 that the electrolytes with more components generally shows higher water content, which is possible because water is more likely to be involved during the process of adding additives and mixing, and additives can also be the source of water.

Table 7-1 Moisture measurements in different electrolytes

Electrolyte solution	Water content (ppm)
Check solution P	3989.95 ± 23.95
H0B01 (EMC only)	3.82 ± 0.2
H01 (EMC+FEC+VC)	8.2 ± 1.6
H02 (EMC+FEC)	4.2 ± 0.6
H03 (EMC+FEC+PES)	4.95 ± 0.95
H04 (EMC+PES)	4.35 ± 0.25
H05 (EMC+VC)	3.75 ± 0.55
RD265 (EC/EMC+FEC+VC)	9.5 ± 1.3
RD165 (EC/EMC)	4.65 ± 1.25

7.3 Oxidative Limitation Analysis of Electrolyte Based on NMC Half-cells

In Figure 7-1, with a galvanostatic measurement under a slow C rate of C/110 upon 5 V, the potential difference will be increased. By the point the potential difference exceeds the potential limit of the electrolyte, the additional current is consumed by electrolyte side reactions that cause an ongoing surface layer formation and decomposition or polymerisation instead of Li extraction or the formation of the stable SEI[147]. Figure 7-1 shows that all electrolytes investigated in this study demonstrate a high oxidative limitation up to 4.9 V except H04 (EMC/PES), which shows a slightly lower oxidative limitation at about 4.8 V. It has been explained in Chapter 3 that while the Si/NMC full cells charged to 4.4 V, the voltage for NMC would be 4.5 V since there was 0.1 V lithiation potential sourced from Si anodes at this SoC. It can be observed in Figure 7-1 that all electrolytes have validated an oxidative stability at 4.5 V. This suggests that oxidative degradation should not occur in the electrolyte during the lithiation due to the high voltage in this study. It can also be noticed that for all NMC cells with EC free electrolytes there are visible bumps appear at the early lithiation stage (at around 25 h). It might result from the slower process of SEI formation compared to EC-containing electrolytes, but the detailed mechanism behind this peak requires a further systematic study on EC-free electrolytes at the low C-rate.

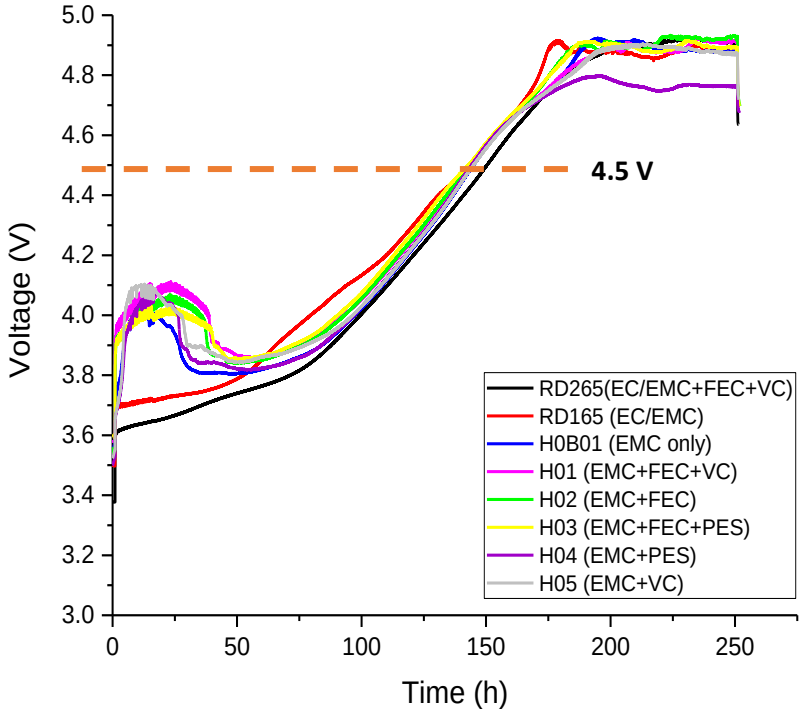

Figure 7-1 Oxidative limitation for NMC half-cells with different electrolytes charging towards 5 V under C rate of C/110.

7.4 Differential Capacity Analysis for the First Lithiation

Figure 7-2 compares the dQ/dV curves of the first lithiation for Si-FLG /NMC full cells with all electrolytes investigated in this study. It can be observed that the reduction of electrolyte components occurs before 2.7 V (*vs.* NMC), after which, the electrodes will undergo the first lithium-Si alloy reaction with lithiation peak located at 3.2 V (equivalent to 0.2 V in Si half cells); this agrees with most Si systems in literatures[114], [117], [123], [157], [165]. According to Figure 7-1 (a), it can be noticed that for Si-FLG /NMC full cell with just EMC solvent, there is only a single reduction peak at 1.73 V. While for the cells with EC/EMC electrolyte, the single peak has been split into a double peak with higher reduction voltage of 1.98 V and 2.17 V, respectively. Typically, the reduction order for electrolyte components on the surface of the Si anode is recognised as $LiPF_6$ salts > electrolyte additives > EC > solvent[166]. Therefore, it is likely that for Si-FLG /NMC full cell with RD165, the SEI formation undergoes different mechanism. In this system, the first peak (1.9 V) refers to the reduction of EC and the second one (2.17 V) refers to the decomposition of EMC; however, there is no information that EC improves the stability of EMC due to the high intensity of EMC reduction. The cell with RD265 shows that there is also a double peak but the first reduction peak becomes broader and there is a slight shift to

the left. This is because the reduction peak of EC is overlapped with that of FEC and VC, which decomposed in prior to EC. Additionally, the second peak which refers to the reduction of EMC has been much suppressed, indicating that a more stable SEI has been formed. To better identify the reduction peak for different additives in each electrolyte system, the dQ/dV spectra of the first lithiation process for Si-FLG /NMC full cell with different EC free electrolytes, is plotted in Figure 7-2 (b). Based on this, the reduction peaks for individual additives are summarised in Table 7-2. This table suggests that in EC free electrolytes, most additives applied in this study could effectively suppress the reduction from electrolyte solvent, which will, in turn, form a more stable SEI layer on Si electrodes. Among all EC free electrolytes, it can be observed that VC could best suppress the solvent reduction, by displaying the smallest reduction peak from EMC and at the highest voltage, compared with others. Whilst for the additive combination of FEC and PES, it seems that the reduction peak from EMC becomes stronger than the electrolytes with the single additive of FEC or PES. It can be a signal that with this combination, there is little improvement in forming the passivated film onto the surface of the Si anode.

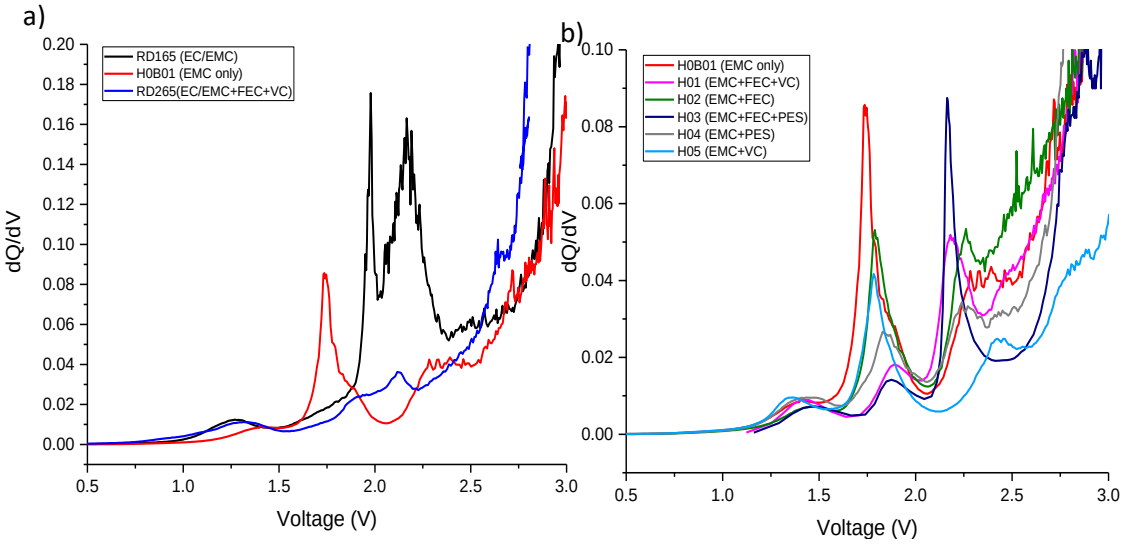

Figure 7-2 dQ/dV plots for the first lithiation of Si/NMC full cells with a) control electrolytes (RD165, RD 265 and H0B01) and b) EC free electrolytes with different additives

Table 7-2 Summary of reduction peaks for different additives in EC free electrolytes

Electrolyte	Reduction peak for VC (V)	Reduction peak for FEC (V)	Reduction peak for PES (V)	Reduction peak for EMC (V)
H0B01	-	-	-	1.73
H01	1.9		-	2.18
H02	-	1.79	-	2.26
H03	-	1.87		2.16
H04	-	-	1.83	2.25
H05	1.78	-	-	2.44

7.5 Constant Current Cycling Performance for Si-FLG/NMC Full Cells with Different Electrolytes

The constant current cycling performance for Si-FLG/NMC full cells with different electrolytes is shown in Figure 7-3. According to Figure 7-3 (a), it can be observed that for cells with EC involved electrolytes (RD265 and RD165), a “step-like” degradation occurs at the early stage cycling. To be more specific, for the cell with RD165, the discharge capacity gradually decreases from the beginning until there is a dramatic capacity drop from 40 cycles, but the drop stops after another 10 cycles, by which point the degradation returns to a gentle decrease and maintains relatively stable until it starts to fail after 100 cycles. Similarly to the cell with RD265, it is cycled stable with a capacity of 155 mAh/g, followed by the significant degradation that occurs from 20 cycles and lasts for another 15 cycles. Aside from the cell with RD165, the one with RD265 demonstrates a longer and more stable cycling performance. Whilst for the cell with only the EMC electrolyte, there is no "step-degradation" during cycling. It starts to gradually fade from the beginning until the "roll-over" effect appears from 65 cycles, which then indicates a severe pulverisation of the Si electrode and the failure of a cell. These results designate that with cycling upon to 4.4 V, EC contained electrodes suffer from the EC oxidation at the surface of the cathode during the early-stage cycling, which causes a significant capacity degradation. This finding is in alignment with previous reports for applying EC free electrolytes in other electrode systems cycling above 4.4 V[22], [27]. This is possible that upon the end of

EC oxidation, by which point EC has been consumed, the cells will demonstrate a relatively stable cycling profile until they start to fail.

Figure 7-3 (b) compares the cycling performance of Si-FLG/NMC full cells with different EC free electrolytes. It shows that without any additives, the cell with only EMC demonstrates the shortest cycle life. However, with only an extra 2 wt% PES additive, there is still no improvement in terms of cyclability. For the cells with the electrolyte of EMC/FEC, a relatively longer cycle life has been achieved, and the "roll-over" effect of the cell upon fading is less obvious compared with the cell containing only the EMC electrolyte. This indicates that FEC could help to improve the cycling stability of the electrode, which is possible because, by providing extra fluoride from FEC, more LiF could be formed to stabilise the SEI layer of Si as well as to enhance the stability of SEI under high voltage[27], [123], [126], [157]. Again, most notably, with additional PES to the EMC/FEC electrolyte system, there is still no obvious improvement for cycling performance. On the contrary, PES involved cells indicate the largest first initial loss compared to all other cells. It could be due to a large amount of EMC reduction in addition to the PES reduction as observed in previous dQ/dV results as shown in Figure 7-2 (b). This result indicates that PES is not suitable for EC free electrolyte systems in Si-FLG/NMC full cells despite the fact that it has been reported for its superior performance in other EC-containing electrolyte systems even under high voltage and high temperature[22], [138], [139]. For single additive in EC free electrolytes, VC demonstrates the best performance especially in terms of high capacity achievement and small initial capacity loss. It could also be explained by previous dQ/dV results that VC could best suppress the EMC reduction and form a relatively stable SEI in the meantime. Among all electrolyte systems, the combination of EMC with FEC and VC displays the longest cycle life, possibly because it combines the benefits of SEI improvement from FEC and the capacity retention from VC. This is also an improvement based on the RD265 electrolyte system, although the cell with RD265 shows a similar performance after the "step-effect", but without EC, it avoids the significant capacity loss at the early stage of cycling.

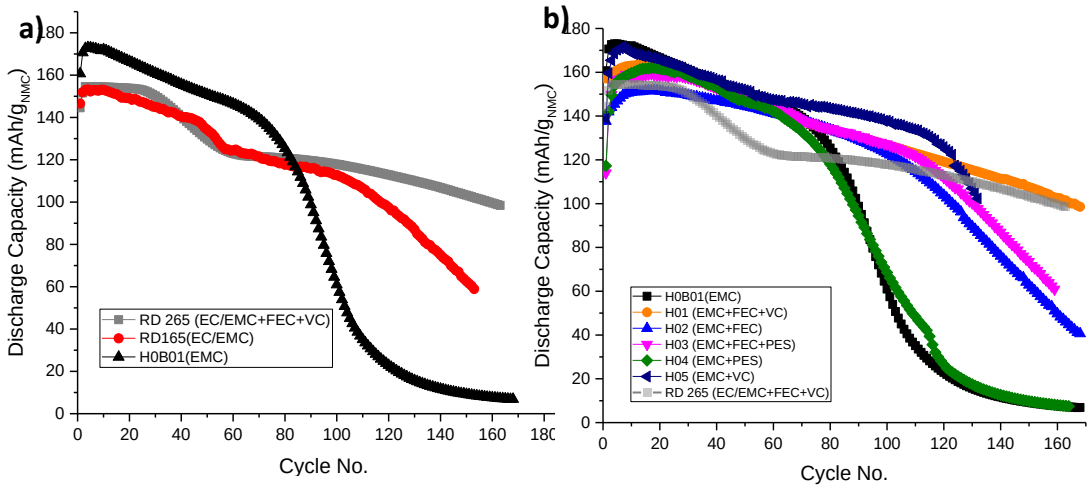

Figure 7-3 Constant current cycling profile under the C rate of C/5 between 2.5 V – 4.4 V for Si-FLG/NMC full cells with a) three control electrolytes and b) EC free electrolytes with different additives.

7.6 Electrochemical Impedance Analysis

Figure 7-4 (a) outlines an example of the variation trend of the Nyquist plots that obtained from potentio electrochemical impedance spectroscopy (PEIS) measurement for Si-FLG/NMC full cell with H01 electrolyte. It displays the negative movement of all spectra, indicating the decrease of series resistance. Also, the size of the first semi-circle in spectra refers to the SEI resistance, which remains stable during the cycling despite there is a significant decrease at the beginning. Moreover, the size of the second semi-circle represents the charge transfer resistance, which also demonstrates a slight decrease for these 100 cycles. These trends are in alignment with the fitting results shown in Figure 7-4 (b)-(d), indicating that the fitting results are reliable for further analysis and comparison.

From Figure 7-4(b), it can be noticed that the cell with only the EMC electrolyte has the highest series resistance, while the cell with RD265, which involves both EC and additives, has the lowest series resistance. This is because lithium ions are known to be preferentially solvated by EC molecules due to the higher binding energy of Li^+...O=C(R) in EC than that of EMC[26], [167]. Therefore, with EC involved, a higher dissociation degree of $LiPF_6$ can be achieved, and it will be easier for lithium ions to move across the electrolyte, thereby resulting in a lower series resistance[168]. It can be observed that with different additives, the series resistance of EC free electrolytes can be reduced to different levels; all of them demonstrate a significant decrease for the first 10 cycles. This decrease is possibly attributed to the low

dissociation constant of $LiPF_6$, which is more likely to appear in ionic pairs or clusters of $LiPF_6$ in the electrolyte[167]. During the process of associating with additives and forming a passivated film on the anode, the dissociation level of $LiPF_6$ becomes higher, which in turn, reduces the viscosity for lithium ions going through the electrolyte. Regarding reducing series resistance for EC free electrolytes under high voltage, the FEC shows the best performance with the lowest series resistance among all EC free electrolytes while VC presents the highest series resistance for EC free electrolytes with additives. The dramatic increase for series resistance of cells with H0B01, RD165 and H04 after 70 cycles can be attributed to the cell fading, which is in agreement with the cycling performance as shown in Figure 7-3.

It can be noted from Figure 7-4 (c) that initially, cells with EMC only, EMC/PES and VC contained EC free electrolytes displayed much higher SEI resistance compared with other cells. Moreover, for cells with EMC only and EMC/PES electrolytes, it takes about 40 cycles to bring the high SEI resistance to a lower and stable level as other cells. These results indicate that the SEI layers formed with EMC only and EMC/PES electrolyte demonstrate the highest resistance and the most instability among those with other electrolytes. It can also be concluded that the SEI layers formed with VC-based electrolytes (H01 and H05) generally present a higher resistance compared with those with FEC-based electrolytes (H02 and H03) for the first 20 cycles. This is in agreement with findings in existing studies that during the SEI forming process, the SEI layers formed with FEC are normally denser and less resistive compared to those formed with VC-based electrolytes[169]. Additionally, it can be noticed that all cells with the FEC additive demonstrate a more stable resistance in SEI compared to others, which proves that FEC could help to form a low resistive and stable SEI layer on the anode surface.

Regarding charge transfer resistance, it can be observed from Figure 7-4 (d) that for cells with EC-containing electrolytes, there is a noticeable increase in charge transfer resistance during the entire cycling process; this is in agreement with EC-involved Si full cell systems[117]. However, for cells with EC-free electrolytes, the charge transfer resistance demonstrates a different level of decrease at the beginning and remains stable until the fading point of the cell, which is quite similar to the trend of charge transfer resistance in Si-based half-cells reported in the previous chapter (as shown in Figure 5-6 and Figure 6-13). This indicates that for the cells with EC involved, the by-

products of EC oxidation on the surface of the NMC cathode could accumulate over cycling, which dominates the increase of charge transfer resistance. Whit the exception of EC from the electrolyte, the trend of charge transfer is most likely dominated by the phase change of the Si surface during the cell fading as explained in Chapter 5. Also, it can be noticed that the general charge transfer resistance is higher for cells with EMC only, EMC/PES and EMC/VC electrolytes compared to those involving FEC, possibly due to the higher resistance of the decomposition products from PES or VC. This is also in alignment with reported impedance results in literatures[27], [117], [140].

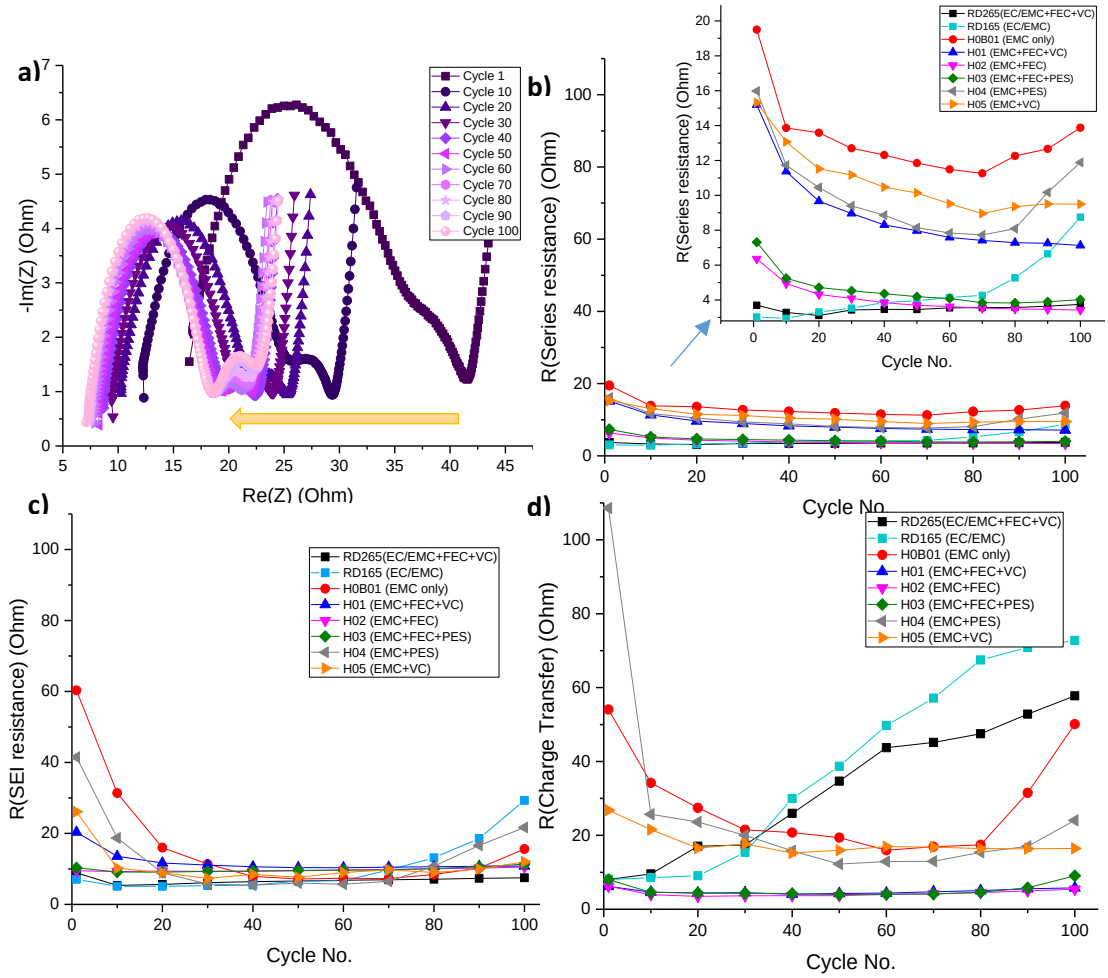

Figure 7-4 a) Electrochemical impedance spectroscopy example for Si-FLG/NMC full cell with H01 electrolyte and the fitting result for b) series resistance (inset: zoom-in of the data set), c) SEI resistance, and d) charge transfer resistance of Si-FLG/NMC full cells with different electrolytes.

7.7 Post-mortem Surface Chemistry Analysis

According to charge transfer results in the last section, the interface charge transfer resistance for all cells with EC free electrolytes are in alignment with Si-based half-

cells, indicating that the Si electrode dominates the charge transfer resistance, which is one of the main fading mechanisms. Therefore, post-mortem XPS analysis has been conducted to investigate the surface chemistry on a pristine Si electrode and the ones with a different electrolytes after 100 cycles. Figure 7-5 summarises the result of a high-resolution survey on Si 2p. It can be observed that for pristine Si electrode, the main components on pristine Si electrode are mainly Si and Si dioxide layer. For most cycled electrodes, the peak for both SiO_2 (~104 eV) and Si (~ 99 eV) disappeared except there is still a reduced peak for Si detected on the electrode with RD165 (EC/EMC), possibly because most Si electrodes were covered by a thick SEI layer after 100 cycles and the weak peak for Si would be likely overlapped with the Li-Si peak. While for Si electrodes with EC/EMC electrolyte, it is likely under the circumstance that by the point of taking XPS measurement, there was electrode cracking on the surface of this Si electrode, which broke the SEI layer covered on Si particles. It has been reported that with EC-based electrolytes without any additives, Si electrode cracking is more likely to occur in the perpendicular direction with the electrode surface and rapidly grow deep into electrode[150].

Regarding the components of the SEI layer on Si electrodes, it can be noticed that all electrodes display a peak at about 101 eV and 102 eV, representing SiO_x. This is a suboxide state of Si and usually exists in the interface between SiO_2 and Si[170]. The presence of SiO_x in SEI layer of Si electrodes has been proven in the literature despite sometimes being difficult to identify when it is overlapped with the peak referred to Li_xSiO_y due to peak shifting with different distribution among Si^+, Si^{2+}, and Si^{3+} oxidation states[125], [171].

Li_xSiO_y is one of the common species of SEI layer that reported in Si electrodes[162], [171][172], which is corresponding to the peak around 100 eV. It has been reported that Li_xSiO_y commonly existed in the inner layer of SEI and with FEC-based electrolytes, the formation of Li_xSiO_y can be suppressed due to FEC promotes the formation of LiF[162], which agrees with the XPS spectra for Si electrodes with RD265, H01 and H02 in Figure 7-5. Also, it has been mentioned in chapter 5 and Chapter 6 that Si particles are likely to be electrochemically fused together through the SEI species Li_xSiO_y. Therefore, the intensity of Li_xSiO_y can also represent the fusion severity within the electrode thus determines the cyclability of the cell. Additionally, there is another SEI component that could be observed in Figure 7-5,

which is the ester polymer (located at 103 eV) that esterified between Si-OH and organics that contained carboxyl groups. It is believed that this polymer component is relatively stable hence it could help to maintain the stability of SEI layer[162]. It can also be noticed that for Si electrodes with EMC/VC there is not Si-ester bond appears in the Si 2p spectra, which possibly because the polymer component formed with this electrolyte system is not likely to be esterified with Si-OH.

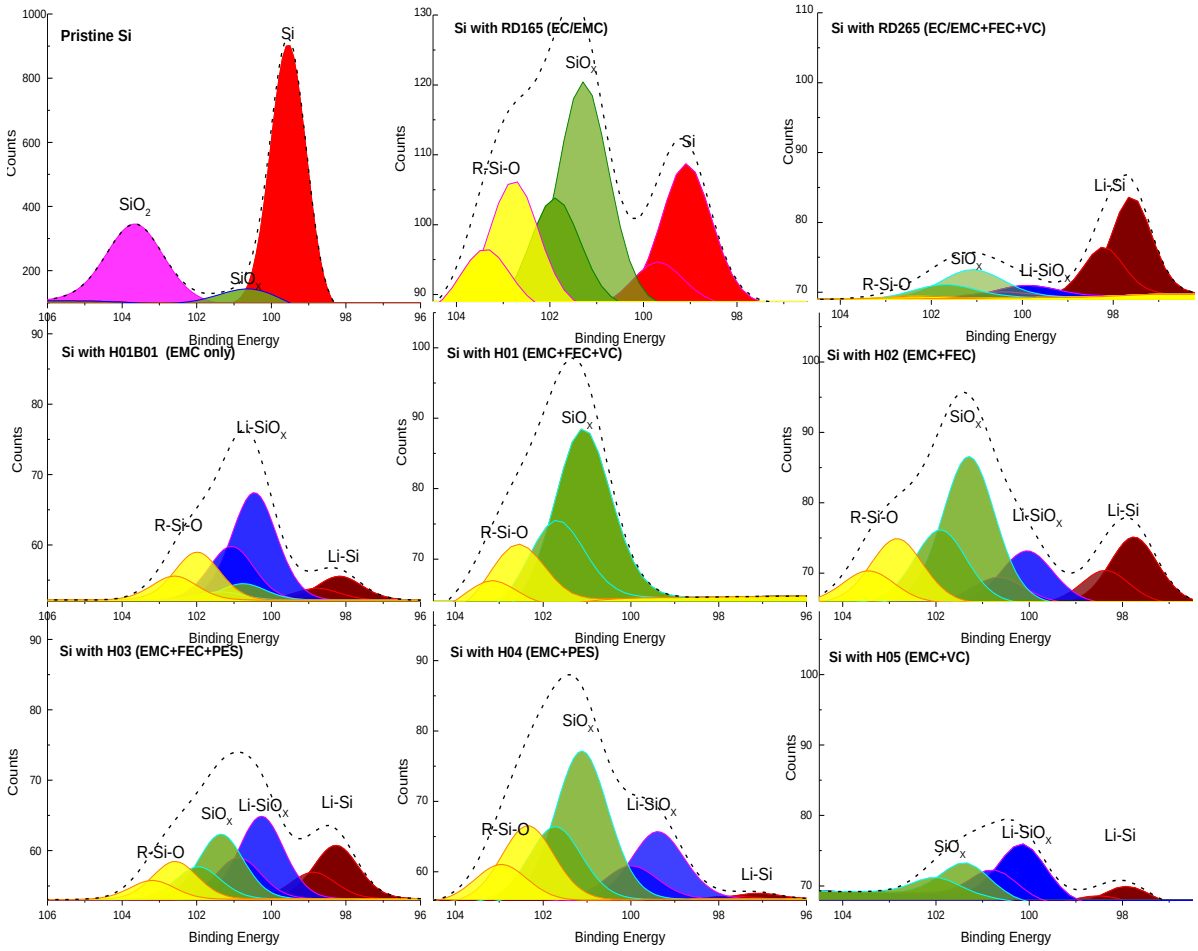

Figure 7-5 High-resolution XPS spectra for the element of Si 2p on Si-FLG electrode: pristine and after 100 cycles in different electrolytes.

Figure 7-6 displays the XPS spectra for the high-resolution survey of F 1s on Si electrodes, which primarily represents the fluorine-contained SEI species. It can be observed that there are two main fluorine-based SEI components for all electrodes, namely LiF (located at 685 eV) and $Li_XPO_YF_Z$ (located at 687 eV). It has been reported in several studies that $Li_XPO_YF_Z$ is the decomposition product from $LiPF_6$, which is less stable than LiF[114], [169]. Therefore, cells with more stable LiF other than $Li_XPO_YF_Z$ are favoured for improving the stability of SEI. In Figure 7-6, it only compares spectra of the cells with RD265 and RD165; it can be noted that the cell

with RD165 (EC/EMC) contains much less LiF and a higher amount of $Li_XPO_YF_Z$ due to the lack of additives and several other SEI components such as LiP_xF_y and fluorocarbon. This possibly comes from the oxidation of EC under high voltage. Interestingly, if we compare Si with RD165 and H0B01, it can be revealed that by simply removing EC from the electrolyte, more LiF could be formed and the formation of $Li_XPO_YF_Z$ will be suppressed, suggesting that under high voltage without the presence of additives, EC will suppress the formation of LiF and generate more organic decomposition products. It can also be noticed that for the VC-containing electrolyte, there are fluorocarbons (referred to peak at 688 eV) that decomposed from $LiPF_6$ presenting in SEI layer, which has been rarely explained in the literature. However, it appears that with these additional fluorocarbons there is no negative impact on the electrochemical stability for the cells with H01 electrolyte compared with those excluding fluorocarbons according to the result in Section 7.5 and Section 7.6.

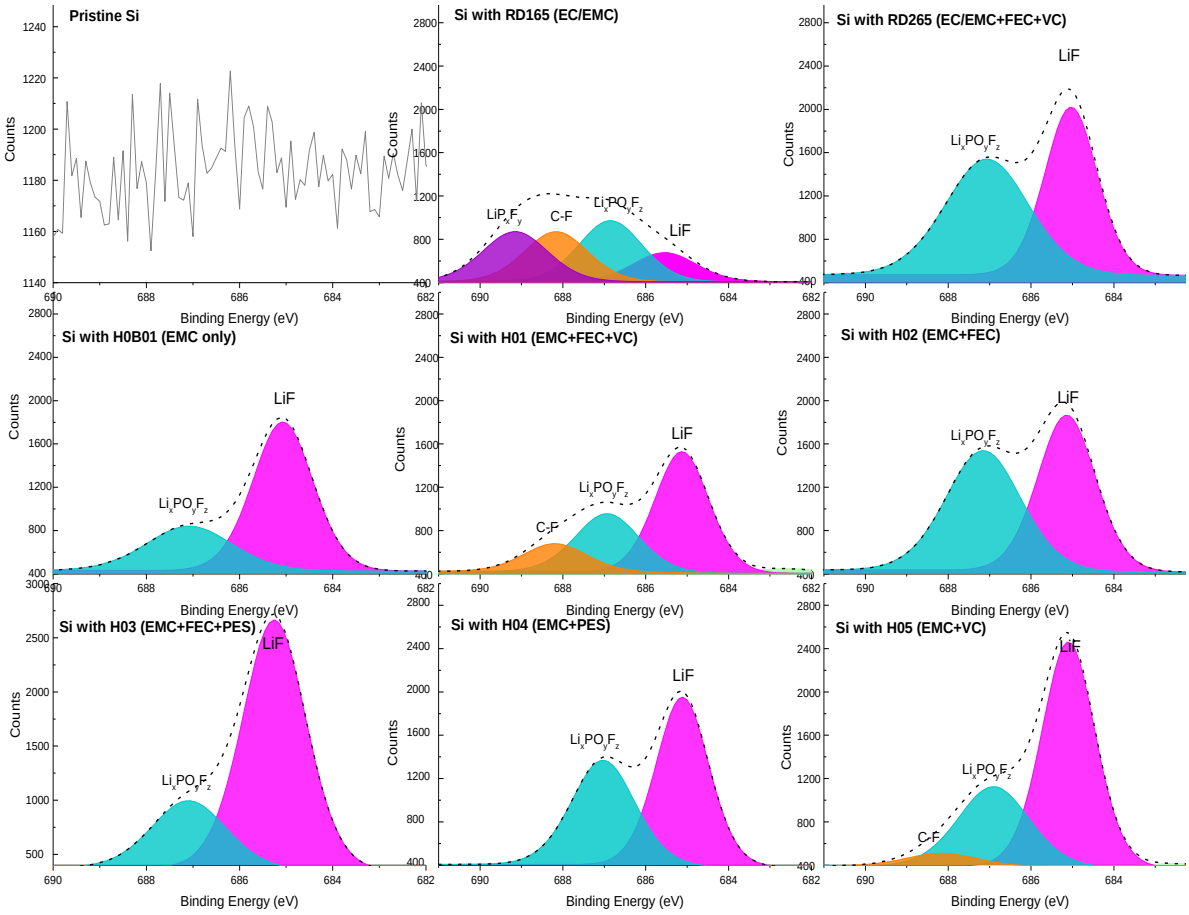

Figure 7-6 High-resolution XPS spectra for the element of F 1s on Si-FLG electrode: pristine and after 100 cycles in different electrolytes.

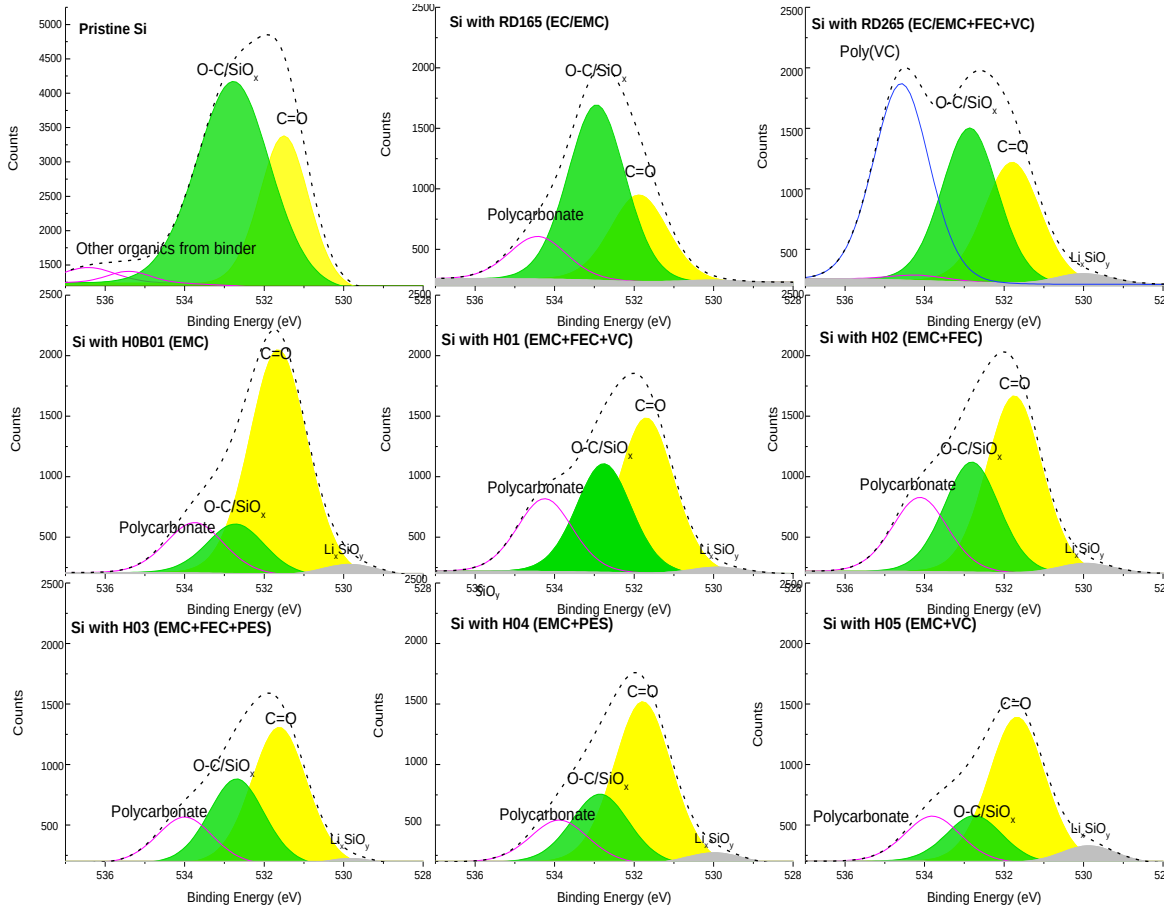

Figure 7-7 High-resolution XPS spectra for the element of O (1s) on Si-FLG electrodes: pristine and after 100 cycles in different electrolytes.

As shown in Figure 7-7, the O 1s spectra displays that there are three main peaks detected on the surface of the Si electrode, located at 531.7 eV, 532.8 eV and 534.4 eV, respectively. O 1s at 531.7 eV can be represented for the C=O group derived from polymer binder as well as from the decomposition products of the electrolyte. The peak at 532.8 eV is the signal overlapped by Si suboxide and C-O group from polymer binder. The O 1s signal at 534.5 eV typically refers to the polycarbonate that comes from other derivation products of either polymer binder or electrolyte components. Generally, it is the weakest signal that can be detected among these three peaks on the Si electrode. However, it can be observed that for the Si electrode cycled with RD265 there is an intensive peak for polycarbonate with a slight shift to a higher energy level (534.8 eV). This phenomenon has also been revealed in several studies, which suggests that this peak could be attributed to the formation of radical poly(VC) in the presence of a VC additive, the reaction is described in Mechanism below[173]–[175]. Interestingly, this intensive peak is not apparent on the Si electrode with H01 (EMC+FEC+VC) and H05 (EMC+VC) with the difference being excluding EC from

the electrolyte. This indicates that the presence of EC could largely assist the formation of radical poly(VC), which is reasonable since it consists of repetition units of EC. The presence of the radical poly(VC) in SEI is considered to contribute a stable SEI layer, and this is one of the advantages of incorporating VC into the electrolyte. Therefore, after excluding EC from the electrolyte, this benefit from VC has been minimised.

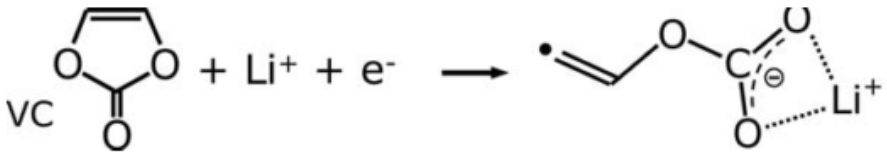

To further investigate the effect of electrolyte decomposition on the surface of the cathode, O 1s spectra on NMC electrodes taken from Si-FLG/NMC full cells has also been analysed. It can be observed from Figure 7-8 that, for pristine NMC electrode, the peak at 529.5 eV represents the O from the metal oxide of NMC, while the other two peaks on the side refer to C=O (531 eV) and C-O bond (532 eV ~ 533.5 eV) that from Li_2CO_3. It can be noted in all cycled electrodes that the O signal from NMC is primarily reduced, while either one or both of C-O and C=O peaks demonstrate a significant growth after cycling, indicating the formation of organic products that decomposed from the electrolyte. There are also polycarbonates (534 eV) existing on the surface of NMC due to the electrolyte decomposition. Constantly, with findings from the anode, the presence of radical poly(VC) can also be detected only on the surface of NMC with RD265, which proves that the decomposition of VC occurs on both sides of the anode and cathode with EC involved. Additionally, there is a small peak at 528.5 eV, which represents Li_2O, detected on some NMC electrodes and it is more evident in the cells with RD165 (EC/EMC), H02 (EMC+FEC) and H04 (EMC+PES). Li_2O is considered as an unstable SEI component since it is generally located at the outermost surface of SEI and can easily react with POF_3 for further oxidation[175], [176]. It can be noted that for cells with VC-involved electrolytes, the intensity of Li_2O can be dramatically decreased or even eliminated, thereby indicating that VC could effectively suppress the formation of Li_2O. While comparing the cells with RD165 and H0B01, it can be concluded that by simply removing EC from the electrolyte, the amount of Li_2O can be significantly reduced since Li_2O has been reported as the predominated product that decomposed from EC; this situation can be

worsened under high voltage due to the instability of EC[177]. This could also explain the improvement of the stability for the cells with H01 (EMC+FEC+VC), compared to those containing RD265 (EC/EMC+FEC+VC). It has been suggested in the literature that PES has the better effect in eliminating Li_2O compared to VC[175]; however, for the EMC/PES system in this study, there is still a noticeable amount of Li_2O detected on NMC, indicating the benefit of PES could not be achieved alone without EC under high voltage.

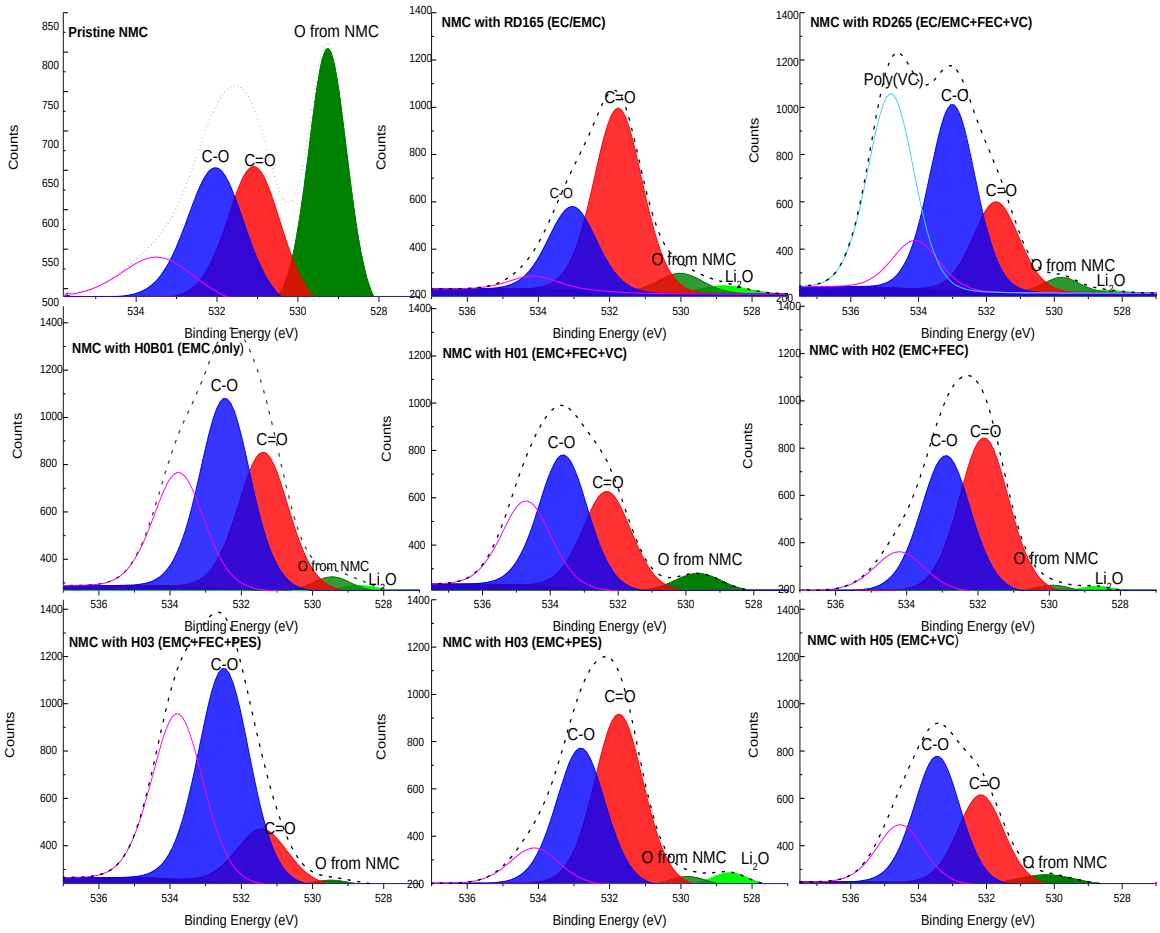

Figure 7-8 High-resolution XPS spectra for the element of O (1s) on NMC electrodes: pristine and after 100 cycles in different electrolytes.

7.8 Chapter Conclusion

It can be concluded from this chapter that cells with EC-involved electrolytes can suffer from the negative effect of EC oxidation on NMC surface under high voltage. With additives of FEC and VC, the cyclability can be improved at the stage when EC has been consumed, but there is still a dramatic capacity loss (13 % of total capcity) for first 50 cycles. Therefore, removing EC from electrolytes can be a practical approach for cells cycling under high voltage (4.4 V), but proper additives are

necessary to enable the formation of the passivated film on electrodes. The results show that EC free electrolyte (H01) with a combination of FEC and VC demonstrates the best performance in terms of improving the cyclability of Si-FLG/NMC full cells with 68.75 % capacity retention after 150 cycles. Removing EC from electrolytes could result in higher impedance for the electrode during lithiation since EC could help to dissociate $LiPF_6$ and improve the rheology property of the electrolyte. With FEC incorporated, cells with the EC free electrolytes could achieve a reasonably low and stable impedance over cycling.

The SEI components formed on the electrode surface with different electrolyte additives have also been investigated through XPS spectra. It revealed that after 100 cycles between 2.5 V – 4.4 V, the main species found in SEI on all Si electrodes are Li_2CO_3, SiO_x, Li_xSiO_y, $Li_XPO_YF_Z$, LiF and polymer components. Li_xSiO_y can also be detected on most electrodes, but since it usually exists in the inner layer of SEI, it does not appear on the electrode with H01 electrolyte, possibly due to a thick and stable SEI layer being formed. Among these SEI components, LiF and ester polymers have been recommended as the most favoured species concerning stabilising SEI layer, while the unstable species such as Li_xSiO_y and $Li_XPO_YF_Z$ are suggested to be suppressed with appropriate additives. It has been proven in this study that FEC could suppress the formation of Li_xSiO_y to some extent, and removing EC from electrolytes could suppress the formation of $Li_XPO_YF_Z$. There is another unstable SEI species - Li_2O detected on some NMC electrodes. It has been proven in this study that removing EC from the electrolyte could reduce or incorporate VC as an electrolyte additive, which could suppress the formation of Li_2O, thus, achieve a more stable electrolyte interface on the cathode side. The only drawback for excluding EC is it could minimise the formation of a stable polymer – radical poly(VC) in the VC-involved electrolytes, which reduces the stability contributed from VC. Therefore, a EC free electrolyte with a combination of FEC and VC additives has been recommended, since FEC could also generate a reasonable amount of polymer species on SEI, which compensates for the lack of a radical poly(VC). This finding is in alignment with the improved electrochemical performance for cells with the electrolyte of EMC/FEC/VC.

Chapter 8 Conclusion and Suggestion for Future Work

8.1 Summary of Main Findings

This primary objective of this thesis is to develop the high-energy Li-ion battery based on Si anode and to improve the cycling performance with addressing a holistic approach that is required to accommodate the dynamic challenges presented by Si undergoing alloying with Li-ions to high storage capacities. This includes problematic volume expansion and a continued loss of Li-ions due to the formation and reformation of SEI layers. To achieve this target, several approaches have been taken including optimising the composite formulation of Si electrodes, developing a robust binder system and investigating a suitable electrolyte for Si full cells that can be stable for cycling under high voltages. Comprehensive studies have been conducted for each approach, which is outlined in more details in different chapters. The main findings of each chapter are summarised as follows.

Chapter 4 and 5 focussed on approaches to develop the optimised composite formulation of the Si electrodes. Chapter 4 investigated three different carbon mixtures and compared them with the standard additive carbon black, which has been the conventional conductive additive used in Li-ion batteries. The results suggested the all cells with carbon mixture showed better performance in terms of rate capacity and the longest cyclability under high C rate compared to those containing only carbon black as the conductive additive. It validates the hypothesis that combining different carbon morphologies allows for maximising both long and short rage conductive networks and structurally stabilises the composite through maximising the physicochemical interactions. Among these carbon mixtures, the one that includes carbon black, graphite and MWCNTs demonstrated the best performance. However, the low viscosity of slurry resulted from the manufacturing process prevented it from being further applied into Si systems in this thesis considering there is a need for a large-

scale coating with this slurry at the later stage. In the end, the carbon mixture containing carbon black, graphite and FLG was considered for further investigation in Si electrodes in this study due to its much-improved cycling performance under high C-rate and its reasonable viscosity of slurry for large-coating on battery pilot line.

Based on the choice of carbon conductive from Chapter 4, Chapter 5 further optimised the Si composite electrode with incorporating FLG as the combined active material. A formulation matrix was conducted to identify the optimized Si-FLG ratio, and as a result, the formulation of 60 wt% Si, 16 wt% FLG, 14 wt% NaPAA and 10 wt% carbon mix was recommended due to its longest cyclability (with 80 % capacity retained after 230 cycles) even under high current density 360 mA/g. Based on this optimized formulation, further characterisation including nano-indentation test, SEM and EDX imaging for cross-section, CC cycling, differential capacity analysis, and different impedance spectroscopy techniques have been conducted to comprehensively understand the contribution from FLG in terms of mechanical and electrochemical behaviours in the Si-FLG electrode as well as to analyse the failure mechanism according to Si phase change. It was concluded that regarding structure optimisation, FLG could improve the tensile property of the electrode and this in turn better tolerate the significant volume change of Si. Also, with incorporation of FLG, the electrochemical fusion in Si electrodes through its SEI components can be prevented to some extent, thus maintaining the stability of the electrode structure. In terms of electrochemical performance, FLG could contribute a capacity of 300 mAh/g in this system. Moreover, due to the superior electronic conductivity, FLG could help to maintain the overall series resistance of the electrode at a lower impedance level. Additionally, Si-FLG electrode demonstrated a much improved electrochemical stability, which postpones the increase of overpotential as well as the phase change to high-resistive crystalline Si phase. Regarding knowledge contribution, this study also introduced SPEIS as a more straightforward characterisation method for Warburg diffusion impedance, which could easily compare the variation trend of Warburg diffusion impedance with different SoC and cycle numbers simultaneously. With this method, it also contributes a novelty to the knowledge system that the Warburg diffusion impedance in the Si electrodes is highly phase-dependant.

Chapter 6 investigated different polymer binder system for Si electrodes, starting with optimising a single polymer system based on PAA. It has been found that with partially

neutralized PAA with 70 mol% NaOH, NaPAA demonstrated much-improved cycling performance while involved into Si electrodes (maintaining stable at 1200 mAh/g for over 100 cycles while comparing only 40 cycles for PAA), due to its enhanced mechanical property in terms of adhesion force and tensile strength. The mechanism behind this improved property could be attributed to with introducing Na^+, the polymer chain within PAA will be extended and stretched, which will present more active carboxyl group to form a strong covalent bond (ester type) with the surface of Si.

Based on the findings with NaPAA, different binary binder systems were further investigated including PAA/PVA system and NaPAA/SBR systems. Due to the limitation condition of crosslinking between PAA and PVA, which is favoured for the acid condition, PAA was only partially neutralised with 8 mol % NaOH in this study. The complete performance of both PAA/PVA and pnPAA/PVA were investigated. It revealed that the optimised ration between PAA/PVA should be 60/40 and the heat-treatment condition should be 150°C for 30 mins. Improved cyclability was achieved for Si-PAA/PVA (60/40) compared to Si-PAA system due to enhanced tensile property contributed from PVA, and further improvement of cyclability was indicated for Si-pnPAA/PVA (60/40) due to the stronger adhesion force with partial neutralisation. For NaPAA/SBR system, two different ratio – 2/1 and 5/1 between NaPAA and SBR were investigated. As a result, NaPAA/SBR (2/1) delivered a slightly longer cycle life than NaPAA/SBR (5/1), but both of them were not as good cyclability as the Si electrodes with NaPAA although they presented much improved tensile property. The failure mechanism could be attributed to the high resistance that induced by SBR, which was proved in the impedance analysis result.

However, both binary systems did not show much improvement in electrochemical cyclability compared to NaPAA; hence a more comprehensive designed binder based on PAA with multi-level crosslinking within the polymer structure was introduced - PAA-Fe^{2+}-FLG. This novel polymer demonstrated significant improvement in terms of tensile strength and adhesion force (similar adhesion force with NaPAA), thus resulted in a dramatic enhancement in half-cell cyclability of Si electrodes compared to Si-NaPAA electrodes, which maintained 1000 mAh/g after 200 cycles even cycled under the full capacity of Si (3579 mAh/g). The additional knowledge contribution from this chapter also addressed that to improve the performance of PAA based binders in Si electrodes, building and strengthening the ionic interaction within

polymer networks can be the most effective approach. Also, among flexibility, high stiffness and adhesion force, the latter two factors are considered as more important factors when designing binders for Si electrodes, since polymers with improved stiffness and adhesion strength generally demonstrate better cycling performance in Si electrodes.

Chapter 7 investigated EC free electrolytes with different additives to be applied into Si-FLG/NMC full cells cycling upon to 4.4 V and compared with the performance of standard EC involved electrolytes. The results proved that EC-involved electrolytes could suffer from problems associated with EC oxidation under high voltage. Improvement in cycle life can be achieved with a combination of FEC and VC additives; however, there was still a dramatic capacity loss for first 50 cycles. Therefore, EC free electrolytes were recommended for Si-FLG/NMC full cells cycled under high voltage with appropriate additives included. To identify the optimised additives, comprehensive studies including water content measurement, oxidative limitation test, differential capacity analysis, CC cycling, impedance analysis and surface chemistry analysis were conducted. The result suggested that Si-FLG/NMC full cells with the electrolyte containing EMC/FEC/VC demonstrated the best performance in terms of cyclability, and also a relatively low and stable overall impedance was achieved. There was no apparent improvement contributed from PES in terms of cell cyclability, indicating that PES may not behave well in EC free electrolytes or that further modification in PES-based electrolyte systems was necessary. Additionally, there proved to be several advantages with removing EC from electrolytes to be cycled under high voltage, including suppressing the formation of unstable SEI species such as $Li_XPO_YF_Z$ on the surface of the anode and Li_2O on the surface of the cathode. Also, FEC and VC have been proven to form a large amount of stable polymer esters that could maintain the stability of SEI. In the meantime, FEC could suppress the formation of Li_xSiO_y on Si and VC could suppress the formation of Li_2O on the surface of NMC, which were also considered to improve the stability of SEI. The only drawback for excluding EC was that it could minimise the amount of the stable polymer - radical poly(VC) that decomposed from VC; however, by combining with FEC, this disadvantage could be compensated.

8.2 Limitation of This Work

Practical approaches for improvement were considered that would add scientific knowledge and also be industrially relevant. For each chapter in this study, the baseline materials chosen for optimisation was based on the good reviews in literature as well as meeting the requirement for easy large-scale manufacture. The materials and the approaches that were concerned as not suitable for battery scale-up pilot line were not considered such as the chemical modification on the material structure and synthesising functional nano-composite materials. However, there can still be a dramatic improvement in cyclability for Si electrodes through those approaches but how to get them industrialised would represent another research direction.

Owing to time constraints during the acquisition of electrochemical cycling data (upto 3 months at times) it was not always possible to carry forward new optimised systems into subsequent chapter territories for comparative purposes. For example, it remains inconclusive whether the optimised binder (PAA-Fe^{2+}-FLG) can further improve the cyclability for Si-FLG/NMC full cells with EMC/FEC/VC. Also, only NMC-622 was chosen as the cathode material as it is considered a relevant material and easily obtainable to study (unlike availability of higher Ni-materials such as NMC-811). Hence the performance for EC free electrolyte for full cells of Si-FLG with other types of NMC chemistries or other high voltage materials such as NCA were not possible to include within the scope of this study.

All of the electrochemical characterisations in this study were conducted in coin cells, hence whether the optimised materials can achieve similar performance in large cell format is yet to be demonstrated but constitutes an interesting possibility for future technology development and transfer. There could be other processing factors to consider at large-scale fabrication also; problems that only emerge whilst manufacturing the battery at pouch cell level. These can include new requirements for the slurry to achieve large area double-sided coating, polymer synthesis at large scale, gas generation problems for electrolytes during formation and relevant other safety issues.

8.3 Suggestion for Research in the Future

Based on the findings in each chapter and the limitation of this work, further investigation on improving Li-ion battery based on Si electrodes can be summarised as follows.

It has been proven in Chapter 4 that the carbon mixture containing carbon black, graphite and MWCNTs demonstrated a much-improved performance in terms of rate capacity and cyclability under high C-rate. However, the manufacturing method for adding MWCNTs into Si slurry needs to be optimised to achieve a higher viscosity for large-scale coating. The research point is how to control the water content while assure to get MWCNTs well dispersed in the meantime. Once this problem is solved, the carbon mixture with MWCNTs is promising to help Li-ion batteries incorporating Si electrodes realise fast charging.

For the Si-FLG electrode that has been optimised in Chapter 5, the binder system and optimised carbon conductive characterised in the future can be incorporated to verify the improvement in this optimised formulation. Concerning the relationship between Warburg diffusion impedance and Si phase change, further operando NMR characterisation can be involved to obtain the accurate phase change of Si at different SoC in this system. This can better establish the knowledge system as in Chapter 5, the phase change of Si at different voltage was referred to literature where NMR conducted on other Si systems, which might have errors with the Si-FLG system in this study.

Regarding the polymer binder investigated for high-content Si electrodes, more binary cross-linking binder systems should be explored that replace PAA with a polymer that could form a stronger covalent bond with the Si particles. Also, with the knowledge finding summarised in Chapter 6, more multi-level cross-linked polymers can be tailor-designed and characterised in Si electrodes. Additionally, the ability of the optimised polymer to be manufactured in a large volume should be considered.

To further improve the energy density and cyclability within Si full cells based on the findings in Chapter 7, a comprehensive study on high-voltage cathodes in pairing with Si anodes needs to be conducted. To reduce the initial loss, methods including pre-lithiated treatment on Si anode, amorphising Si particles and alloying with other materials that could help with buffering expansion issues could be investigated.

Regarding the choice of electrolyte to be applied under high voltage, the EC free electrolyte are considered to be a good start since cyclability improvement for Si-FLG/NMC full cell has been proven in this study, but more candidates and combination of additives can be further investigated. To better understand whether PES is suitable for EC free electrolyte systems under high voltage in Si-FLG/NMC full cells, modifications on PES or incorporation with other additive candidates can be considered.

With the optimised materials identified for Si full cells, manufacture and characterisation at the pouch cell level are suggested to be conducted, since it will address new challenges for the manufacturing process, electrode and electrolyte behaviours, and safety issues.

Bibliography

[1] G. T. K. Fey, “Introduction to Lithium Ion Batteries.”

[2] J. B. Goodenough and K. S. Park, “The Li-ion rechargeable battery: A perspective,” *J. Am. Chem. Soc.*, vol. 135, pp. 1167–1176, 2013.

[3] The Institution for Mathematics and Its Applications, “Abstracts and Talk Materials,” *Kybernetes*, Jul-2005. [Online]. Available: http://www.emeraldinsight.com/doi/abs/10.1108/k.2005.06734fac.004. [Accessed: 26-Jan-2015].

[4] I. Buchmann, “Basic to Advanced Battery Information from Battery University,” 2012. [Online]. Available: http://batteryuniversity.com/. [Accessed: 18-Dec-2014].

[5] E. Science, “A Better Anode Design to Improve Lithium-Ion Batteries,” *The Advanced Light Source Communications Group*.

[6] H. Fujimoto, K. Tokumitsu, A. Mabuchi, N. Chinnasamy, and T. Kasuh, “The anode performance of the hard carbon for the lithium ion battery derived from the oxygen-containing aromatic precursors,” *J. Power Sources*, vol. 195, no. 21, pp. 7452–7456, Nov. 2010.

[7] M. N. Obrovac and L. J. Krause, “Reversible Cycling of Crystalline Silicon Powder,” *J. Electrochem. Soc.*, vol. 154, p. A103, 2007.

[8] M. N. Obrovac and L. Christensen, “Structural Changes in Silicon Anodes during Lithium Insertion/Extraction,” *Electrochem. Solid-State Lett.*, vol. 7, no. 5, p. A93, 2004.

[9] T. D. Hatchard and J. R. Dahn, “In Situ XRD and Electrochemical Study of the Reaction of Lithium with Amorphous Silicon,” *J. Electrochem. Soc.*, vol. 151, p. A838, 2004.

[10] J. Li and J. R. Dahn, “An In Situ X-Ray Diffraction Study of the Reaction of Li with Crystalline Si,” *J. Electrochem. Soc.*, vol. 154, no. 3, p. A156, 2007.

[11] J. H. Ryu, J. W. Kim, Y.-E. Sung, and S. M. Oh, “Failure Modes of Silicon Powder Negative Electrode in Lithium Secondary Batteries,” *Electrochem. Solid-State Lett.*, vol.

7, no. 10, p. A306, 2004.

[12] B. Key, M. Morcrette, J.-M. Tarascon, and C. P. Grey, “Pair distribution function analysis and solid state NMR studies of silicon electrodes for lithium ion batteries: understanding the (de)lithiation mechanisms.,” *J. Am. Chem. Soc.*, vol. 133, no. 3, pp. 503–12, 2011.

[13] J. Shim and K. A. Striebel, “The dependence of natural graphite anode performance on electrode density,” *J. Power Sources*, vol. 130, no. 1–2, pp. 247–253, 2004.

[14] M. Singh, J. Kaiser, and H. Hahn, “Thick Electrodes for High Energy Lithium Ion Batteries,” *J. Electrochem. Soc.*, vol. 162, no. 7, pp. A1196–A1201, 2015.

[15] Z. Du *et al.*, “Enabling aqueous processing for crack-free thick electrodes,” *J. Power Sources*, vol. 354, pp. 200–206, 2017.

[16] J. R. Szczech and S. Jin, “Nanostructured silicon for high capacity lithium battery anodes,” *Energy Environ. Sci.*, vol. 4, no. 1, p. 56, 2011.

[17] H. Wu and Y. Cui, “Designing nanostructured Si anodes for high energy lithium ion batteries,” *Nano Today*, vol. 7, no. 5, pp. 414–429, Oct. 2012.

[18] S. Goriparti, E. Miele, F. De Angelis, E. Di Fabrizio, R. Proietti Zaccaria, and C. Capiglia, “Review on recent progress of nanostructured anode materials for Li-ion batteries,” *J. Power Sources*, vol. 257, pp. 421–443, Jul. 2014.

[19] R. Teki, R. Krishnan, T. C. Parker, T. M. Lu, P. N. Kumta, and N. Koratkar, “Nanostructured silicon anodes for lithium Ion rechargeable batteries,” *Small*, vol. 5, no. 20, pp. 2236–2242, 2009.

[20] D. Mazouzi *et al.*, “Critical roles of binders and formulation at multiscales of silicon-based composite electrodes,” *J. Power Sources*, vol. 280, pp. 533–549, Apr. 2015.

[21] A. Kraytsberg, Y. Ein-Eli, a. Kraytsberg, and Y. Ein-Eli, “Higher, stronger, better ... A review of 5 volt cathode materials for advanced lithium-ion batteries,” *Adv. Energy Mater.*, vol. 2, pp. 922–939, 2012.

[22] R. Petibon, J. Xia, L. Ma, M. K. G. Bauer, K. J. Nelson, and J. R. Dahn, “Electrolyte System for High Voltage Li-Ion Cells,” *J. Electrochem. Soc.*, vol. 163, no. 13, pp. A2571–A2578, 2016.

[23] K. J. Nelson, D. W. Abarbanel, J. Xia, Z. Lu, and J. R. Dahn, "Effects of Upper Cutoff Potential on $LaPO_4$-Coated and Uncoated $Li[Ni_{0.42}Mn_{0.42}Co_{0.16}]O_2$/Graphite Pouch Cells," *J. Electrochem. Soc.*, vol. 163, no. 2, pp. A272–A280, 2016.

[24] K. J. Nelson, G. L. d'Eon, A. T. B. Wright, L. Ma, J. Xia, and J. R. Dahn, "Studies of the Effect of High Voltage on the Impedance and Cycling Performance of Li[Ni0.4Mn0.4Co0.2]O2/Graphite Lithium-Ion Pouch Cells," *J. Electrochem. Soc.*, vol. 162, no. 6, pp. A1046–A1054, 2015.

[25] J. C. Burns *et al.*, "Predicting and Extending the Lifetime of Li-Ion Batteries," *J. Electrochem. Soc.*, vol. 160, no. 9, pp. A1451–A1456, 2013.

[26] Y. Wang and P. B. Balbuena, "Theoretical studies on cosolvation of Li ion and solvent reductive decomposition in binary mixtures of aliphatic carbonates," *Int. J. Quantum Chem.*, vol. 102, no. 5 SPEC. ISS., pp. 724–733, 2005.

[27] L. Ma *et al.*, "A Guide to Ethylene Carbonate-Free Electrolyte Making for Li-Ion Cells," *J. Electrochem. Soc.*, vol. 164, no. 1, pp. A5008–A5018, 2017.

[28] D. Aurbach *et al.*, "Design of electrolyte solutions for Li and Li-ion batteries: A review," *Electrochim. Acta*, vol. 50, no. 2–3 SPEC. ISS., pp. 247–254, 2004.

[29] S. Tan, Y. J. Ji, Z. R. Zhang, and Y. Yang, "Recent progress in research on high-voltage electrolytes for lithium-ion batteries," *ChemPhysChem*, vol. 15, no. 10, pp. 1956–1969, 2014.

[30] A. J. Gmitter, I. Plitz, and G. G. Amatucci, "High Concentration Dinitrile, 3-Alkoxypropionitrile, and Linear Carbonate Electrolytes Enabled by Vinylene and Monofluoroethylene Carbonate Additives," *J. Electrochem. Soc.*, vol. 159, no. 4, p. A370, 2012.

[31] H. Li, "A High Capacity Nano-Si Composite Anode Material for Lithium Rechargeable Batteries," *Electrochem. Solid-State Lett.*, vol. 2, no. 11, p. 547, 1999.

[32] H. Kim, M. Seo, M. H. Park, and J. Cho, "A critical size of silicon nano-anodes for lithium rechargeable batteries," *Angew. Chemie - Int. Ed.*, vol. 49, no. 12, pp. 2146–2149, 2010.

[33] C. K. Chan *et al.*, "High-performance lithium battery anodes using silicon nanowires.," *Nat. Nanotechnol.*, vol. 3, no. 1, pp. 31–35, 2008.

[34] L. Cui, R. Ruffo, C. K. Chan, H. Peng, and Y. Cui, “Crystalline-Amorphous Core - Shell Silicon Nanowires for High Capacity and High Current Battery Electrodes 2009,” 2009.

[35] T. Song *et al.*, “Arrays of sealed silicon nanotubes as anodes for lithium ion batteries,” *Nano Lett.*, vol. 10, no. 5, pp. 1710–1716, 2010.

[36] J. P. Maranchi, a. F. Hepp, and P. N. Kumta, “High Capacity, Reversible Silicon Thin-Film Anodes for Lithium-Ion Batteries,” *Electrochem. Solid-State Lett.*, vol. 6, no. 9, p. A198, 2003.

[37] S. Ohara, J. Suzuki, K. Sekine, and T. Takamura, “A thin film silicon anode for Li-ion batteries having a very large specific capacity and long cycle life,” *J. Power Sources*, vol. 136, no. 2, pp. 303–306, Oct. 2004.

[38] D. Ma, Z. Cao, and A. Hu, “Si-Based Anode Materials for Li-Ion Batteries: A Mini Review,” *Nano-Micro Lett.*, vol. 6, no. 4, pp. 347–358, 2014.

[39] B. M. Bang, J. I. Lee, H. Kim, J. Cho, and S. Park, “High-performance macroporous bulk silicon anodes synthesized by template-free chemical etching,” *Adv. Energy Mater.*, vol. 2, no. 7, pp. 878–883, 2012.

[40] D. Chen *et al.*, “Reversible lithium-ion storage in silver-treated nanoscale hollow porous silicon particles,” *Angew. Chemie - Int. Ed.*, vol. 51, no. 10, pp. 2409–2413, 2012.

[41] N. Liu *et al.*, “A pomegranate-inspired nanoscale design for large-volume-change lithium battery anodes,” *Nat Nano*, vol. 9, no. 3, pp. 187–192, Mar. 2014.

[42] M. Zhou *et al.*, “Graphene/carbon-coated si nanoparticle hybrids as high-performance anode materials for li-ion batteries,” *ACS Appl. Mater. Interfaces*, vol. 5, no. 8, pp. 3449–3455, 2013.

[43] S. D. Beattie, D. Larcher, M. Morcrette, B. Simon, and J.-M. Tarascon, “Si Electrodes for Li-Ion Batteries—A New Way to Look at an Old Problem,” *J. Electrochem. Soc.*, vol. 155, p. A158, 2008.

[44] J. Saint *et al.*, “Towards a fundamental understanding of the improved electrochemical performance of silicon-carbon composites,” *Adv. Funct. Mater.*, vol. 17, no. 11, pp. 1765–1774, 2007.

[45] X. Yang, Z. Wen, X. Xu, B. Lin, and Z. Lin, “High-Performance

Silicon/Carbon/Graphite Composites as Anode Materials for Lithium Ion Batteries," *J. Electrochem. Soc.*, vol. 153, no. 7, p. A1341, 2006.

[46] W. Xu and J. C. Flake, "Composite Silicon Nanowire Anodes for Secondary Lithium-Ion Cells," *J. Electrochem. Soc.*, vol. 157, no. 1, p. A41, 2010.

[47] U. Farooq *et al.*, "Effect of binder and composition ratio on electrochemical performance of silicon/graphite composite battery electrode," *Mater. Lett.*, vol. 136, pp. 254–257, Dec. 2014.

[48] T. Yim *et al.*, "Effect of binder properties on electrochemical performance for silicon-graphite anode: Method and application of binder screening," *Electrochim. Acta*, vol. 136, pp. 112–120, Aug. 2014.

[49] S. Komaba *et al.*, "Comparative Study of Sodium Polyacrylate and Poly- (vinylidene fluoride) as Binders for High Capacity Si À Graphite Composite Negative Electrodes in Li-Ion Batteries," *J. Phys. Chem.*, pp. 1380–1389, 2012.

[50] J.-G. Ren *et al.*, "Silicon-Graphene Composite Anodes for High-Energy Lithium Batteries," *Energy Technol.*, vol. 1, no. 1, pp. 77–84, 2013.

[51] G. Zhou *et al.*, "Graphene-wrapped Fe3O4 anode material with improved reversible capacity and cyclic stability for lithium ion batteries," *Chem. Mater.*, vol. 22, no. 18, pp. 5306–5313, 2010.

[52] S.-L. Chou, J.-Z. Wang, M. Choucair, H.-K. Liu, J. A. Stride, and S.-X. Dou, "Enhanced reversible lithium storage in a nanosize silicon/graphene composite," *Electrochem. commun.*, vol. 12, no. 2, pp. 303–306, Feb. 2010.

[53] Y. Q. Zhang *et al.*, "Silicon/graphene-sheet hybrid film as anode for lithium ion batteries," *Electrochem. commun.*, vol. 23, pp. 17–20, Sep. 2012.

[54] H. Xiang *et al.*, "Graphene/nanosized silicon composites for lithium battery anodes with improved cycling stability," *Carbon N. Y.*, vol. 49, no. 5, pp. 1787–1796, 2011.

[55] A. Gohier *et al.*, "High-rate capability silicon decorated vertically aligned carbon nanotubes for li-ion batteries," *Adv. Mater.*, vol. 24, no. 19, pp. 2592–2597, 2012.

[56] J. Y. Eom, J. W. Park, H. S. Kwon, and S. Rajendran, "Electrochemical Insertion of Lithium into Multiwalled Carbon Nanotube/Silicon Composites Produced by

Ballmilling," *J. Electrochem. Soc.*, vol. 153, no. 9, p. A1678, 2006.

[57] L. Dai, D. W. Chang, J.-B. Baek, and W. Lu, "Carbon nanomaterials for advanced energy conversion and storage.," *Small*, vol. 8, no. 8, pp. 1130–66, 2012.

[58] N. Li, C. R. Martin, J. E. Soc, and P. A-a, "A High-Rate , High-Capacity , Nanostructured Sn-Based Anode Prepared Using Sol-Gel Template Synthesis service A High-Rate , High-Capacity , Nanostructured Sn-Based Anode Prepared Using Sol-Gel Template Synthesis," vol. 148, no. 2, pp. 164–170, 2001.

[59] H.-J. Ahn, Y.-S. Kim, K.-W. Park, and T.-Y. Seong, "Use of Sn-Si nanocomposite electrodes for Li rechargeable batteries.," *Chem. Commun. (Camb).*, no. 1, pp. 43–45, 2005.

[60] J. Liu, K. Song, P. A. Van Aken, J. Maier, and Y. Yu, "Self-Supported Li 4 Ti 5 O 12 − C Nanotube Arrays as High-Rate and Long- Life Anode Materials for Flexible Li-Ion Batteries," *Nano Lett.*, vol. 14, pp. 2597–2603, 2014.

[61] N. Sharma, D. Puthusseri, M. O. Thotiyl, and S. Ogale, "Hard Carbon and $Li_4Ti_5O_{12}$ -Based Physically Mixed Anodes for Superior Li-Battery Performance with Significantly Reduced Li Content: A Case of Synergistic Materials Cooperation," *ACS Omega*, vol. 2, no. 12, pp. 8818–8824, 2017.

[62] J. M. Feckl, K. Fominykh, M. Döblinger, D. Fattakhova-Rohlfing, and T. Bein, "Nanoscale porous framework of lithium titanate for ultrafast lithium insertion," *Angew. Chemie - Int. Ed.*, vol. 51, no. 30, pp. 7459–7463, 2012.

[63] Y. Sun *et al.*, "Direct atomic-scale confirmation of three-phase storage mechanism in Li4Ti5O12anodes for room-temperature sodium-ion batteries," *Nat. Commun.*, vol. 4, no. May, pp. 1810–1870, 2013.

[64] C. Chen, R. Agrawal, and C. Wang, "High Performance Li4Ti5O12/Si Composite Anodes for Li-Ion Batteries," *Nanomaterials*, pp. 1469–1480, 2015.

[65] H. K. Arlavinda Rezqita a, b, Raad Hamida, Sabine Schwarzc and A. Trifonovaa, "Conductive Additive for Si/Mesoporous Carbon Anode for Li-Ion Batteries: Commercial Graphite vs Super C65 Arlavinda Rezqita," *ECS Trans.*, vol. 66, no. 9, pp. 17–27, 2015.

[66] I. Lahiri and W. Choi, "Carbon Nanostructures in Lithium Ion Batteries: Past, Present,

and Future," *Crit. Rev. Solid State Mater. Sci.*, vol. 38, no. 2, pp. 128–166, 2013.

[67] B. Fuchsbichler, C. Stangl, H. Kren, F. Uhlig, and S. Koller, "High capacity graphite–silicon composite anode material for lithium-ion batteries," *J. Power Sources*, vol. 196, no. 5, pp. 2889–2892, Mar. 2011.

[68] a Magasinski, P. Dixon, B. Hertzberg, a Kvit, J. Ayala, and G. Yushin, "High-performance lithium-ion anodes using a hierarchical bottom-up approach.," *Nat. Mater.*, vol. 9, no. 4, pp. 353–358, 2010.

[69] M. E. Spahr, D. Goers, A. Leone, S. Stallone, and E. Grivei, "Development of carbon conductive additives for advanced lithium ion batteries," *J. Power Sources*, vol. 196, no. 7, pp. 3404–3413, 2011.

[70] M. E. Spahr, "Carbon-Conductive Additives for Lithium-Ion Batteries BT - Lithium-Ion Batteries: Science and Technologies," M. Yoshio, R. J. Brodd, and A. Kozawa, Eds. New York, NY: Springer New York, 2009, pp. 117–154.

[71] B. Lestriez, S. Desaever, J. Danet, P. Moreau, D. Plée, and D. Guyomard, "Hierarchical and Resilient Conductive Network of Bridged Carbon Nanotubes and Nanofibers for High-Energy Si Negative Electrodes," *Electrochem. Solid-State Lett.*, vol. 12, no. 4, p. A76, 2009.

[72] S. Chou, Y. Pan, J. Wang, H. Liu, and S. Dou, "Small things make a big difference: binder effects on the performance of Li and Na batteries.," *Phys. Chem. Chem. Phys.*, vol. 16, pp. 20347–20359, 2014.

[73] M. Yoshio, R. J. Brodd, and A. Kozawa, *Lithium-Ion Batteries*, vol. 49, no. 0. Springer, 2009.

[74] M. Yoo, C. W. Frank, S. Mori, and S. Yamaguchi, "Effect of poly(vinylidene fluoride) binder crystallinity and graphite structure on the mechanical strength of the composite anode in a lithium ion battery," *Polymer (Guildf).*, vol. 44, no. 15, pp. 4197–4204, 2003.

[75] J. Li, L. Christensen, M. N. Obrovac, K. C. Hewitt, and J. R. Dahn, "Effect of Heat Treatment on Si Electrodes Using Polyvinylidene Fluoride Binder," *J. Electrochem. Soc.*, vol. 155, p. A234, 2008.

[76] A. Magasinski *et al.*, "Toward efficient binders for Li-ion battery Si-based anodes: Polyacrylic acid," *ACS Appl. Mater. Interfaces*, vol. 2, pp. 3004–3010, 2010.

[77] S. Komaba *et al.*, “Polyacrylate Modifier for Graphite Anode of Lithium-Ion Batteries,” *Electrochem. Solid-State Lett.*, vol. 12, no. 5, p. A107, 2009.

[78] Z.-J. Han, N. Yabuuchi, K. Shimomura, M. Murase, H. Yui, and S. Komaba, “High-capacity Si–graphite composite electrodes with a self-formed porous structure by a partially neutralized polyacrylate for Li-ion batteries,” *Energy Environ. Sci.*, vol. 5, no. 10, p. 9014, 2012.

[79] R. P. Babu, K. O’Connor, and R. Seeram, “Current progress on bio-based polymers and their future trends,” *Prog. Biomater.*, vol. 2, no. 1, p. 8, 2013.

[80] I. Kovalenko *et al.*, “A major constituent of brown algae for use in high-capacity Li-ion batteries.,” *Science*, vol. 334, no. 6052, pp. 75–9, Oct. 2011.

[81] B. Lestriez, S. Bahri, I. Sandu, L. Roue, and D. Guyomard, “On the binding mechanism of CMC in Si negative electrodes for Li-ion batteries,” *Electrochem. commun.*, vol. 9, no. 12, pp. 2801–2806, Dec. 2007.

[82] H. Buqa, M. Holzapfel, F. Krumeich, C. Veit, and P. Novák, “Study of styrene butadiene rubber and sodium methyl cellulose as binder for negative electrodes in lithium-ion batteries,” *J. Power Sources*, vol. 161, no. 1, pp. 617–622, Oct. 2006.

[83] L. Yue, L. Zhang, and H. Zhong, “Carboxymethyl chitosan: A new water soluble binder for Si anode of Li-ion batteries,” *J. Power Sources*, vol. 247, pp. 327–331, Feb. 2014.

[84] A. M. Chockla, T. D. Bogart, C. M. Hessel, K. C. Klavetter, C. B. Mullins, and B. A. Korgel, “Influences of gold, binder and electrolyte on silicon nanowire performance in Li-ion batteries,” *J. Phys. Chem. C*, vol. 116, no. 34, pp. 18079–18086, 2012.

[85] M. Ge, J. Rong, X. Fang, and C. Zhou, “Porous doped silicon nanowires for lithium ion battery anode with long cycle life,” *Nano Lett.*, vol. 12, no. 5, pp. 2318–2323, 2012.

[86] J.-H. Lee, U. Paik, V. a. Hackley, and Y.-M. Choi, “Effect of Carboxymethyl Cellulose on Aqueous Processing of Natural Graphite Negative Electrodes and their Electrochemical Performance for Lithium Batteries,” *J. Electrochem. Soc.*, vol. 152, p. A1763, 2005.

[87] W.-R. Liu, M.-H. Yang, H.-C. Wu, S. M. Chiao, and N.-L. Wu, “Enhanced Cycle Life of Si Anode for Li-Ion Batteries by Using Modified Elastomeric Binder,” *Electrochem. Solid-State Lett.*, vol. 8, no. 2, p. A100, 2005.

[88] J. Li, R. B. Lewis, and J. R. Dahn, “Sodium Carboxymethyl Cellulose,” *Electrochem. Solid-State Lett.*, vol. 10, no. 2, p. A17, 2007.

[89] M. N. . Ravi Kumar, “A review of chitin and chitosan applications,” *React. Funct. Polym.*, vol. 46, no. 1, pp. 1–27, Nov. 2000.

[90] L. Chai, Q. Qu, L. Zhang, M. Shen, L. Zhang, and H. Zheng, “Chitosan, a new and environmental benign electrode binder for use with graphite anode in lithium-ion batteries,” *Electrochim. Acta*, vol. 105, pp. 378–383, Aug. 2013.

[91] H. Tang, Q. Weng, and Z. Tang, “Chitosan oligosaccharides: A novel and efficient water soluble binder for lithium zinc titanate anode in lithium-ion batteries,” *Electrochim. Acta*, vol. 151, pp. 27–34, Jan. 2015.

[92] L. Zhang, Z. Liu, G. Cui, and L. Chen, “Biomass-derived materials for electrochemical energy storages,” *Prog. Polym. Sci.*, Oct. 2014.

[93] B. Koo, H. Kim, Y. Cho, K. T. Lee, N. S. Choi, and J. Cho, “A highly cross-linked polymeric binder for high-performance silicon negative electrodes in lithium ion batteries,” *Angew. Chemie - Int. Ed.*, vol. 51, no. 35, pp. 8762–8767, 2012.

[94] J. Song *et al.*, “Interpenetrated gel polymer binder for high-performance silicon anodes in lithium-ion batteries,” *Adv. Funct. Mater.*, 2014.

[95] M. H. Ryou *et al.*, “Mussel-inspired adhesive binders for high-performance silicon nanoparticle anodes in lithium-ion batteries,” *Adv. Mater.*, vol. 25, no. 11, pp. 1571–1576, 2013.

[96] S. Choi, T. woo Kwon, A. Coskun, and J. W. Choi, “Highly elastic binders integrating polyrotaxanes for silicon microparticle anodes in lithium ion batteries,” *Science (80-.).*, vol. 357, no. 6348, pp. 279–283, 2017.

[97] N. X. Chen and J. H. Zhang, “The role of hydrogen-bonding interaction in poly(vinyl alcohol)/ poly(acrylic acid) blending solutions and their films,” *Chinese J. Polym. Sci. (English Ed.*, vol. 28, no. 6, pp. 903–911, 2010.

[98] K. Kumeta, I. Nagashima, S. Matsui, and K. Mizoguchi, “Crosslinking reaction of poly(vinyl alcohol) with poly(acrylic acid) (PAA) by heat treatment: Effect of neutralization of PAA,” *J. Appl. Polym. Sci.*, vol. 90, no. 9, pp. 2420–2427, 2003.

[99] G. Liu *et al.*, “Polymers with tailored electronic structure for high capacity lithium battery electrodes,” *Adv. Mater.*, vol. 23, no. 40, pp. 4679–4683, 2011.

[100] H. Wu *et al.*, “Stable Li-ion battery anodes by in-situ polymerization of conducting hydrogel to conformally coat silicon nanoparticles.,” *Nat. Commun.*, vol. 4, p. 1943, 2013.

[101] F. Goto, K. Abe, K. Ikabayashi, T. Yoshida, and H. Morimoto, “The polyaniline/lithium battery,” *J. Power Sources*, vol. 20, no. 3–4, pp. 243–248, 1987.

[102] A. Ray, G. E. Asturias, D. L. Kershner, A. F. Richter, A. G. MacDiarmid, and A. J. Epstein, “Polyaniline: Doping, structure and derivatives,” *Synth. Met.*, vol. 29, no. 1, pp. 141–150, Mar. 1989.

[103] T. R. Jow and L. W. Shacklette, “Electrochemical --- and science,” no. 1, 1988.

[104] C. Wang, H. Wu, Z. Chen, M. T. McDowell, Y. Cui, and Z. Bao, “Self-healing chemistry enables the stable operation of silicon microparticle anodes for high-energy lithium-ion batteries.,” *Nat. Chem.*, vol. 5, no. 12, pp. 1042–8, 2013.

[105] T. W. Kwon, Y. K. Jeong, I. Lee, T. S. Kim, J. W. Choi, and A. Coskun, “Systematic molecular-level design of binders incorporating Meldrum’s acid for silicon anodes in lithium rechargeable batteries,” *Adv. Mater.*, vol. 26, no. 47, pp. 7979–7985, 2014.

[106] M. Zhong, Y. Liu, and X. Xie, “Self-healable, super tough graphene oxide–poly(acrylic acid) nanocomposite hydrogels facilitated by dual cross-linking effects through dynamic ionic interactions,” *J. Mater. Chem. B*, vol. 3, pp. 4001–4008, 2015.

[107] H. Kawai, M. Nagata, H. Tukamoto, and A. R. West, “High-voltage lithium cathode materials,” *J. Power Sources*, vol. 81–82, pp. 67–72, Sep. 1999.

[108] D. Miranda, C. M. Costa, and S. Lanceros-Mendez, “Lithium ion rechargeable batteries: state of the art and future needs of microscopic theoretical models and simulations,” *J. Electroanal. Chem.*, vol. 739, pp. 97–110, Dec. 2014.

[109] I. Bloom *et al.*, “Effect of cathode composition on capacity fade, impedance rise and power fade in high-power, lithium-ion cells,” *J. Power Sources*, vol. 124, no. 2, pp. 538–550, 2003.

[110] Y. Itou and Y. Ukyo, “Performance of LiNiCoO2 materials for advanced lithium-ion batteries,” *J. Power Sources*, vol. 146, no. 1–2, pp. 39–44, 2005.

[111] T. Ohzuku and R. J. Brodd, “An overview of positive-electrode materials for advanced lithium-ion batteries,” *J. Power Sources*, vol. 174, no. 2, pp. 449–456, Dec. 2007.

[112] T. Mueller, G. Hautier, a Jain, and G. Ceder, “Evaluation of Tavorite-Structured Cathode Materials for Lithium-Ion Batteries Using High-Throughput Computing,” *Chem. Mater.*, vol. 23, no. 17, pp. 3854–3862, 2011.

[113] G. Remarks, “Diffusion in Nanocrystalline Materials,” *Notes*, 1988.

[114] C. C. Nguyen and B. L. Lucht, “Development of Electrolytes for Si-Graphite Composite Electrodes,” *J. Electrochem. Soc.*, vol. 165, no. 10, pp. A2154–A2161, 2018.

[115] S. D. Beattie *et al.*, “Understanding capacity fade in silicon based electrodes for lithium-ion batteries using three electrode cells and upper cut-off voltage studies,” *J. Power Sources*, vol. 302, pp. 426–430, Jan. 2016.

[116] M. J. Loveridge *et al.*, “Towards High Capacity Li-ion Batteries Based on Silicon-Graphene Composite Anodes and Sub-micron V-doped LiFePO 4 Cathodes,” *Sci. Rep.*, vol. 6, no. November, pp. 1–11, 2016.

[117] H. Shobukawa, J. Alvarado, Y. Yang, and Y. S. Meng, “Electrochemical performance and interfacial investigation on Si composite anode for lithium ion batteries in full cell,” *J. Power Sources*, vol. 359, pp. 173–181, 2017.

[118] Y. Huang, X. Hou, X. Fan, S. Ma, S. Hu, and K. Lam, “Advanced Li-Rich Cathode Collaborated with Graphite/Silicon Anode for High Performance Li-Ion Batteries in Half and Full Cells,” *Electrochim. Acta*, vol. 182, pp. 1175–1187, Nov. 2015.

[119] The Boston Consulting Group, “Focus Batteries for Electric Cars,” 2010.

[120] N.-S. Choi, K. H. Yew, H. Kim, S.-S. Kim, and W.-U. Choi, “Surface layer formed on silicon thin-film electrode in lithium bis(oxalato) borate-based electrolyte,” *J. Power Sources*, vol. 172, no. 1, pp. 404–409, Oct. 2007.

[121] K. Xu, S. Zhang, T. R. Jow, W. Xu, and C. A. Angell, “LiBOB as Salt for Lithium-Ion Batteries:A Possible Solution for High Temperature Operation,” *Electrochem. Solid-State Lett.*, vol. 5, no. 1, p. A26, 2002.

[122] S. S. Zhang, “A review on electrolyte additives for lithium-ion batteries,” *J. Power Sources*, vol. 162, no. 2, pp. 1379–1394, Nov. 2006.

[123] N.-S. Choi, K. H. Yew, K. Y. Lee, M. Sung, H. Kim, and S.-S. Kim, “Effect of fluoroethylene carbonate additive on interfacial properties of silicon thin-film electrode,” *J. Power Sources*, vol. 161, no. 2, pp. 1254–1259, Oct. 2006.

[124] G.-B. Han, M.-H. Ryou, K. Y. Cho, Y. M. Lee, and J.-K. Park, “Effect of succinic anhydride as an electrolyte additive on electrochemical characteristics of silicon thin-film electrode,” *J. Power Sources*, vol. 195, no. 11, pp. 3709–3714, Jun. 2010.

[125] L. Chen, K. Wang, X. Xie, and J. Xie, “Effect of vinylene carbonate (VC) as electrolyte additive on electrochemical performance of Si film anode for lithium ion batteries,” *J. Power Sources*, vol. 174, no. 2, pp. 538–543, Dec. 2007.

[126] S. Dalavi, P. Guduru, and B. L. Lucht, “Performance Enhancing Electrolyte Additives for Lithium Ion Batteries with Silicon Anodes,” *J. Electrochem. Soc.*, vol. 159, no. 5, p. A642, 2012.

[127] F. Lin *et al.*, “Surface reconstruction and chemical evolution of stoichiometric layered cathode materials for lithium-ion batteries,” *Nat. Commun.*, vol. 5, pp. 1–9, 2014.

[128] J. Xia, M. Nie, J. C. Burns, A. Xiao, W. M. Lamanna, and J. R. Dahn, “Fluorinated electrolyte for 4.5 V Li(Ni0.4Mn0.4Co0.2)O2/graphite Li-ion cells,” *J. Power Sources*, vol. 307, pp. 340–350, Mar. 2016.

[129] Z. Zhang *et al.*, “Fluorinated electrolytes for 5 v lithium-ion battery chemistry,” *Energy Environ. Sci.*, vol. 6, no. 6, pp. 1806–1810, 2013.

[130] S. T. Myung *et al.*, “Nickel-Rich Layered Cathode Materials for Automotive Lithium-Ion Batteries: Achievements and Perspectives,” *ACS Energy Lett.*, vol. 2, no. 1, pp. 196–223, 2017.

[131] Y. Zhu, M. D. Casselman, Y. Li, A. Wei, and D. P. Abraham, “Perfluoroalkyl-substituted ethylene carbonates: Novel electrolyte additives for high-voltage lithium-ion batteries,” *J. Power Sources*, vol. 246, pp. 184–191, Jan. 2014.

[132] R. Rohan, T. C. Kuo, J. H. Lin, Y. C. Hsu, C. C. Li, and J. T. Lee, “Dinitrile-Mononitrile-Based Electrolyte System for Lithium-Ion Battery Application with the Mechanism of Reductive Decomposition of Mononitriles,” *J. Phys. Chem. C*, vol. 120, no. 12, pp.

6450–6458, 2016.

[133] Y. Abu-Lebdeh and I. Davidson, “High-Voltage Electrolytes Based on Adiponitrile for Li-Ion Batteries,” *J. Electrochem. Soc.*, vol. 156, no. 1, p. A60, 2009.

[134] J. Xia, J. Self, L. Ma, and J. R. Dahn, “Sulfolane-Based Electrolyte for High Voltage Li(Ni0.42Mn0.42Co0.16)O2 (NMC442)/Graphite Pouch Cells,” *J. Electrochem. Soc.*, vol. 162, no. 8, pp. A1424–A1431, 2015.

[135] A. Abouimrane, I. Belharouak, and K. Amine, “Sulfone-based electrolytes for high-voltage Li-ion batteries,” *Electrochem. commun.*, vol. 11, no. 5, pp. 1073–1076, May 2009.

[136] E. M. Erickson *et al.*, “Publisher’s Note: Review—Development of Advanced Rechargeable Batteries: A Continuous Challenge in the Choice of Suitable Electrolyte Solutions [*J. Electrochem. Soc.*, 162, A2424 (2015)],” *J. Electrochem. Soc.*, vol. 164, no. 4, pp. X5–X5, 2017.

[137] H. Duncan, N. Salem, and Y. Abu-Lebdeh, “Electrolyte Formulations Based on Dinitrile Solvents for High Voltage Li-Ion Batteries,” *J. Electrochem. Soc.*, vol. 160, no. 6, pp. A838–A848, 2013.

[138] B. Li, M. Xu, T. Li, W. Li, and S. Hu, “Prop-1-ene-1,3-sultone as SEI formation additive in propylene carbonate-based electrolyte for lithium ion batteries,” *Electrochem. commun.*, vol. 17, no. 1, pp. 92–95, 2012.

[139] Y. K. Han, J. Yoo, and J. Jung, “Reductive Decomposition Mechanism of Prop-1-ene-1,3-sultone in the Formation of a Solid-Electrolyte Interphase on the Anode of a Lithium-Ion Battery,” *J. Phys. Chem. C*, vol. 120, no. 50, pp. 28390–28397, 2016.

[140] J. Xia, L. Ma, C. P. Aiken, K. J. Nelson, L. P. Chen, and J. R. Dahn, “Comparative Study on Prop-1-ene-1,3-sultone and Vinylene Carbonate as Electrolyte Additives for Li(Ni1/3Mn13Co1/3)O2/Graphite Pouch Cells,” *J. Electrochem. Soc.*, vol. 161, no. 10, pp. A1634–A1641, 2014.

[141] M. D. Radin *et al.*, “Narrowing the Gap between Theoretical and Practical Capacities in Li-Ion Layered Oxide Cathode Materials,” *Adv. Energy Mater.*, vol. 7, no. 20, pp. 1–33, 2017.

[142] W. Haselrieder, B. Westphal, H. Bockholt, A. Diener, S. Höft, and A. Kwade,

"Measuring the coating adhesion strength of electrodes for lithium-ion batteries," *Int. J. Adhes. Adhes.*, vol. 60, pp. 1–8, 2015.

[143] E. Radvanyi *et al.*, "Study and modeling of the Solid Electrolyte Interphase behavior on nano-silicon anodes by Electrochemical Impedance Spectroscopy," *Electrochim. Acta*, vol. 137, pp. 751–757, 2014.

[144] and D. A. Elad Pollak,* Gregory Salitra, Valentina Baranchugov, "In Situ Conductivity, Impedance Spectroscopy, and Ex Situ Raman Spectra of Amorphous Silicon during the Insertion/Extraction of Lithium," *J. Phys. Chem. C*, vol. 111, no. 30, pp. 11437–11444, 2007.

[145] J. Guo, A. Sun, X. Chen, C. Wang, and A. Manivannan, "Cyclability study of silicon–carbon composite anodes for lithium-ion batteries using electrochemical impedance spectroscopy," *Electrochim. Acta*, vol. 56, no. 11, pp. 3981–3987, Apr. 2011.

[146] M. Gaberscek, J. Moskon, B. Erjavec, R. Dominko, and J. Jamnik, "The Importance of Interphase Contacts in Li Ion Electrodes: The Meaning of the High-Frequency Impedance Arc," *Electrochem. Solid-State Lett.*, vol. 11, p. A170, 2008.

[147] A. Hofmann, F. Werth, A. Ho weling, and T. Hanemann, "Investigation of the Oxidative Stability of Li-Ion Battery Electrolytes Using Cathode Materials," *ECS Electrochem. Lett.*, vol. 4, no. 12, pp. A141–A144, 2015.

[148] M. J. Loveridge *et al.*, "Enhancing cycling durability of Li-ion batteries with hierarchical structured silicon–graphene hybrid anodes," *Phys. Chem. Chem. Phys. Phys. Chem. Chem. Phys*, vol. 18, no. 18, pp. 30677–30685, 2016.

[149] M. Petzl, M. Kasper, and M. A. Danzer, "Lithium plating in a commercial lithium-ion battery – A low-temperature aging study," *J. Power Sources*, vol. 275, pp. 799–807, 2015.

[150] F. Shi, Z. Song, P. N. Ross, G. A. Somorjai, R. O. Ritchie, and K. Komvopoulos, "Failure mechanisms of single-crystal silicon electrodes in lithium-ion batteries," *Nat. Commun.*, vol. 7, no. May, p. 11886, 2016.

[151] Y. Oumellal *et al.*, "The failure mechanism of nano-sized Si-based negative electrodes for lithium ion batteries," *J. Mater. Chem.*, vol. 21, no. 17, p. 6201, 2011.

[152] K. Karki *et al.*, "Lithium-assisted electrochemical welding in silicon nanowire battery

electrodes," *Nano Lett.*, vol. 12, no. 3, pp. 1392–1397, 2012.

[153] K. Ogata *et al.*, "Revealing lithium-silicide phase transformations in nano-structured silicon-based lithium ion batteries via in situ NMR spectroscopy.," *Nat. Commun.*, vol. 5, p. 3217, 2014.

[154] B. Lu, Y. Song, Q. Zhang, J. Pan, Y.-T. Cheng, and J. Zhang, "Voltage hysteresis of lithium ion batteries caused by mechanical stress," *Phys. Chem. Chem. Phys.*, vol. 18, no. 6, pp. 4721–4727, 2016.

[155] D. K. Kang and H. C. Shin, "Investigation on cell impedance for high-power lithium-ion batteries," *J. Solid State Electrochem.*, vol. 11, no. 10, pp. 1405–1410, 2007.

[156] L. Baggetto *et al.*, "On the electrochemistry of an anode stack for all-solid-state 3D-integrated batteries," *J. Power Sources*, vol. 189, no. 1, pp. 402–410, 2009.

[157] T. Swamy and Y.-M. Chiang, "Electrochemical Charge Transfer Reaction Kinetics at the Silicon-Liquid Electrolyte Interface," *J. Electrochem. Soc.*, vol. 162, no. 13, pp. A7129–A7134, 2015.

[158] T. L. Kulova, A. M. Skundin, Y. V. Pleskov, E. I. Terukov, and O. I. Kon'kov, "Lithium intercalation in thin amorphous-silicon films," *Russ. J. Electrochem.*, vol. 42, no. 4, pp. 363–369, 2006.

[159] J. Dong, Y. Ozaki, and K. Nakashima, "FTIR studies of conformational energies of poly (acrylic acid) in cast films," *J. Polym. Sci. …*, pp. 507–515, 1997.

[160] S. Dubinsky, G. S. Grader, G. E. Shter, and M. S. Silverstein, "Thermal degradation of poly(acrylic acid) containing copper nitrate," *Polym. Degrad. Stab.*, vol. 86, no. 1, pp. 171–178, 2004.

[161] M. Wu *et al.*, "Toward an ideal polymer binder design for high-capacity battery anodes," *J. Am. Chem. Soc.*, vol. 135, no. 32, pp. 12048–12056, 2013.

[162] M. Nie, D. P. Abraham, Y. Chen, A. Bose, and B. L. Lucht, "Silicon solid electrolyte interphase (SEI) of lithium ion battery characterized by microscopy and spectroscopy," *J. Phys. Chem. C*, vol. 117, no. 26, pp. 13403–13412, 2013.

[163] S. M. M. Quintero, R. V. Ponce F, M. Cremona, A. L. C. Triques, A. R. d'Almeida, and A. M. B. Braga, "Swelling and morphological properties of poly(vinyl alcohol) (PVA)

and poly(acrylic acid) (PAA) hydrogels in solution with high salt concentration," *Polymer (Guildf).*, vol. 51, no. 4, pp. 953–958, Feb. 2010.

[164] Q. Huang, M. J. Loveridge, R. Genieser, M. J. Lain, and R. Bhagat, "Electrochemical Evaluation and Phase-related Impedance Studies on Silicon–Few Layer Graphene (FLG) Composite Electrode Systems," *Sci. Rep.*, vol. 8, no. 1, p. 1386, 2018.

[165] R. Nölle, A. J. Achazi, P. Kaghazchi, M. Winter, and T. Placke, "Pentafluorophenyl isocyanate as effective electrolyte additive for improved performance of silicon-based lithium ion full cells," *ACS Appl. Mater. Interfaces*, 2018.

[166] J. M. Martinez De La Hoz, F. A. Soto, and P. B. Balbuena, "Effect of the electrolyte composition on SEI reactions at Si anodes of Li Ion batteries," *J. Phys. Chem. C*, vol. 119, no. 13, pp. 7060–7068, 2015.

[167] S. N. Shkerin, I. A. Profatilova, and S. Roh, "Effect of ethylene carbonate concentration on the conductivity of carbonate-based electrolytes with LiPF6 for Li-ion batteries," *Ionics (Kiel).*, vol. 15, no. 6, pp. 761–764, 2009.

[168] I. A. Profatilova, N. S. Choi, K. H. Yew, and W. U. Choi, "The effect of ethylene carbonate on the cycling performance of a Si electrode," *Solid State Ionics*, vol. 179, no. 40, pp. 2399–2405, 2008.

[169] C. C. Nguyen and B. L. Lucht, "Comparative Study of Fluoroethylene Carbonate and Vinylene Carbonate for Silicon Anodes in Lithium Ion Batteries," *J. Electrochem. Soc.*, vol. 161, no. 12, pp. A1933–A1938, 2014.

[170] P. J. Grunthaner, M. H. Hecht, F. J. Grunthaner, and N. M. Johnson, "The localization and crystallographic dependence of Si suboxide species at the SiO2/Si interface," *J. Appl. Phys.*, vol. 61, no. 2, pp. 629–638, 1987.

[171] B. Philippe *et al.*, "Nanosilicon electrodes for lithium-ion batteries: Interfacial mechanisms studied by hard and soft X-ray photoelectron spectroscopy," *Chem. Mater.*, vol. 24, no. 6, pp. 1107–1115, 2012.

[172] K. Schroder *et al.*, "The Effect of Fluoroethylene Carbonate as an Additive on the Solid Electrolyte Interphase on Silicon Lithium-Ion Electrodes," *Chem. Mater.*, vol. 27, no. 16, pp. 5531–5542, 2015.

[173] L. Madec *et al.*, "Effect of sulfate electrolyte additives on

LiNi1/3Mn1/3Co1/3O2/graphite pouch cell lifetime: Correlation between xps surface studies and electrochemical test results," *J. Phys. Chem. C*, vol. 118, no. 51, pp. 29608–29622, 2014.

[174] L. El Ouatani *et al.*, "The Effect of Vinylene Carbonate Additive on Surface Film Formation on Both Electrodes in Li-Ion Batteries," *J. Electrochem. Soc.*, vol. 156, no. 2, p. A103, 2009.

[175] L. Madec, R. Petibon, J. Xia, J.-P. Sun, I. G. Hill, and J. R. Dahn, "Understanding the Role of Prop-1-ene-1,3-Sultone and Vinylene Carbonate in LiNi $_{1/3}$ Mn $_{1/3}$ Co $_{1/3}$ O $_{2}$ /Graphite Pouch Cells: Electrochemical, GC-MS and XPS Analysis," *J. Electrochem. Soc.*, vol. 162, no. 14, pp. A2635–A2645, 2015.

[176] T. Eriksson, a M. Andersson, C. Gejke, T. Gustafsson, and J. O. Thomas, "Influence of Temperature on the Interface Chemistry of Li x Mn 2 O 4 Electrodes," *Langmuir*, vol. 18, no. 9, pp. 3609–3619, 2002.

[177] S. P. Kim, A. C. T. V. Duin, and V. B. Shenoy, "Effect of electrolytes on the structure and evolution of the solid electrolyte interphase (SEI) in Li-ion batteries: A molecular dynamics study," *J. Power Sources*, vol. 196, no. 20, pp. 8590–8597, 2011.